A Supramolecular Approach to the Development of Luminescent Lanthanide Complexes

Steven W. Magennis

A thesis presented for the degree of

Doctor of Philosophy

in the Faculty of Science and Engineering at the

University of Edinburgh, 2000

To Mum and Dad

Declaration

I am the author of this thesis. The work is original and my own; where this is not so credit has been duly given. This thesis has not been submitted, in whole or in part, for any degree at this or any other university.

Steven Magennis

Acknowledgements

List of Abbreviations

NMR	nuclear magnetic resonance
s	singlet
d	doublet
t	triplet
q	quartet
m	multiplet
br	broad
δ	chemical shift
ppm	parts per million
J	coupling constant
COSY	correlation spectroscopy
IR	infrared
MS	mass spectrometry
FAB	fast atom bombardment
EI	electron impact
ES	electrospray
m/z	mass/charge ratio
UV	ultraviolet
λ	wavelength
ε	molar absorption coefficient
τ	lifetime
em	emission
ex	excitation
v	very
w	weak
s	strong
m	medium

Abstract

The development of photoactive molecular architectures is a recurring theme in supramolecular chemistry. In this respect, lanthanide complexes continue to play an important role owing to the attractive photophysical properties of the trivalent metal ion. Of particular interest are those complexes in which lanthanide luminescence is sensitised by the ligand, thereby combining many of the favourable characteristics inherent in both species.

Work undertaken for this thesis involved the preparation and characterisation of lanthanide complexes and the study of their luminescent properties; this work is divided into three sections. Firstly, it has been shown that imidodiphosphinates, acting as sensitising ligands, form a hydrophobic shell around lanthanide ions, to give long-lived, highly luminescent complexes. Modification of the imidodiphosphinate ligand allows the first coordination sphere of the metal to be altered, which prevents the binding of deactivating water molecules in solution. Secondly, reaction of a bis(β-diketonate) ligand with lanthanide ions leads to the formation of a novel triple-stranded dinuclear complex. The europium complex is very attractive, with a large absorption coefficient and high luminescence quantum yield. Finally, lanthanide complexes of lariat crown ethers, and their interaction with aromatic acids, have been investigated with a view to the development of new homogeneous immunoassays.

Contents

Chapter One

Introduction

Interest in the process of luminescence continues to increase as a result of the vast array of associated applications; these range from the conspicuous examples of lamps and television displays to the more esoteric use of molecular sensors. Exploitation of the luminescence phenomenon requires a detailed understanding of the interaction of light and matter, and considerable progress has been made in this respect, particularly in solid-state photophysics and molecular photochemistry. The recent developments in the field of supramolecular chemistry provide a conceptual grounding for the design of more complex luminescent systems, which have an attendant increase in function.

The excellent luminescent properties of lanthanide ions make them well suited for use in supramolecular systems. Furthermore, these properties are modulated upon complexation, so that the luminescence characteristics are determined by the interaction and organisation of the trivalent metal ion and the ligand(s). The work undertaken for this thesis is concerned with the development of luminescent lanthanide complexes, in which new luminescent features can be tailored for a specific application by the suitable choice of metal and ligand.

The thesis is organised as follows:

Chapter 2 provides a background to the study of luminescent lanthanide complexes, illustrating the unique benefits of utilising such species, whilst also highlighting their place within the wider framework of photoactive systems. Firstly, the field of supramolecular photochemistry is introduced as a conceptual foundation for the development of photochemical molecular devices. A discussion of the luminescent and physicochemical properties of lanthanides follows, paying particular attention to the functioning of their complexes as light-conversion molecular devices. This chapter concludes with a discussion of the present applications of luminescent lanthanide complexes.

Chapter 3 describes the preparation of neutral lanthanide complexes by a simple complexation approach, using three anionic imidodiphosphinate ligands instead of a synthetically challenging polydentate ligand. The photophysical properties of these complexes are examined in detail.

Chapter 4 is concerned with the synthesis and luminescence properties of novel dinuclear lanthanide complexes of a bis(β-diketonate) ligand. The motivation for studying such bimetallic complexes is discussed, and the applicability of bis(β-diketonate) ligands to the construction of dinuclear lanthanide complexes is examined. Subsequent sections detail the investigation of the complexation of lanthanide ions, focussing on the sensitisation of Eu^{3+} emission via the coordinated ligands.

Chapter 5 describes a new approach to luminescent labelling, based on the controlled formation of ternary lanthanide complexes. The preparation and characterisation of lanthanide complexes of lariat crown ethers is discussed first, followed by analysis of their interaction with aromatic acids.

Chapter 6 details the experimental procedures used throughout the course of this work.

Chapter Two

Background

2.1   SUPRAMOLECULAR PHOTOCHEMISTRY

The field of *supramolecular chemistry* covers the structures and functions of organised molecular systems formed by association of two or more chemical species via intermolecular forces.[1] Conceptually, it can be thought of as the next step in a logical progression of chemical complexity, from atom to molecule to supermolecule.

Supramolecular species can be characterised by both the spatial arrangement of their components and by the type of intermolecular forces present. These forces range from the weak, such as hydrogen bonds, to the relatively strong, such as electrostatic ion-ion interactions. Intermolecular forces are in general weaker than covalent bonds, making supramolecular species thermodynamically less stable and kinetically more labile than molecules. If desired, however, supramolecular stability can be greatly increased by a combination of these forces, and the influence of other factors (*e.g.* chelate and macrocyclic effects[2]).

Many of the intrinsic properties of individual components are preserved on forming a supermolecule, with only small changes due to mutual perturbations between components. Processes resulting from component interactions, however, may strongly affect certain intrinsic properties or give rise to entirely new properties. When a supramolecular system is formed from photoactive components, the new photochemical and photophysical characteristics that may subsequently arise are the subject of *supramolecular photochemistry*.[3]

It would be an impossible task to adequately summarise the progress made in the area of supramolecular photochemistry in this chapter; such a summary can be found, however, in several excellent monographs.[3,4] Rather than diluting the description of the supramolecular approach with assorted examples, this section will focus on those concepts pertinent to luminescent lanthanide complexes, in particular photophysical processes within supermolecules.

5

2.1.1 Photophysical properties of molecular components

Defining supermolecules in terms of molecular subunits with intrinsic properties can be very useful when classifying systems. For example, in transition metal coordination compounds the electronic interaction between metal and ligand is normally so strong that it is more appropriate to consider the entire complex as a "molecular" component rather than as a multicomponent supermolecule.

Deciding which properties are relevant when characterising molecular components depends on their role within the supermolecule. The active components may take part in a range of elementary processes, for instance: light absorption, light emission, energy or electron transfer and isomerisation. The most important photophysical processes are shown schematically in Figure 2.1.[3]
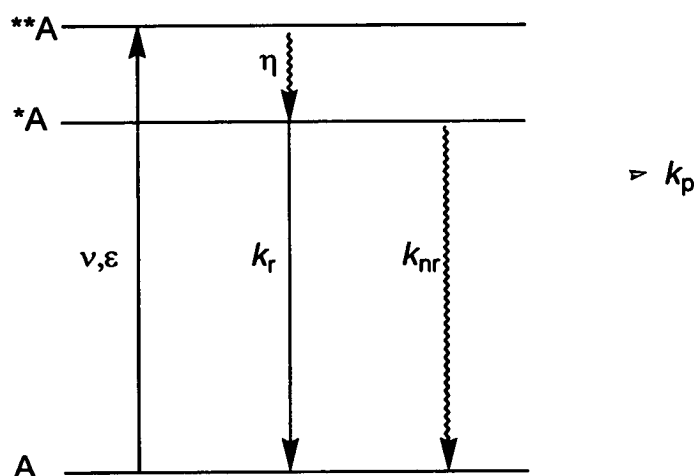
Figure 2.1 Photophysical processes within a molecular component

After light absorption, component A in Figure 2.1 is excited to state **A. A conversion process to a lower excited state, *A, follows and this can either decay to the ground-state, via radiative (k_r) or radiationless (k_{nr}) processes, or follow reactive (k_p) pathways. This system can be further defined by the frequency of incident light (v), the molar absorption coefficient (ε), the lifetime of the excited state *A ($\tau = 1/(k_r + k_{nr} + k_p)$), the quantum yields of emission ($\Phi_r = k_r\tau$) and photoreaction ($\Phi_p = k_p\tau$), and the efficiency

of formation of the excited state *A (η).

Other important properties that are necessary to characterise components in certain photoactive systems include redox behaviour, acid-base properties of the ground and excited states, and the coordination properties of components in the ground and excited states.[3]

2.1.2 Intercomponent energy-transfer processes

A characteristic feature of electronically excited species is their potential to transfer energy to another species.[5] A large number of the photophysical properties of supermolecules are a result of intercomponent energy-transfer processes, whereby an energy acceptor (A) receives energy from a donor (D) (scheme 2.1). The excited state properties of the donor are said to be quenched, while the excited state properties of the acceptor are sensitised.

$$D.A \xrightarrow{\ h\nu\ } *D.A \xrightarrow[\ \ ]{\ energy\ transfer\ } D.*A \qquad (2.1)$$

The electronic interaction between two species can be split into two additive terms, a coulombic term and an exchange term. Depending on the specific system, either of the terms can predominate leading to two mechanisms termed coulombic and electron-exchange energy transfer, also named Förster-type and Dexter-type respectively.[6] Both mechanisms require energy conservation, with the acceptor level generally below the donor level to ensure the process is exothermic.

Coulombic energy transfer mechanism

Coulombic energy transfer is dominated by electrostatic interactions that perturb the electronic structures of the energy donor and acceptor. This interaction takes place via the electromagnetic field, therefore no physical contact between donor (D) and acceptor

(A) is required. The result of this interaction is that *D is deexcited to D with the simultaneous excitation of A to *A, as shown in Figure 2.2.
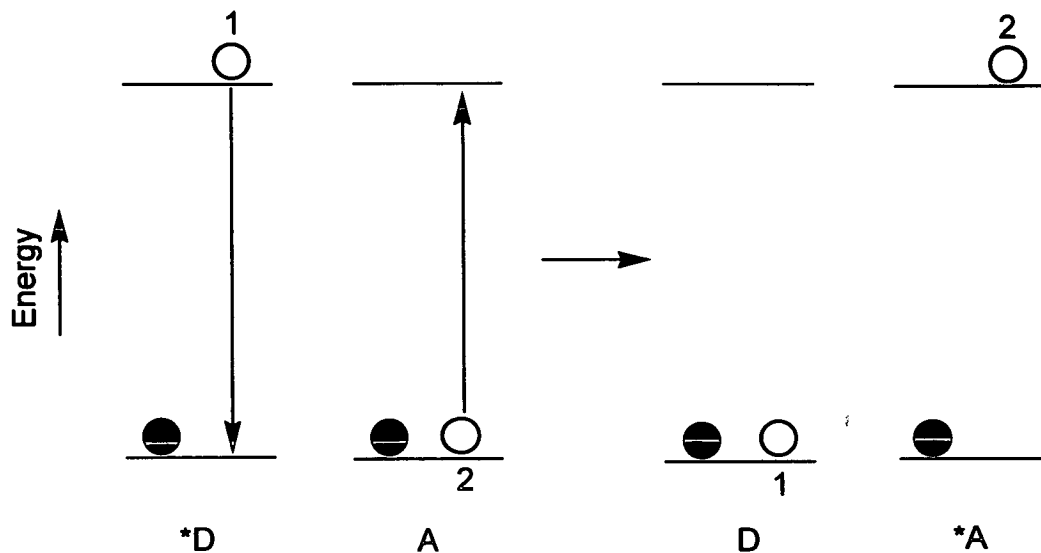
Figure 2.2 Simplified representation of non-radiative energy transfer by coulombic interaction

The most important term within the coulombic interaction is the dipole-dipole term, which obeys the same selection rules as the corresponding electric dipole transitions for A→*A and D→*D. In addition, this mechanism requires good overlap of the donor emission and acceptor absorption spectrum. For a dipole-dipole interaction, theory predicts that the strength of the interaction has a $1/r^6$ dependence, where r is the donor-acceptor distance, thus relatively long-range energy transfer is possible (in the order of 100 Å).

Electron-exchange energy transfer mechanism

Unlike the coulombic mechanism, the exchange mechanism requires much closer contact between donor and acceptor since it involves the physical transfer of electrons. It can be visualised as an exchange of two electrons, as shown in Figure 2.3, and like any chemical reaction it requires favourable overlap of the appropriate orbitals. Unlike, the coulombic mechanism, the rate of energy transfer is independent of the intensity of A→*A and D→*D transitions. The spin selection rules for this process are dependent

upon spin conservation of the reacting donor-acceptor supermolecule as a whole.
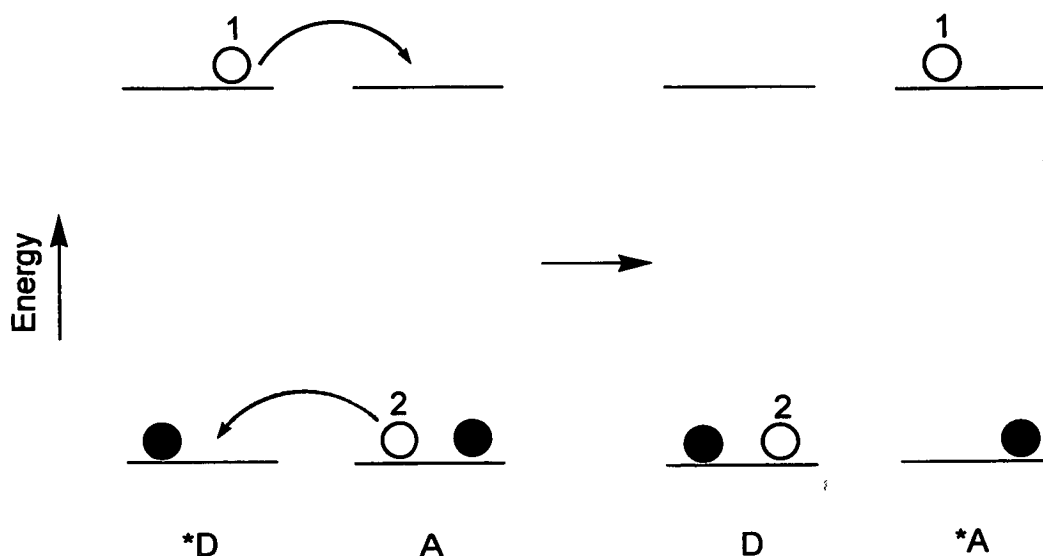
Figure 2.3 Simplified representation of non-radiative energy transfer by exchange interaction

2.1.3 The design of photochemical molecular devices

In *molecular photochemistry*, there are a number of pathways open to an electronically excited molecule, some of which have been mentioned.[7] Chemical pathways include dissociation leading to fragmentation of the molecule, charge-transfer reactions, in which a reaction pathway is opened to the excited species, and isomerisation. New electronic excited states are generated by energy transfer pathways and these may be intermolecular, when a different molecule is excited, or intramolecular, where a different excited state of the same molecule is populated. Finally, the excited species may lose energy by a radiative process, luminescence, or by non-radiative deactivation, collisional quenching. These primary processes can find many applications such as photochemical synthesis, photoluminescent materials and photochromic technology; however, more complex functions can only be performed by several components in concert. A cooperative assembly of components with designed, light-induced functions can be described as a *photochemical molecular device* (PMD).[3]

Much of supramolecular chemistry is inspired by natural systems and nature provides many examples of PMDs performing functions essential to life: photosynthesis and vision being among the most notable.[8] While these systems are highly complicated, suitably designed artificial PMDs can or could perform valuable photoinduced functions providing the necessary spatial, temporal and energetic requirements are met. Current research into PMDs embraces many areas, from sensor technology[9] and solar energy conversion[10] to the more futuristic possibility of information processing at the molecular level,[11] emphasising the utility and diversity of this supramolecular approach.

2.1.4 Light-conversion molecular devices

Having absorbed light, one useful function for a PMD is the transfer of this localised electronic energy to another component, where the energy can be used for a chemical reaction or be reconverted into light.[3] Even in the simplest case of a two-component donor-acceptor system a number of specific requirements must be fulfilled. For the donor these include stability towards photochemical decomposition reactions, high absorption efficiency, long-lived excited state and appropriate kinetic factors to favour energy transfer. When the acceptor is a lumophore, it must have photochemical stability and high luminescence efficiency. Where there are bonds or bridging groups connecting components, these must also display high stability, bring the components in close proximity and facilitate energy transfer.

An interesting design of PMDs involves the utilisation of several molecular components as donors, which increase the overall cross-section for light absorption, connected to a common acceptor component. This is known as the *antenna effect* and is shown schematically in Figure 2.4.[12] The donor components are designated as light-harvesting centres (LHCs), drawing inspiration from photosynthesis in which solar energy is harvested by pigment molecules acting as antennas.[3] In photosynthesis, the solar energy is used for chemical reaction whereas in Figure 2.4 the energy is channelled to a lumophore (L), which then re-emits light of a different wavelength.
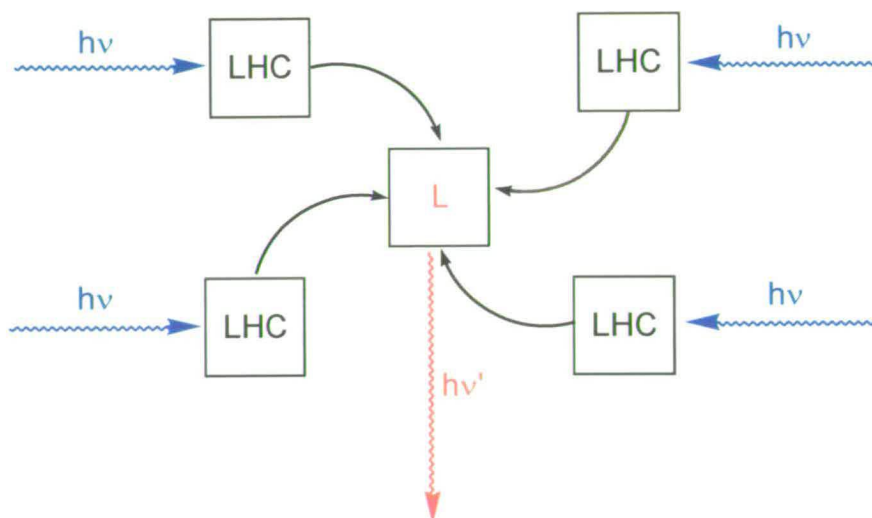
Figure 2.4 Schematic diagram illustrating the antenna effect

While conversion of light from one wavelength to another occurs in any luminescent species, the multicomponent nature of a PMD means the absorption and emission steps occur independently and can thus be optimised as required. The PMD illustrated in Figure 2.4 can be described as a *light-conversion molecular device* (LCMD),[1] involving an absorption-energy transfer-emission (A-ET-E) process.

2.2   CHEMICAL PROPERTIES OF LANTHANIDE COMPLEXES

A conceptual route from molecules to supermolecules to photochemical devices has been outlined in the previous section, without actually specifying which real atoms and molecules might be applicable. This section provides a background to the chemical properties of lanthanide complexes as a prelude to discussing the photophysics of real systems that embody some of those supramolecular concepts.

2.2.1 Chemical properties of lanthanide atoms and ions

The lanthanide elements (represented by the general symbol Ln) conventionally lie

between lanthanum and hafnium as shown by the blue shaded row in Figure 2.5. Along with the actinide row, situated below the lanthanides, they form the *f* block. Unlike the actinides, the only radioactive lanthanide is promethium, for which no stable isotope exists. The lanthanides, yttrium and lanthanum are also collectively called the rare earths, though it is now known that many of them are quite abundant.

H																	He
Li	Be											B	C	N	O	F	Ne
Na	Mg											Al	Si	P	S	Cl	Ar
K	Ca	Sc	Ti	V	Cr	Mn	Fe	Co	Ni	Cu	Zn	Ga	Ge	As	Se	Br	Kr
Rb	Sr	Y	Zr	Nb	Mo	Tc	Ru	Rh	Pd	Ag	Cd	In	Sn	Sb	Te	I	Xe
Cs	Ba	La	Hf	Ta	W	Re	Os	Ir	Pt	Au	Hg	Tl	Pb	Bi	Po	At	Rn
Fr	Ra	Ac	Rf	Db	Sg	Bh	Hs	Mt									

Ce	Pr	Nd	Pm	Sm	Eu	Gd	Tb	Dy	Ho	Er	Tm	Yb	Lu
Th	Pa	U	Np	Pu	Am	Cm	Bk	Cf	Es	Fm	Md	No	Lr

Figure 2.5 The modern periodic table with the lanthanide elements shaded in blue and the Group Three elements of Y and La shaded in green

The chemistry of the lanthanides is dominated by the +3 oxidation state, and this is the case whether in solution or in the solid state. The electronic configurations of the Ln^{3+} ions are shown in Table 2.1. Although the predominance of this oxidation state is often ascribed to the filling or half-filling of the $4f$ sub-shell, a full explanation of this requires a detailed thermodynamic analysis using Born-Haber cycles.[13] Cerium can exist in the tetravalent state in solid and aqueous solution and, less importantly, certain other elements (Pr, Nd, Tb, and Dy) give Ln^{4+} in solids. All of the lanthanides can exist in the divalent state under certain conditions, but only Eu, Yb and Sm have significant chemistry in this oxidation state, as indicated by the reduction potentials for Ln(III)/Ln(II) shown in Table 2.1.

Table 2.1 Selected properties of lanthanide atoms and lanthanide(III) ions

Element	Electronic configuration of metal	Electronic configuration of M^{3+}	Ln(III)/Ln(II) / volts[†]	Ionic Radius / Å[*]
Lanthanum	$[Xe]5d^16s^2$	$[Xe]$	(-3.1)	1.16
Cerium	$[Xe]4f^15d^16s^2$	$[Xe]4f^1$	(-3.2)	1.14
Praseodymium	$[Xe]4f^36s^2$	$[Xe]4f^2$	(-2.7)	1.13
Neodymium	$[Xe]4f^46s^2$	$[Xe]4f^3$	-2.6 (in THF)	1.11
Promethium	$[Xe]4f^56s^2$	$[Xe]4f^4$	(-2.6)	1.09
Samarium	$[Xe]4f^66s^2$	$[Xe]4f^5$	-1.55	1.08
Europium	$[Xe]4f^76s^2$	$[Xe]4f^6$	-0.34	1.07
Gadolinium	$[Xe]4f^75d^16s^2$	$[Xe]4f^7$	(-3.9)	1.05
Terbium	$[Xe]4f^96s^2$	$[Xe]4f^8$	(-3.7)	1.04
Dysprosium	$[Xe]4f^{10}6s^2$	$[Xe]4f^9$	-2.5 (in THF)	1.03
Holmium	$[Xe]4f^{11}6s^2$	$[Xe]4f^{10}$	(-2.9)	1.02
Erbium	$[Xe]4f^{12}6s^2$	$[Xe]4f^{11}$	(-3.1)	1.00
Thulium	$[Xe]4f^{13}6s^2$	$[Xe]4f^{12}$	-2.3 (in THF)	0.99
Ytterbium	$[Xe]4f^{14}6s^2$	$[Xe]4f^{13}$	-1.05	0.99
Lutetium	$[Xe]4f^{14}5d^16s^2$	$[Xe]4f^{14}$	—	0.98
Yttrium	$[Kr]4d^15s^2$	$[Kr]$	—	1.02

† Values in parentheses are calculated values[13]; * ionic radii for C.N. = 8 from R. D. Shannon[14]

The 4f orbitals are the determining factor in many of the properties of the lanthanides, and these 4f electrons can be thought of as inner electrons because their shielding by the 5s and 5p orbitals, and high kinetic energy, means interaction with the surroundings is a small perturbation.[15] As a result, 4f electrons do not take part in bonding to any significant extent, simply because the region of electron density does not extend out far enough.[16]

The Ln^{3+} ions resemble each other so closely in chemical and physical properties because they are all highly electropositive elements of similar size with little involvement of their valence electrons in bonding. Likewise, the elements yttrium and lanthanum from Group Three (shaded in green in Figure 2.5) are also included in this

discussion because of their similarities to the lanthanides. The Y^{3+} ion with a [Kr] noble gas core, for example, has an ionic radius close to those of Dy^{3+} and Ho^{3+}.

One important feature of the lanthanides is the decrease in their atomic and ionic radii across the series. This is known as the lanthanide contraction and can also be accounted for by the $4f$ electrons. In this case, the $5s$ and $5p$ orbitals contract with increasing nuclear charge as a result of the poor screening ability of f electrons. The ionic radii for Ln^{3+}, along with La^{3+} and Y^{3+}, are shown in Table 2.1. These show a steady decrease from 1.16 Å for La^{3+} to 0.98 Å for Lu^{3+}. The chemistry of lanthanides generally shows a corresponding gradual trend across the series as would be expected for an increasing charge to radius ratio.

2.2.2 Complexation properties of lanthanide(III) ions

General considerations

All of the Ln^{3+} ions share a number of characteristic coordination properties, and the most important of these are summarised as follows:[15]

(a)   The Ln^{3+} ions are classified as hard acids in the Pearson classification scheme and thus exhibit a strong preference for negatively charged donor groups that are also hard bases. Water molecules are very strong ligands towards Ln^{3+} ions and compete for coordination sites. As a result, in aqueous solution only ligands containing negatively charged donors such as O and F can bind strongly. Donor groups containing neutral oxygen or nitrogen atoms can bind but usually only when part of a multidentate ligand. Generally, the preference for donor atoms is O>N>S, although donors with large dipole moments or polarisable atoms can alter this pattern. Complexes formed from weaker ligands may have to be prepared under anhydrous conditions and tend to be very susceptible to hydrolysis. In addition, hydroxide ions bind so strongly to Ln^{3+} ions that lanthanide hydroxides, which have very low solubility, precipitate under neutral or alkaline conditions unless the ligands bind strongly.

(b)   Since the $4f$ orbitals cannot interact to any great degree with their environment,
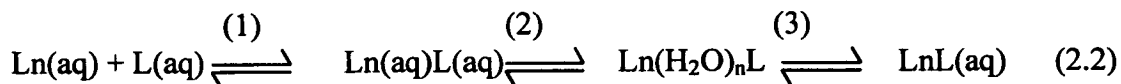
complex formation is dominated by electrostatic interactions. As a result of this ionic bonding, there is a lack of directionality to the Ln^{3+}-ligand interactions. The stereochemistry of the complexes formed is determined almost completely by the ionic radius of the Ln^{3+} ion; ligand characteristics such as charge, number of donor atoms and steric bulk; and solvation effects.

(c)   A wide range of coordination numbers are adopted by the Ln^{3+} ion in both the solid state and solution. In solids, coordination numbers from 3 to 12 are known to exist, reflecting the combination of electronic and steric requirements of the Ln^{3+} ion. In solution, there are the same requirements along with the effect of solvation. The most common coordination numbers in solution, including coordinated solvent molecules, are 8 and 9. For example, studies in aqueous solutions show that the lighter, larger ions (Ce^{3+} to Nd^{3+}) usually have hydration states of nine, whereas the heavier, smaller ions (Dy^{3+} to Lu^{3+}) predominantly have hydration states of eight. The ions from Sm^{3+} to Tb^{3+} are in equilibrium between eight- and nine-coordination.

(d)   The stability constants are, in general, much less than those of transition metal ions but greater than those of alkali and alkaline earth metal ions. The stability constants increase across the period, as would be expected for a smaller ion with greater charge density, and a similar correlation exists for other cations. For example, Sc^{3+} and Fe^{3+} form more stable complexes than Ln^{3+}, whereas the complexes of Ca^{2+} (which is of similar size to the lanthanides but has a smaller charge) are less stable. While complex stability does increase across the lanthanide row, there is often a slight irregularity at gadolinium, the gadolinium break, and this is thought to be partly a result of the change-over from coordination number 8 to 9.

(e)   Lanthanide complexes are ionic in nature; therefore, the kinetics of complexation are normally rapid for simple ligands. For example, the lifetime for water exchange is of the order of 10^{-9} s, so that this exchange is effectively controlled by the rate of diffusion to and from the inner coordination sphere.[17] The reaction sequence for Ln^{3+} complexation with a different ligand in aqueous solution is outlined below

15

(scheme 2.2):

$$\underset{\text{(1)}}{\text{Ln(aq)} + \text{L(aq)} \rightleftharpoons} \quad \underset{\text{(2)}}{\text{Ln(aq)L(aq)} \rightleftharpoons} \quad \underset{\text{(3)}}{\text{Ln}(H_2O)_n L \rightleftharpoons} \quad \text{LnL(aq)} \quad (2.2)$$

The fastest step is the diffusion controlled formation of Ln(aq)L(aq). In step (2) an outer sphere complex is formed, with the Ln^{3+} and ligand separated by at least one water molecule. In step (3) an inner sphere complex is formed, which is the case for all strongly binding ligands. In some instances, involving weakly basic inorganic and monodentate organic ligands, the complexation can be outer sphere.[18] For simple ligands, steps (2) and (3) may be comparable in rate. For polydentate ligands, however, step (3) is much slower, giving kinetically inert complexes.[19]

Chelate and macrocyclic complexes
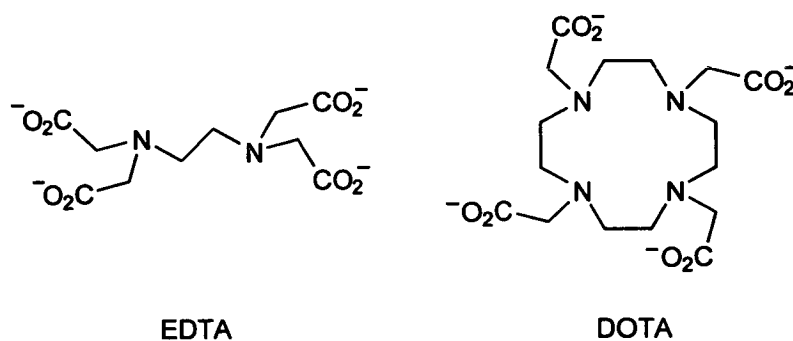
EDTA

DOTA

Figure 2.6 Examples of a chelating (EDTA) and a macrocyclic (DOTA) ligand

Complexes of chelating or macrocyclic ligands are among the most widely studied due to their thermodynamic stability and, often, increased kinetic inertness. Two typical examples, shown in Figure 2.6, are the polydentate aminopolycarboxylate EDTA and the macrocyclic DOTA, with stability constants for 1:1 complex formation in the region of 10^{17} and 10^{26} respectively. The increase in kinetic inertness, in aqueous solutions, is usually a combination of factors such as shielding the Ln^{3+} ion from attack by water and stability towards proton- and cation-mediated dissociation pathways.[19]

16

2.3   SPECTROSCOPY AND MAGNETISM OF LANTHANIDE (III) IONS

2.3.1 Spectroscopic terms

So far the Ln^{3+} ions have been described by their electronic configuration only. It is now necessary to consider the spectroscopically distinguishable energy levels that arise, in a particular configuration, as a result of interactions between the electrons and with the environment of the Ln^{3+} ion.

The electronic energy levels of a Ln^{3+} ion are reasonably well described by the Russell-Saunders coupling scheme. This scheme is appropriate where spin-orbit coupling is weak compared with interelectronic repulsion. These two interactions are actually of similar magnitude in Ln^{3+} ions and, if required, the more complicated intermediate coupling scheme can give a more accurate description of the electronic structure.[20] In the Russell-Saunders scheme, the individual orbital angular momenta of all the electrons are combined to give a total orbital angular momentum of the ion with quantum number L. Similarly, the individual electronic spin angular momenta combine into a total spin angular momentum for the ion with quantum number S. The total angular momentum is then given by the spin orbit coupling between S and L, described by the quantum number J. The energy levels of the ion can then be given a term symbol $^{(2S+1)}L_J$. The ground state of the Ln^{3+} ions can then be determined by Hund's rules (Table 2.2).[20]

A free Ln^{3+} ion has spherical symmetry that is removed on placing the ion in a chemical environment, such as in a complex. As a result, the $(2J + 1)$ degeneracy of the $^{(2S+1)}L_J$ spectroscopic levels can be partially or completely removed by the crystal field splitting. In contrast to transition metals, this crystal field splitting is very small due to the shielding of the $4f$ electrons and is of the order of 100 cm^{-1}. It is necessary to emphasise the relative separations for interelectronic repulsion, spin-orbit coupling and ligand field (10^4 cm^{-1}, 10^3 cm^{-1} and 10^2 cm^{-1} respectively), since in d-block transition metal complexes the importance of the latter two effects is reversed.

This description of the splitting of degenerate $4f^n$ states is in good agreement with the experimental evidence and energy level schemes for each of the free Ln^{3+} ions have been constructed, as shown in Figure 2.7.[21]

Table 2.2 Spectroscopic and magnetic properties of lanthanide(III) ions

| M^{3+}	$^{(2S+1)}L_J$ Ground state	Colour	μ_{eff}/ BM (Hund)	μ_{eff}/ BM (Van Vleck)
La^{3+}	$^1S_0$	Colourless	0	0
Ce^{3+}	$^2F_{5/2}$	Colourless	2.54	2.56
Pr^{3+}	$^3H_4$	Green	3.58	3.62
Nd^{3+}	$^4I_{9/2}$	Lilac-red	3.62	3.68
Pm^{3+}	$^5I_4$	Pink	2.68	2.83
Sm^{3+}	$^6H_{5/2}$	Pale yellow	0.845	1.55-1.65
Eu^{3+}	$^7F_0$	Very pale pink	0	3.4-3.5
Gd^{3+}	$^8S_{7/2}$	Colourless	7.94	7.94
Tb^{3+}	$^7F_6$	Very pale pink	9.72	9.7
Dy^{3+}	$^6H_{15/2}$	Pale yellow	10.60	10.6
Ho^{3+}	$^5I_8$	Yellow	10.61	10.6
Er^{3+}	$^4I_{15/2}$	Pink	9.58	9.6
Tm^{3+}	$^3H_6$	Pale green	7.56	7.6
Yb^{3+}	$^2F_{7/2}$	Colourless	4.54	4.54
Lu^{3+}	$^1S_0$	Colourless	0	0
Y^{3+}	$^1S_0$	Colourless	0	0
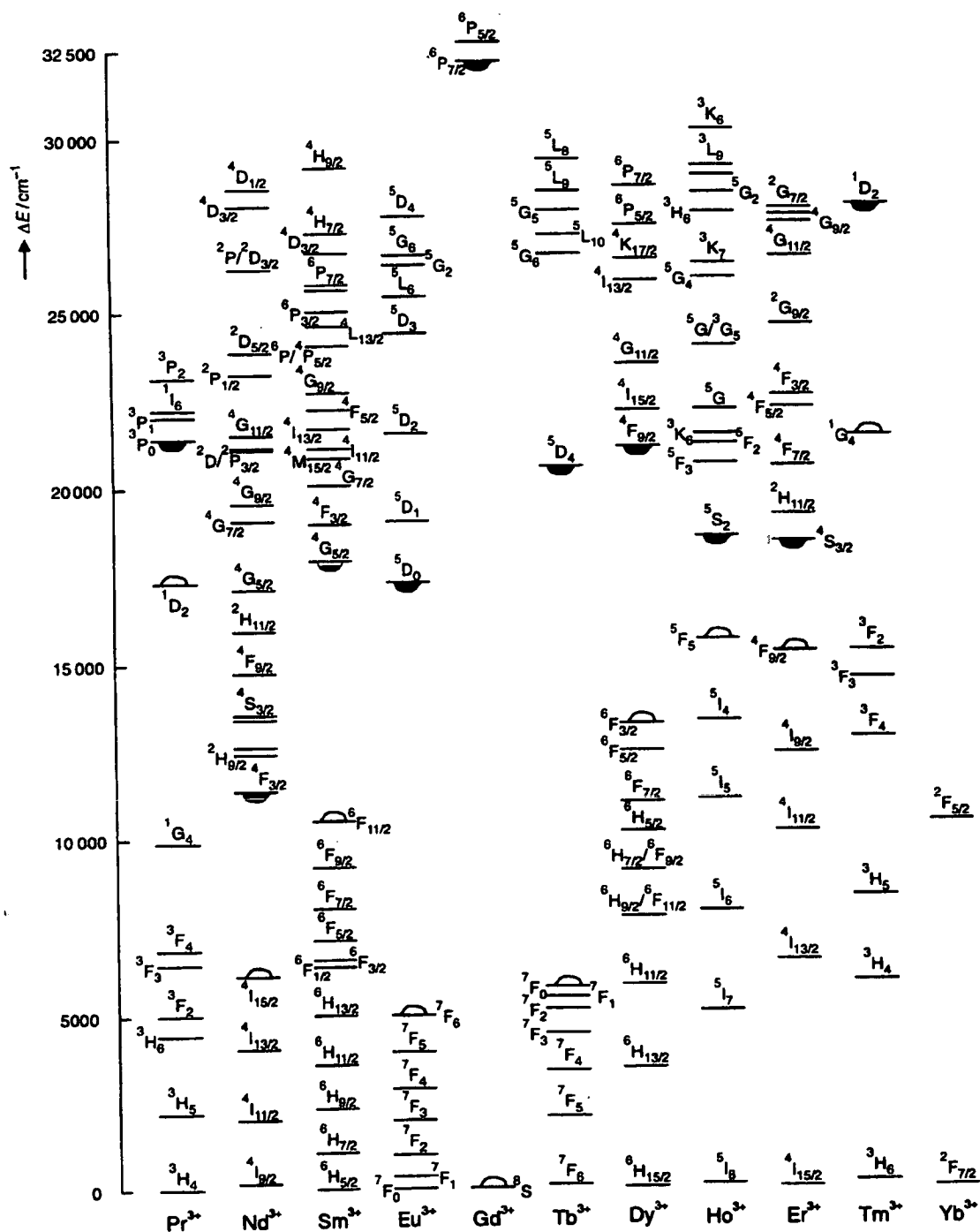
Figure 2.7 Energy level diagram for free Ln^{3+} ions in aqueous solutions; shaded semi-circles represent the lowest luminescent level, unshaded semi-circles represent the highest level of the ground state (reproduced from *J. Chem. Soc., Perkin Trans. 2*, 1998, 2141)

2.3.2 Magnetic properties

The magnetic properties of the free Ln^{3+} ions are a result of unpaired $4f$ electrons, which have little interaction with the environment. The paramagnetism of Ln^{3+} complexes is therefore similar to the free ions. Unlike transition metals the quenching of orbital angular momentum is negligible. According to Hund, the effective magnetic moment μ_{eff} is given by:

$$\mu_{eff} = g_J \sqrt{[J(J + 1)]} \tag{2.3}$$

where

$$g_J = \frac{S(S + 1) + 3J(J + 1) - L(L + 1)}{2J(J + 1)} \tag{2.4}$$

The values calculated using the above equation are shown in Table 2.2. These values are in good agreement with the observed values for all the Ln^{3+} ions, with the exception of Sm^{3+} and Eu^{3+}. This discrepancy arises because equation 2.3 neglects any contribution from the low-lying excited states of these ions, which are thermally populated at room temperature. Good agreement is obtained when this factor is taken into account (Van Vleck μ_{eff} in Table 2.2).[13]

The intrinsic paramagnetism of Ln^{3+} ions has many important applications, primarily as a result of their effect on the NMR spectra of other species. Some lanthanide complexes are used as NMR shift reagents, where the complex induces changes in the NMR spectra of coordinated molecules via through-space interactions.[22] This can often spread the resonances over a larger chemical shift range, thereby simplifying the spectrum and providing structural information, as the effect of the Ln^{3+} ion is distance-dependent. The use of chiral lanthanide shift reagents permits the resolution of enantiomers since the resulting diastereomers will have different lanthanide induced shifts.

A particularly important medical application of paramagnetic lanthanide complexes is as

contrast agents in magnetic resonance imaging (MRI).[23] In MRI the ^{1}H NMR signals of water in the tissues and fluids are monitored. The use of gradient coils means that each part of the patient's body feels a different field and therefore gives slightly different resonance frequencies, allowing spatial resolution. The lanthanide complexes, which are preferentially absorbed in brain tumours, cause signal enhancements of nearby ^{1}H nuclei by shortening relaxation times.

2.3.3 Selection rules and intensities of electronic transitions

The most important electronic transitions for Ln^{3+} ions are intraconfigurational *f-f* transitions within the 4*f* subshell, where the energy levels are arranged in reasonable agreement with the Russell-Saunders coupling scheme outlined previously. The *f-f* transitions are caused by both electric-dipole radiation and magnetic-dipole radiation.

Electric-dipole transitions

As with *d-d* electric-dipole transitions, the *f-f* transitions are parity-forbidden (Laporte rule). This rule forbids transitions among orbitals having the same symmetry properties towards an inversion centre. However, the *f-f* transitions can gain intensity through mixing in higher electronic states of opposite parity to the 4*f* wave functions. This mixing can take place through the ligand field (if the Ln^{3+} environment is without an inversion centre) or via asymmetric vibrations (vibronic coupling).[24] These transitions are known as forced (or induced) electric-dipole transitions and because the 4*f* orbitals are shielded, the molar absorption coefficients are very low (of the order of 1 $dm^3 mol^{-1} cm^{-1}$).

The most important selection rules for electric-dipole transitions are summarised as follows:[25]

– $\Delta l = \pm 1$ Laporte rule

– $\Delta S = 0$ Valid as long as J is a "good" quantum number

$-\ \Delta L \leq 6$ Valid as long as J is a "good" quantum number

$-\ \Delta J \leq 6$ $J = 0 \rightarrow J' = 0$ forbidden; $\Delta J = 2, 4, 6$ if J or $J' = 0$

The S and L selection rules are valid in the limit of Russell-Saunders coupling (*i.e.* if J is "good") and so are not rigid. Although the selection rules for J are more rigidly adhered to, they can be broken by "J-mixing", which is a weak effect resulting from the ligand field mixing electronic states with different J but same S and L values.[20]

Most f-f transitions are little affected by the environment of the Ln^{3+} ion, although there are some transitions whose intensities exhibit sensitivity to the surroundings. These transitions are referred to as hypersensitive transitions and usually follow the selection rules $\Delta J \leq 2$, $\Delta L \leq 2$ and, sometimes, $\Delta S = 0$. At the present time, however, no mechanism has been found that can adequately explain this hypersensitivity.[26]

Magnetic-dipole transitions

Magnetic-dipole transitions between $4f$ states are parity-allowed, but their oscillator strength is very low. They are normally much weaker than electric-dipole transitions, but the shielding of the f-electrons makes this transition comparable in intensity. The selection rules for magnetic-dipole transitions are as follows:[25]

$-\ \Delta l = 0$

$-\ \Delta S = 0$ Valid as long as J is a "good" quantum number

$-\ \Delta L = 0$ Valid as long as J is a "good" quantum number

$-\ \Delta J = 0, \pm 1$ $J = 0 \rightarrow J' = 0$ forbidden

The S and L selection rules are relaxed due to intermediate coupling. The intensity of magnetic-dipole transitions are relatively insensitive to the environment of the Ln^{3+} ion.

It should also be noted that the nature of the electronic transitions (electric or magnetic dipole) is not always clear-cut and some transitions may possess characteristics of both.

Many of the *f-f* transitions of Ln^{3+} ions lie in the visible region of the electromagnetic spectrum, but as they are weak the colours of lanthanide compounds (see Table 2.2) tend to be much less intense than those of the *d* block transition metals. Another consequence of the small interaction of the 4*f* orbitals of Ln^{3+} with the surroundings is that the ground and excited states of *f-f* transitions have the same equilibrium geometry. The absorption and emission are bands are therefore very sharp, with transitions in solids and solution almost as sharp as for the gaseous ions. The typical width at half height of absorption and emission bands are between 0.01 Å and 0.5 Å. The minor perturbation by the ligand field also means that the energy of *f-f* transitions vary little between compounds. It should also be emphasised that *f-f* excitation should not produce species that differ in reactivity or structure from the ground state.[20]

In addition to the selection rules already mentioned, a transition must fulfil the selection rules imposed by the symmetry of the Ln^{3+} ion. This symmetry not only determines the removal of the degeneracy of the *J* states, as previously discussed, but also dictates which of the electric- and magnetic-dipole transitions will be allowed.[20] In theory, analysis of the observed bands for these transitions should allow the symmetry of the Ln^{3+} to be determined. These experiments need to be performed at low temperature with high resolution (< 0.01 nm) laser spectroscopy. Even under these conditions there are a number of additional factors which must be considered; the intensity of certain transitions may be so weak as to be almost unobservable, additional vibronic lines may be present and crystal defects or sample inhomogeneities may cause slight differences in Ln^{3+} ion environments resulting in additional lines.[20]

2.3.4 Radiative and non-radiative relaxation processes of Ln^{3+} ions

The Ln^{3+} ions can be divided into three groups depending on their luminescence characteristics:[27]

(a) La^{3+} and Lu^{3+} (and Y^{3+}) - for these ions, no *f-f* transitions are possible

(b) Sm^{3+}, Eu^{3+}, Gd^{3+}, Tb^{3+} and Dy^{3+} - for these ions luminescence is relatively efficient as a result of the large energy gap between the excited and ground states, thus minimising non-radiative pathways

(c) Ce^{3+}, Pr^{3+}, Nd^{3+}, Ho^{3+}, Er^{3+}, Th^{3+} and Yb^{3+} - for these ions there are only small energy differences between the excited and ground states, thus non-radiative energy transfer is efficient

The Eu^{3+} and Tb^{3+} ions have particularly attractive luminescent properties, and the majority of complexes studied have contained one of these ions. Therefore, the remainder of this section will concentrate on the luminescence spectroscopy of Eu^{3+} and Tb^{3+} ions, though most of the theory applies equally well to the other luminescent Ln^{3+} ions.

The red emission of Eu^{3+} consists mainly of transitions from the ^5D manifold to the ^7F manifold, as shown in Figure 2.7. In solution, most of the emission is associated with the $^5D_0 \rightarrow {}^7F_J$ ($J = 0-6$) transitions; emission from the $^5D_1$ level is usually weak. The strongest lines are the $^5D_0 \rightarrow {}^7F_{1,2,4}$ transitions and the $^5D_0 \rightarrow {}^7F_2$ transition is hypersensitive. The selection rules for electric-dipole transitions allow the $^5D_0 \rightarrow {}^7F_{2,4,6}$ transitions, the $^5D_0 \rightarrow {}^7F_1$ transition is allowed for magnetic-dipole transitions, while the $^5D_0 \rightarrow {}^7F_{0,3,5}$ are strictly forbidden (as mentioned previously this rule can be broken). In the solid state, stronger emission can sometimes be observed from the $^5D_{1,2,3}$ levels. One interesting feature of the $^5D_0 \rightarrow {}^7F_0$ transition is that both states are non-degenerate; therefore, only one line should be observed for each unique Eu^{3+} environment. High resolution excitation spectroscopy can be used to check for the presence of more than one line though, as with the site symmetry determination, this is experimentally difficult.[28]

Table 2.3 Typical features of the $^5D_0 \rightarrow {}^7F_J$ and $^5D_4 \rightarrow {}^7F_J$ luminescent transitions for Eu^{3+} and Tb^{3+} complexes respectively in solution (adapted from reference 20)

J	Range / nm	Intensity	Comments
europium			
0	577-581	vw	non-degenerate
1	585-600	s	allowed (magnetic-dipole)
2	610-625	s-vs	hypersensitive
3	640-655	vw	always weak
4	680-710	m-s	sensitive to environment
5	740-770	vw	seldom observed
6	810-840	vw	seldom measured
terbium			
6	480-505	m-s	sensitive to environment
5	535-555	s-vs	–
4	580-600	m-s	sensitive to environment
3	615-625	m	–
2	640-655	w	sensitive to environment
1	660-670	vw	always weak
0	675-680	vw	always weak

Similarly, the green emission of Tb^{3+} consists mainly of the $^5D_4 \rightarrow {}^7F_J$ ($J = 0-6$) transitions (see Figure 2.7), the most intense being the $^5D_4 \rightarrow {}^7F_5$ line, with the $^5D_4 \rightarrow {}^7F_{3,5}$ transitions having magnetic-dipole character. The salient features of the $^5D_0 \rightarrow {}^7F_J$ transitions of Eu^{3+} and $^5D_4 \rightarrow {}^7F_J$ transitions of Tb^{3+} in solution are summarised in Table 2.3.

Vibrational deactivation

Since the *f-f* transitions are highly forbidden, the corresponding lifetimes of the Ln^{3+} excited states are long (millisecond range). The calculated radiative lifetimes (the

lifetime in the absence of other deactivating pathways) of Eu^{3+} ($^5D_0$) and Tb^{3+} ($^5D_4$) in aqueous solution are 9.67 ms and 9.02 ms, respectively.[26] The measured luminescence lifetimes of the $^5D_0$ level of Eu^{3+} in aqueous solution are normally much shorter, in the range 0.1-1.0 ms. The lifetimes in anhydrous solutions are longer, in deuterated solvents they can reach 4-4.5 ms and in the solid state they can be as long as 6 ms. The lifetime of the $^5D_1$ level of Eu^{3+} is much shorter (< 0.05 ms). The lifetime of the $^5D_4$ level of Tb^{3+} is generally longer than that of the $^5D_0$ level of Eu^{3+}: for example, the lifetime in aqueous solution is in the range 0.4-5 ms. Unlike organic fluorophores, Ln^{3+} ion luminescence is not directly quenched by O_2.[29]

It is obvious that there are large deviations of these lifetimes from the radiative rate and between the two Ln^{3+} ions. These differences were first explained by considering non-radiative deactivation in the solid state. This deactivation was interpreted in terms of multiphonon processes,[26] whereby non-radiative relaxation occurs by the simultaneous emission of several phonons (a phonon is a quantum of vibrational energy in a crystal lattice). The probability of this process occurring decreases rapidly with the number of phonons required to bridge the energy gap. The difference in energy between the $^5D_4$ and $^7F_0$ levels for Tb^{3+} is 15000 cm^{-1}, the difference for the $^5D_0$ and $^7F_6$ levels of Eu^{3+} is in the region of 10000 cm^{-1}, while the energy gap between $^5D_1$ and $^5D_0$ levels is around 2000 cm^{-1}. In these cases, for a typical lattice phonon of 1000 cm^{-1}, the multiphonon process would require approximately 15, 10 and 2 phonons.

The intensities and lifetimes are greater for both Eu^{3+} and Tb^{3+} in D_2O compared to H_2O, and the greater effect in the case of Eu^{3+} is attributed to the larger energy gap.[29,30] The vibrations of coordinated water molecules deactivate the Ln^{3+} excited state by an energy transfer process and the rate is proportional to the number of O–H or O–D oscillators associated with the Ln^{3+} ion. The appropriate energy levels of Eu^{3+} and Tb^{3+} are shown in Figure 2.8, along with the vibrational levels of coordinated O–H and O–D oscillators.
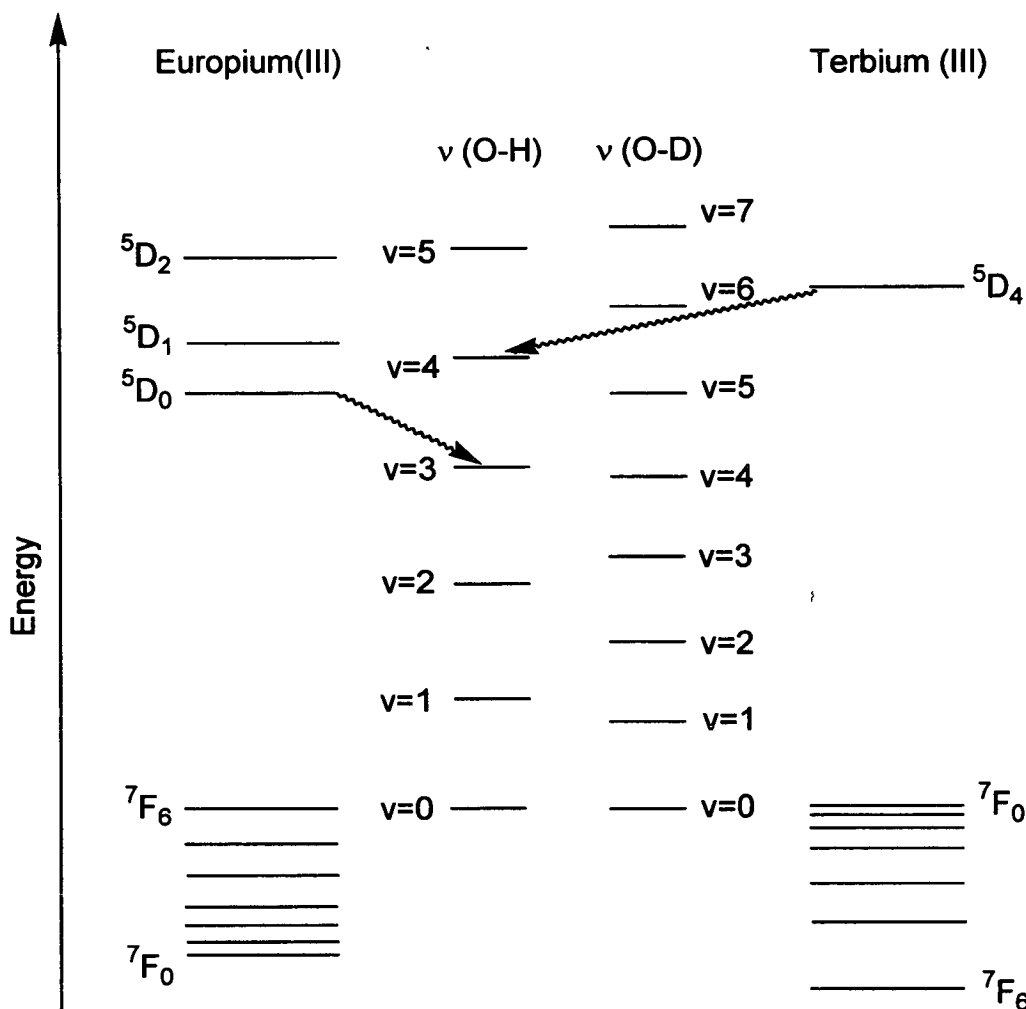
Figure 2.8 Radiationless deexcitation of Eu^{3+} and Tb^{3+} by coupling of the emissive states to the O–H and O–D vibrational overtones of coordinated solvent molecules; the energy level diagrams have been positioned to coincide the highest acceptor state of the ground ^7F term with the zero-point energies of the vibrational overtone ladders (adapted from reference 28)

The probability of exciting an oscillator from the ground vibrational level to an overtone level decreases rapidly as the overtone level involved increases, as a result of poor Franck-Condon overlap between wavefunctions. Since O–D vibrations are of lower frequency than O–H, energy transfer to D_2O will involve excitation to a higher vibrational level than H_2O, and will therefore be less efficient for a given energy gap. This explains the increase in lifetime in D_2O and the longer lifetime for Tb^{3+} compared

to Eu^{3+}.

The rate constant for deactivation of the Ln^{3+} excited state in H_2O may be partitioned into the different modes of quenching as shown in equation 2.5:

$$k_{H_2O} = k_r + \Sigma k_{nr} + k_{OH} \tag{2.5}$$

where k_{H_2O} is the observed decay rate in H_2O, k_r is the radiative rate constant, k_{OH} is the rate constant for non-radiative deexcitation to coordinated O–H oscillators and Σk_{nr} is the sum of the rate constants for all other non-radiative processes. In D_2O the k_{OH} term can be neglected, giving equation 2.6.

$$k_{D_2O} = k_r + \Sigma k_{nr} \tag{2.6}$$

The difference between the observed rates of decay in H_2O and D_2O is k_{OH} and this, together with the fact that the oscillators act independently,[31] was used to derive an expression for the determination of the number of water molecules (q) in the primary coordination sphere (equation 2.7):

$$q = A(k_{H_2O} - k_{D_2O}) \tag{2.7}$$

where A is a proportionality constant for a given ion.[28] The error in q is given as ± 0.5. The constant A was empirically derived in a study of solids in which the hydration state was known from X-ray crystallography. A good correlation was also found between the solid state and the same samples in solution, indicating that the rate of quenching by O–H oscillators is independent of the state of matter.[32] The value of A for Eu^{3+} and Tb^{3+} was found to be 1.05 and 4.2 respectively, illustrating the greater sensitivity of Eu^{3+} to O–H quenching.

While equation 2.7 will give a good estimate of the hydration state of a Ln^{3+} ion, it is an empirical result and must therefore have limitations. Firstly, there is the possibility that

a complex exists in solution as a mixture of isomers, each of which has a different q-value. Since water molecules exchange on a faster timescale than the Ln^{3+} lifetime, an average q-value is obtained. However, in many cases this can be ruled out by NMR or high-resolution emission studies, which show that only one isomer is present in solution.[33] Secondly, the equation is based on the number of coordinated water molecules without consideration of any contribution from outer-sphere water molecules. Finally, since there is an energy transfer from the Ln^{3+} ion to the O–H / O–D oscillator, the rate of energy transfer should be distance-dependent.

A quantitative theory of the relaxation of Ln^{3+} ions in solution does not exist at the present time. There are, however, certain theoretical models which give reasonable agreement with experimental results (one such model is based on the coulombic dipole-dipole mechanism of energy transfer).[34] In view of this, attempts have been made recently to improve the empirical calculation of hydration states.[35] The new expression, equation 2.8, takes into account the quenching effect of closely diffusing water molecules:

$$q_{corr} = A' \, (k_{H_2O} - k_{D_2O})_{corr} \qquad (2.8)$$

where q_{corr} represents the corrected hydration state of the Ln^{3+} ion, A' is a new proportionality constant (1.2 ms for Eu^{3+}, 5 ms for Tb^{3+}) and the corrections to $(k_{H_2O} - k_{D_2O})$ are -0.25 ms^{-1} for Eu^{3+} and -0.06 ms^{-1} for Tb^{3+}.

While high energy O–H vibrations are the most efficient quenchers, whether the solvent is water or another molecule such as methanol, other oscillators can also contribute to the quenching process. It is well established that N–H, C–H and C=O vibrations can deactivate the excited states of Ln^{3+} ions.[29] In particular, the quenching by amine and amide N–H oscillators has been shown to be very effective,[36] and corrections have been applied to equation 2.8 to take into account H/D exchange for these groups. Coordinated anions can also have a large effect on the lifetime of the Ln^{3+} excited state. The displacement of water molecules from the inner coordination sphere by ions such as F$^-$

leads to an increased lifetime and intensity of emission, while some other coordinated anions, for example CNS^-, have the opposite effect by introducing new deactivating pathways, such as charge transfer from the anion to the Ln^{3+} ion .[37]

Charge transfer transitions

Electron transfer can occur from filled ligand molecular orbitals to the partly filled $4f$ shell of Ln^{3+} ions. For a given Ln^{3+} ion, the more reducing the ligand, the lower the energy of the charge transfer (CT) transition.[38] The energy of the charge transfer transition follows the sequence:

$$Eu^{3+} < Yb^{3+} < Sm^{3+} < Tm^{3+}$$
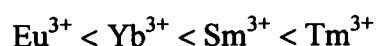
The luminescence of the $^5D_0$ level of Eu^{3+} can be increased or decreased by the charge transfer states. Whilst the $4f$ levels can be efficiently excited by energy transfer from charge transfer bands, thereby increasing the emission intensity, if these bands are low-lying they can also serve to thermally deactivate the Eu^{3+} excited states, leading to a decrease in emission lifetime and intensity.[38] The charge transfer states for Tb^{3+} occur at such a high energy that they cannot influence the *f-f* luminescence of this ion.

Effect of 4f levels higher than the emissive state

In addition to the effect of charge transfer, there can also be important processes involving $4f$ excited states that lie above the emitting state of a Ln^{3+} ion. As with the charge transfer process, this manifests itself in one of two ways. Either the closely spaced higher electronic states can relax to the lower emissive levels, resulting in an increase in luminescence, or the upper excited states may deactivate the lower state. The $^5D_1$ and $^5D_0$ states of Eu^{3+} are involved in both these mechanisms. Excitation into the $^5D_1$ state can result in radiationless deactivation to the $^5D_0$ state or in deactivation to the ground state.[20] However, since the $^5D_1$ is only slightly higher in energy than the $^5D_0$ state, the $^5D_0$ state can be deactivated at higher temperatures by thermally populating the $^5D_1$ state.[39]

2.3.5 4f-5d transitions

In addition to the 4*f* intraconfigurational transitions of Ln^{3+} complexes, it is necessary to mention briefly one other electronic transition that can occur in the region of interest (*i.e.*, the experimentally-accessible near-UV to near-IR region), namely the interconfigurational 4*f*-5*d* transition. These Laporte-allowed transitions are very intense but for most Ln^{3+} ions are of such high energy that they are located in the vacuum ultraviolet region. However, Ce^{3+}, Tb^{3+} and sometimes Pr^{3+} exhibit absorption bands above 200 nm.[26] These transitions are easily identifiable as they are much broader than *f-f* transitions, reflecting the greater interaction of the 5*d* orbital with the surroundings of the Ln^{3+} ion.

2.4 DESIGNING LUMINESCENT LANTHANIDE COMPLEXES

In this section, the design of luminescent lanthanide complexes will be discussed, illustrating their place within supramolecular photochemistry. Having examined in detail the spectroscopic and coordination properties of Ln^{3+} ions, the main advantages and disadvantages of the Ln^{3+} ion as a lumophore can be summarised as follows:

Advantages of Ln^{3+} as lumophore
- very well-defined, narrow line emission
- long lifetime in excited state
- efficient luminescence, even in solution at room temperature (most metal ions and their complexes are not very luminescent in solution at temperatures above 77 K)
- emission in the visible region

Disadvantages of Ln^{3+} as lumophore
- very poor light absorbers
- efficient vibrational quenching by coordinated molecules
- complexes are kinetically labile

2.4.1 Sensitised lanthanide emission

Overcoming the problems of vibrational quenching and lability involves designing polydentate ligands that complex the Ln^{3+} ion, preventing the coordination of deactivating solvent molecules and increasing kinetic stability; examples of this will be discussed later. The problem of the low absorption coefficient is solved by sensitisation of the lanthanide emission; in other words, by another species transferring energy to the excited state of the Ln^{3+} ion, without the Ln^{3+} absorbing the light directly. This process was first discovered in lanthanide complexes in 1942, when characteristic Ln^{3+} emission was observed from certain lanthanide complexes of β-diketone ligands when they were irradiated by ultraviolet light.[40] This led to a vast amount of research on the photophysics of β-diketonate complexes, providing a detailed mechanism of the sensitisation process.[41] This mechanism is illustrated in Figure 2.9.

The first part of the mechanism involves absorption from the ground-state singlet of the organic ligand to the excited singlet state. Non-radiative decay brings the ligand to the lowest vibrational level of the excited singlet state. The ligand can then either deactivate to the ground state by a non-radiative or radiative (fluorescence) pathway, or it can cross over to the excited triplet state via an intersystem crossing (ISC). The presence of the Ln^{3+} ion increases the rate of this intersystem crossing due to the paramagnetism and/or heavy atom effect of the metal. From the triplet state, the ligand can either return to the ground state, again via non-radiative or radiative (phosphorescence) pathways, or it can transfer its energy to an excited state of the Ln^{3+} ion (with energy transfer rates in the region 10^6-10^9 s^{-1}). Following energy transfer, the Ln^{3+} ion can decay via any of the available pathways (as if the Ln^{3+} ion had itself absorbed the light). When the Ln^{3+} is Eu^{3+} or Tb^{3+}, luminescence will be very efficient, as discussed earlier. In the case of Gd^{3+}, for which luminescence is also very efficient, this mechanism does not apply because the lowest excited state of Gd^{3+}, at 32200 cm^{-1}, is far higher than the triplet state of most organic ligands.
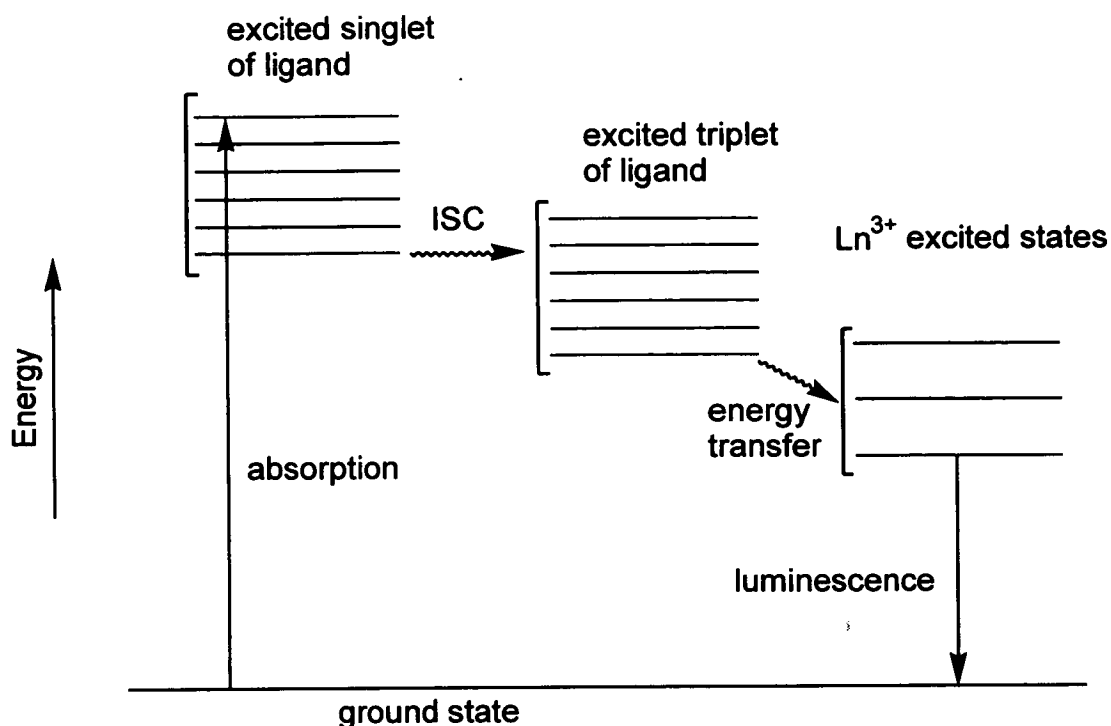
excited singlet
of ligand

excited triplet
of ligand

ISC

Ln^{3+} excited states

Energy

absorption

energy
transfer

luminescence

ground state

Figure 2.9 The energy transfer mechanism from organic ligand to Ln^{3+} ion in lanthanide complexes

.The mechanism shown in Figure 2.9 is generally thought to account for the short-range energy transfer process in lanthanide complexes.[41] The energy transfer in this instance most probably proceeds by the Dexter electron-exchange mechanism.[42] In addition, it has been demonstrated that energy transfer can also occur from the singlet state of the organic ligand to the excited state of the Ln^{3+} ion, with the long-range Förster dipole-dipole mechanism operating.[43] As mentioned previously, energy transfer can also occur to and from charge transfer states. The charge transfer state may be populated thermally, optically or following an electron transfer process from a ligand-localised excited state [photoinduced electron transfer (PET)].[3] Recently, Yb^{3+} luminescence in a Yb^{3+}-protein system was attributed to sensitisation due to a PET process; the lack of Eu^{3+} emission from the analogous Eu^{3+}-protein system was ascribed to the charge transfer state being lower in energy than the excited state of Eu^{3+}, preventing sensitisation.[44]

Having established a solution to the problem of the weak absorbance of Ln^{3+} ions, it is

necessary to quantitatively assess the sensitisation process. Overall efficient sensitisation requires each step to compete effectively with the other deactivating pathways. In other words, the quantum yield for ligand-sensitised luminescence (the ratio of photons emitted by the Ln^{3+} ion to photons absorbed by the ligand) must be high. The main limiting factors are the formation of the donor level (ligand triplet state), the energy transfer process and deactivation of the Ln^{3+} excited states.

One requirement for efficient energy transfer is good matching of the energy levels of donor and acceptor, ideally with the acceptor level slightly lower than the donor level (*i.e.* energy transfer is exothermic). In fact, it has been demonstrated that if the energy gap is too small, a thermally activated back energy transfer process can occur from the excited state of the lanthanide to the ligand triplet state, which then deactivates to the ground state.[12] It has been shown that back energy transfer occurs when the ligand level is less than 1850 cm^{-1} above the metal's excited state.[45] In this case, the excited state of the Ln^{3+} ion is in thermal equilibrium with the ligand triplet state, and dissolved oxygen is able to quench the lanthanide luminescence by deactivating this triplet state.[12] Deactivation of Ln^{3+} ions via charge transfer states has already been discussed, but it should be emphasised again that the relatively low reduction potential means that for efficient luminescence of Eu^{3+}, ligands that are hard to oxidise are required.

2.4.2 Luminescent lanthanide complexes of polydentate ligands

Photophysical studies have been performed on the lanthanide complexes of a wide range of polydentate ligands. The complexes described next are some of the most important structural types, focussing on those in which energy transfer from ligand to metal occurs. This serves to illustrate the design criteria discussed previously.

Cryptates

The development of kinetically-stable lanthanide cryptate complexes revitalised the study of luminescent lanthanide complexes.[46] Initial work focussed on the 2.2.1 cryptand ligand (1).[47]
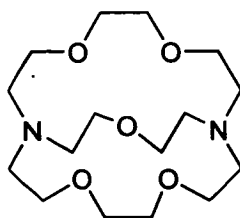
1

This cryptate serves two purposes; it encapsulates the Ln^{3+} ion, providing high kinetic and thermodynamic stability, and it shields the ion from most of the water molecules (three waters are still coordinated). The low absorption coefficient is overcome somewhat by the presence of a ligand-to-metal charge transfer (LMCT) state through which the Ln^{3+} ion can be excited; however, the efficiency of energy transfer is poor. The breakthrough for these systems came when the ether arms were replaced with 2,2'-bipyridine (bpy) groups (2).[12] The bpy units absorb strongly in the UV region, sensitising Ln^{3+} emission. The drawbacks of the Eu^{3+} and Tb^{3+} complexes are the presence of low-lying CT states (Eu^{3+}) and a deactivating back energy transfer process (Tb^{3+}), in addition to the 2-3 waters which are still coordinated to the metal.
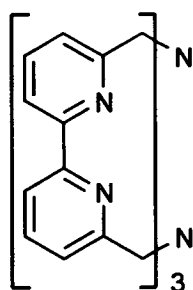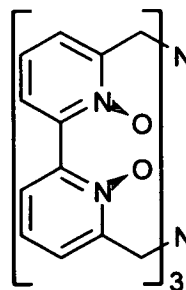

2   **3**

Perhaps the most significant aspect of this work was the realisation that these complexes could be described as light-conversion molecular devices, performing the absorption-energy transfer-emission process mentioned earlier. The bpy components transfer energy to the Ln^{3+} component, which then emits. The minimal perturbation by the ligands on the spectroscopic properties of the Ln^{3+} ions makes them ideal as components in such systems. The desirable emitting properties of the Ln^{3+} ion are maintained, whilst the

problem of low absorption is circumvented by utilising the antenna effect.[12] In this type of device, simply changing the Ln^{3+} ion used results in a range of different colours of emitted light for the same excitation wavelength.

A number of other cryptates, incorporating other chromophores, have also been synthesised. The europium complexes of cryptands containing N-oxide groups, ligand 3 for example, exhibit higher conversion efficiency than the bpy analogue. This is due to a decrease in the number of coordinated water molecules and possibly increased energy transfer efficiency, as a result of a stronger binding interaction. However, the europium complexes show an increased quenching due to LMCT states that are lower than in the bpy system.[46]

Complexes of bipyridine-based branched-macrocyclic ligands

The bipyridine ligand has also been used as a building block of branched macrocyclic ligands (*e.g.* 4 and 5).[46] In most cases, these ligands are better at shielding the Ln^{3+} ion from solvent molecules than the cryptands. The bpy-branched triazacyclononane (4) is particularly good in this respect, with very little change in lifetime for the Eu^{3+} and Tb^{3+} complexes in either H_2O or D_2O, demonstrating the absence of coordinated water molecules. The close proximity of the CH_2 groups to the metal, which can potentially quench the luminescence, explains the relatively short lifetime of these complexes.
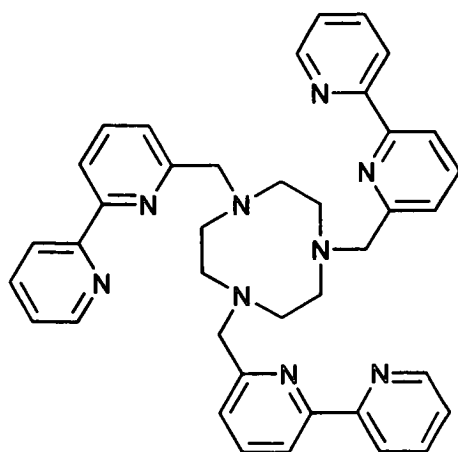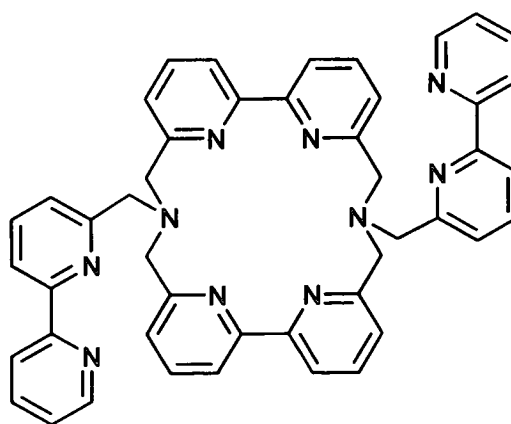
4   5

Podates

Podand ligands, in particular tripodal ligands, are another class of polydentate ligands that have proved to be very effective at encapsulating Ln^{3+} ions.[48] The photophysical properties of suitably designed podates have been investigated. Ligand **6**, which is a tripodal ligand with bpy chromophoric arms, forms a 1:1 complex with Eu^{3+}.[46] This structure lacks the stability of the cryptates, so that while it is has reasonable luminescent properties in methanol it decomposes in water. A better ligand is the hexadentate N-donor podand, ligand **7**, which forms stable 1:1 complexes with Eu^{3+}, Tb^{3+} and Gd^{3+} in water, methanol and CH_2Cl_2.[49] Energy transfer from the ligand to the metal is very efficient for Tb^{3+} but poor for Eu^{3+} due to deactivating LMCT states. Lifetime studies show that three water molecules are coordinated in aqueous solution.
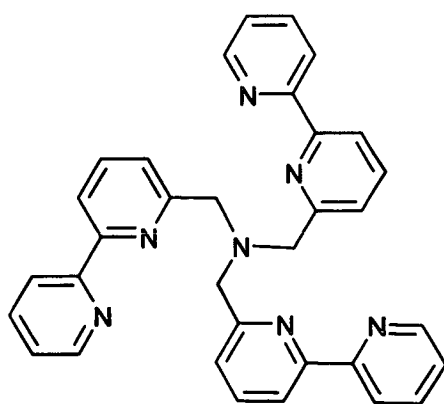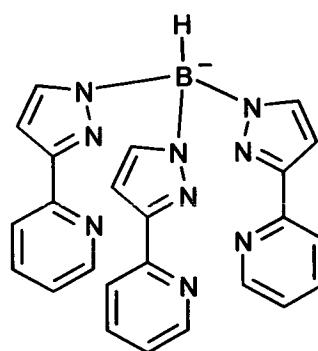

**6**   **7**
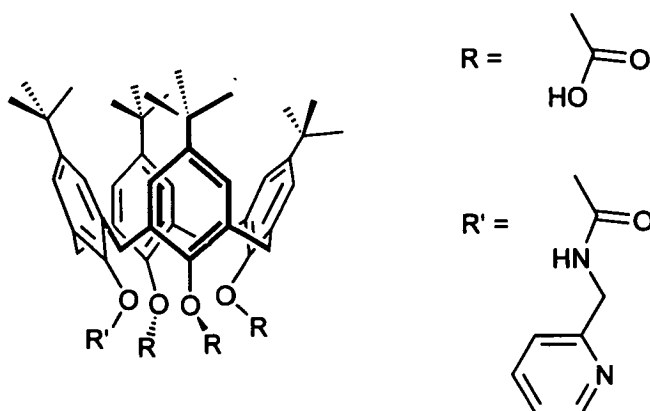
Complexes of functionalised calixarenes

Calixarenes are versatile ligands for metal complexation as they can be functionalised at the phenolic OH groups (lower rim) and at the *para* positions of the phenol rings (upper rim). This leads to selective and strong complexation and the ability to control the metal environment. The majority of studies with Ln^{3+} ions have involved the calix[4]arenes, such as the *p*-t-butylcalix[4]arene-tetra-acetamide (**8**). This ligand was shown to encapsulate Ln^{3+} ions, forming kinetically-inert complexes in water with good shielding from solvent molecules.[50] Upon excitation of the phenyl groups, energy transfer occurs to Eu^{3+} and Tb^{3+}. The luminescence quantum yield is high for the Tb^{3+} complex but

1000 times lower for the Eu^{3+} complex as a result of LMCT deactivation.

8
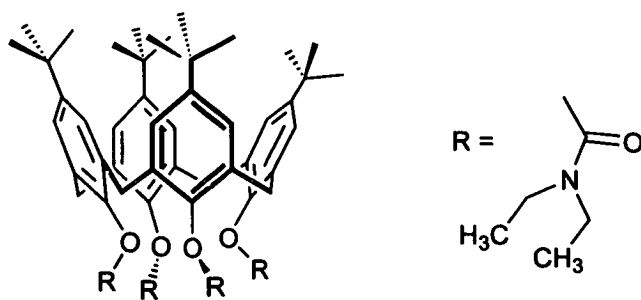
Subsequent studies concentrated on complexes in which the calix[4]arenes were functionalised with an appropriate sensitising group to increase the absorbance and modulate the energy transfer process. Calix[4]arenes functionalised with three amide groups and one sensitiser group on the lower rim, such as (**9**), demonstrated the possibility of energy transfer from the appended sensitiser to the encapsulated Ln^{3+} ion.[51] While high quantum yields are obtained in acetonitrile, the efficiencies are substantially reduced in methanolic solutions due to poor shielding from solvent molecules. Similar results were obtained with the neutral Ln^{3+} complexes of calix[4]arene triacids, such as (**10**).[52]

9

R = [structure]

R' = [structure]
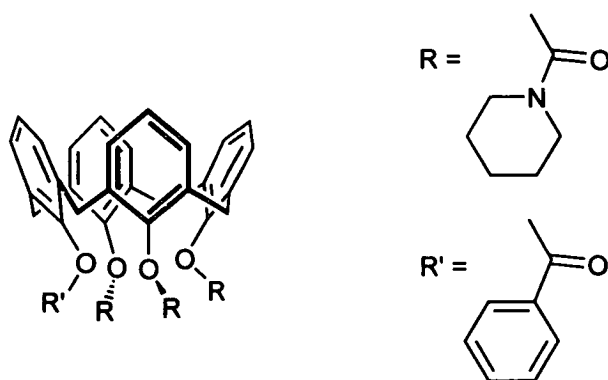
10

In a design progression analogous to that of the cryptates, calix[4]arenes functionalised with bipyridine groups have also been studied. Ligand (**11**) is a calix[4]arene with two (2,2'-bipyridin-6-yl)methyl groups.[53] The corresponding complexes have high absorption coefficients and reasonably good quantum yields. Recent developments include the synthesis of N-oxide derivatives (ligand **12**); the complexes of this ligand exhibit much better stability in coordinating solvents than those of **11**.[54]

11 R = [structure] **12** R = [structure]
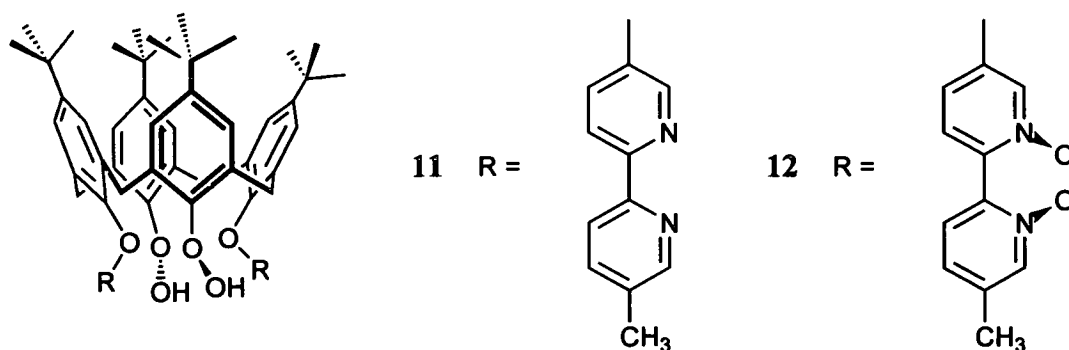
Cyclodextrin-functionalised macrocyclic complexes

In the complexes described so far, the sensitiser has been an integral part of the ligand system. An entirely different approach employs a cyclodextrin appended with a Ln^{3+} ion macrocycle. Cyclodextrins are ideally suited to form inclusion complexes with many hydrophobic species and it has been shown that in the presence of aromatic guests, an energy transfer process can take place from the guest to the appended Ln^{3+} ion. This

system functions, therefore, as a sensor for the appropriate aromatic hydrocarbon, since Ln^{3+} luminescence can only occur upon guest inclusion in the cyclodextrin. The initial system involved inclusion of benzene in complex **13** with the Eu^{3+} ion in an aza crown ether.[55] Work on this, and other systems, has led to a detailed mechanism for the energy transfer process and the synthesis of improved complexes. In complex **14**, for example, the ligand is a diethylenetriaminepentaacetic acid (DTPA) derivative, which provides overall neutrality of the complex, facilitating inclusion of the neutral guest.[56]
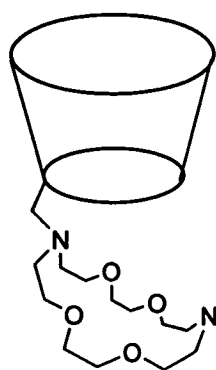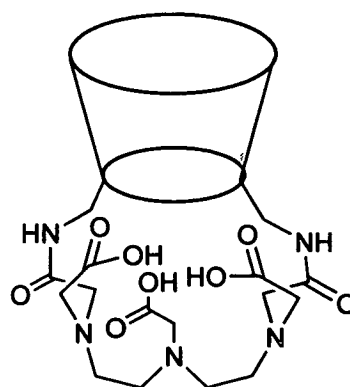
13   **14**

Acyclic polyaminocarboxylate complexes

The Ln^{3+} complexes of acyclic polyaminocarboxylate ligands are thermodynamically (and often kinetically) very stable and have been widely studied, particularly for application as MRI contrast reagents.[23] The ligands DTPA and triethylenetetraaminehexaacetic acid (TTHA) have been functionalised with the chromophore 7-amino-4-methyl-2(1*H*)-quinolinone (carbostyril 124) to give **15** and **16** respectively.[57] The luminescent properties of the Eu^{3+} and Tb^{3+} complexes (which were not isolated) in aqueous solution show the metal is well shielded from water and the sensitiser is not bound. Energy transfer does occur from this sensitiser, though quantum yields of luminescence are not reported.
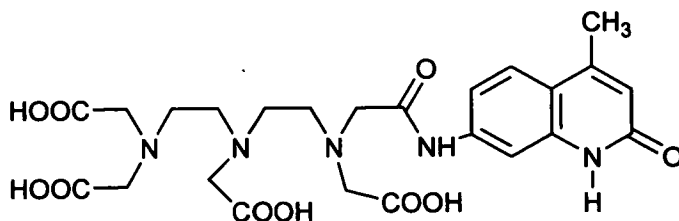
15
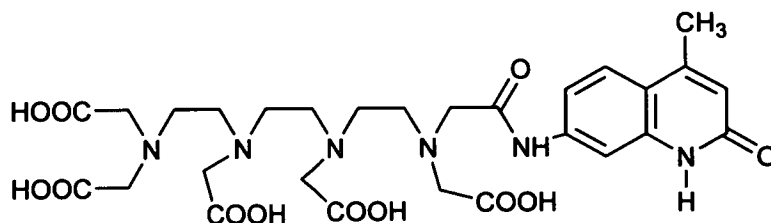
16

Complexes of polyazamacrocyclic ligands

Extensive work has been carried out on lanthanide complexes of functionalised derivatives of 1,4,7,10-tetraazacyclododecane (cyclen) such as ligands **17**, **18** and **19**.
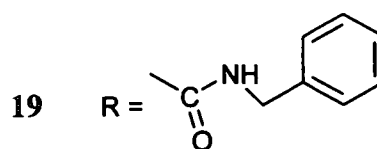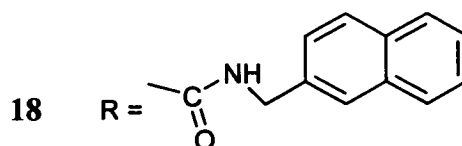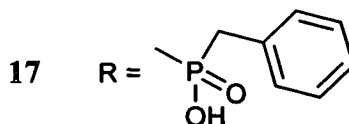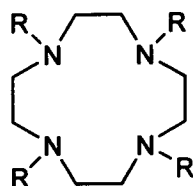
The lanthanide complexes have very high thermodynamic and kinetic stability, and this type of ligand allows a great deal of variation in the coordinating pendant arm (phosphinate, carboxylate and carboxamide substituents have all been used).[36] Ligand

17 forms stable complexes with Eu^{3+} and Tb^{3+} and excludes all water molecules from the inner coordination sphere.[58] This results in very long-lived species, especially the Tb^{3+} complex which has a lifetime in H_2O of 4.13 ms. Excitation of the phenyl groups sensitises the Ln^{3+} luminescence with high quantum yields for Tb^{3+}; the low quantum yield of the Eu^{3+} complex is probably due to LMCT states.

Polyamide ligands such as **18** have been prepared where one or more arms are replaced with naphthyl groups.[59] The Eu^{3+} complex has a low quantum yield, ascribed to a PET process. The calculated hydration state of 1.37 water molecules for this complex is of interest. This value is rather high considering only one water molecule is coordinated to a related, and more hydrophilic, complex.[60] This discrepancy has been accounted for by an N–H/N–D exchange process. Since N–H oscillators can quench the $^5D_0$ state of Eu^{3+}, exchange in D_2O would give a much larger difference in lifetimes than would be expected for one water molecule alone. As with many other Ln^{3+}-sensitiser systems, a photophysical analysis of the Tb^{3+} complex of **18** gives good evidence that the energy transfer process occurs via the ligand triplet state. Recent studies with related ligands, such as **19**, continue to illustrate the versatility of cyclen-based systems.[61]

Complexes of pyridine-based ligands

A number of complexes have been synthesised using pyridine-based building blocks, often with carboxylate or aminocarboxylate arms. A typical example is the terpyridine derivative, **20**, which forms very stable, 9-coordinate complexes with Ln^{3+} ions.[45] High quantum yields and long lifetimes are achieved for both Eu^{3+} and Tb^{3+} in aqueous solution. Investigation of a range of derivatives of **20** showed a very good correlation between ligand triplet state and luminescence quantum yield, and this information was used to successfully design some improved derivatives such as ligand **21**. This ligand combines high absorption and efficient energy transfer with the stability of a 9-coordinate chelate.[45]
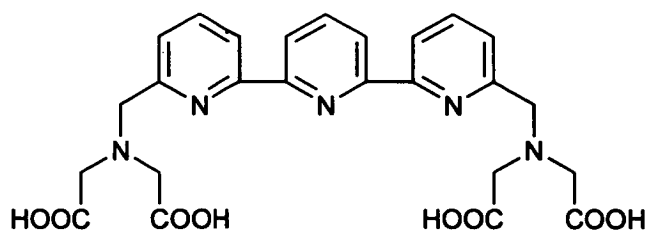
20
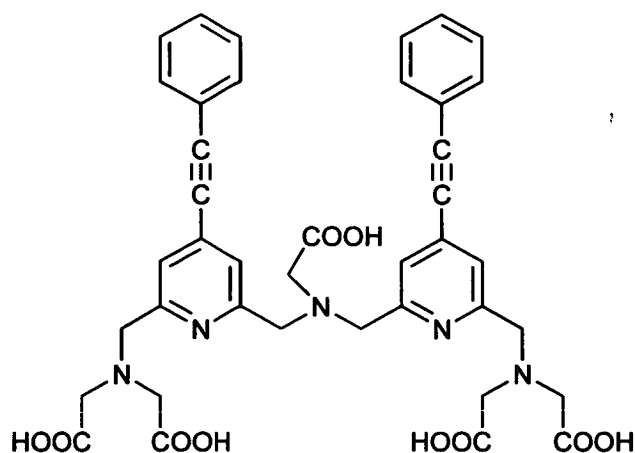
21

An interesting terpyridine derivative (**22**) incorporates two azacrown units and a terpyridyl diester unit. In the Eu^{3+} complex of this ligand, the lone pairs of the azacrown nitrogen participate in a PET process that serves to deactivate the excited state of the metal.[62] If the azacrown units bind K^+ ions, however, it becomes harder to remove electrons from the nitrogen lone pairs, thereby suppressing the PET process and increasing Eu^{3+} luminescence. Such a system can be viewed as a sensor for K^+ ions or as a luminescent switch, triggered by the presence of the alkali cation.
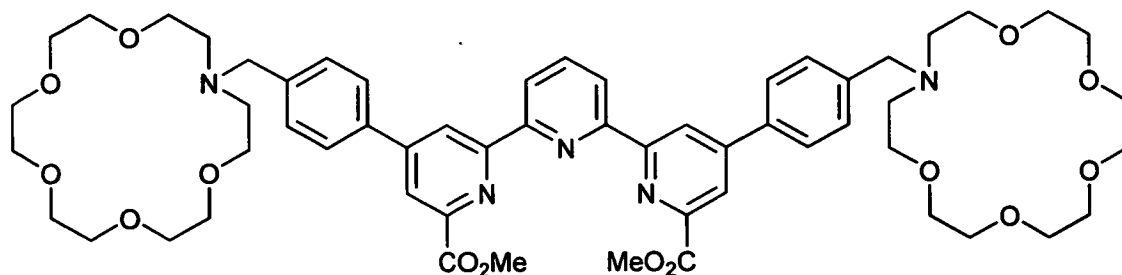
22

2.5 APPLICATIONS OF LUMINESCENT LANTHANIDE COMPLEXES

The intention of the preceding sections was to build a theoretical framework for the study of lanthanide complexes, so that their unique luminescent properties can be fully appreciated. In this section, the most significant of the current, practical applications of luminescent lanthanide complexes will be discussed.

2.5.1 Immunoassay

Immunoassay, the technique of using antibodies or antibody-related reagents to determine sample components, is the most important analytical method of *in vitro* diagnosis.[63] It has allowed the routine detection of substances such as drugs, hormones, viruses and proteins in body fluids. The high affinity and specificity of immunological interactions allows selective binding of trace amounts of an antigen to its corresponding antibody, even in the place of chemically similar substances. Having bound the analyte, a suitable means of detection of the immunocomplex is required. The technique of radioimmunoassay (RIA) was developed in 1959 and used antibodies labelled with radioactive isotopes, combining the selectivity of immunological interactions with the great sensitivity of detection of the radioactive signal.[64] Despite its success, this technique has a number of disadvantages including the health hazard associated with radioactive substances, the strict licensing and disposal regulations, and the limited shelf-life of radioactive reagents.

The search for non-radioactive labelling methods led to the development of luminescent labels. The first labels used were fluorescent organic dyes such as fluorescein but these fluoroimmunoassays (FIA) could not offer the sensitivity of radioimmunoassays due to interference from the intrinsic background fluorescence (fluorescence of serum components covers a broad wavelength region from 320 nm to 515 nm), instrumental light scattering and self-quenching.[63] Good alternatives to RIA were only realised after the use of lanthanide complexes as labels.

The main advantages of using lanthanide complexes as labels are as follows:

(a)   The energy transfer between ligand and Ln^{3+} ion can be very efficient.

(b)   The Stokes shift is large (>250 nm), allowing easy spectral discrimination between the Ln^{3+} emission and background fluorescence and scattering.

(c)   The lanthanide emission is very narrow which allows efficient collection using filters, and distinction of the specific emission from any background signal or from the emission of any other Ln^{3+} ion that may be employed.

(d)   The lifetime of the Ln^{3+} luminescence is long, which allows its temporal resolution from the short-lived background signal. This simply requires a time delay between excitation and detection to allow the fluorescence to decay before measuring the Ln^{3+} emission.

The use of lanthanide complexes in time-resolved fluoroimmunoassay, however, is not just a question of photophysics. Labelling an antibody with Ln^{3+} ions requires high complex stability (kinetic and thermodynamic) and biocompatability. Stable complexes that have appropriate functionality to allow covalent coupling to an antibody have been synthesised. Derivatives such as DTPA, TETA and DOTA have all been successfully employed.[65]

The assay process involves formation of the immunocomplex with the labelled antibody, followed by purification and signal detection steps. This is most commonly achieved by a heterogeneous assay such as the Dissociation Enhanced Lanthanide Fluorescence Immunoassay (DELFIA) system.[66] In this system an antibody is multiply labelled with covalently bound Eu^{3+} chelates to increase the overall sensitivity of the system. The antigen is immobilised on a solid support so that following formation of the immunocomplex, unreacted reagents can be simply washed away. To quantify the amount of bound antibody, the Eu^{3+} has to be dissociated from its relatively weakly luminescent chelate into an "enhancement solution" consisting of β-diketone ligands and trioctylphosphine oxide. This is achieved by lowering the pH with an acidic enhancement solution, thereby forming a Eu^{3+} complex with the β-diketone ligands. Trioctylphosphine oxide can coordinate Ln^{3+} ions and is thought to shield the metal from deactivating solvent molecules. The luminescence of the resultant Eu^{3+} species is detected by time-resolved techniques and often gives linear calibration curves over 2-4 orders of magnitude.

The use of lanthanide complexes as luminescent labels is now well established, and in addition to improving the speed and simplicity of immunoassays, they can provide previously unattainable levels of sensitivity.

2.5.2 Luminescent probes of biomolecular structure

Of the biologically important metal ions, many lack the useful spectroscopic or magnetic properties that would allow the structure of metal-containing systems to be probed. These "silent" ions can often be replaced by metal ions with useful properties, and an important example of this is the substitution of Ca^{2+} ions with Ln^{3+} ions.[67]

This substitution is facilitated by the similar ionic radii and coordination properties of Ca^{2+} and Ln^{3+} ions.[20] The major difference is, of course, the higher charge of the Ln^{3+} ions, which results in slower ligand exchange rates and higher formation constants with biomolecules. In fact, it is the size of the ions that is the most important factor since the

additional charge on the Ln^{3+} ion can be compensated for by charged groups or counterions.

Before initiating a spectroscopic study of Ln^{3+}-substituted species, however, it is necessary to be certain that the substitution has not caused significant structural alterations. In a number of cases, X-ray crystallography has demonstrated the isomorphous substitution of Ca^{2+} by Ln^{3+} ions.[28] In other instances, the retention of biological activity provided good evidence that substitution produced only a minor perturbation.[28] Having ascertained effective Ca^{2+} replacement by the luminescent probe, the structural information obtainable is dependent on the specific spectroscopic technique.

Characterisation of metal binding sites by excitation spectroscopy

As mentioned previously, the $^7F_0 \rightarrow {}^5D_0$ transition of Eu^{3+} consists of a single line for each unique metal environment. Excitation spectroscopy, monitoring this transition, can be used to characterise distinct binding sites in biomolecules, and by measuring the lifetimes of each species, information on the coordination environment is also obtained.[68]

Energy-transfer distance measurements

It is possible to measure the distances between different parts of a biomolecule by studying inter-site energy transfer. The energy transfer process normally occurs via the long-range dipole-dipole mechanism discussed previously, and it has become a standard spectroscopic technique to calculate donor and acceptor distances in the 10-70 Å region.[69] Applications involving Ln^{3+} ions include inter-metal energy transfer, such as Tb^{3+} to Nd^{3+} transfer in the protein thermolysin,[70] and energy transfer from intrinsic protein fluorophores to Ln^{3+} ions, such as tryptophan to Tb^{3+} transfer in the protein parvalbumin.[43]

2.5.3 Luminescent materials

Perhaps the key application of Ln^{3+} ions, and certainly the one which has had the largest impact on everyday life, is in phosphors: the term phosphor being a general term for a luminescent material.[71] The archetypal inorganic phosphor consists of a host lattice with luminescent ions doped into it. Two types of dopant may be distinguished: those that interact weakly with the lattice such as Ln^{3+} ions and those that interact strongly with the lattice such as Mn^{2+}.[72] The overall processes involved depend intimately on the nature of the lattice, the excitation source and the luminescent ion.[71]

Phosphors incorporating Ln^{3+} ions have been studied intensively, resulting in many useful materials and greatly extending the knowledge of the excited-state processes of Ln^{3+} ions. They are currently utilised in colour television screens, fluorescent tubes and X-ray detectors, to name just a few examples.[72]

The advantages of lanthanide-containing phosphors includes the narrow emission bands, the relative invariance of the spectral position of the emission bands and the specific emission wavelengths of some Ln^{3+} ions (Eu^{3+} and Tb^{3+} in particular), which allows high lumen efficiencies and efficient generation of white light. The specific requirements of the phosphor depend upon its use. For example, lumen efficiency is a quantity that relates the phosphor emission to the actual spectral sensitivity of the human eye, making it important for lighting applications. Similarly, to obtain white light with high lumen efficiency, a phosphor mixture must have very sharp emission lines in a region where eye sensitivity is reasonably high.[72]

Although the phosphors used in many of the classic applications such as colour television and fluorescent lamps are almost fully optimised,[73] there is a great deal of interest in new applications such as light-emitting diodes (LEDs) and electroluminescence (EL). As discussed next, it is in these areas that coordination compounds of lanthanides may play a role.

Applications of lanthanide complexes to light-emitting diodes

The possibility of generating white light by the direct conversion of electricity in LEDs with an efficiency superior to halogen lamps now exists.[72] One way to generate white light is to combine blue, green and red diodes. Another, cheaper, possibility is to produce a single white LED by combining a UV LED with blue, green and red emitting phosphors.[74] The phosphor material must have sufficient absorption and high quantum yield at the emission wavelength and also have narrow emission bands. There is, therefore, the possibility of employing phosphors in which Eu^{3+} and Tb^{3+} ions are complexed to ligands that absorb efficiently in the UV, providing these materials have sufficient stability.[74]

Applications of lanthanide complexes to electroluminescent materials

One of the most promising developments in flat screen technology is that of the electroluminescent display, and this is analogous to the LED in that it involves the direct conversion of electricity into light. Electroluminescent materials fall into two distinct categories: inorganic and organic. Although inorganic EL is reasonably well established, organic EL is a technology in its infancy, and it is here that coordination compounds of Ln^{3+} ions may prove useful.[72] Initial work on organic EL focussed on organic fluorescent dyes, demonstrating the generation of light by the direct recombination of charge carriers. The charge recombination step leads to the formation of excited singlet and triplet states in a 1:3 ratio. The excited triplet species are lost via non-radiative processes or, possibly, in side reactions. These drawbacks have prompted the use of complexes of Eu^{3+} and Tb^{3+} with organic sensitising ligands as emitters in organic EL materials.[75] Since triplet states can effectively sensitise the Ln^{3+} excited state, high efficiencies are possible. As with the LED phosphors, stability may be the deciding factor in potential applications.

2.6   REFERENCES

1.   J.-M. Lehn, *Angew. Chem. Int. Ed. Engl.*, 1988, **27**, 89.

2.   F. A. Cotton and G. Wilkinson, *Advanced Inorganic Chemistry*, Wiley-Interscience, New York, 5th edn., 1988, ch. 2.

3.   V. Balzani and F. Scandola, *Supramolecular Photochemistry*, Ellis Horwood, Chichester, 1991.

4.   J.-M. Lehn, *Supramolecular Chemistry*, VCH, Weinheim, 1995.

5.   V. Balzani and F. Scandola, *J. Chem. Educ.*, 1983, **60**, 814.

6.   N. J. Turro, *Modern Molecular Photochemistry*, The Benjamin / Cummings Publishing Company, California, 1978, ch. 9.

7.   A. Gilbert and J. Baggott, *Essentials of Molecular Photochemistry*, Blackwell Scientific Publications, Oxford, 1991.

8.   R. P. Wayne, *Principles and Applications of Photochemistry*, Oxford University Press, Oxford, 1991.

9.   A. P. de Silva, H. Q. N. Gunaratne, T. Gunnlaugsson, A. J. M. Huxley, C. P. McCoy, J. T. Rademacher and T. E. Rice, *Chem. Rev.*, 1997, **97**, 1515.

10. G. J. Meyer, *J. Chem. Educ.*, 1997, **74**, 652.

11. V. Balzani, M. Gómez-López, J. F. Stoddart, *Acc. Chem. Res.*, 1998, **31**, 405.

12. B. Alpha, R. Ballardini, V. Balzani, J.-M. Lehn, S. Perathoner and N. Sabbatini, *Photochem. Photobiol.*, 1990, **52**, 299.

13. S. Cotton, *Lanthanides and Actinides*, Macmillan Education, London, 1991, ch. 2.

14. R. D. Shannon, *Acta Crystallogr.*, 1976, **A32**, 751.

15. G. R. Choppin, in *Lanthanide Probes in Life, Chemical and Earth Sciences*, eds. J.-C. G. Bünzli and G. R. Chopin, Elsevier, Amsterdam, 1989, ch. 1.

16. H. G. Friedman, jun., G. R. Choppin and D. G. Feuerbacher, *J. Chem. Educ.*, 1964, **41**, 354.

17. L. Helm and A. E. Merbach, *Coord. Chem. Rev.*, 1999, **187**, 151.

18. G. R. Choppin, *J. Alloys Compd.*, 1997, **249**, 9.

19. G. R. Choppin, *J. Alloys Compd.*, 1997, **249**, 1.

20. J.-C. G. Bünzli, in *Lanthanide Probes in Life, Chemical and Earth Sciences*, eds.

J.-C. G. Bünzli and G. R. Chopin, Elsevier, Amsterdam, 1989, ch. 7.

21. G. Stein and E. Würzberg, *J. Chem. Phys.*, 1975, **62**, 208.

22. J. Reuben, in *Progress in Nuclear Magnetic Resonance Spectroscopy*, eds. J. W. Emsley, J. Feeney and L. H. Sutcliffe, Pergamon Press, 1973, **9**, 1.

23. Z. Guo and P. J. Sadler, *Angew. Chem. Int. Ed. Engl.*, 1999, **38**, 1512.

24. A. B. P. Lever, *Inorganic Electronic Spectroscopy*, Elsevier, 1968, ch. 6.

25. R. D. Peacock, *Struct. Bonding (Berlin)*, 1975, **22**, 83.

26. W. T. Carnall, in *Handbook on the Physics and Chemistry of Rare Earths*, eds. K.A. Gschneidner, Jr., and L. Eyring, North Holland, Amsterdam, 1979, **3**, ch. 24.

27. L. C. Thompson, in *Handbook on the Physics and Chemistry of Rare Earths*, eds. K.A. Gschneidner, Jr., and L. Eyring, North Holland, Amsterdam, 1979, **3**, ch. 25.

28. W. DeW. Horrocks, Jr., and D. R. Sudnick, *Acc. Chem. Res.*, 1981, **14**, 384.

29. J. L. Kropp and M. W. Windsor, *J. Chem. Phys.*, 1965, **42**, 1599.

30. J. L. Kropp and M. W. Windsor, *J. Chem. Phys.*, 1963, **39**, 2769.

31. Y. Haas and G. Stein, *J. Phys. Chem.*, 1971, **75**, 3677.

32. W. DeW. Horrocks, Jr., and D. R. Sudnick, *J. Am. Chem. Soc.*, 1979, **101**, 334.

33. D. Parker and J. A. G. Williams, *J. Chem. Soc., Dalton Trans.*, 1996, 3613.

34. V. L. Ermolaev and E. B. Sveshnikova, *Chem. Phys. Lett.*, 1973, **23**, 349.

35. A. Beeby, I. M. Clarkson, R. S. Dickins, S. Faulkner, D. Parker, L. Royle, A. S. de Sousa, J. A. G. Williams, and M. Woods, *J. Chem. Soc., Perkin Trans. 2*, 1999, 493.

36. D. Parker and J. A. G. Williams, *J. Chem. Soc., Perkin Trans. 2*, 1995, 1305.

37. S. P. Sinha, in *Systematics and the Properties of the Lanthanides*, ed. S. P. Sinha, D. Reidel Publishing Company, Dordrecht, 1983, ch. 10.

38. G. Blasse, *Struct. Bonding (Berlin)*, 1976, **26**, 43.

39. Y. Haas and G. Stein, *Chem. Phys. Lett.*, 1971, **8**, 366.

40. S. I. Weissman, *J. Chem. Phys.*, 1942, **10**, 214.

41. W. DeW. Horrocks, Jr., and M. Albin, in *Progress in Inorganic Chemistry*, ed. S. J. Lippard, Wiley, New York, 1984, **31**, 1.

42. G. E. Buono-Core, H. Li and B. Marciniak, *Coord. Chem. Rev.*, 1990, **99**, 55.

43. W. DeW. Horrocks, Jr., and W. E. Collier, *J. Am. Chem. Soc.*, 1981, **103**, 2856.

44. W. DeW. Horrocks, Jr., J. P. Bolender, W. D. Smith and R. M. Supkowski, *J. Am. Chem. Soc.*,1997, **119**, 5972.

45. M. Latva, H. Takalo, V.-M. Mukkala, C. Matachescu, J. C. Rodríguez-Ubis and J. Kankare, *J. Luminescence*, 1997, **75**, 149.

46. N. Sabbatini, M. Guardigli and J.-M. Lehn, *Coord. Chem. Rev.*, 1993, **123**, 201.

47. N. Sabbatini, S. Dellonte, M. Ciano, A. Bonazzi and V. Balzani, *Chem. Phys. Lett.*, 1984, **107**, 212.

48. S. Liu, L.-W. Yang, S. J. Rettig and C. Orvig, *Inorg. Chem.*, 1993, **32**, 2773.

49. N. Armaroli, V. Balzani, F. Barigelletti, M. D. Ward and J. A. McCleverty, *Chem. Phys. Lett.*, 1997, **276**, 435.

50. N. Sabbatini, M. Guardigli, A. Mecati, V. Balzani, R. Ungaro, E. Ghidini, A. Casnati and A. Pochini, *Chem. Commun.*, 1990, 878.

51. N. Sato and S. Shinkai, *J. Chem. Soc., Perkin Trans. 2*, 1993, 621.

52. D. M. Rudkevich, W. Verboom, E. van der Tol, C. J. van Staveren, F. M. Kaspersen, J. W. Verhoeven and D. N. Reinhoudt, *J. Chem. Soc., Perkin Trans. 2*, 1995, 131.

53. G. Ulrich, R. Ziessel, I. Manet, M. Guardigli, N. Sabbatini, F. Fraternali and G. Wipff, *Chem. Eur. J.*, 1997, **3**, 1815.

54. L. Prodi, S. Pivari, F. Bolletta, M. Hissler and R. Zeissel, *Eur. J. Inorg. Chem.*, 1998, 1959.

55. Z. Pikramenou and D. G. Nocera, *Inorg. Chem.*, 1992, **31**, 532.

56. C. M. Rudzinski, D. S. Engebretson, W. K. Hartmann and D. G. Nocera, *J. Phys. Chem. A*, 1998, **102**, 7442.

57. M. Li and P. R. Selvin, *J. Am. Chem. Soc.*,1995, **117**, 8132.

58. M. Murru, D. Parker, G. Williams and A. Beeby, *Chem. Commun.*, 1993, 1116.

59. A. Beeby, D. Parker and J. A. G. Williams, *J. Chem. Soc., Perkin Trans. 2*, 1996, 1565.

60. S. Amin, D. A. Voss, Jr., W. DeW. Horrocks, Jr., C. H. Lake, M. R. Churchill and J. R. Morrow, *Inorg. Chem.*, 1995, **34**, 3294.

61. G. Zucchi, R. Scopelliti, P.-A. Pittet, J.-C. G. Bünzli and R. D. Rogers, *J. Chem. Soc., Dalton Trans.*, 1999, 931.

62. A. P. de Silva, H. Q. N. Gunaratne, T. E. Rice and S. Stewart, *Chem. Commun.*, 1997, 1891.

63. A. Mayer and S. Neuenhofer, *Angew. Chem. Int. Ed. Engl.*, 1994, **33**, 1044.

64. R. S. Yalow and S. A. Berson, *J. Clin. Invest.*, 1959, **38**, 1996.

65. I. Hemillä, *J. Alloys Compd.*, 1995, **225**, 480.

66. E. P. Diamandis and T. K. Christopoulos, *Anal. Chem.*, 1990, **62**, 1449A.

67. F. S. Richardson, *Chem. Rev.*, 1982, **82**, 541.

68. J. Bruno, W. DeW. Horrocks, Jr., and R. J. Zauhar, *Biochemistry*, 1992, 31, 7016.

69. C. F. Meares and T. G. Wensel, *Acc. Chem. Res.*, 1984, **17**, 202.

70. A. P. Snyder, D. R. Sudnick, V. K. Arkle and W. DeW. Horrocks, Jr., *Biochemistry*, 1981, **20**, 3334.

71. G. Blasse, in *Handbook on the Physics and Chemistry of Rare Earths*, eds. K.A. Gschneidner, Jr., and L. Eyring, North Holland, Amsterdam, 1979, **4**, ch. 34.

72. T. Jüstel, H. Nikol and C. Ronda, *Angew. Chem. Int. Ed. Engl.*, 1998, **37**, 3084.

73. G. Blasse, *J. Alloys Compd.*, 1995, **225**, 529.

74. C. Ronda, T. Jüstel and H. Nikol, *J. Alloys Compd.*, 1998, **275-277**, 669.

75. J. Kido, K. Nagai, Y. Okamoto and T. Skotheim, *Chem. Lett.*, 1991, 1267.

Chapter Three

Imidodiphosphinate antenna ligands in lanthanide complexes

3.1   INTRODUCTION

The main requirements of antenna systems based on Ln^{3+} ions, for application as light-conversion molecular devices, are high ligand absorption coefficients, efficient ligand to metal energy transfer and minimal non-radiative deactivation of the excited state of the metal. As discussed in Chapter 2, the most common method employed to satisfy these design criteria is via the encapsulation of the Ln^{3+} ion by a polydentate ligand.

The aims of this work were to develop lanthanide complexes in which the metal ion is completely encapsulated by simple ligands, rather than highly designed and synthetically challenging polydentate ligands, and to control the formation of the desired species by straightforward complexation principles. These ligands must have strong binding units and bulky aromatic groups to play the dual role of antenna and solvent shield, forming a hydrophobic shell around the metal ion. Ideally, the binding and antenna domains should also be independent of each other. In this way the sensitising group can be optimised for a particular Ln^{3+} ion, without changing the binding characteristics of the ligand (unlike those ligands in which the antennas are also the binding units, *e.g.* polypyridines). Although remote light-harvesting units have previously been successfully employed to sensitise Ln^{3+} luminescence, this was restricted to more intricate macrocyclic supramolecular structures.[1-6]

The ligand tetraphenylimidodiphosphinate (tpip) was chosen as an ideal candidate to investigate this new approach. The two tautomeric structures of the parent compound tetraphenylimidodiphosphinic acid (Htpip) (**23**) are shown in Figure 3.1. In the crystalline state, it has been shown by X-ray crystallography[7] that Htpip exists in the tautomeric form (b) shown in Figure 3.1. These molecules are linked, in infinite chains, by OH···O hydrogen bonds making Htpip insoluble in most solvents. This hydrogen bonding can only be overcome in strongly protic or basic media.

$$\underset{\text{Ph}}{\overset{\text{Ph}}{\text{O=P}}} \overset{\overset{\text{H}}{|}}{\underset{}{\text{N}}} \underset{\text{Ph}}{\overset{\text{Ph}}{\text{P=O}}}$$

(a)

$$\underset{\text{Ph}}{\overset{\text{Ph}}{\text{O=P}}} - \text{N=} \underset{\text{Ph}}{\overset{\text{Ph}}{\text{P}}} - \text{OH}$$
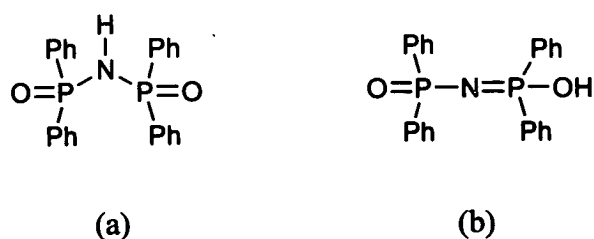
(b)

Figure 3.1 Structures of the tautomeric forms of Htpip

Tetraphenylimidodiphosphinate is one member of a series of imidodiphosphinate ligands that have the general formula $[R_2P(E)NP(E)R_2]^-$ (E = O, S, Se; R = Me, Ph, OPh).[8] Studies of the coordination chemistry of tpip with various metal ions show that the ligand adopts a bidentate binding mode.[9] Imidodiphosphinates can be viewed as inorganic analogues of β-diketonates, and it is well known that the latter form highly luminescent lanthanide complexes (see Chapter 2).

However, imidodiphosphinates have a number of distinct advantages over β-diketonates for use as antenna ligands. Firstly, the chelating unit of tpip does not contain any O–H, C–H or N–H bonds (which will minimise non-radiative deactivation of the excited states of bound Ln^{3+} ions) unlike β-diketonates, which contain a C–H bond in the binding unit. Secondly, four aromatic groups can be attached to an imidodiphosphinate ligand (two on each phosphorus atom), whereas only two aromatic groups can be attached to a β-diketonate (one on each carbonyl carbon), allowing the imidodiphosphinate to collect a greater amount of light for a given chromophoric substituent. Finally, the aromatic substituents of a β-diketonate are in conjugation with the chelate, thereby preventing their use as remote light-harvesting ligands.

Prior to this study, there were seven literature reports involving lanthanide complexes of tpip.[10-16] A combination of elemental analysis, thermogravimetric analysis, IR spectroscopy and single-crystal X-ray crystallography (for Ln = Dy, Pr) had demonstrated the formation of anhydrous $[Ln(tpip)_3]$ complexes in the solid state, with bidentate coordination of each tpip ligand.[10,11,15] On the basis of ^{1}H NMR and ^{31}P NMR spectroscopy and metal-centred electronic spectroscopy of a number of the complexes it

was concluded that the solid state and solution structures are similar.[10,11,15] The majority of this research was motivated by the search for new NMR shift reagents, and it was shown[12-16] that some of the complexes, in particular [Pr(tpip)₃] and [Gd(tpip)₃], are extremely useful for this purpose, especially as a result of their high stability in aqueous and acidic media (in contrast to lanthanide β-diketonates).[17] With the exception of the aforementioned study of the metal-centred absorptions of some of these complexes,[11] no photophysical investigations of Ln(tpip)₃ complexes have been reported.

3.2 LANTHANIDE COMPLEXES OF TPIP

3.2.1 Preparation and characterisation of Htpip

The ligand Htpip is prepared by the reaction of chlorodiphenylphosphine and hexamethyldisilazane followed by oxidation with H_2O_2 and recrystallisation from MeOH, according to a method reported in the literature (26% yield).[18] The FAB-MS of the ligand shows peaks at m/z 418 and 219, corresponding to $[M + H]^+$ and $[M\text{-}Ph_2PO + 2H]^+$ respectively. The ^1H NMR spectrum of the ligand in CDCl₃ shows two multiplets at δ 7.27-7.48 and 7.65-7.80 in a 3:2 ratio for the phenyl protons. Although the ^1H NMR of Htpip is unreported, the spectrum of the product matches that of a known sample of Htpip.[19] The ^{31}P NMR spectrum in CDCl₃ shows a single resonance at δ 21.0, corresponding to two equivalent phosphorus atoms.

The absorption spectrum of Htpip in EtOH (Figure 3.2) shows peaks with λ_{max}/nm (ε/dm³ mol⁻¹ cm⁻¹) of 261 (2060), 266 (2460) and 273 (1940), which is in agreement with a previously reported spectrum in EtOH that had peaks with λ_{max}/nm (ε/dm³ mol⁻¹ cm⁻¹) of 260 (1982), 266 (2479) and 273 (1982).[20] The absorption spectra of aromatic compounds are characterised by three sets of bands due to $\pi \rightarrow \pi^*$ transitions. Benzene, for example, has a band at 184 nm (ε = 60 000 dm³ mol⁻¹ cm⁻¹), a band called the *K*-band at 203.5 nm (ε = 7400 dm³ mol⁻¹ cm⁻¹) and a band called the *B*-band at 254 nm (ε = 204 dm³ mol⁻¹ cm⁻¹).[21] The *B*-band is forbidden, but gains intensity by the loss of symmetry caused by molecular vibration; therefore, it is characterised by its vibrational

fine structure. All of the bands for benzene are strongly affected by ring substitution. The position of the bands for benzene is particularly affected by substituents that cause an increase in the conjugation of the benzene π-system, thereby increasing the wavelength and intensity of the bands.

In the case of Htpip, it is particularly important to assess the effect of any conjugation as the ligand was chosen because the aromatic groups are distinct electronically from the binding unit. It can be seen in Figure 3.1 that the tautomeric forms (a) and (b) resemble the keto and enol forms respectively of β-diketones. It is well known that the aromatic substituents are in conjugation with the chelate ring in the enol form of β-diketones.[22]
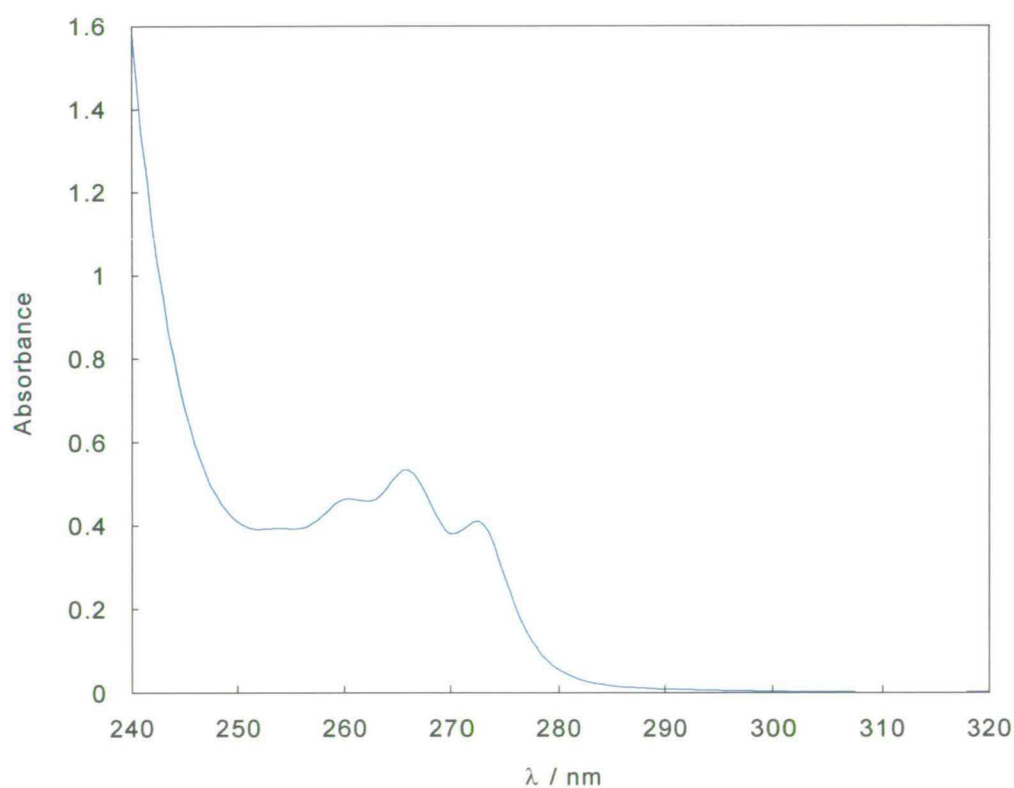

Figure 3.2 Absorption spectrum of Htpip (2×10^{-4} mol dm^{-3}) in EtOH

The structured band centred at 266 nm for the Htpip sample can be assigned as the *B*-band of the phenyl groups. As noted previously,[20] the observed absorption maximum suggests that this band is due to a phosphorus-substituted benzene in which there is no

conjugation of the phenyl groups with –P=N– in the binding unit. In support of this, diphenylphosphinic acid, [(C$_6$H$_5$)$_2$P(O)OH], in which there is obviously no –P=N– conjugation, shows the same spectral pattern as Htpip.[20] The *B*-band for Htpip is situated at the tail end of a far more intense band at shorter wavelength, which can be attributed to the *K*-band of the phenyl groups.

3.2.2 Preparation and characterisation of lanthanide complexes of tpip

The potassium salt of Htpip is prepared by a similar method to that reported for the potassium salt of the monothio analogue of tpip.[23] Htpip is dissolved in a methanolic KOH solution, the solvent is reduced and a white solid precipitated by the addition of diethyl ether. Recrystallisation from ethanol gives the desired product in reasonable yield (58%). The FAB-MS of the product shows an intense peak at *m/z* 456 corresponding to [*M* + H]$^+$. The ^{1}H NMR spectrum in D$_2$O shows two multiplets at δ 7.52-7.41 and 7.79-7.73 in a 3:2 ratio, which are assigned to the phenyl protons. The ^{31}P NMR spectrum in D$_2$O shows a singlet at δ 17.0, which is in agreement with the previously reported value of δ 16.4.[15]

Reaction of Ktpip with a lanthanide chloride was performed according to the reported literature procedure;[10] one equivalent of an aqueous solution of LnCl$_3$·6H$_2$O (Ln = Sm, Eu, Gd, Tb, Dy) was reacted with three equivalents of an aqueous solution of Ktpip, giving [Ln(tpip)$_3$] in 70-80% yield. These complexes are very soluble in solvents such as CHCl$_3$, CH$_2$Cl$_2$ and acetone, and are reasonably soluble in more polar solvents such as acetonitrile. The Eu^{3+}, Tb^{3+}, Sm^{3+} and Dy^{3+} ions were chosen for complexation studies with tpip because these ions are all strongly luminescent in the visible region (see Chapter 2).

Whilst the [Ln(tpip)$_3$] (Ln = Sm, Eu, Gd, Tb, Dy) complexes have been partially characterised previously, an important part of this work involved their full characterisation. All of the [Ln(tpip)$_3$] complexes studied have been characterised for the first time by mass spectrometry. In each case, FAB-MS confirms the complex formation, showing intense signals corresponding to [*M* + H]$^+$ and [*M*–tpip]$^+$.

The previously reported NMR spectroscopic data for these complexes were limited to a ^{31}P NMR spectrum for each complex and a ^1H NMR spectrum of the Eu^{3+} and Dy^{3+} complexes. A full NMR study has now been performed for these complexes and the ^1H, ^{13}C and ^{31}P NMR spectra obtained are summarised in Table 3.1. Previously reported data are indicated and are in good agreement with the new results. No NMR spectra were acquired for [Gd(tpip)₃] due to the severe paramagnetic broadening caused by the Gd^{3+} ion.

The NMR spectra of the complexes have broadly similar features, with the exception of the characteristic differences that arise from the magnetic properties of the different Ln^{3+} ions. As will be discussed, however, the complexes can also be divided into two groups based on their NMR spectra; Eu^{3+} and Sm^{3+} form one group and their spectra differ from those of the other group, consisting of Tb^{3+} and Dy^{3+}. The ^1H, ^{31}P and ^{13}C NMR spectra of [Eu(tpip)₃] and [Tb(tpip)₃] are shown in Figures A1-3 in Appendix I as representative examples of the two different kinds of spectra obtained.

The presence of a Ln^{3+} ion in a complex can have a profound effect on the appearance of the NMR spectra of the ligand nuclei. As mentioned, [Ln(tpip)₃] complexes were first studied as NMR shift reagents, whereby a weak "addition complex" can be formed between the lanthanide complex and an organic molecule, causing shifts in the resonances of the organic molecule and aiding resolution of its spectrum. In general, the chemical shifts arising from the interaction of ligand nuclei with a paramagnetic Ln^{3+} ion can be described in terms of two additive interactions: contact and pseudocontact.[24]

The pseudocontact shift is caused by a through-space interaction between the electron and nuclear magnetic dipoles. The contact shift arises from covalent bonding interactions, where there is transfer of unpaired electron density onto the ligand. This effect is important for nuclei that are very close to the metal ion. Theoretical and experimental studies of paramagnetic lanthanide complexes have allowed the relative magnitude and sign of the contact or pseudocontact shifts for Ln^{3+} ions in a given complex to be deduced.[24] The well-documented effect of Ln^{3+} ions on the NMR spectra of ligand nuclei will be used in a qualitative manner to aid characterisation of the

[Ln(tpip)₃] complexes.

Table 3.1 NMR data for [Ln(tpip)₃]

Complex[a]	δ (^{1}H)	δ (^{13}C)	δ (^{31}P)
Sm(tpip)₃	7.58-7.66 (24H, m, Ar)	131.1, 131.0, 130.9, 129.8,	25.1 (s)[b]
	7.19-7.26 (12H, m, Ar)	127.5, 127.4, 127.3	
	7.03-7.08 (24H, m, Ar)	[(s), (d), (d), (d)]	
Eu(tpip)₃	7.48-7.54 (24H, m, Ar)	129.8 (d, ^1J(P,C) 137 Hz)	37.7 (s)[d]
	7.21 (12H, t, Ar)	129.4 (s)	
	6.95-6.99 (24H, m, Ar)[c]	128.9 (d, J(P,C) 10 Hz)	
		127.0 (d, J(P,C) 13 Hz)	
Tb(tpip)₃	7.97 (24H, br s, Ar)	159.3 (br s, quart. C)	200.7 (s)[e]
	7.35 (12H, s, *p*-Ar)	134.5 (s)	
	6.28 (24H, s, Ar)	130.4 (s)	
		128.6 (s)	
Dy(tpip)₃	8.1 (24H, br s, Ar)	154 (br s, quart. C)	147.9 (s)[g]
	7.45 (12H, s, *p*-Ar)	132.6 (s)	
	6.57 (24H, s, Ar)[f]	130.2 (s)	
		128.3 (s)	

[a] CDCl₃ solvent at room temperature; [b] Reported[11] δ_P 24.2; [c] Reported[15] δ_H 7.0(m), 7.2(m), 7.5(m); [d] Reported[15] δ_P 38.1; [e] Reported[11] δ_P 195.0; [f] Reported[15] δ_H 7.4(m), 6.5(m); [g] Reported[15] δ_P 147.0

Each of the complexes gives a ^{1}H NMR spectrum with three signals in a 2:1:2 ratio. These signals are very sharp multiplets for the Sm^{3+} and Eu^{3+} complexes whereas for the Tb^{3+} and Dy^{3+} complexes, each of them is broadened into a singlet. For the Dy^{3+} and Tb^{3+} complexes the resonance at high frequency is especially broad, perhaps explaining why this resonance was not previously reported for [Dy(tpip)₃].[15] This signal can be assigned to the *ortho* protons. These are nearest to the paramagnetic Ln^{3+} ion. Therefore, they would be expected to be more strongly affected than the *meta* and *para*

protons, to which the other two signals can be attributed. Relative to Htpip, the *ortho* resonances for the Dy^{3+} and Tb^{3+} complexes are shifted to high frequency whereas the *meta* resonance is shifted to low frequency. This may reflect a predominantly contact interaction with the metal for the *ortho* protons and a predominantly pseudocontact interaction for the *meta* protons.

These assignments suggest that each of the phenyl rings is equivalent, and this is confirmed by the ^{13}C NMR spectra. For [Eu(tpip)$_3$], seven signals are observed. This corresponds to three doublets, due to coupling between P and each of the quaternary, *ortho* and *meta* carbons, and a singlet that can be assigned to the *para* carbon. Similarly, the seven signals in the ^{13}C NMR spectrum of the Sm^{3+} complex must also be due to ^{31}P-^{13}C couplings; three doublets and one singlet. In this case, however, the peaks are too close together to identify them further. Similar ^{31}P-^{13}C couplings have been reported for complexes of tpip with tin(IV) with ^1J (P,C) *ca.* 139 Hz, ^2J (P,C) *ca.* 11 Hz and ^3J (P,C) *ca.* 14 Hz.[25] Any fine structure is lost in the ^{13}C NMR spectra of the Dy^{3+} and Tb^{3+} complexes, as it was for the ^1H NMR spectrum; four broad peaks are observed due to the quaternary, *ortho*, *meta* and *para* resonances respectively. One peak, which is attributable to the quaternary carbon, is significantly shifted to higher frequency for the Tb^{3+} and Dy^{3+} complexes, and this agrees with the shifts for the *ortho* protons in the ^1H NMR spectra.

In the ^{31}P NMR spectrum of each of the complexes, a single resonance is obtained for all of the phosphorus atoms, and these are all shifted to higher frequency with respect to the value of δ 20.3 reported[11] for the diamagnetic analogue [Y(tpip)$_3$]. Broad ^{31}P signals are observed for the Tb^{3+} and Dy^{3+} complexes, with large shifts to higher frequency. For a predominant pseudocontact interaction, the ^{31}P signals of the Tb^{3+} and Dy^{3+} complexes would be expected to show large shifts in one direction, the Sm^{3+} complex would shift a small amount in the same direction and the Eu^{3+} complex would show shifts in the opposite direction.[26] If the contact interaction predominates, the order of ^{31}P shifts to higher frequency should be Tb > Dy > Eu > Sm, as is observed for the tpip complexes.

These results provide good evidence that there is only one species in solution, with a single ligand environment. The possibility that a dynamic equilibrium (that is fast on the NMR timescale) exists between free and complexed ligand was also examined. The ^{1}H and ^{31}P spectrum of a mixture of [Eu(tpip)$_3$] and [Tb(tpip)$_3$] shows only those signals observed for the original pure samples, which rules out the possibility of a fast exchange process. In support of this, the only changes that occur in the ^{31}P NMR spectrum of [Tb(tpip)$_3$] in acetone-d_6 on cooling down the solution from 297 K to 240 K, is a slight broadening and a shift from δ 206.7 to 269.9. Such temperature-dependent shifts are not uncommon for lanthanide complexes.[24] Similarly, the ^{31}P NMR spectrum of [Eu(tpip)$_3$] in CD$_2$Cl$_2$ at 297 K shows a singlet at δ 39.8, and at 260 K shows a singlet at δ 39.6. This further evidence confirms that the only species that exists in solution is [Ln(tpip)$_3$].

In order to investigate the structure of [Ln(tpip)$_3$] in the solid state, single-crystal X-ray diffraction studies of [Tb(tpip)$_3$] and [Eu(tpip)$_3$] were performed. The crystal structure of [Tb(tpip)$_3$], grown by slow evaporation from CHCl$_3$, is shown in Figure 3.3. The three anionic tpip ligands each adopt a bidentate binding mode giving a six-coordinated Tb^{3+} ion.

Coordination numbers of 3-5 are found in the lanthanide complexes of very bulky ligands, such as [N(SiMe$_3$)$_2$].[27] For complexes of bidentate ligands (mostly β-diketonates), the most common coordination numbers are 7-9. Six-coordinate Ln^{3+} ions are relatively unusual in the solid state for complexes of bidentate ligands, except when the ligand is very bulky. For example, 2,2,6,6-tetramethylheptane-3,5-dione forms anhydrous six-coordinate complexes with smaller Ln^{3+} ions (Ln = Ho-Lu), though they do rehydrate readily.[27] The absence of any coordinated water molecules in the [Tb(tpip)$_3$] structure, despite their presence in the crystal lattice, can be attributed to the steric bulk of the tpip ligands. The twelve phenyl groups form a hydrophobic shell around the central metal ion.
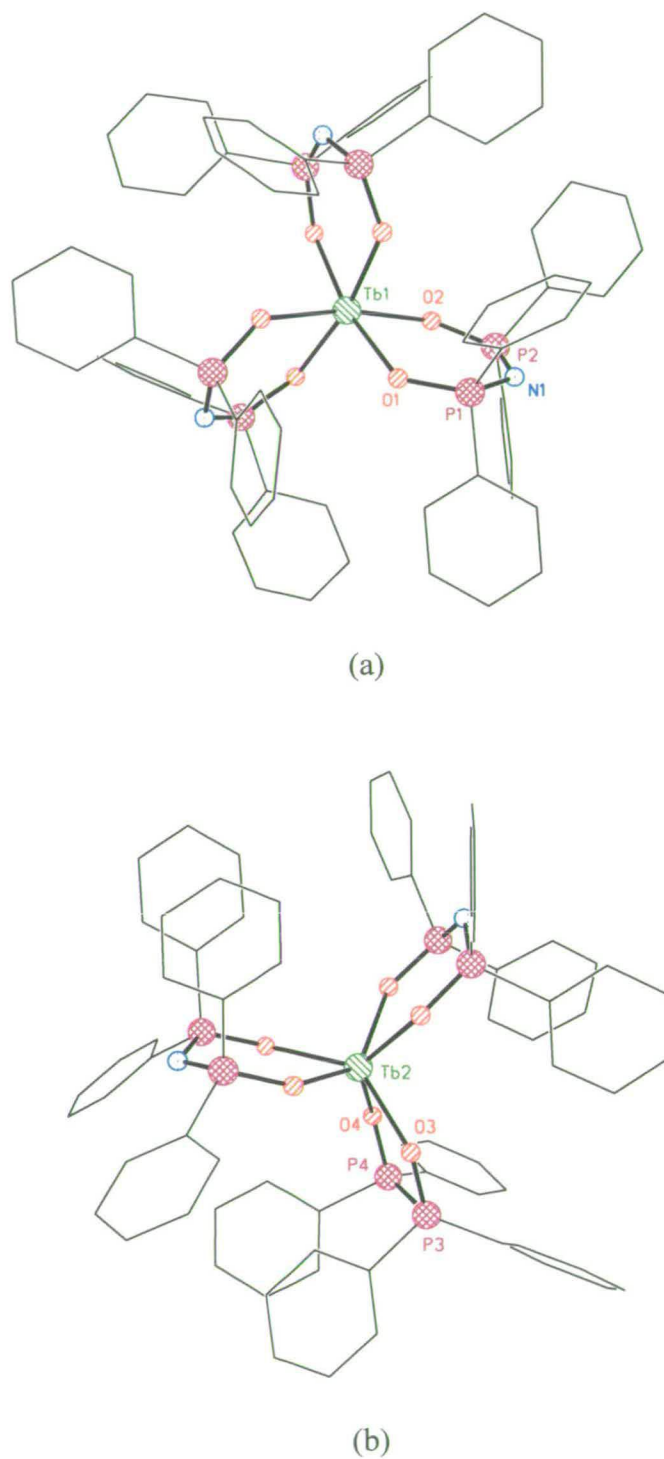
(a)

(b)

Figure 3.3 Molecular structure of Tb(tpip)$_3$ showing the atomic numbering scheme; selected bond distances (Å): (a) Tb(1)–O(1) 2.259(5), Tb(1)–O(2) 2.244(5), P(1)–O(1) 1.526(5), P(2)–O(2) 1.521(5), P(1)–N(1) 1.575(6), P(2)–N(1) 1.593(6); (b) Tb(2)–O(3) 2.272(5), Tb(2)–O(4) 2.295(5), P(3)–O(3) 1.519(5), P(4)–O(4) 1.508(5), P(3)–N(2) 1.599(6), P(4)–N(2) 1.582(6)

There are two structures adopted by [Tb(tpip)₃] in the unit cell of the crystal, which differ only in the symmetry around the Tb^{3+} ion. In both structures, the three tpip ligands are crystallographically equivalent to each other. In one instance, the complex adopts a distorted octahedral structure [(a) in Figure 3.3] whereas in the other instance, the symmetry is better described as trigonal prismatic [(b) in Figure 3.3]. While the structure of [Tb(tpip)₃] is notable for the lack of coordinated water molecules, closer inspection of (b) does reveal a short van der Waals contact between the Tb^{3+} ion and a water molecule situated at the top of the trigonal prism, with a Tb–O distance of 3.85 Å (expected van der Waals 4.08 Å). No such contact is observed in the octahedral structure.

In both structures, tpip displays a symmetrical chelate coordination to Tb^{3+}, with average Tb–O bond distances of 2.25 Å and 2.28 Å for (a) and (b) respectively. The average P–N bond distances are 1.58 Å and 1.59 Å for (a) and (b) respectively, whilst the average P–O bond distances are 1.52 Å and 1.51 Å for (a) and (b) respectively. These bond lengths can also be compared with those for the free ligand [(b) in Figure 3.1], which were 1.519 Å for P–O and 1.535 Å for P–N.[7] This indicates that, as in the free ligand, the five atoms of the imidodiphosphinate chelate are involved in substantial · π-delocalisation. For the free acid, the exceptionally short P–N bond is associated with the linear P–N–P arrangement.[7] The typical length of a P–N single bond, for comparison, is 1.75-1.80 Å.[28]

The crystal structure of [Eu(tpip)₃], grown by slow evaporation from $CHCl_3$, is shown in Figure 3.4. It is the same as the [Tb(tpip)₃] structure except that there are three structurally unique complexes in the unit cell; the symmetry is trigonal prismatic in two of these complexes (one of these is shown in Figure 3.4), and distorted octahedral in the other complex. As with [Tb(tpip)₃], the three ligands of a given complex are identical. The structure of [Eu(tpip)₃] shows an absence of any coordinated water molecules, but in the trigonal prismatic structures a short van der Waals contact exists between the Eu^{3+} ion and a water molecule, as was found in the [Tb(tpip)₃] structure.

The average Eu–O bond distance for the trigonal prismatic structure shown in Figure

3.4 is 2.29 Å with average P–N and P–O bond lengths of 1.59 and 1.52 Å respectively. These bond lengths are almost identical to those of the other two structures in the unit cell and are similar to those of the [Tb(tpip)$_3$] structure.
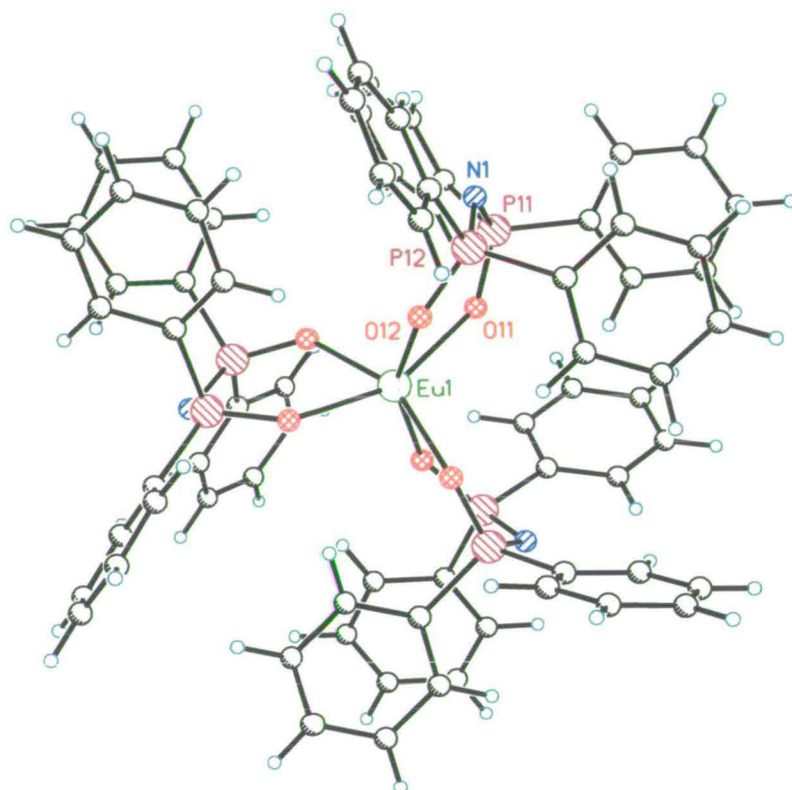

Figure 3.4 Molecular structure of Eu(tpip)$_3$, grown from CHCl$_3$, showing the atomic numbering scheme; selected bond distances (Å): Eu(1)–O(11) 2.280(3), Eu(1)–O(12) 2.308(3), P(11)–O(11) 1.518(3), P(12)–O(12) 1.519(3), P(11)–N(1) 1.593(4), P(12)–N(1) 1.590(4)

While the bond lengths show that a certain amount of π-delocalisation occurs in [Eu(tpip)$_3$], examination of this crystal structure shows that the six-membered ring formed by the imidodiphosphinate binding unit and Eu^{3+} is not planar, but instead adopts a puckered geometry. In fact, imidodiphosphinate ligands with the general formula [R$_2$P(E)NP(E)R$_2$]$^-$ (E = O, S, Se), seem to have no requirement for planarity associated with π-delocalisation.[8] This is in contrast to complexes of β-diketonates where the six-membered ring system is extensively π-delocalised and planar. It is well documented, however, that other ring systems that have delocalised P–N–P bonds, such

as the cyclic phosphazenes, also show a great deal of conformational flexibility.[28]

Whilst imidodiphosphinate ligands do appear to be structurally flexible, another possible explanation for the lack of planarity of the chelate rings is the presence of intramolecular interactions. The steric bulk of the tpip ligand means that there are a large number of possible phenyl-phenyl contacts, which will probably vary depending on factors such as the ionic radius of the Ln^{3+} ion. In support of the latter explanation, the structures for [Eu(tpip)$_3$] and [Tb(tpip)$_3$] show edge-to-face π-stacking interactions between phenyl groups of different tpip ligands (*e.g.* both structures of [Tb(tpip)$_3$] have C–H to centroid distances of *ca.* 3.0 Å).

The few crystal structures that have been reported for lanthanide complexes of tpip are detailed here, for comparison with the structures obtained in this work. The structures of [Pr(tpip)$_3$] and [Dy(tpip)$_3$] have been determined[15] and are similar to the Eu^{3+} and Tb^{3+} structures discussed previously, with no water molecules coordinated to the metal ion. The structures for both complexes are reported to be distorted octahedral, with average Pr–O and Dy–O distances of 2.36 and 2.26 Å respectively. Comparison of these bond lengths with the complexes of Eu (2.29 Å) and Tb (2.25 and 2.28 Å) shows a gradual decrease across the series, as would be expected on the basis of the lanthanide contraction.

The other relevant, reported crystal structures are those involving the formation of adducts of Ln(tpip)$_3$. For example, a crystal of Pr(tpip)$_3$(H$_2$O) was isolated from the reaction of ethanoic acid and [Pr(tpip)$_3$],[15] and a 1:1 adduct was formed between [La(tpip)$_3$] and ethyl acetate, which coordinates through the C=O of the ester group.[12] As both La^{3+} and Pr^{3+} are larger than the Ln^{3+} ions used in this study, it was thought that the formation of such adducts may become more restricted across the series.

Attempts were made to crystallise the Eu^{3+} complex from ethyl acetate to examine the possibility of adduct formation. Slow evaporation of an ethyl acetate solution yields crystals of [Eu(tpip)$_3$] with no coordinated solvent molecules, as shown in Figure 3.5. Half an equivalent of ethyl acetate is present in the unit cell. Only one structural type is

found in the unit cell and, in this case, the complex adopts a distorted octahedral structure. Unlike the structures of [Eu(tpip)$_3$] crystals grown from CHCl$_3$, the three ligands are not equivalent, though they are very similar. The average Eu–O bond is 2.30 Å, with average P–N and P–O bond lengths of 1.59 and 1.52 Å respectively, which are almost identical to the distances observed in the other [Eu(tpip)$_3$] structure. The absence of coordinated ethyl acetate in the structure in Figure 3.5 can probably be attributed to the size of the central metal ion.
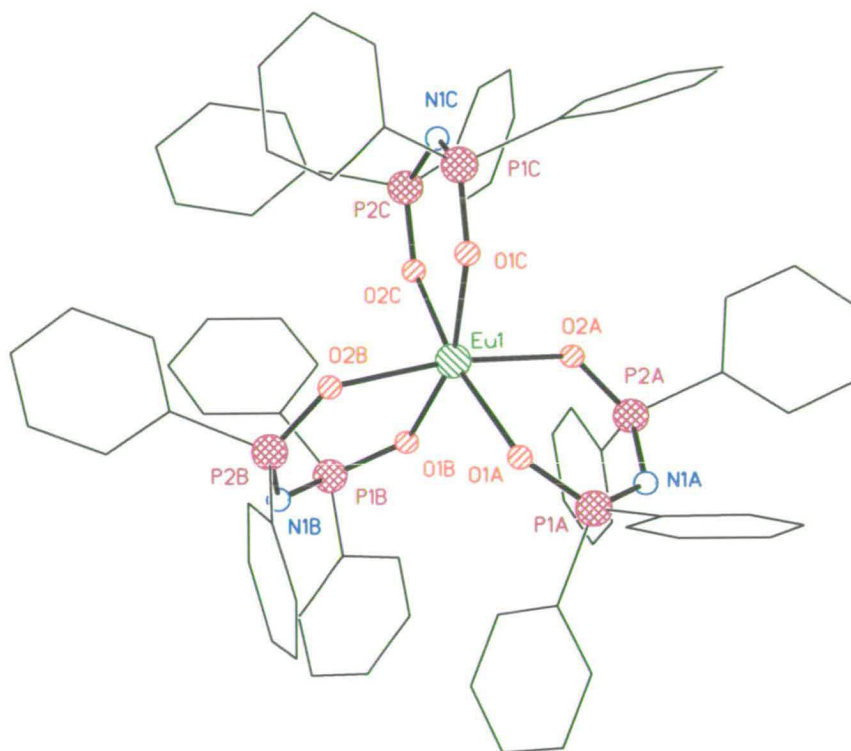
Figure 3.5 Molecular structure of Eu(tpip)$_3$ grown from ethyl acetate, showing the atomic numbering scheme; selected bond distances (Å): Eu(1)–O(1A) 2.291(2), Eu(1)–O(2A) 2.301(2), P(1A)–O(1A) 1.522(2), P(2A)–O(2A) 1.520(2), P(1A)–N(1A) 1.591(3), P(2A)–N(1A) 1.584(3), Eu(1)–O(1B) 2.315(2), Eu(1)–O(2B) 2.326(2), P(1B)–O(1B) 1.519(2), P(2B)–O(2B) 1.518(2), P(1B)–N(1B) 1.584(3), P(2B)–N(1B) 1.594(3), Eu(1)–O(1C) 2.283(2), Eu(1)–O(2C) 2.291(2), P(1C)–O(1C) 1.522(2), P(2C)–O(2C) 1.517(2), P(1C)–N(1C) 1.585(3), P(2C)–N(1C) 1.590(3)

3.2.3 Photophysical studies of lanthanide complexes of tpip

Ligand-centred levels

The absorption spectrum of [Eu(tpip)$_3$] in CH$_3$CN is shown in Figure 3.6; the inset is an expansion of the 250-320 nm region of this spectrum. This absorption spectrum has a structured band centred on 270 nm (λ_{max}/nm = 265 and 272) at the tail of an intense band at shorter wavelength; the absorption profile in CHCl$_3$ is identical, with the exception of a slight shift (*ca.* 1 nm) to longer wavelength (ε_{273} = 5000 dm^3 mol^{-1} cm^{-1}). Absorption spectra were measured in the concentration range 7 × 10^{-6} to 1 × 10^{-4} mol dm^{-3} in CHCl$_3$, and the Beer-Lambert law was obeyed throughout.

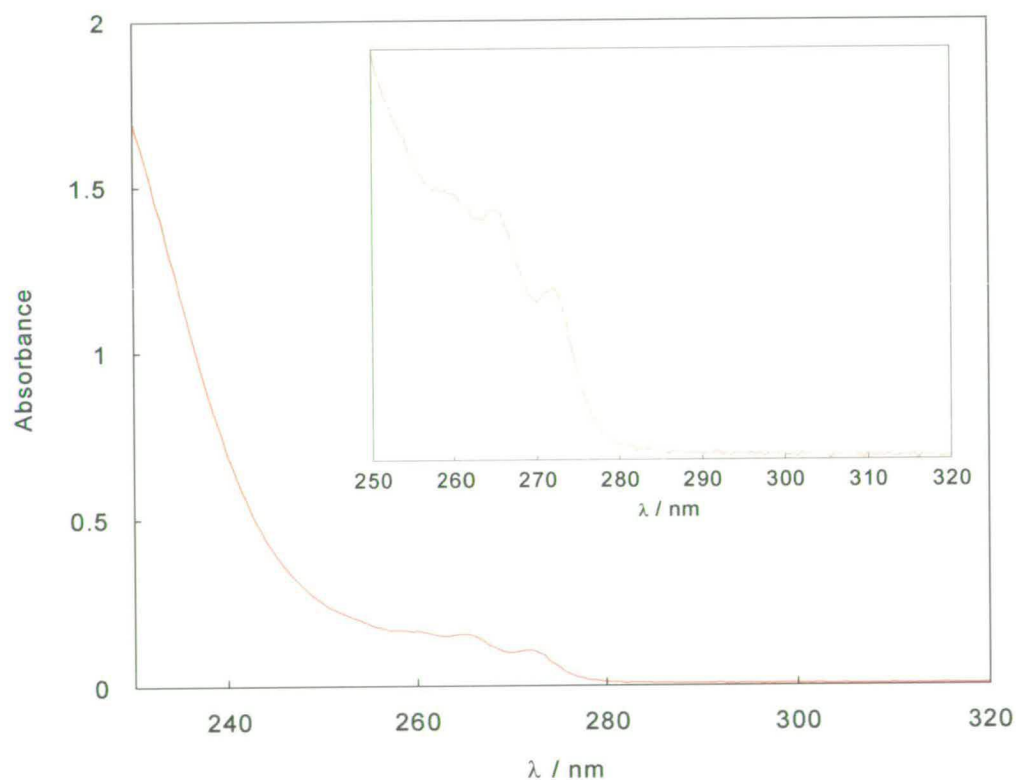**Figure 3.6** Absorption spectrum of [Eu(tpip)$_3$] (2 × 10^{-5} mol dm^{-3}) in CH$_3$CN; the inset shows an expanded section of the spectrum

The spectrum in Figure 3.6 is very similar to the absorption spectrum of Htpip in EtOH (Figure 3.2). The absorption spectra of the other [Ln(tpip)$_3$] complexes are identical to

that shown in Figure 3.6, confirming that they have the same complex formulation and that the bands observed are characteristic of the tpip ligand. Since deprotonation of the ligand and its subsequent binding to a tripositive metal ion has little effect on the absorption spectrum of the ligand, this confirms that the phosphorus-substituted phenyl groups of tpip can be considered as being remote from the imidodiphosphinate binding unit.

Metal-centred levels

The emission and excitation spectra of a CH_3CN solution of [Eu(tpip)$_3$] are shown in Figure 3.7. Excitation at 273 nm leads to strong red emission due to the characteristic $^5D_0 \rightarrow {}^7F_J$ (J = 0-4) transitions of Eu^{3+}. The dominant band in the corrected emission spectrum is the hypersensitive $^5D_0 \rightarrow {}^7F_2$ transition, which is split into two components (within the resolution of the instrument) that are centred on 610 and 620 nm. The excitation spectrum shows a structured band with peaks at 267 and 273 nm. This band resembles the absorption spectrum of [Eu(tpip)$_3$] very closely, which demonstrates that the Eu^{3+} emission is sensitised by an energy transfer process from the tpip ligand. The excitation profile also extends to wavelengths shorter than 250 nm, in agreement with the intense band observed at higher energy in the absorption spectrum of [Eu(tpip)$_3$].

Excitation and emission spectra for [Tb(tpip)$_3$], [Sm(tpip)$_3$] and [Dy(tpip)$_3$] in CH_3CN are shown in Figures 3.8, 3.9 and 3.10 respectively, and they show that the same sensitisation process discussed for [Eu(tpip)$_3$] also occurs in these complexes. Excitation at a wavelength corresponding to ligand-centred bands results in luminescence characteristic of the Ln^{3+} ion.

The excitation spectra for these complexes, monitoring the strongest *f-f* transition in each case, are essentially identical to that of [Eu(tpip)$_3$]. The only differences are minor changes in the band profile. Such deviations may arise from small variations in lamp output over the wavelength range examined or because of slightly different efficiencies of energy transfer from the ligand-centred levels to the excited states of the Ln^{3+} ion.
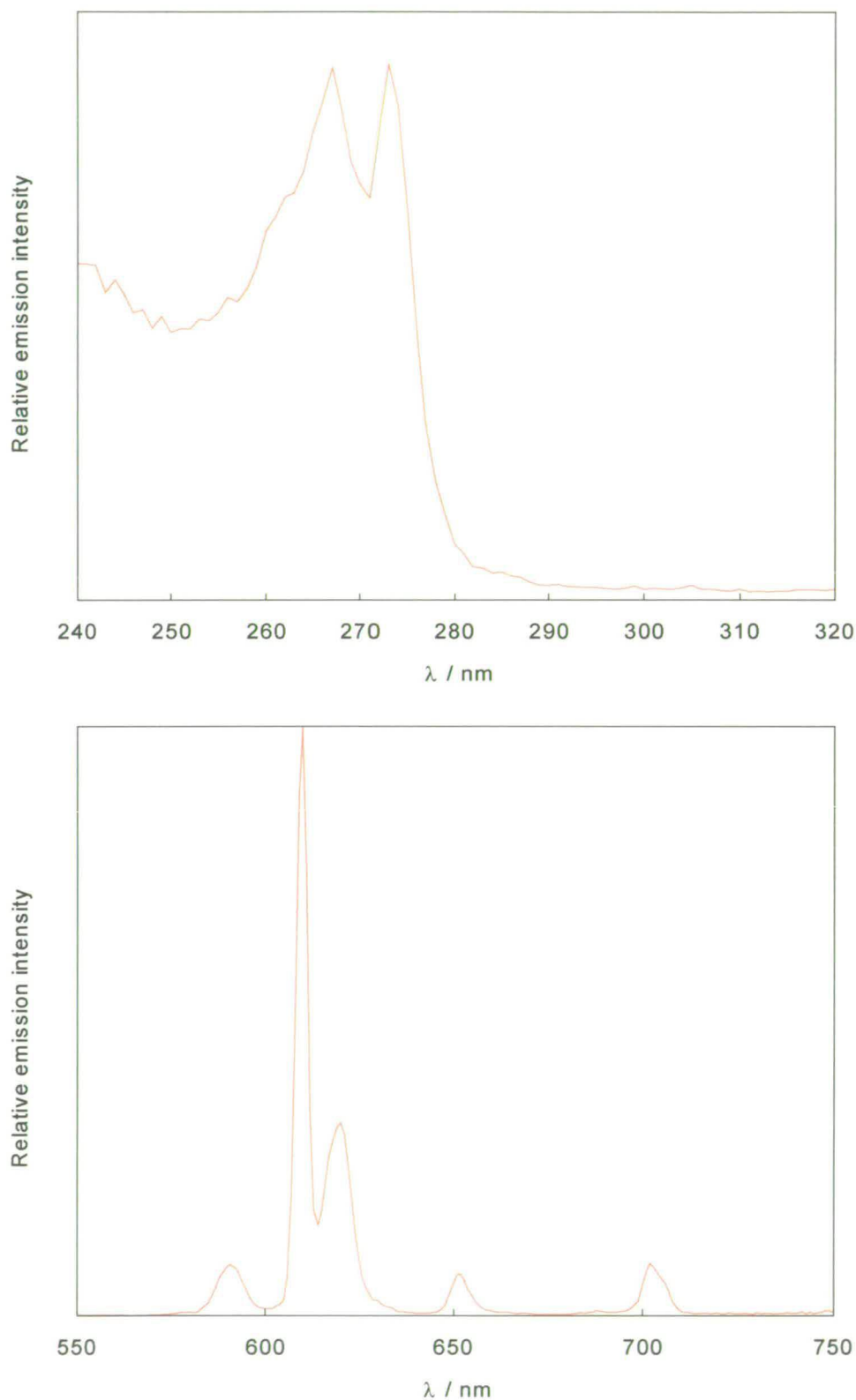
Figure 3.7 Top: excitation spectrum of [Eu(tpip)$_3$] (6×10^{-6} mol dm^{-3}) in CH$_3$CN, $\lambda_{em} = 610$ nm, 1 nm bandpass (ex.); Bottom: corrected emission spectrum of [Eu(tpip)$_3$] (2×10^{-5} mol dm^{-3}), in CH$_3$CN, $\lambda_{ex} = 273$ nm, 2 nm bandpass (em.)
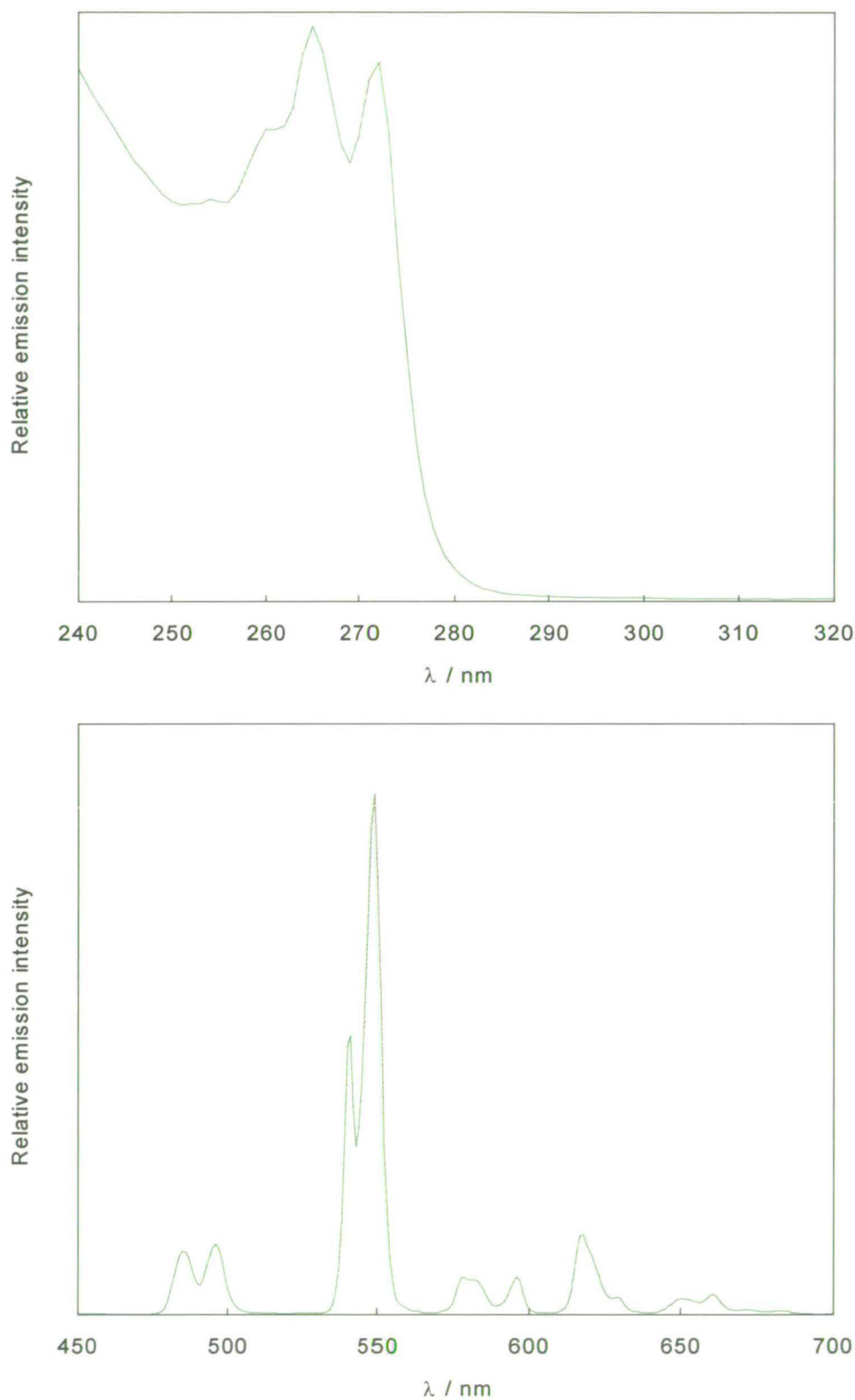
Figure 3.8 Top: excitation spectrum of [Tb(tpip)$_3$] (1 × 10^{-5} mol dm^{-3}) in CH$_3$CN, λ_{em} = 550 nm, 1 nm bandpass (ex.); Bottom: corrected emission spectrum of [Tb(tpip)$_3$] (2 × 10^{-5} mol dm^{-3}) in CH$_3$CN, λ_{ex} = 273 nm, 2 nm bandpass (em.)
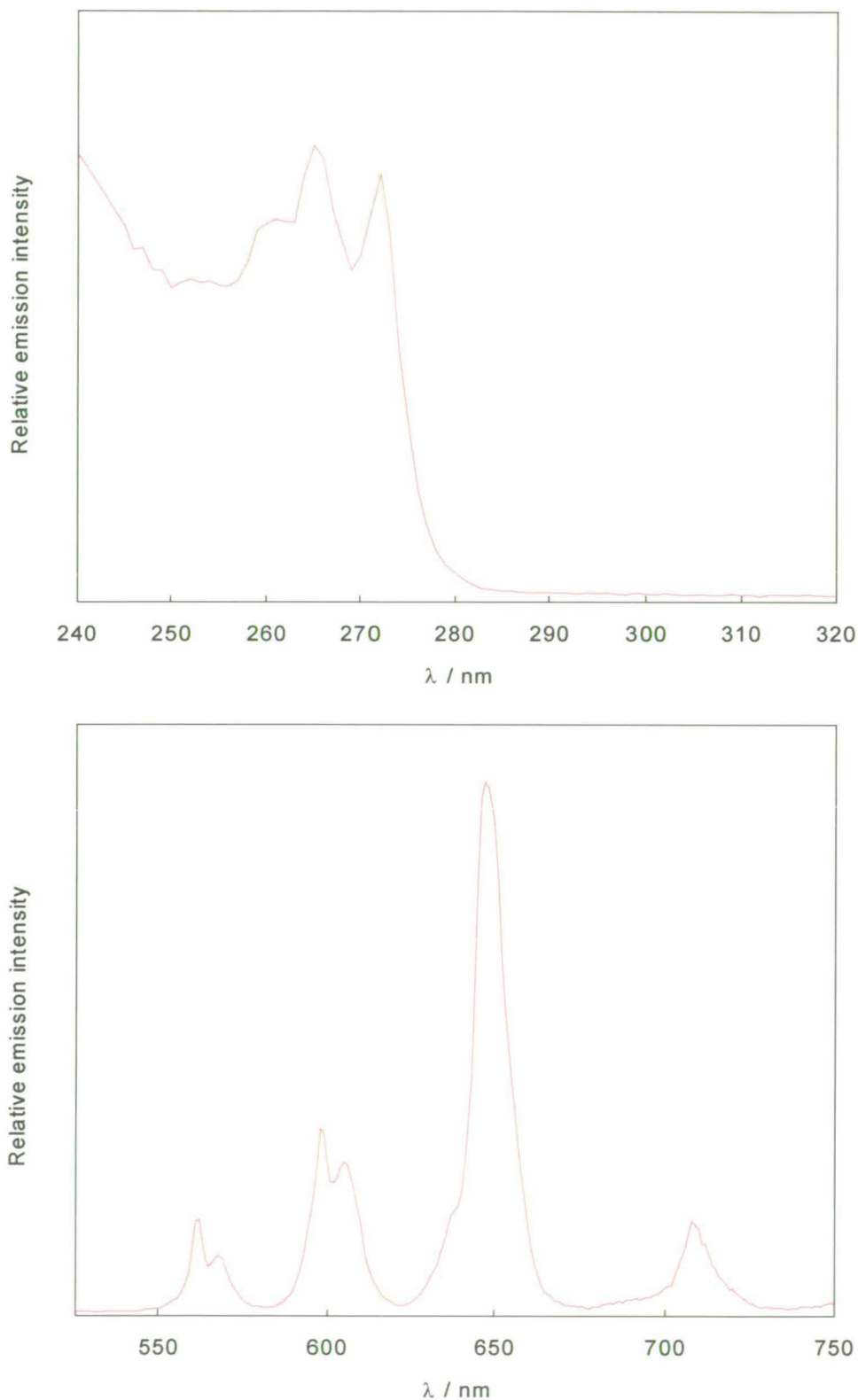
Figure 3.9 Top: excitation spectrum of $[Sm(tpip)_3]$ $(1 \times 10^{-5}$ mol dm$^{-3})$ in CH$_3$CN, $\lambda_{em} = 649$ nm, 1 nm bandpass (ex.); Bottom: corrected emission spectrum of $[Sm(tpip)_3]$ $(1 \times 10^{-5}$ mol dm$^{-3})$ in CH$_3$CN, $\lambda_{ex} = 270$ nm, 2 nm bandpass (em.)
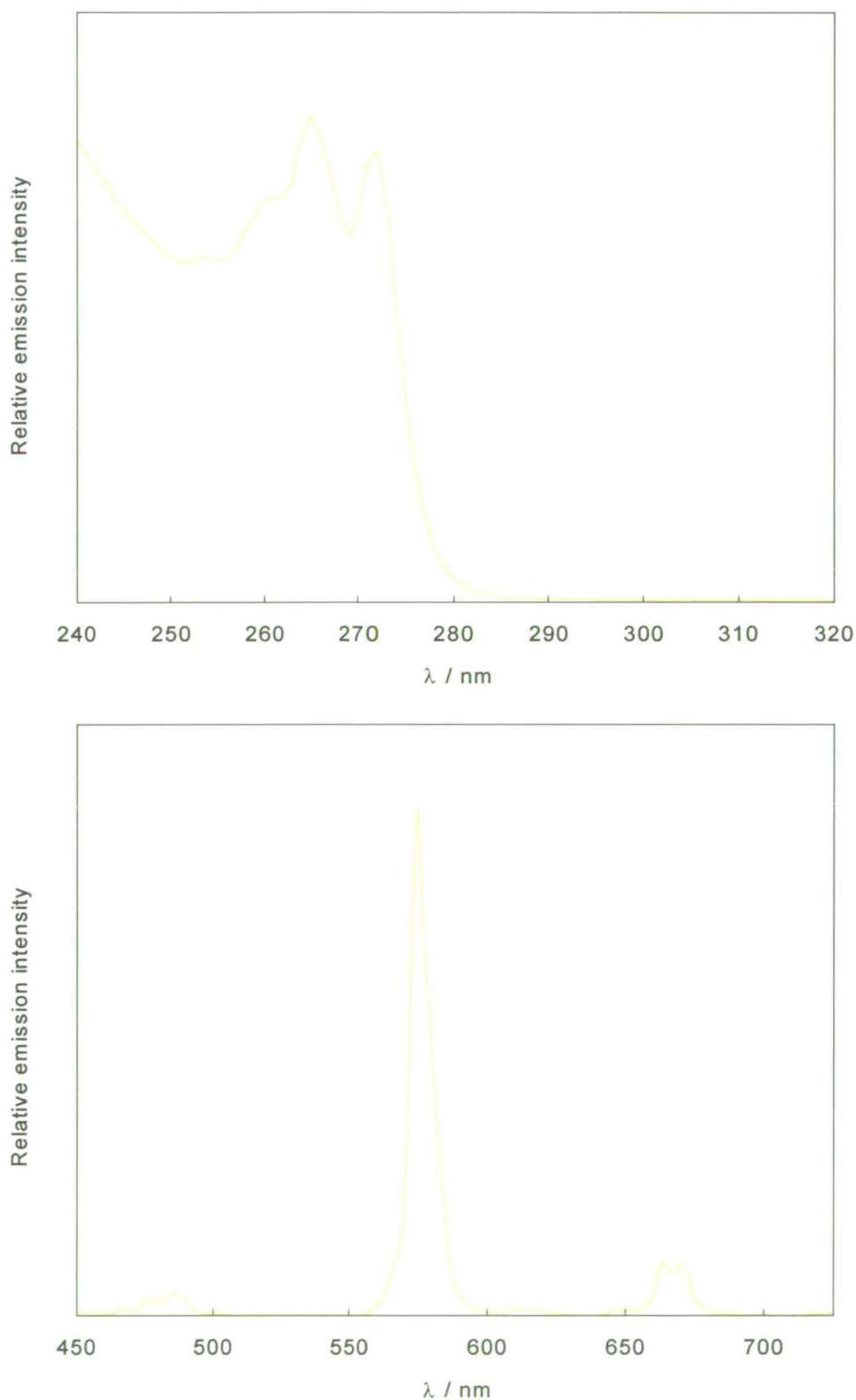
Figure 3.10 Top: excitation spectrum of [Dy(tpip)$_3$] in CH$_3$CN (1×10^{-5} mol dm^{-3}), λ_{em} = 575 nm, 1 nm bandpass (ex.); Bottom: corrected emission spectrum of [Dy(tpip)$_3$] (1×10^{-5} mol dm^{-3}) in CH$_3$CN, λ_{ex} = 270 nm, 2 nm bandpass (em.)

The emission spectrum of [Tb(tpip)$_3$] shows strong green emission due to the $^5D_4 \rightarrow ^7F_J$ (J = 2-6) transitions of Tb^{3+}, with an intense structured $^5D_4 \rightarrow ^7F_5$ band with peaks at 541 and 549 nm. Excitation of [Sm(tpip)$_3$] at 270 nm leads to the pink emission of Sm^{3+} due to $^4G_{5/2} \rightarrow ^6H_J$ (J = 5/2, 7/2, 9/2, 11/2) transitions; the most intense peak is the hypersensitive transition $^4G_{5/2} \rightarrow ^6H_{9/2}$ at 647 nm. Similarly, the sensitisation process in [Dy(tpip)$_3$] results in the typical yellow luminescence from Dy^{3+}, with the $^4F_{9/2} \rightarrow ^6H_J$ (J = 15/2, 13/2, 11/2) transitions observable. The latter spectrum is dominated by the hypersensitive $^4F_{9/2} \rightarrow ^6H_{13/2}$ transition at 575 nm.

In order to further assess the photophysical processes involved in the luminescence of [Ln(tpip)$_3$] (Ln = Eu, Tb, Sm, Dy), the complexes were studied by time-resolved spectroscopy. The measured luminescence lifetimes, following excitation into ligand-centred bands (λ_{ex} = 266 nm), are displayed in Table 3.2. All of the luminescence lifetimes measured for these complexes are monoexponential, as expected for one discrete [Ln(tpip)$_3$] solution species.

Table 3.2 Luminescence lifetimes of the Eu^{3+} ($^5D_0$), Tb^{3+} ($^5D_4$), Sm^{3+} ($^4G_{5/2}$) and Dy^{3+} ($^4F_{9/2}$) levels in [Ln(tpip)$_3$] (Ln = Eu, Tb, Sm, Dy) (λ_{ex} = 266 nm)

Ln	Conditions[a]	τ / ms
Eu	solid (powder)	2.2
	dry CH$_3$CN solution	1.8
	dry CH$_3$CN solution + H$_2$O[b]	0.82
Tb	solid (powder)	3.1
	dry CH$_3$CN solution	2.8
	dry CH$_3$CN solution + H$_2$O[b]	1.4
Sm	dry CH$_3$CN solution	0.15
	dry CH$_3$CN solution + H$_2$O[b]	0.06
Dy	dry CH$_3$CN solution	0.18
	dry CH$_3$CN solution + H$_2$O[b]	0.12

[a] Lifetimes measured at room temperature; concentration of CH$_3$CN solutions = 1 × 10^{-4} mol dm^{-3}, except for [Dy(tpip)$_3$] with concentration = 1 × 10^{-5} mol dm^{-3}, [b] [H$_2$O] = 10 mol dm^{-3}

The lifetimes of [Eu(tpip)$_3$] and [Tb(tpip)$_3$] in the solid state are 2.2 and 3.1 ms respectively. These very long lifetimes are characteristic of an absence of deactivating, non-radiative pathways.[29] This is in agreement with the lack of coordinated water molecules in the single-crystal X-ray structures of [Eu(tpip)$_3$] and [Tb(tpip)$_3$] reported in this work, and the analyses, IR spectroscopy and thermogravimetric analyses reported elsewhere.[10,11] The tpip ligand was partly chosen because of the absence of any potentially quenching oscillators (*e.g.* N–H and C–H) in the imidodiphosphinate binding unit, and the measured lifetimes suggest that the role of any other oscillators is minimal. The results for the tpip complexes compare favourably with the reported luminescence lifetimes (at 298 K) of other solid-state samples that have no coordinated H$_2$O molecules. For example [EuCl$_2$(D$_2$O)$_6$]Cl and [TbCl$_2$(D$_2$O)$_6$]Cl have lifetimes of 1.64 and 2.38 ms respectively,[29] while Na[Eu(EDTA)(D$_2$O)$_3$]·5D$_2$O and Na[Tb(EDTA)(D$_2$O)$_3$]·5D$_2$O have lifetimes of 1.79 and 2.27 ms for respectively.[29]

In dry acetonitrile, [Eu(tpip)$_3$] and [Tb(tpip)$_3$] also exhibit long-lived luminescence, with lifetimes of 1.8 and 2.8 ms respectively. These values are only slightly reduced in comparison with the solid state results, confirming that no water molecules are complexed in the first coordination sphere of the Ln^{3+} ion. The lifetimes of [Sm(tpip)$_3$] and [Dy(tpip)$_3$] in dry CH$_3$CN are 0.15 and 0.18 ms respectively. While these are short in comparison with the isostructural Eu^{3+} and Tb^{3+} complexes, relative to other Sm^{3+} and Dy^{3+} complexes they are quite long. For comparison, the lifetimes of perchlorate salts of Sm^{3+} and Dy^{3+} in D$_2$O are reported [30] to be 0.054 and 0.038 ms, while more recently an *m*-terphenyl-based, tricarboxylate ligand was used to form 1:1 complexes with Sm^{3+} and Dy^{3+}, with lifetimes in CD$_3$OD reported to be 0.090 and 0.079 ms respectively.[31]

Upon addition of H$_2$O (10 mol dm^{-3}) to the dry CH$_3$CN solutions of [Eu(tpip)$_3$] and [Tb(tpip)$_3$], there is a significant reduction in the lifetimes (54 and 50% decrease for Eu^{3+} (^{5}D$_0$) and Tb^{3+} (^{5}D$_4$) lifetimes respectively, as shown in Table 3.2). The [Sm(tpip)$_3$] and [Dy(tpip)$_3$] lifetimes decrease to 0.06 and 0.12 ms respectively upon addition of H$_2$O (10 mol dm^{-3}) to the dry CH$_3$CN solutions. This corresponds to an increase in the decay rate of 0.64, 0.35, *ca.* 10 and *ca.* 2 ms^{-1} for the Eu^{3+}, Tb^{3+}, Sm^{3+}

and Dy^{3+} complexes respectively. Such a large lifetime decrease upon adding water is consistent with the coordination of water molecules to the Ln^{3+} ion.

The ability of [Tb(tpip)$_3$] and [Eu(tpip)$_3$] to coordinate a water molecule in solution can be related to the crystal structures of these species in Figures 3.3 and 3.4, in which the trigonal prismatic structures were found to have a short van der Waals contact between the Ln^{3+} ion and a water molecule. In solution, where there is more conformational freedom, it is possible that such a contact can proceed to inner-sphere coordination.

The observed lifetimes differ for each Ln^{3+} complex; this can be explained by considering the energy gap between the luminescent state and the highest J level of the ground state. This energy gap is similar for Sm^{3+} and Dy^{3+} and amounts to *ca.* 7500 cm^{-1} and 7800 cm^{-1} respectively, whereas for Eu^{3+} and Tb^{3+} the gap is larger at 12, 300 cm^{-1} and 14, 800 cm^{-1} respectively.[32] For Tb^{3+} and Eu^{3+}, the energy gap is large enough that, to a first approximation, only the high-energy O−H oscillators contribute to vibrational quenching. The smaller gap for Sm^{3+} and Dy^{3+} results in lower frequency vibrations causing significant deactivation.[30] This explains why the lifetimes of the Sm^{3+} and Dy^{3+} complexes are much shorter than those of the Tb^{3+} and Eu^{3+} complexes in dry CH_3CN.

The decay rate of the Eu^{3+} complex is increased to a greater extent than that of the Tb^{3+} complex upon addition of H_2O to the dry CH_3CN solution, and this effect is well documented. Similarly, Sm^{3+} and Dy^{3+} luminescence is more efficiently quenched by addition of H_2O because the energy gap is bridged by lower vibrational overtones of H_2O.[30] The decay rate of Sm^{3+} luminescence is increased far more than that of the Dy^{3+}, despite the similar energy gap for these two ions. This may be due to the larger Sm^{3+} ion accommodating an additional deactivating water molecule compared with the Dy^{3+} ion.

To estimate the number of water molecules coordinated to Eu^{3+} or Tb^{3+} in aqueous solutions, an empirical relation (equation 2.7) can be used.[33] This equation can also be used with CH_3CN as the solvent by measuring the lifetimes following the addition of equal amounts of H_2O or D_2O to the CH_3CN solution.[34] As the lifetime upon adding

D_2O should not be greatly different to that in the anhydrous solvent alone, it is possible to estimate the hydration state of the Ln^{3+} ion using equation 3.1:

$$q = A(k_{H_2O} - k_{CH_3CN}) \qquad (3.1)$$

where q is the number of water molecules in the primary coordination sphere, A is the proportionality constant used in equation 2.7 ($A_{Eu} = 1.05$, $A_{Tb} = 4.2$), k_{H_2O} is the observed decay rate in aqueous CH_3CN, k_{CH_3CN} is the observed decay rate in dry CH_3CN. This approach has been used recently with Eu^{3+} and Tb^{3+} complexes of a ligand derived from 1,4,7,10-tetraazacyclododecane.[35] Applying equation 3.1 to the values in Table 3.2 gives $q = 0.71$ and 1.5 for [Eu(tpip)₃] and [Tb(tpip)₃] respectively in aqueous CH_3CN, confirming the inner-sphere coordination of water molecules to the Ln^{3+} ion in these complexes.

Equation 2.7 can be modified to take into account the contribution of outer-sphere water molecules (equation 2.8).[36] If the same corrections are applied to equation 3.1, the q-values obtained are 0.47 and 1.5 for Eu^{3+} and Tb^{3+} respectively. The corrected q-value for Eu^{3+} is slightly reduced, while there is no change for the Tb^{3+} value. However, equation 2.8 was derived empirically, based on lifetimes measured for charged, hydrophilic complexes, which may make it less reliable for the neutral, hydrophobic tpip complexes. Based on the q-values obtained from equation 3.1, there is probably one water molecule coordinated to the metal ion of [Eu(tpip)₃] and [Tb(tpip)₃]. Although the q-value is much larger in the Tb^{3+} complex, it seems unlikely that there are more water molecules coordinated to the smaller Tb^{3+} ion, especially in view of the crystal structure of [Tb(tpip)₃].

These studies in aqueous CH_3CN are notable for a number of other reasons. For applications in biological, and therefore aqueous, systems it is important to consider the charge of the complex. It is an advantage to have neutral complexes, like [Ln(tpip)₃], as it minimises possible aspecific binding.[29] While this may seem irrelevant because [Ln(tpip)₃] is prepared by precipitation from water, it may be possible to functionalise the ligand to give the complex higher aqueous solubility. The stability of the complex

towards hydrolysis is very promising in this respect. Many lanthanide complexes that are very luminescent in organic solvents are severely prone to hydrolysis. Nitrogen-donor ligands, such as benzimidazole-based ligands [37] or bpy-based ligands such as the podand **6** [38] demonstrate particular sensitivity to water. The main exceptions to this are cryptate complexes, which are extremely stable.[38]

In addition to luminescence decay measurements of [Eu(tpip)$_3$], the growth of Eu (^{5}D$_0$) luminescence has been examined and found to increase exponentially, with a rise time of 7.5 μs (Figure 3.11). This initial rise, before the luminescence decay, can be attributed to the non-radiative decay from the upper ^{5}D$_1$ level to the ^{5}D$_0$ level, from which emission subsequently occurs. The population of the ^{5}D$_1$ level following an energy transfer process from suitably matched ligand excited states has been noted on numerous occasions. Many europium β-diketonates, for example, have rise times in the region of 2-3 μs, in agreement with the value determined for [Eu(tpip)$_3$].[39]
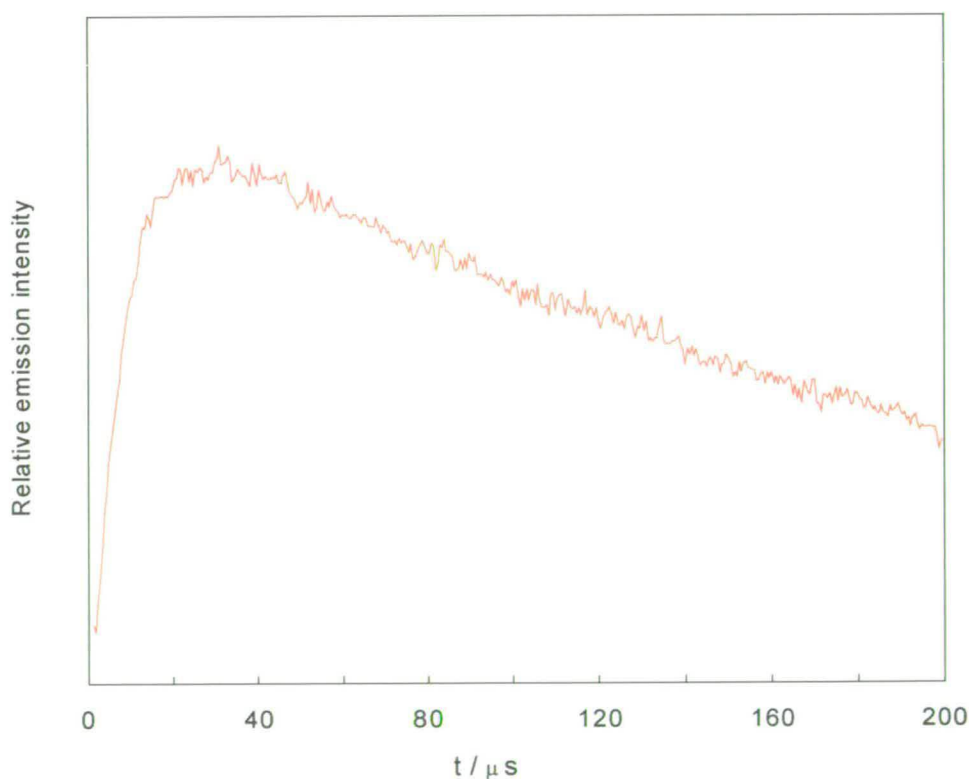
Figure 3.11 Growth of Eu (^{5}D$_0$) luminescence with time (t) for [Eu(tpip)$_3$] (1×10^{-4} mol dm^{-3}) in CHCl$_3$

Having assessed the factors that control the relative rate of luminescence from the excited Ln^{3+} states, it is important to consider the overall efficiency of the sensitisation process. Luminescence quantum yields were measured for [Eu(tpip)$_3$] and [Tb(tpip)$_3$] in dry CH_3CN upon excitation at 273 nm, using [Ru(2,2'-bipyridyl)$_3$]Cl$_2$ in aerated H_2O and quinine sulfate in 0.5 mol dm^{-3} H_2SO_4 as standards. The values obtained are 1.3% for [Eu(tpip)$_3$] and 20% for [Tb(tpip)$_3$], showing that the overall efficiency of the antenna effect is high.

The high quantum yields for both Eu^{3+} and Tb^{3+} are very encouraging because no particular attention was given to the energy levels of the tpip ligand. For many complexes, sensitisation is only efficient with either Eu^{3+} or Tb^{3+}. For example, the room temperature quantum yield of Eu(acac)$_3$, where acac is the β-diketonate acetylacetonate, is < 0.2%, whereas the corresponding value for Tb(acac)$_3$ is 19%.[40] Similarly, for the Tb^{3+} complex with *p*-t-butylcalix[4]arene-tetra-acetamide (**8**), the luminescence quantum yield is 20% (the same as measured for [Tb(tpip)$_3$]), but is three orders of magnitude lower for the Eu^{3+} complex (0.02%).[41] In both the acac and the calixarene complexes, the low quantum yield of Eu^{3+} emission was attributed to LMCT deactivation.

In contrast, a low quantum yield for Tb^{3+} luminescence suggests that there is a back energy transfer process occurring from the Tb^{3+} ($^5D_4$) level to a ligand excited state. This is the case for the Tb^{3+} complex of the cryptand **2**; the quantum yield at room temperature is 3% in H_2O.[42] This decay process, which is also common for other polypyridine ligands,[38] normally involves energy transfer to the triplet state of the ligand.

Attempts were made to measure the triplet state of the tpip ligands in [Ln(tpip)$_3$] by measuring the phosphorescence of [Gd(tpip)$_3$], since Gd^{3+} does not possess any excited states that could lie below the triplet states. Unfortunately, the emission obtained for this experiment was very weak, preventing an analysis of the data. In view of the high energy of the $\pi \rightarrow \pi^*$ band of the phenyl groups of tpip, however, it seems unlikely that the ligand state from which energy transfer takes place, whether it is a singlet or triplet

state, is low enough to allow a back energy transfer process to occur.

The high quantum yield obtained for [Tb(tpip)₃] complexes can be attributed to a combination of the shielding of the Ln^{3+} ions from quenching solvent molecules (as shown by the lifetime measurements), efficient ligand-to-metal energy transfer and the absence of back energy transfer. In view of the reasonably high quantum yield and long luminescence lifetime of [Eu(tpip)₃], LMCT states do not appear to play a prominent role in the deactivation of the metal ion. The difference in quantum yield is probably due to a better match between ligand and metal excited states in [Tb(tpip)₃].

3.3   LANTHANIDE COMPLEXES OF TTIP

The preceding section demonstrated that an imidodiphosphinate ligand can be employed very effectively to form stable, highly luminescent complexes with Ln^{3+} ions. Any attempt to improve upon the photophysical properties of [Ln(tpip)₃] complexes requires alteration of the imidodiphosphinate ligand used. One possibility is to modulate the first coordination sphere of the Ln^{3+} ion to prevent the coordination of water molecules in solution that is observed for [Ln(tpip)₃] complexes. It was thought that this could be achieved by replacing the phenyl groups of tpip with *o*-tolyl groups, thereby increasing the steric bulk close to the metal.

3.3.1 Preparation and characterisation of Httip

The preparation of the new ligand N-(P,P-di-2-methylphenylphosphinoyl)-P,P-di-2-methylphenyl-phosphinimidic acid (Httip, 25), which is the *o*-tolyl analogue of Htpip, is accomplished in two steps as shown in Scheme 3.1. The reagent chlorodi-2-methylphenylphosphine (24) is prepared by the reaction of PCl₃ with the Grignard reagent of 2-bromotoluene, following a similar method to that described in the literature (the reported preparation used 2-chlorotoluene).[43] Characterisation of chlorodi-2-methylphenylphosphine was performed by ¹H and ³¹P NMR spectroscopy and agreed with the reported spectra. Due to the sensitivity of this material it was used

immediately. The second step in Scheme 3.1 is reaction of chlorodi-2-methylphenylphosphine and hexamethyldisilazane followed by oxidation with H_2O_2, according to the method used for the synthesis of Htpip[18] to give pure Httip (15% yield).
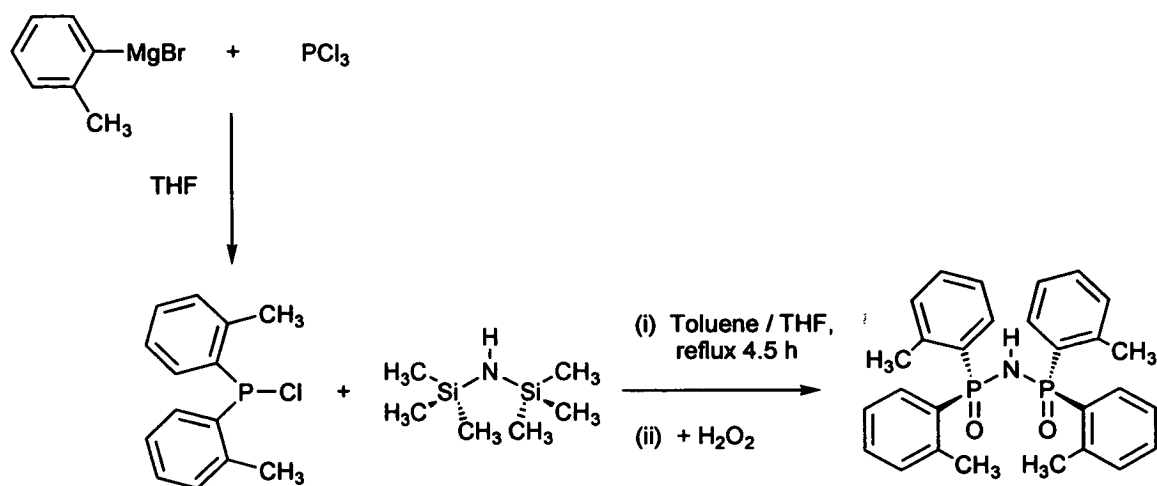
Scheme 3.1

The FAB-MS of the Httip ligand shows an intense peak at *m/z* 474, corresponding to $[M + H]^+$. The ^1H NMR spectrum of the ligand in $CDCl_3$ shows three multiplets at δ 7.82-7.74, 7.33-7.27 and 7.14-7.00, corresponding to the phenyl protons and a singlet at δ 2.18 for the protons of the methyl group. The ^{31}P NMR spectrum, also in $CDCl_3$, shows one singlet at δ 25.4 for the equivalent phosphorus atoms of the ligand. As for Htpip, this ligand has a very low solubility in common organic solvents, and appears to be generally less soluble than Htpip. This suggests the ligand is adopting a hydrogen-bonded structure in the solid state [*cf.* Htpip structure (b) in Figure 3.1]. This is confirmed by IR spectroscopy which shows strong absorptions at 1196, 1215 and 1229 cm^{-1}, characteristic of the vibrations of $-P=N-$ systems,[20] and strong absorptions at 1068 and 1094 cm^{-1} assigned to P–O stretching vibrations. These two sets of vibrations agree with those observed in many complexes of imidodiphosphinates,[10] suggesting that there is much delocalisation of electron density in the solid-state structure of the free ligand.

3.3.2 Preparation and characterisation of lanthanide complexes of ttip

Potassium salt of ttip

The potassium salt of Httip, Kttip, is prepared by dissolving Httip in a methanolic KOH solution, removing the solvent and recrystallising the resultant white solid from ethanol to give the desired product in reasonable yield (59%). The FAB-MS of this product shows intense peaks at *m/z* 512 and 550 corresponding to $[M + H]^+$ and $[M + K]^+$ respectively. The ^{1}H NMR spectrum of the ligand in CD$_3$OD shows two multiplets at δ 8.31-8.20 and 7.29-6.99, corresponding to the phenyl protons, and a singlet at δ 2.12 for the protons of the methyl group. The ^{31}P NMR spectrum, also in CD$_3$OD, shows one singlet at δ 9.1 for the equivalent phosphorus atoms. The shift to lower frequency relative to the ^{31}P resonance of Htpip (*ca.* 8 ppm difference), is probably a solvent effect. The solid analyses satisfactorily as Kttip·3.5H$_2$O and the large amount of solvent of crystallisation is in agreement with the crystal structure of Kttip grown from a methanolic solution (Figure 3.12).

The crystal structure is a hydrogen-bonded network with the formula [K(ttip)(MeOH)$_2$(H$_2$O)]$_n$. One oxygen atom of each ligand is bonded directly to one K$^+$ ion and hydrogen bonded to a water molecule, while the other oxygen atom of the ligand is hydrogen bonded to both a water and a MeOH molecule; the K$^+$ ion is bonded to the same MeOH molecule, another MeOH and a water. The network is built by various additional interactions involving bridging solvent molecules, such as the hydrogen bonding of the oxygen atom of adjacent ligands to the same water molecule. The P–N and P–O bond lengths of the imidodiphosphinate are short and comparable to those found for the tpip complexes, indicative of electron delocalisation around the binding unit.
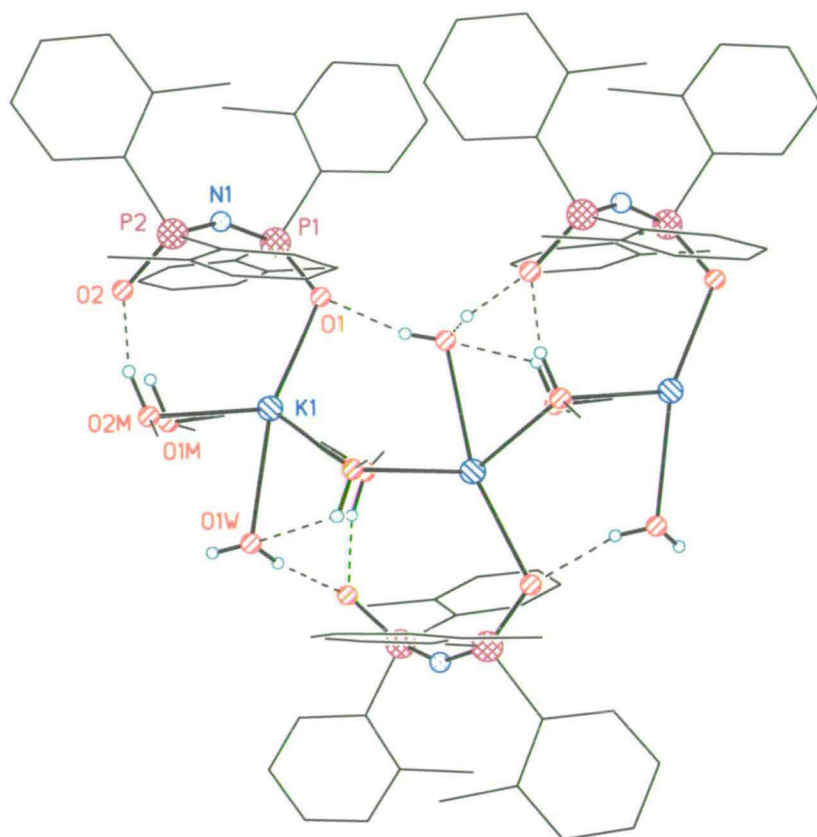
Figure 3.12 Molecular structure of Kttip showing the atomic numbering scheme; selected bond distances (Å): K(1)–O(1) 2.713(8), K(1)–O(2M) 2.799(10), K(1)–O(1M) 2.822(10), K(1)–O(1W) 2.842(7), P(1)–O(1) 1.508(7), P(1)–N(1) 1.586(9), P(2)–N(1) 1.546(9), P(2)–O(2) 1.510(8)

The absorption spectrum of Kttip in MeOH is shown in Figure 3.13; the inset is an expansion of the 250-320 nm region of this spectrum. This absorption spectrum has a similar profile to that observed for Htpip and [Ln(tpip)₃], with a structured band centred on 270 nm [λ_{max}/nm (ε/dm³ mol⁻¹ cm⁻¹) 270 (2700), 277 (2500)]. The absorption maxima are at slightly longer wavelengths than the Htpip and [Ln(tpip)₃] absorptions; such minor changes upon substitution of phenyl rings with methyl groups are common.[21] As discussed previously, there are three characteristic UV absorption bands for substituted benzene rings, and on this occasion it appears that they are all present; the aforementioned band is attributed to the *B*-band of the tolyl groups. At shorter wavelength, an intense band is observed that has a shoulder around 230 nm, and this shoulder is attributed to the *K*-band.
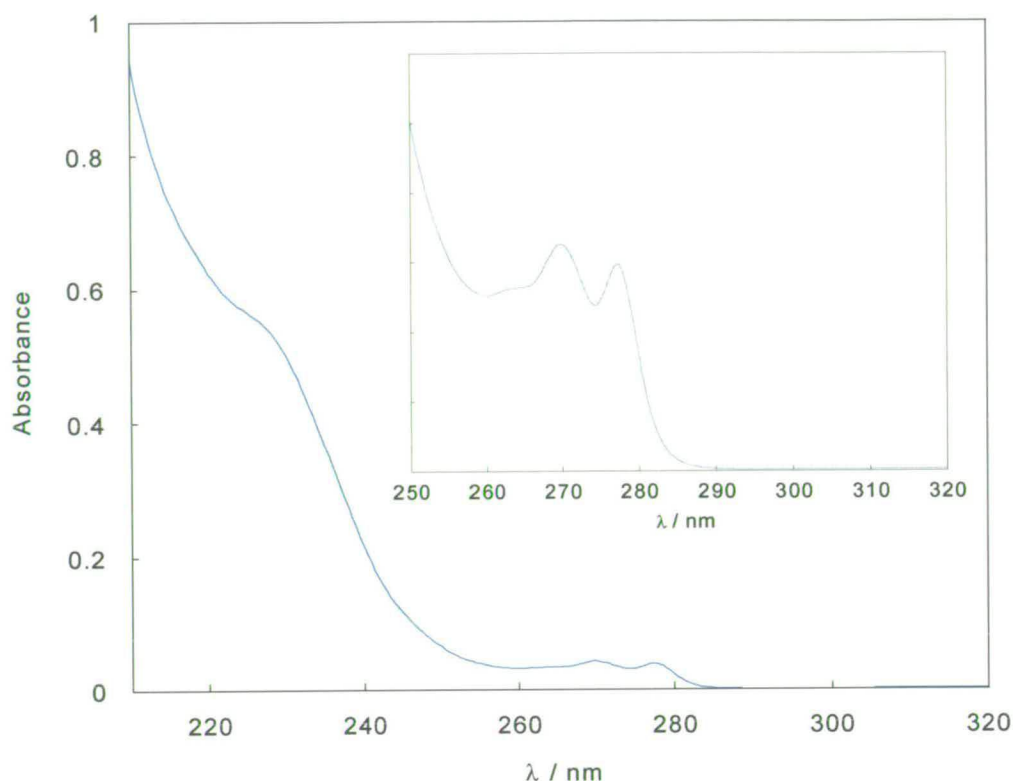
Figure 3.13 Absorption spectrum of Kttip (1.2×10^{-4} mol dm^{-3}) in MeOH

Lanthanide complexes of ttip

The potassium salt of ttip is less soluble in water then Ktpip, therefore the complexes were prepared in MeOH. One equivalent of a methanolic solution of LnCl$_3$·6H$_2$O (Ln = Eu, Tb) is added dropwise to three equivalents of a methanolic solution of Kttip. The white solid that immediately precipitates is filtered, washed with MeOH and dried under vacuum and analyses as [Ln(ttip)$_3$] in 70-90% yield. Whilst these complexes and the corresponding tpip complexes dissolve in similar solvents, the former have, in general, a lower solubility, presumably due to the additional twelve methyl groups.

Both [Eu(ttip)$_3$] and [Tb(ttip)$_3$] have been characterised by FAB-MS, showing intense signals corresponding to [M + H]$^+$ and [M–ttip]$^+$. The ^{1}H NMR spectrum of [Eu(ttip)$_3$] in CDCl$_3$ shows two multiplets, in a 1:1 ratio, for the aromatic protons at δ 7.15-7.16 and 6.10-6.31 and a singlet for the methyl protons at δ 3.06. In the ^{31}P NMR spectrum of the same sample, a single resonance is obtained at δ 25.7 for all of the phosphorus atoms. As [Tb(ttip)$_3$] was less soluble in CDCl$_3$ than [Eu(ttip)$_3$], only a ^{31}P NMR

spectrum was obtained. Although this spectrum is weak, a broad singlet at δ 142 is clearly observed. As expected, the patterns and lanthanide-induced shifts observed in the [Ln(ttip)₃] NMR spectra are in agreement with NMR data for the corresponding [Ln(tpip)₃] complexes.

The IR spectra of these complexes show strong absorptions assigned to PO and PNP stretching vibrations. For both [Eu(ttip)₃] and [Tb(ttip)₃], these occur at 1224 and 1195 cm⁻¹ [v(PNP)] and 1098 and 1071 cm⁻¹ [v(PO)]. These absorptions are similar to those observed for the free ligand, probably due to the hydrogen bonding in the latter molecule. The lack of absorbance in the region between 3100 and 4000 cm⁻¹ suggests that there are no H_2O or MeOH molecules coordinated to the Ln^{3+} ion.
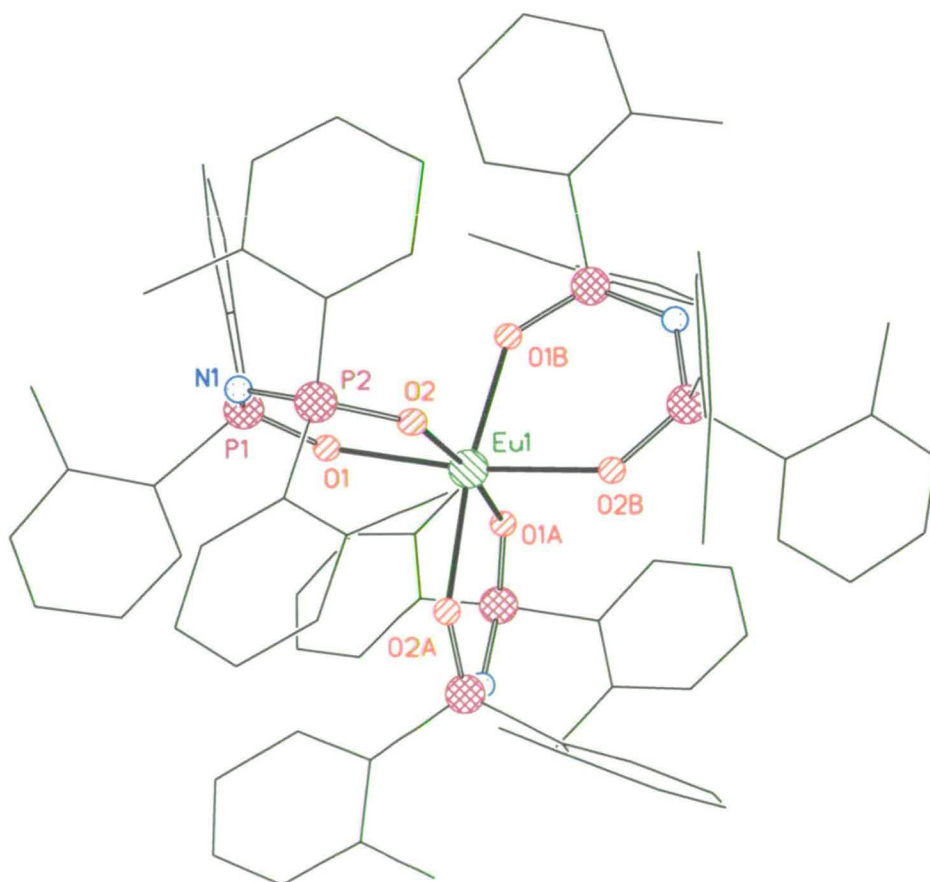
Figure 3.14 Molecular structure of Eu(ttip)₃ showing the atomic numbering scheme; selected bond distances (Å): Eu(1)–O(1) 2.28(3), Eu(1)–O(2) 2.27(3), P(1)–O(1) 1.50(3), P(2)–O(2) 1.51(3), P(1)–N(1) 1.591(9), P(2)–N(1) 1.580(9)

Single crystals of [Eu(ttip)$_3$], suitable for X-ray diffraction analysis, were grown by slow evaporation from a CHCl$_3$ solution. The crystal structure of [Eu(ttip)$_3$] is shown in Figure 3.14. The lower degree of accuracy of this structure, relative to the determinations performed for the [Ln(tpip)$_3$] previously discussed, precludes a detailed analysis of bond parameters. However, it is clear that the structure is very similar to those discussed for the [Ln(tpip)$_3$] complexes. There are three anionic ttip ligands adopting a bidentate coordination mode to the Eu^{3+} ion and no coordinated solvent molecules (one CHCl$_3$ molecule per complex is found in the crystal lattice), giving a six-coordinate metal ion. The *o*-tolyl groups bound to the same P atom orient themselves such that the two methyl groups are pointing away from each other. As with the tpip structures, the low coordination number is attributed to the twelve *o*-tolyl groups forming a hydrophobic shell around the central metal ion. The average Eu–O bond distance for the structure is 2.28 Å, with average P–N and P–O bond lengths of 1.59 and 1.51 Å respectively, which compare well with those observed for [Ln(tpip)$_3$].

3.3.3 Photophysical studies of lanthanide complexes of ttip

The absorption spectrum of [Eu(ttip)$_3$] in CH$_3$CN is shown in Figure 3.15; the inset is an expansion of the 240-290 nm region of this spectrum. This spectrum is very similar to that of Kttip (Figure 3.13). The absorption coefficients are *ca.* three times greater, corresponding to the absorption of three ttip ligands [λ_{max}/nm (ε/dm^3 mol^{-1} cm^{-1}), 278 (6800), 271 (6200)], with the same band assignments discussed for Kttip. Steady-state luminescence spectra (emission and excitation) of CH$_3$CN solutions of [Eu(ttip)$_3$] and [Tb(ttip)$_3$] are shown in Figures 3.16 and 3.17 respectively.

Excitation at a wavelength corresponding to ligand-centred bands results in luminescence characteristic of the Ln^{3+} ion. The uncorrected excitation spectra of both solutions show one structured band with peaks at 270 and 277 nm. This band matches the *B*-band observed for the *o*-tolyl groups in the absorption spectrum of [Eu(ttip)$_3$]; the extension of the excitation profile to higher energy matches the shoulder seen in the same absorption spectrum (the *K*-band). This demonstrates that the sensitisation process that occurs in [Ln(tpip)$_3$] (Ln = Sm, Eu, Tb, Dy) complexes also operates in [Eu(ttip)$_3$]

and [Tb(ttip)$_3$].

For [Eu(ttip)$_3$], the characteristic $^5D_0 \rightarrow {}^7F_J$ ($J = 0$-4) transitions of Eu^{3+} are observed in the emission spectrum, with the hypersensitive $^5D_0 \rightarrow {}^7F_2$ transition resolved into two components centred on 611 and 621 nm. Similarly, the $^5D_4 \rightarrow {}^7F_J$ ($J = 2$-6) transitions of Tb^{3+} are observed for [Tb(ttip)$_3$], with an intense structured $^5D_4 \rightarrow {}^7F_5$ band that has peaks at 542 and 551 nm. In terms of the splitting and relative intensities of the *f–f* transitions, the emission spectra of [Eu(ttip)$_3$] and [Tb(ttip)$_3$] are almost identical to the spectra recorded for their respective tpip analogues, indicative of a high degree of structural similarity between [Ln(tpip)$_3$] and [Ln(ttip)$_3$] complexes in solution.
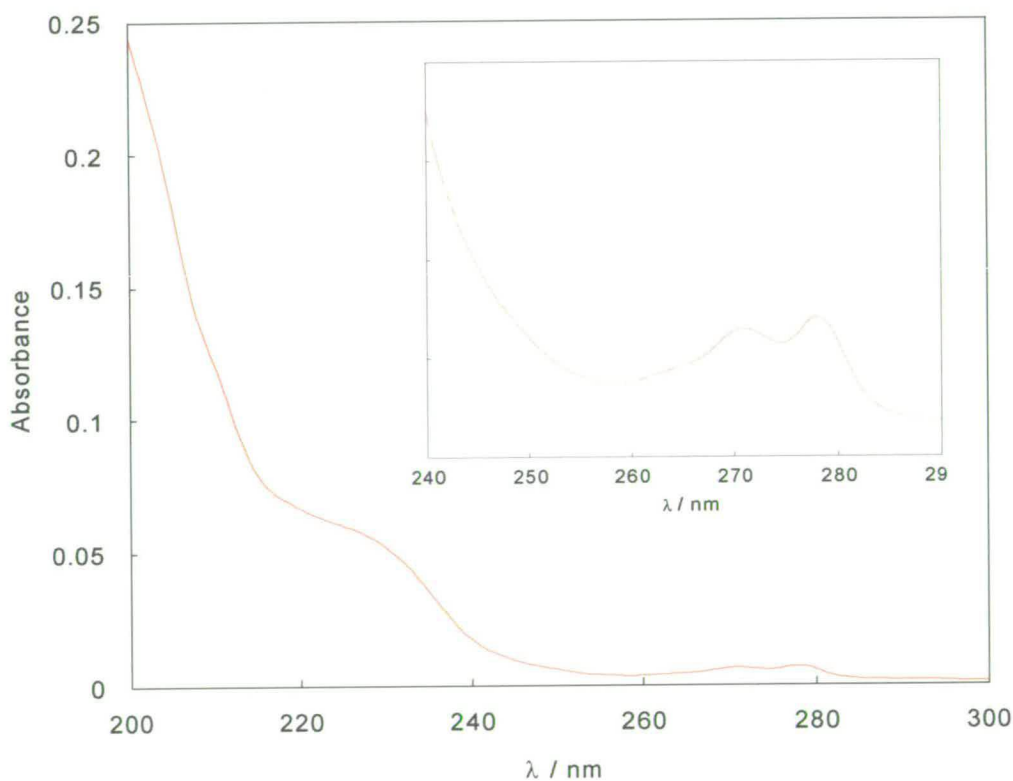
Figure 3.15 Absorption spectrum of [Eu(ttip)$_3$] (1×10^{-6} mol dm^{-3}) in CH$_3$CN; the inset shows an expanded section of the spectrum
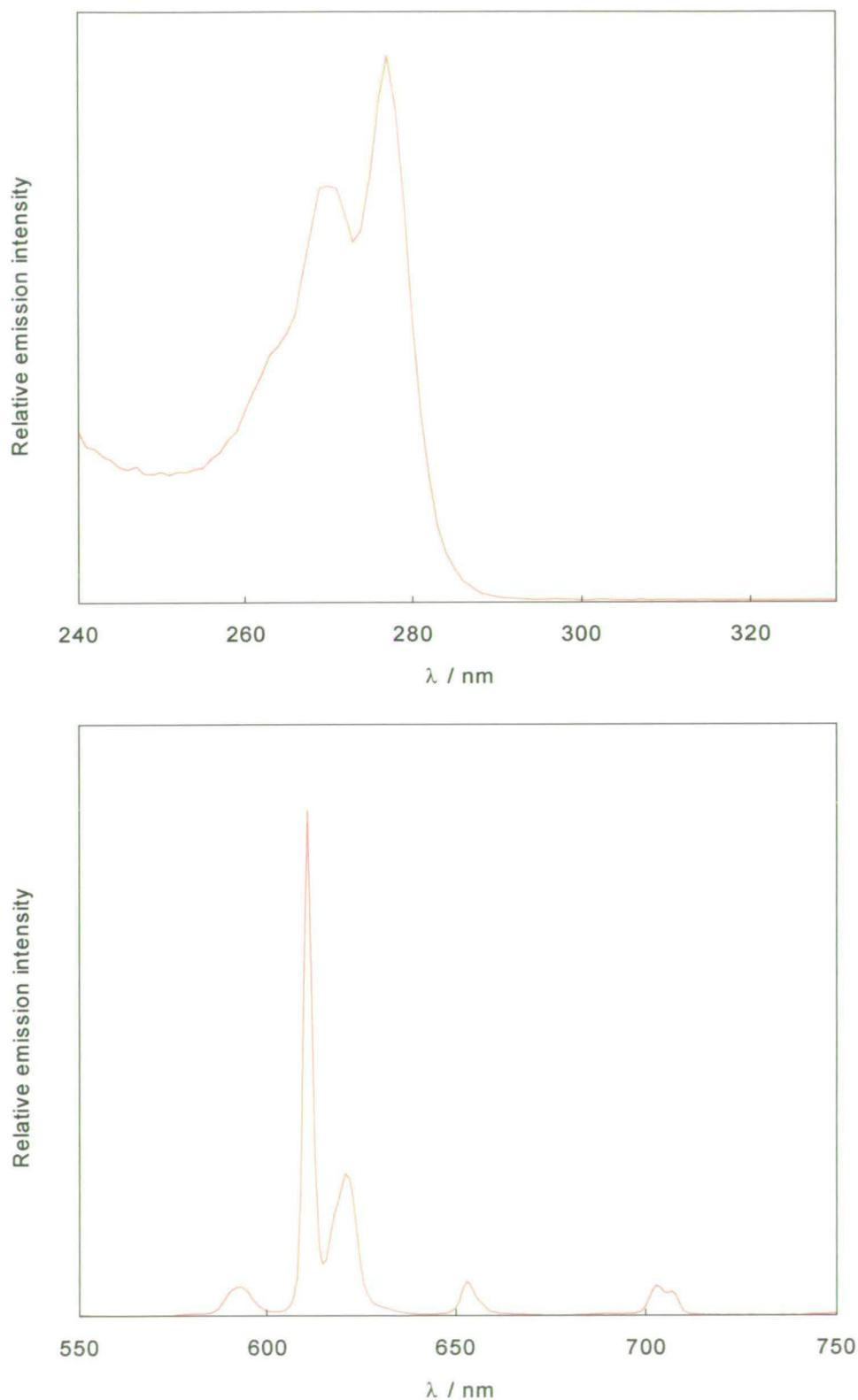
Figure 3.16 Top: excitation spectrum of $[Eu(ttip)_3]$ $(1 \times 10^{-6}$ mol dm$^{-3})$ in CH_3CN, $\lambda_{em} = 610$ nm, 1 nm bandpass (ex.); Bottom: corrected emission spectrum of $[Eu(ttip)_3]$ $(1 \times 10^{-6}$ mol dm$^{-3})$ in CH_3CN, $\lambda_{ex} = 273$ nm, 2 nm bandpass (em.)
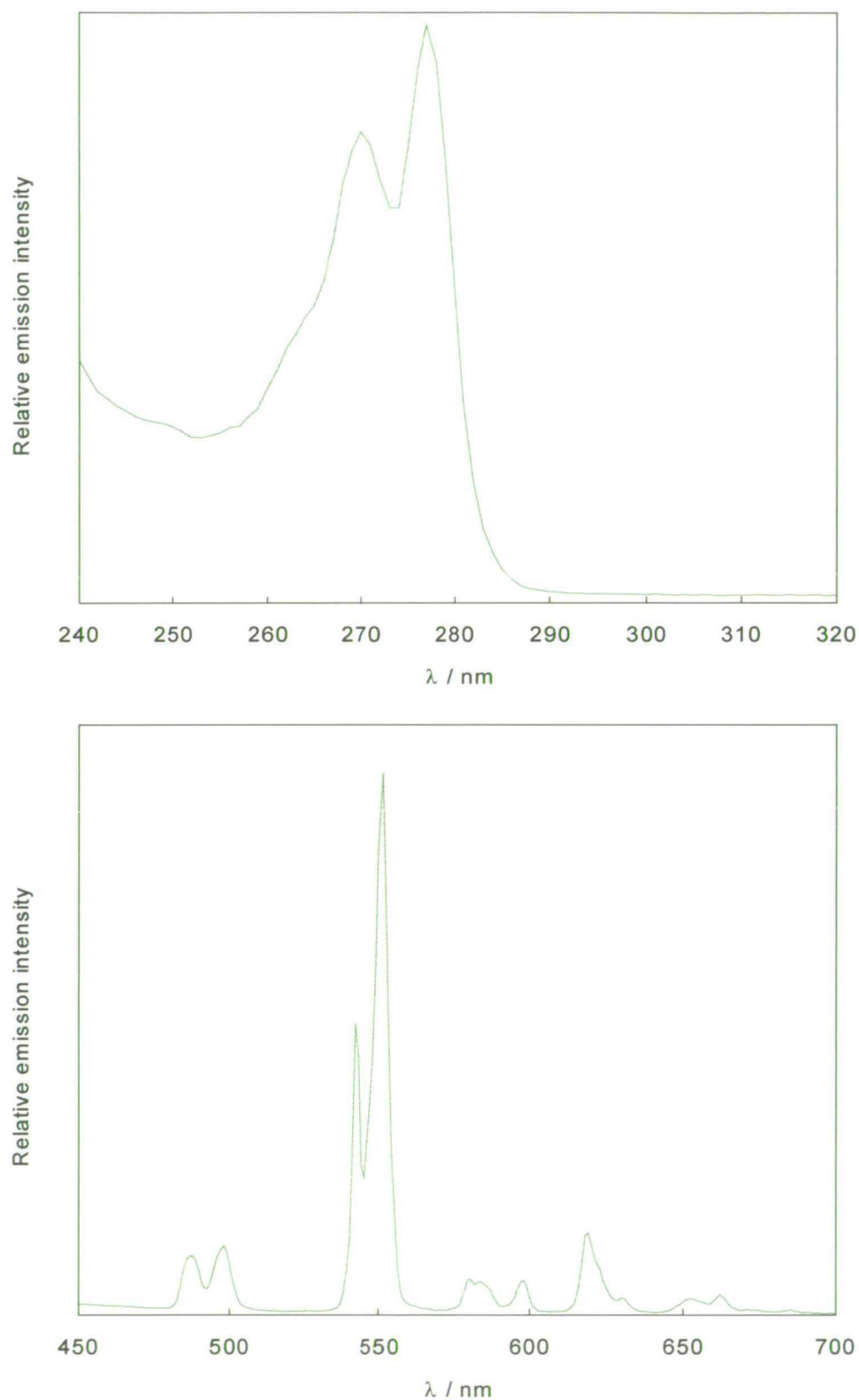
Figure 3.17 Top: excitation spectrum of [Tb(ttip)$_3$] (1×10^{-6} mol dm^{-3}) in CH$_3$CN, λ_{em} = 550 nm, 1 nm bandpass (ex.); Bottom: corrected emission spectrum of [Eu(ttip)$_3$] (1×10^{-6} mol dm^{-3}) in CH$_3$CN, λ_{ex} = 273 nm, 2 nm bandpass (em.)

In order to investigate the possibility of solvent coordination in solution, time-resolved luminescence spectroscopy has been performed on [Eu(ttip)$_3$] and [Tb(ttip)$_3$] in both the solid state and in solution. The measured luminescence lifetimes, following excitation into ligand-centred bands (λ_{ex} = 266 nm), are displayed in Table 3.3. All of the decays are monoexponential.

The measured lifetimes at room temperature of [Eu(ttip)$_3$] and [Tb(ttip)$_3$] as powdered solids appear to be rather short in comparison with the analogous tpip complexes. The increase in decay rate for [Eu(ttip)$_3$] compared with [Eu(tpip)$_3$] is 550 s^{-1}; the increase for [Tb(ttip)$_3$] compared with [Tb(tpip)$_3$] is 390 s^{-1}. However, the crystal structure of [Eu(ttip)$_3$], elemental analyses and IR spectroscopy give no evidence of solvent content in [Ln(ttip)$_3$] (Ln = Eu and Tb) in the solid state.

This significant increase in the decay rate may be due to the presence of a new deactivating pathway. A temperature-dependent pathway can be eliminated, as the solid-state luminescence lifetimes do not change upon lowering the temperature to 77 K (Table 3.3). This means the higher decay rate is not due to back energy transfer to ligand excited states or to a charge transfer mechanism.[38]

Table 3.3 Luminescence lifetimes of the Eu^{3+} ($^5D_0$) and Tb^{3+} ($^5D_4$) levels in [Ln(ttip)$_3$] (Ln = Eu, Tb) (λ_{ex} = 266 nm)

Ln	Conditions[a]	τ / ms
Eu	solid (powder, RT)	1.0
	solid (powder, 77 K)	0.99
	dry CH$_3$CN solution	1.3
	dry CH$_3$CN solution + H$_2$O[b]	1.1
Tb	solid (powder, RT)	1.4
	solid (powder, 77 K)	1.4
	dry CH$_3$CN solution	1.9
	dry CH$_3$CN solution + H$_2$O[b]	1.7

[a] Solution lifetimes measured at room temperature; Concentration of CH$_3$CN solutions = 1 × 10^{-6} mol dm^{-3}; [b] [H$_2$O] = 10 mol dm^{-3}

The increase in decay rate for [Ln(ttip)₃] could be associated with vibrational deactivation, and in the absence of coordinated solvent molecules such deactivation would be due to the ligand itself. The replacement of phenyl with *o*-tolyl results in the presence of 36 additional C–H oscillators close to the metal ion in the ttip complexes. Although C–H vibrations are much less efficient than O–H vibrations, the cumulative effect can be large. In the Eu^{3+} complex of a substituted 1,4,7,10-tetraazacyclododecane, for example, the average contribution of each C–H oscillator to the decay rate was either 5 s^{-1} or 26 s^{-1} depending on the oscillator to Ln^{3+} ion distance.[44] This distance was *ca.* 0.7 Å longer in the former case, hence the reduced contribution. Studies of other lanthanide complexes have produced similar estimates.[45]

On the basis of the literature values, the increase in decay rate observed for [Eu(ttip)₃] contains a contribution from the methyl C–H oscillators. If the increase in decay rate for [Ln(ttip)₃] is due solely to C–H quenching, the average contribution from each C–H oscillators is 15 s^{-1} for Eu^{3+} and 11 s^{-1} for Tb^{3+}. The increase in rate observed for [Tb(ttip)₃] is quite large considering the larger energy gap that must be bridged to deactivate the Tb^{3+} ($^5D_4$) level. In a recent study, the average contribution of C–H oscillators to the decay rate of the Tb^{3+} ($^5D_4$) and Eu^{3+} ($^5D_0$) level were estimated to be *ca.* 1 s^{-1} and 18 s^{-1} respectively.[31] However, vibrational quenching is strongly dependent on the metal-oscillator distance, so it is not unfeasible that this distance is shorter, especially for the smaller Tb^{3+} ion. Although not attempted as part of this work, lifetime measurements performed on complexes with deuterated methyl groups might help to clarify the cause of the faster decay rates in [Ln(ttip)₃], since C–D should be less effective at quenching the Ln^{3+} ion luminescence.

In dry CH_3CN, the lifetimes of the Eu^{3+} ($^5D_0$) level in [Eu(ttip)₃] and the Tb^{3+} ($^5D_4$) level in [Tb(ttip)₃] increase to 1.33 and 1.89 ms respectively. A longer lifetime in solution compared with the solid state is not uncommon and is good evidence that solvent molecules are not deactivating the excited state. For example, it has recently been shown that nine-coordinate complexes of Eu^{3+} with tripodal ligands, in which there are no coordinated water molecules, have shorter lifetimes in the solid state than in dry CH_3CN.[34]

In agreement with the solid state results, the lifetimes of the ttip complexes are still significantly shorter than for the tpip analogues in dry CH_3CN. Upon addition of H_2O (10 mol dm^{-3}) to these anhydrous solutions, there is a small reduction in the lifetimes of both the Eu^{3+} ($^5D_0$) and the Tb^{3+} ($^5D_4$) lifetimes to 1.13 and 1.67 ms respectively. This reduction upon adding water is much smaller than that observed with [Eu(tpip)$_3$] and [Tb(tpip)$_3$] (in spite of the 100-fold increase in the H_2O:complex ratio for [Ln(ttip)$_3$] compared with [Ln(tpip)$_3$]), and is consistent with H_2O molecules solely interacting in the second coordination sphere of the Ln^{3+} ion.

Applying equation 3.1 to the values in Table 3.3 gives q = 0.14 and 0.29 for [Eu(ttip)$_3$] and [Tb(ttip)$_3$] respectively in aqueous CH_3CN, supporting the conclusion that there are only second-sphere interactions of water in these complexes, in contrast with [Ln(tpip)$_3$] in aqueous CH_3CN (q = 0.71 and 1.5 for [Eu(tpip)$_3$] and [Tb(tpip)$_3$] respectively). If corrections are applied for outer-sphere water molecules, then q < 0. This change to outer-sphere coordination is attributed to the greater shielding of the Ln^{3+} ion by the bulky *o*-tolyl groups of the ttip ligand.

3.4   CONCLUSIONS

Imidodiphosphinates have been studied for the first time as antenna ligands in the search for new luminescent lanthanide complexes for application as photonic devices and sensors. Photophysical studies of lanthanide complexes of either tetraphenylimidodiphosphinate (tpip) or ttip, a new *o*-tolyl derivative of tpip, suggest they are attractive candidates for such purposes.

Each imidodiphosphinate in the complexes [Ln(tpip)$_3$] (Ln = Sm, Eu, Tb, Dy) and [Ln(ttip)$_3$] (Ln = Eu, Tb) strongly coordinates in a bidentate fashion and the bulky aromatic groups ensure that the Ln^{3+} ions are six-coordinate in the solid state. The complexes, which are very stable, retain their structure in organic solvents and are resistant to hydrolysis. Inner-sphere coordination of water occurs in acetonitrile solutions of the tpip complexes; however, this is prevented in the ttip complexes by the

extra shielding provided by the *o*-tolyl groups. Although the exclusion of coordinating solvent molecules by structurally-complex polydentate ligands is not uncommon, the same result using only three bidentate ligands is very unusual and suggests that this simple complexation approach could be extended to other simple ligand systems.

In addition to providing a hydrophobic shell around the Ln^{3+} ion, the aromatic groups act as light antennas; they collect light and channel it to the bound Ln^{3+} ion. In all of the complexes studied, excitation into ligand-centred bands is followed by energy transfer to the Ln^{3+} ion, with subsequent characteristic line emission. The long luminescent lifetimes of the [Ln(tpip)$_3$] complexes suggest that non-radiative deactivating pathways (such as LMCT and back energy transfer) are absent; the high quantum yields of both [Eu(tpip)$_3$] and [Ln(tpip)$_3$] show that the overall sensitisation process is efficient. While the ligand ttip prevents the coordination of deactivating water molecules, it does appear to provide an additional deactivating pathway. However, if this quenching process is, as thought, due to C–H vibrations, simply substituting C–H with C–D can eliminate it.

With regards to the photophysical properties of the [Ln(tpip)$_3$] complexes, one disadvantage is that they have a relatively low absorption coefficient (*ca.* 5×10^3 dm^3 mol^{-1} cm^{-1}). Although the Tb^{3+} complex of the cryptand **2** is seven times less efficient at converting the incident light, the greater amount of light absorbed ($\varepsilon_{272} = 29 \times 10^3$ dm^3 mol^{-1} cm^{-1}) compensates.[42] While the relative importance of quantum yield and absorbance will vary depending on the application, this is one area where a superior imidodiphosphinate may be found (perhaps at the expense of overall efficiency).

It is the flexibility of imidodiphosphinates that makes them most useful as antenna ligands, since they offer a wealth of possibilities for further derivitisation. Since the binding and antenna domains are not in conjugation, imidodiphosphinate complexes can be altered whilst maintaining binding properties. Simply exchanging one Ln^{3+} ion for another allows the complex to be tuned so that light emission is centred on four different wavelengths, with no attendant changes to structure or absorption wavelength. It should be possible to further modify the ligands to optimise the antenna groups for a particular Ln^{3+} ion, and to incorporate new physical properties (*e.g.* solubility) as

required.

3.5   REFERENCES

1. S. Aime, M. Botta, R. S. Dickins, C. L. Maupin, D. Parker, J. P. Riehl and J.A.G. Williams, *J. Chem. Soc., Dalton Trans.*, 1998, 881.

2. P. R. Selvin, J. Jancarik, M. Li and L.-W. Hung, *Inorg. Chem.*, 1996, **35**, 700.

3. N. Sato and S. Shinkai, *J. Chem. Soc., Perkin Trans. 2*, 1993, 621.

4. M.A. Mortellaro and D.G. Nocera, *J. Am. Chem. Soc.*, 1996, **118**, 7414.

5. Z. Pikramenou, J.-A. Yu, A. Ponce and D.G. Nocera, *Coord. Chem. Rev.*, 1994, **132**, 181.

6. Z. Pikramenou and D.G. Nocera, *Inorg. Chem.*, 1992, **31**, 532.

7. H. Nöth, *Z. Naturforsch., Teil B*, 1982, **37**, 1491.

8. A. M. Z. Slawin, M. B. Smith and J. D. Woolins, *J. Chem. Soc., Dalton Trans.*, 1996, 3659 and references therein.

9. C. Silvestru, I. Haiduc, R, Cea-Olivares and A. Zimbron, *Polyhedron*, 1994, **13**, 3159 and references therein.

10. I. Rodríguez, C. Alvarez, J. Gómez-Lara and R. Cea-Olivares, *Lanthanide-Actinide Res.*, 1986, **1**, 253.

11. A. O. Gudima, E. O. Berezhnoi and V. A. Kalibabchuk, *Koord. Khim.*, 1990, **16**, 1147.

12. I. Rodríguez, C. Alvarez, J. Gómez-Lara, R. A. Toscano, N. Platzer, C. Mulheim and H. Rudler, *Chem. Commun.*, 1987, 1502.

13. C. Alvarez, N. Goasdoué, N. Platzer, I. Rodríguez and H. Rudler, *Chem. Commun.*, 1988, 1002.

14. C. Alvarez, L. Barkaoui, N. Goasdoué, J.-C. Daran, N. Platzer, H. Rudler, and B. J. Vaissermann, *Chem. Commun.*, 1989, 1507.

15. N. Platzer, H. Rudler, C. Alvarez, L. Barkaoui, B. Denise, N. Goasdoué, M.-N. Rager, J. Vaissermann and J.-C. Daran, *Bull. Soc. Chim. Fr.*, 1995, **132**, 95.

16. L. Barkaoui, M. Charrouf, M.-N. Rager, B. Denise, N. Platzer and H. Rudler, *Bull. Soc. Chim. Fr.*, 1997, **134**, 167.

17. I. B. Bliss and W. G. Bos, *J. Inorg. Nucl. Chem.*, 1977, **39**, 443.

18. D. J. Williams, *Inorg. Nucl. Chem. Lett.*, 1980, **16**, 189.

19. A pure sample of Htpip was kindly supplied by Professor J. D. Woolins (Department of Chemistry, Loughborough University).

20. K. L. Paciorek, *Inorg. Chem.*, 1964, **3**, 96.

21. D. H. Williams and I. Fleming, *Spectroscopic Methods in Organic Chemistry*, McGraw-Hill Book Co., London, 5th edn., 1995, ch. 1.

22. D. F. Martin, M. Shamma and W.C. Fernelius, *J. Am. Chem. Soc.*,1958, **80**, 4891 and references therein.

23. A. Schmidpeter and H. Groeger, *Chem. Ber.*, 1967, **100**, 3979.

24. J. Reuben, *Progress in NMR Spectroscopy*, 1975, **9**, 1.

25. R. O. Day, R. R. Holmes, A. Schmidpeter, K. Stoll and L. Howe, *Chem. Ber.*, 1991, **124**, 2443

26. A. D. Sherry and C. F. G. C. Geraldes, in *Lanthanide Probes in Life, Chemical and Earth Sciences*, eds. J.-C. G. Bünzli and G. R. Chopin, Elsevier, Amsterdam, 1989, ch. 4.

27. L. C. Thompson, in *Handbook on the Physics and Chemistry of Rare Earths*, eds. K.A. Gschneidner, Jr., and L. Eyring, North Holland, Amsterdam, 1979, **3**, ch. 25.

28. F. A. Cotton and G. Wilkinson, *Advanced Inorganic Chemistry*, Wiley-Interscience, New York, 5th edn., 1988, ch. 11.

29. J.-C. G. Bünzli, in *Lanthanide Probes in Life, Chemical and Earth Sciences*, eds. J.-C. G. Bünzli and G. R. Chopin, Elsevier, Amsterdam, 1989, ch. 7 and references therein.

30. G. Stein and E. Würzberg, *J. Chem. Phys.*, 1975, **62**, 208.

31. M. P. Oude Wolbers, F. C. J. M. van Veggel, B. H. M. Snellink-Ruël, J. W. Hofstraat, F. A. J. Guerts and D. N. Reinhoudt, *J. Chem. Soc., Perkin Trans. 2*, 1998, 2141.

32. W. T. Carnall, in *Handbook on the Physics and Chemistry of Rare Earths*, eds. K.A. Gschneidner, Jr., and L. Eyring, North Holland, Amsterdam, 1979, **3**, ch. 24.

33. W. DeW. Horrocks, Jr., and D. R. Sudnick, *Acc. Chem. Res.*, 1981, **14**, 384.

34. F. Renaud, C. Piguet, G. Bernardinelli, J.-C. Bünzli and G. Hopfgartner, *J. Am. Chem. Soc.*,1999, **121**, 9326.

35. G. Zucchi, R. Scopelliti, P.-A. Pittet, J.-C. G. Bünzli and R. D. Rogers, *J. Chem. Soc., Dalton Trans.*, 1999, 931.

36. A. Beeby, I. M. Clarkson, R. S. Dickins, S. Faulkner, D. Parker, L. Royle, A. S. de Sousa, J. A. G. Williams, and M. Woods, *J. Chem. Soc., Perkin Trans. 2*, 1999, 493.

37. C. Piguet, J.-C. Bünzli, G. Bernardinelli, G. Hopfgartner and A. F. Williams, *J. Am. Chem. Soc.*,1993, **115**, 8197.

38. N. Sabbatini, M. Guardigli and J.-M. Lehn, *Coord. Chem. Rev.*, 1993, **123**, 201.

39. H. Richter-Lustig, A. Ron and S. Speiser, *Chem. Phys. Lett.*, 1982, **85**, 576.

40. W. R. Dawson, J. L. Kropp and M. W. Windsor, *J. Chem Phys.*1966, **45**, 2410.

41. N. Sabbatini, M. Guardigli, A. Mecati, V. Balzani, R. Ungaro, E. Ghidini, A. Casnati and A. Pochini, *Chem. Commun.*, 1990, 878.

42. B. Alpha, R. Ballardini, V. Balzani, J.-M. Lehn, S. Perathoner and N. Sabbatini, *Photochem. Photobiol.*, 1990, **52**, 299.

43. P. W. Clark and B. J. Mulraney, *J. Organomet. Chem.*, 1981, **217**, 51.

44. R. S. Dickins, D. Parker, A. S. de Souza and J. A. G. Williams, *Chem. Commun.*, 1996, 697.

45. T. C. Schwendemann, P. S. May, M. T. Berry, Y. Hou and C. Y. Meyers,*J. Phys. Chem. A*, 1998, **102**, 8690 and references therein.

Chapter Four

Dinuclear lanthanide complexes of a

bis(β-diketonate) ligand

4.1 INTRODUCTION

4.1.1 Dinuclear lanthanide complexes

Most of the lanthanide complexes that have been studied, and which have practical use, are monometallic. The variability of the coordination numbers of Ln^{3+} ions can make their incorporation into organised supramolecular architectures difficult, explaining why relatively little work has been carried out on polymetallic *f-f* complexes (where *f-f* signifies that the metals involved are all Ln^{3+} ions).[1] Despite this, well-defined polynuclear lanthanide systems have potential applications in many exciting areas of chemical research.[2] Interest in the optical properties of such systems is currently focused on the study of metal-metal interactions for laser and phosphor applications,[3] the design of advanced devices performing functions such as directional intermetallic energy transfer,[4] and the development of more efficient luminescent labels.[5]

Research has concentrated on the simplest type of *f-f* cluster, namely the bimetallic complex, which can be divided into homo- and heterobimetallic complexes. With the exception of one dinuclear complex in the solid state,[6] the heterobimetallic complexes prepared to date have been statistical mixtures of homo- and hetero-species. The difficulty in preparing pure heterobimetallic complexes is a result of the very slight variance in chemical properties between Ln^{3+} ions. In general, two main strategies have been adopted for the preparation of bimetallic lanthanide complexes.

The first approach involves using one receptor ligand that is preorganised to incorporate two metal ions into distinct metal binding sites. The most successful ligands have been phenolic Schiff base ligands such as **26**. The Ln^{3+} ions often act as templates for the formation of these ditopic macrocyclic ligands and have been used to form both homo- and heterobimetallic complexes.[2] More recently, Ln^{3+} ions have been used as templates in the formation of dinuclear complexes of the macrobicyclic iminophenolate cryptand (**27**).[7]

26   **27**

The other synthetic strategy is to self-assemble dinuclear complexes. The process of *self-assembly* consists of the spontaneous generation of a well-defined supramolecular structure from a given set of components under specific conditions.[8] It is a process that allows access to structures that might otherwise be unattainable by conventional covalent synthetic methodology. When the components are metal ions and ligands, the strong and highly directional metal-ligand interactions can direct the formation of polymetallic clusters, potentially with novel properties and structural features.[9] One or more reasonably flexible acyclic ligands can form a cavity around the metal ions and the flexibility allows an optimisation of the metal-ligand interactions.

A common method of self-assembling dinuclear complexes is by using a combination of bis(polydentate) ligands and metal ions.[10] If the ligands are designed so that their two binding sites cannot bind with the same metal, then a dinuclear complex may be formed, with the number and arrangement of the ligands determined by the steric and electronic requirements of the metal and ligand.

The complex formed from the linking of two metal ions by three identical ligands can be described either as a triple helicate, if the ligands wrap in a helical fashion, or a triple mesocate, if the ligands do not have a helical twist (Figure 4.1).[11] This approach has been used with Ln[3+] ions and segmental bis-tridentate ligands based on benzimidazole-pyridine units, such as ligands **28** and **29**.[12] Many triple helical complexes using three

ligands of this type and two Ln^{3+} ions have been synthesised, providing much insight into the factors controlling both their structure and photophysical properties.[1]

triple mesocate
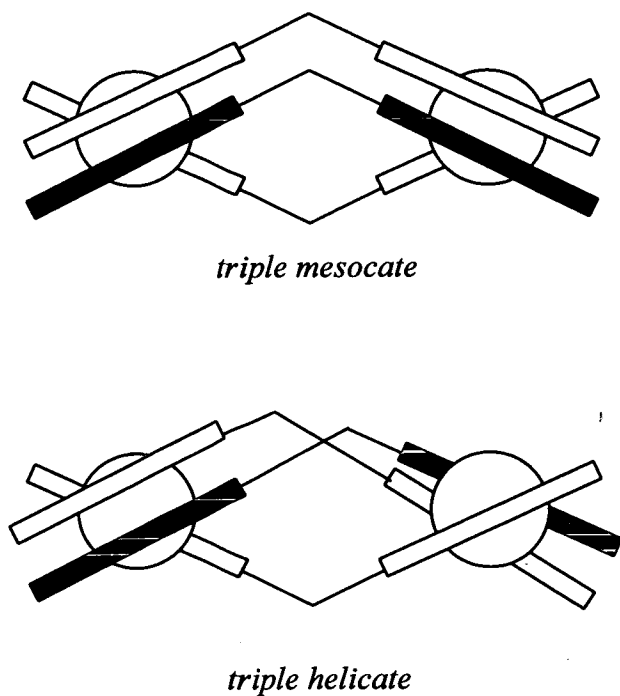
triple helicate

Figure 4.1 Schematic of dinuclear, triple-stranded mesocates and helicates (adapted from reference 25)

28   **29**
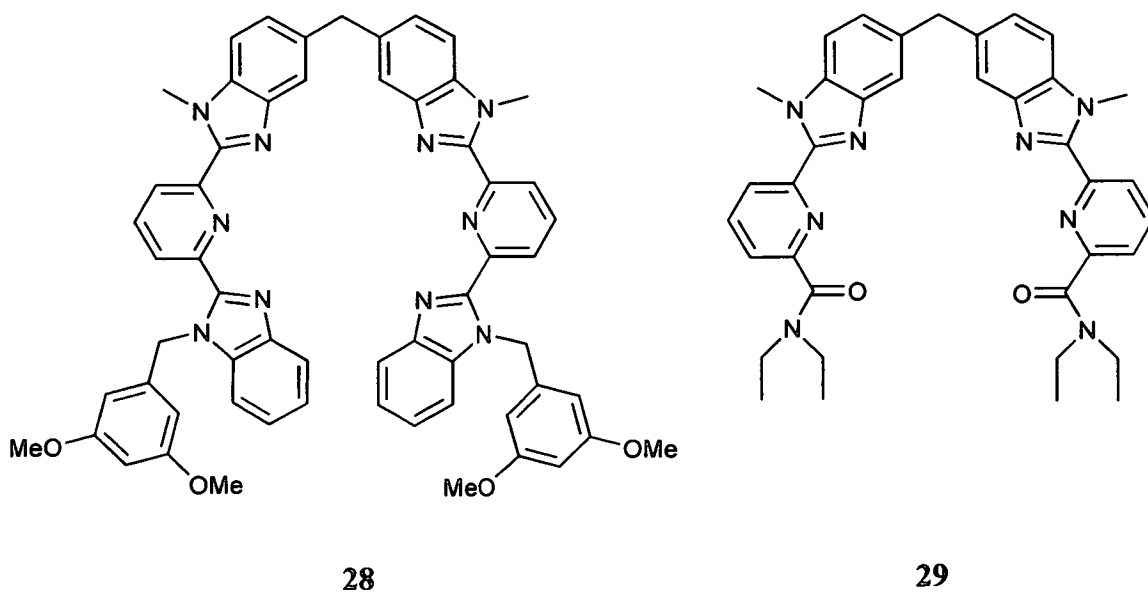
4.1.2 Dinuclear complexes with bis(β-diketonate) ligands

The approach taken in the present study is to utilise bis(bidentate) ligands in a manner analogous to that described for the helicates formed from neutral benzimidazole-pyridine ligands, but using anionic ligands to increase thermodynamic and kinetic stability. The desired structural features of the ligands are two anionic groups separated by a rigid spacer, which prevents both these groups binding the same metal. As the ligand has two anionic sites, charge neutrality could be achieved by the combination of two Ln^{3+} ions and three ligands, giving a neutral dinuclear complex. During the course of this study a report was published that examined helicate formation with a benzimidazole-pyridine anionic ligand that was functionalised with a carboxylic acid.[13] These helicates, the first lanthanide-containing helicates self-assembled in water, have high thermodynamic stability and are kinetically inert, illustrating the advantage of using anionic ligands.

For this study, the bis(β-diketonate) ligand 1,3-bis(3-phenyl-3-oxopropanoyl)benzene (30), hereafter referred to as H_2bis-DBM because of its similarity to dibenzoylmethane (HDBM), has been selected for the role of bis(bidentate) ligand. In general, β-diketonates are an ideal choice as anionic ligands because they are strongly chelating species and can form complexes with virtually every metal cation.[14] In terms of this project, there are two distinct advantages in using a bis(β-diketonate).
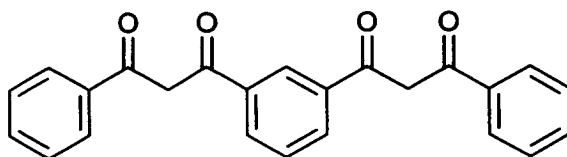
H_2bis-DBM, **30**

Firstly, there is a precedent in the literature for the formation of dinuclear complexes with bis(β-diketonate) ligands. The ligand bis-DBM itself has recently been shown to form triple helical M_2L_3 complexes with Ti(III), V(III), Mn(III) and Fe(III).[15] Similarly,

the cofacial copper complex $Cu_2(XBA)_2$ (**31**) was one of the first examples of a dinuclear transition metal complex of a bis(β-diketonate) ligand.[16] These types of complexes were studied in view of their potential to coordinate other species in the cavity of the complex. Complex **32**, for example, was the first self-assembled macrocyclic host, selectively binding the difunctional Lewis base, 1,4-diazabicyclo[2,2,2]octane.[17]

31   **32**
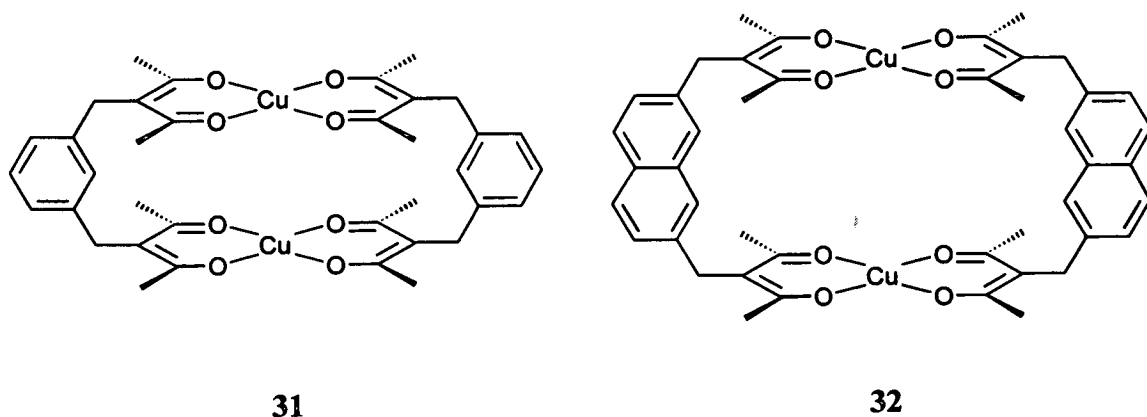
In addition to the ability of these ligands to form dinuclear complexes, the other attraction is that the mononuclear lanthanide complexes of β-diketonate ligands have been extensively studied and are among the most luminescent lanthanide complexes known. As mentioned in Chapter 2, the process of sensitised lanthanide emission via energy transfer from coordinated organic ligands was first established for mononuclear β-diketonate complexes. The mononuclear lanthanide complexes of β-diketonates fall into three main categories as shown in Figure 4.2; tris complexes, anionic tetrakis complexes and adducts of tris complexes with neutral Lewis bases.[18,19] In each case the β-diketonate coordinates in a bidentate fashion to form a six-membered chelate ring.

In view of this, it was envisaged that reaction of bis-DBM with a lanthanide might lead to the formation of two different dinuclear complexes (Figure 4.3). The neutral and dianionic complexes in Figure 4.3 are analogous to the mononuclear tris and tetrakis complexes respectively. A study of dinuclear complexes of bis(β-diketonate) ligands has the added advantage that, in many instances, their chemical and photophysical properties can be compared directly with the corresponding mononuclear species.
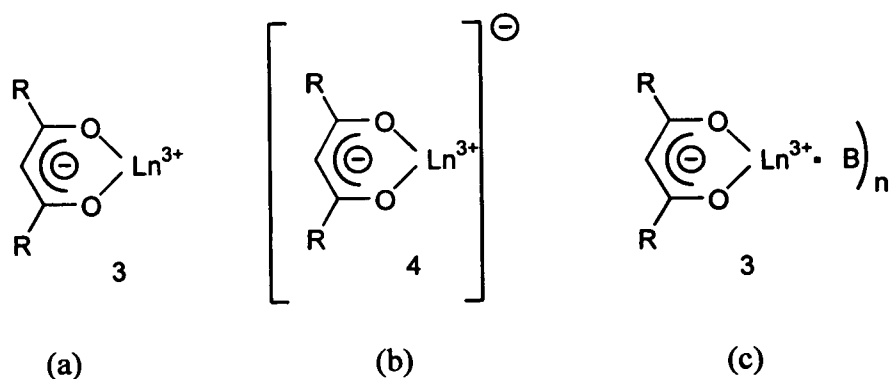
Figure 4.2 Structures of lanthanide β-diketonates; (a) tris complexes, (b) tetrakis complexes and (c) adducts of tris complexes with neutral Lewis base (B)
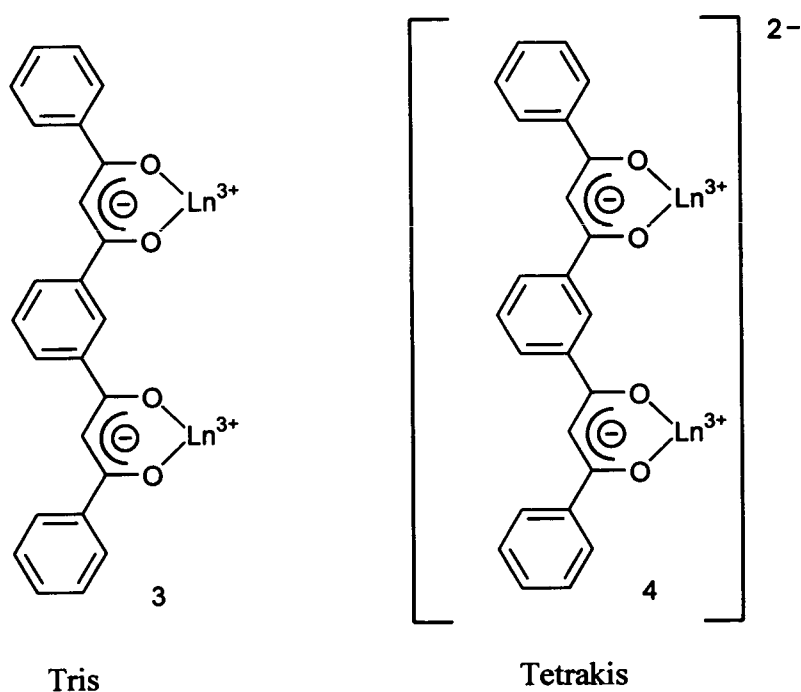
Figure 4.3 Structures of tris and tetrakis dinuclear lanthanide complexes of bis-DBM

Although there are no reports in the literature of the formation of dinuclear lanthanide complexes with bis(β-diketonate) ligands, some studies of Eu^{3+} and bis(β-diketonate) ligands have been reported. Ligand **33** forms a stable 1:1 complex with Eu^{3+} in aqueous solution, and energy transfer occurs from the ligand to the metal.[20] The mononuclear

complex is probably a result of the flexibility of the ligand, allowing both β-diketonate binding units to coordinate to the same metal. Ligand **34**, which can be covalently bound to proteins, forms a luminescent complex with Eu^{3+} in aqueous solution and has been used successfully as a luminescent label in time-resolved fluoroimmunoassays.[21] The large complex formation constant is attributed to the tetradentate coordination of the ligand.
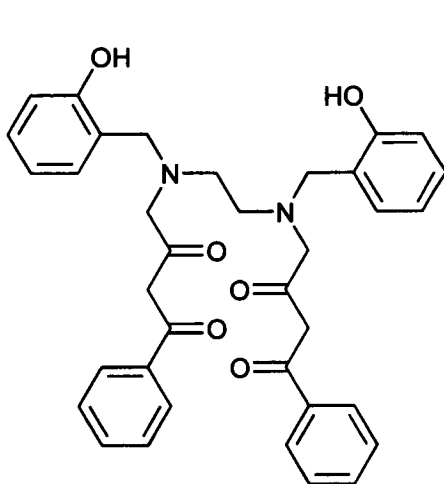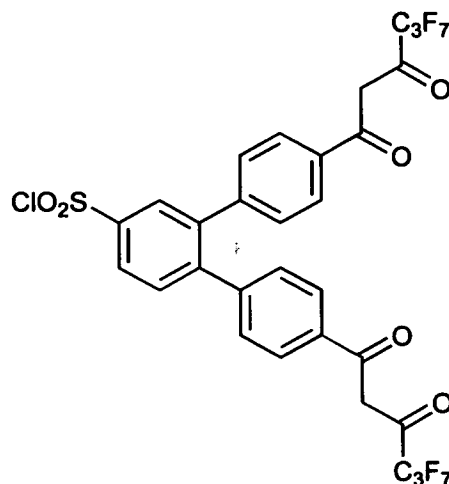
33   **34**

4.2   SYNTHESIS AND CHARACTERISATION OF H₂BIS-DBM

The ligand H₂bis-DBM is obtained in reasonable yield (18%) by the Claisen condensation of dimethyl isophthalate and acetophenone; the previously reported preparation[22] was modified by using NaH and THF in place of $NaNH_2$ and diethyl ether respectively due to the availability of these materials.

The structures of free β-diketone ligands have been reported extensively in the literature, primarily because of their interesting tautomerism. A free β-diketone can exist in either the keto or enol tautomeric forms and these are related by a 1,3 proton shift. In addition, each of these tautomeric forms can exist as a number of conformers. The predominant conformers for β-diketones are the *cis*-diketo and *cis*-enol forms.[23]

These two conformers are shown for dibenzoylmethane (HDBM) in Figure 4.4. As mentioned previously, HDBM can be viewed as the parent β-diketone of H_2bis-DBM.

(a)   (b)
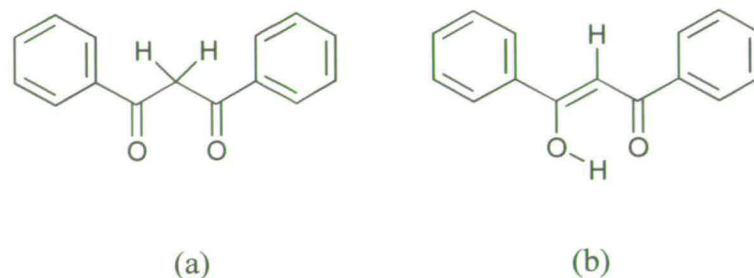
Figure 4.4 Structures of the *cis*-diketo (a) and *cis*-enol (b) tautomeric forms of dibenzoylmethane

A previously reported IR study of this ligand suggests H_2bis-DBM exists in the enol form in the solid state, with strong bands at 1563 and 1608 cm^{-1} assigned to absorption by the enol-chelate.[22] The crystal structure of H_2bis-DBM (Figure 4.5), which does not contain any solvent molecules, confirms that this bis(β-diketone) exists in the enol form in the solid state. The two enolic rings adopt a *trans* orientation with respect to the central phenyl ring. Examination of the packing of H_2bis-DBM in the crystal structure shows an absence of hydrogen bonding interactions, but indicates the adopted structure is influenced by π-π stacking of the aromatic molecules.
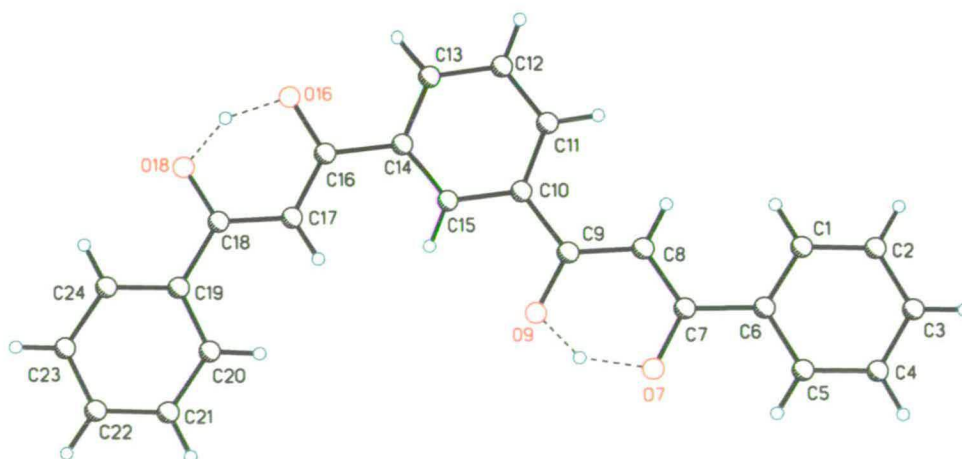
Figure 4.5 Molecular structure of H_2bis-DBM showing the atomic numbering scheme

This structure can be compared with the reported structure of HDBM.[24] The average C-C distance for the phenyl rings is 1.39 Å for both H_2bis-DBM and HDBM. In HDBM, the C-O bonds are not equidimensional (1.292 Å and 1.317 Å), implying that the enolic proton is not shared symmetrically with the carbonyl oxygen.[23] For H_2bis-DBM, the carbonyl bond lengths for C(7)-O(7), C(9)-O(9), C(16)-O(16) and C(18)-O(18) are; 1.290(4), 1.297(4), 1.300(5) and 1.283 (5) Å, respectively. Though the differences are not as significant as for HDBM, in H_2bis-DBM the O(7)/O(9) ring appears to be symmetrical, whereas the O(16)/O(18) ring does not. What is of more significance is that the chemical inequivalence of the carbonyl groups in each chelate ring in H_2bis-DBM (unlike those in HDBM) does not appear to manifest itself in the electronic distribution. In this respect, the solid state structure of H_2bis-DBM is like a superposition of two HDBM molecules.

In solution, β-diketones exist as mixtures of keto and enol forms.[23] In most organic solvents, however, β-diketones are predominately (> 90%) enolised. These conformers normally have a sufficiently distinct set of resonances in their ^{1}H NMR spectra that the molar proportions can be obtained. In the ^{1}H NMR spectrum of H_2bis-DBM in CDCl$_3$ (Figure 4.6), only resonances attributable to the enol form can be distinguished, most noticeably the singlet at δ 6.94 for the two equivalent methine protons (*i.e.* the ligand is C_2-symmetric). HDBM is also known to be 100% enolised in CCl$_4$.[23] Aided by a ^{1}H-^{1}H COSY spectrum (Figure A4 in Appendix I), the other resonances can be assigned as follows; the triplet at δ 8.65 is due to the proton that is *ortho* to both carbonyl substituents of the central phenyl ring, a doublet of doublets at δ 8.17 is due to the other *o*-Ar protons, a multiplet at δ 7.98-8.04 is assigned to the *o*-Ar protons of the outside phenyl rings and the multiplet at δ 7.50-7.66 is due to the seven *m*- and *p*-Ar protons.

Confirmation that H_2bis-DBM is in the enol form is provided by the UV absorption spectrum in methanol (Figure 4.7). The intense band with λ_{max} = 357 nm (ε_{max} = 48 000 dm^3 mol^{-1} cm^{-1}) is attributed to singlet-singlet $\pi \rightarrow \pi^*$ enol absorption and is characteristic of the enol form of β-diketones. This spectrum is in agreement with the previously reported data of an ethanolic solution of the ligand.[22]
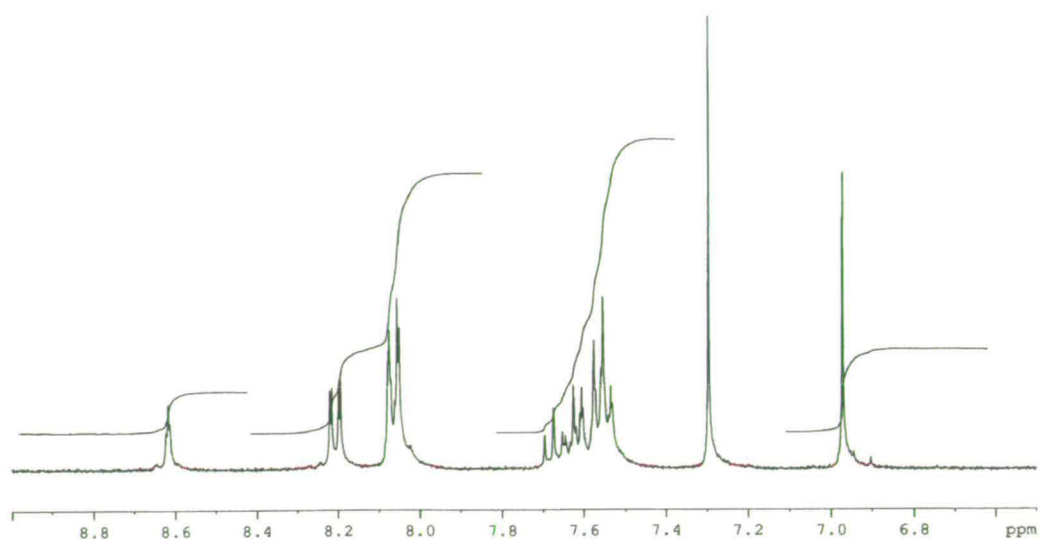
Figure 4.6 ^{1}H NMR spectrum of H_2bis-DBM in CDCl$_3$ (360 MHz)
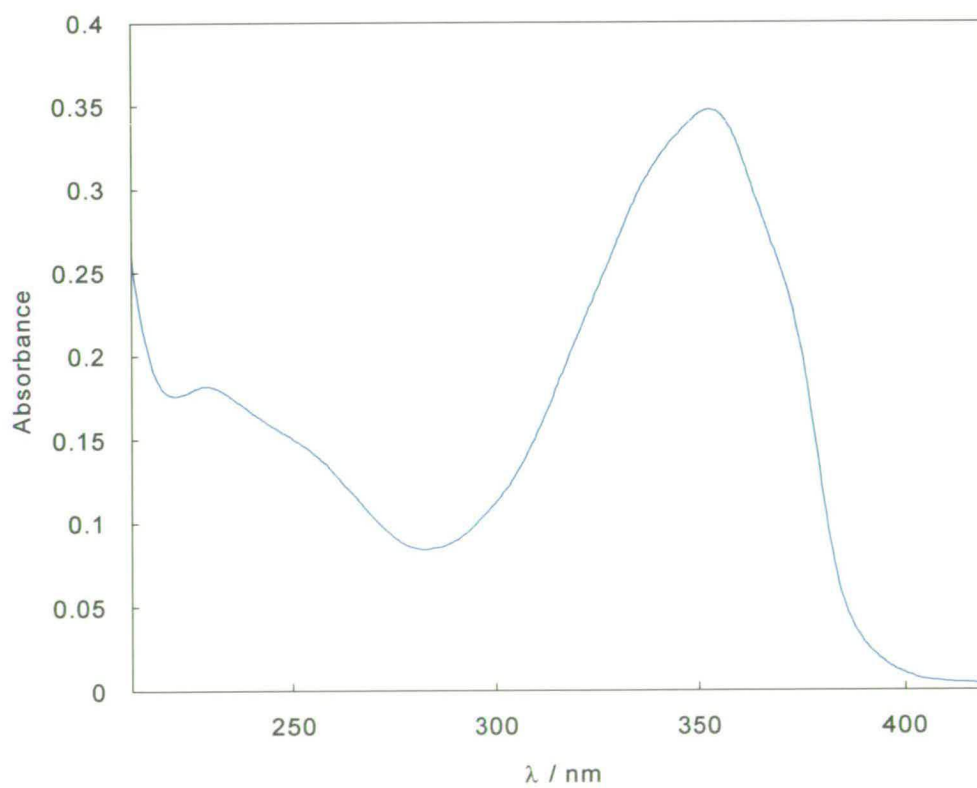
Figure 4.7 Absorption spectrum of H_2bis-DBM in MeOH (7.3×10^{-6} mol dm^{-3})

4.3   DINUCLEAR TRIS CHELATES OF BIS-DBM

4.3.1 Synthesis and characterisation of tris chelates of bis-DBM

The simplest dinuclear complex of a Ln^{3+} ion and bis-DBM was expected to be the "tris" complex, as shown in Figure 4.3, therefore this was the first synthetic target. The reaction of H_2bis-DBM (3 equiv.) with hydrated europium or yttrium chloride (2 equiv.) and triethylamine (6 equiv.) in a mixed $CHCl_3$/MeOH solvent leads to the precipitation of a pale yellow compound which, after washing, analyses as M_2(bis-DBM)$_3 \cdot n H_2O$ with $n = 1$ for M = Eu and $n = 2$ for M = Y. The solids are soluble in DMF and slightly soluble in alcoholic solvents.

Although the stoichiometry of these products matches that of the target M_2L_3 dinuclear complex, any cluster of general formula $[M_{2x}L_{3x}]$ would give the same analysis. There are only two ways to unambiguously assign the structural formulae of dinuclear complexes in practice;[11] mass spectrometry and crystallography. While mass spectrometry was very informative, attempts to grow crystals of the europium or yttrium complexes were unsuccessful, yielding only powders.

The FAB(+)-MS spectrum of the isolated europium product exhibits intense peaks with mass distribution $m/z = 1407\text{-}1414$, corresponding to $[Eu_2(\text{bis-DBM})_3 + H]^+$. Similarly the FAB(+)-MS spectrum of the yttrium product exhibits an intense peak with $m/z = 1283$, corresponding to the dinuclear species $[Y_2(\text{bis-DBM})_3 + H]^+$. Confirmation of these peak assignments is given by the accurate FAB(+)-MS spectrum of the europium sample (Figure 4.8). Since the Eu^{3+} ions exist as either the ^{151}Eu (48 %) or ^{153}Eu (52 %) isotopes, the accurate mass spectrum provides conclusive identification of a dinuclear complex.
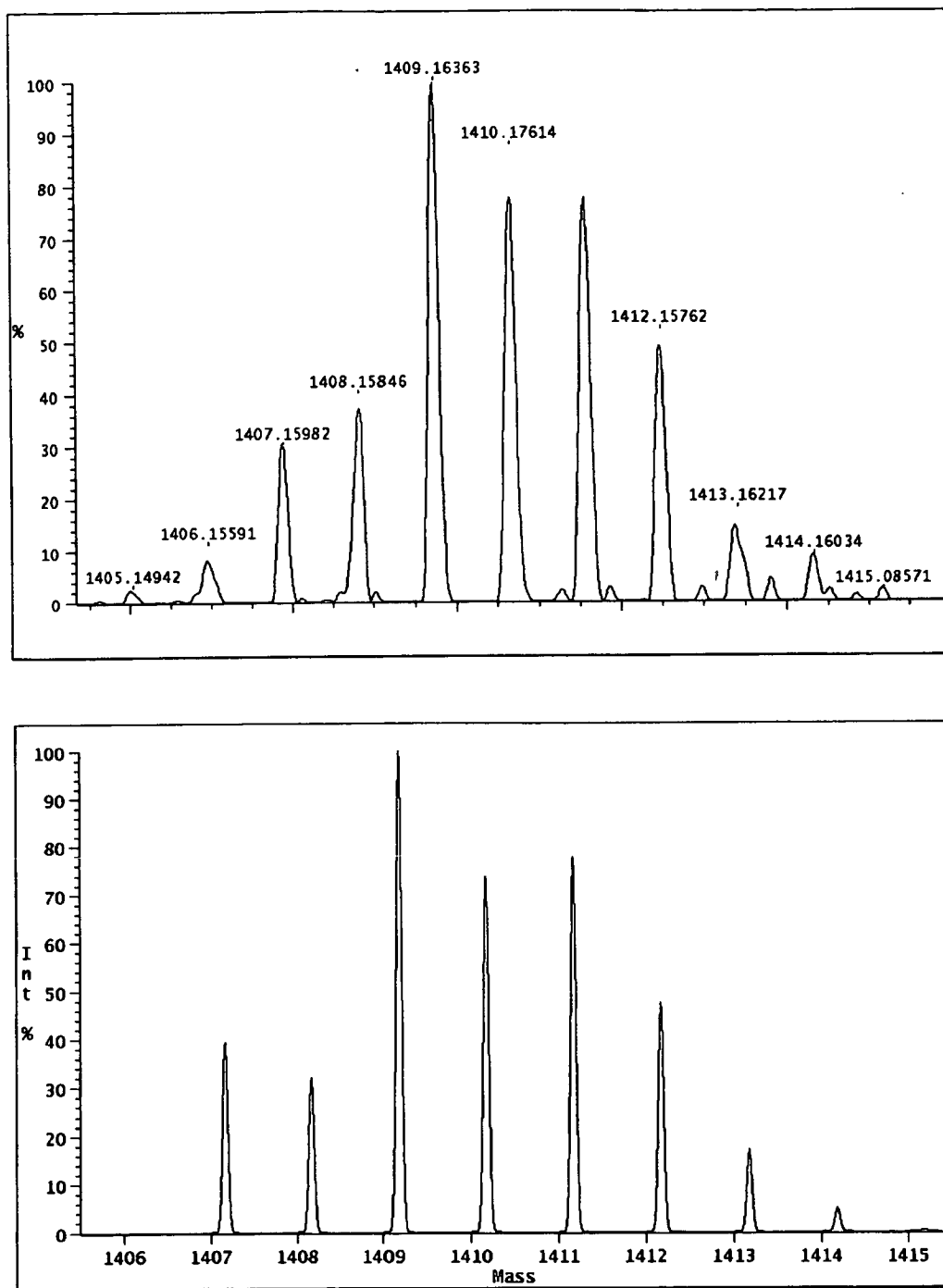
Figure 4.8 Accurate FAB(+)-MS spectrum of [Eu₂(bis-DBM)₃] (top) and theoretical isotopic

profile (bottom)

Further evidence for the structural formulation is given by electrospray mass spectrometry (ES-MS). This is a particularly useful technique because it probes the

nature of the species that exist in solution. The ES(+)-MS spectrum of [Eu₂(bis-DBM)₃] in a DMF/CH₃CN solution is shown in Figure 4.9. The peaks centred on *m/z* 1410 can undoubtedly be assigned as $[M + H]^+$ for the dinuclear complex, by comparison with the accurate FAB(+)-MS in Figure 4.8.
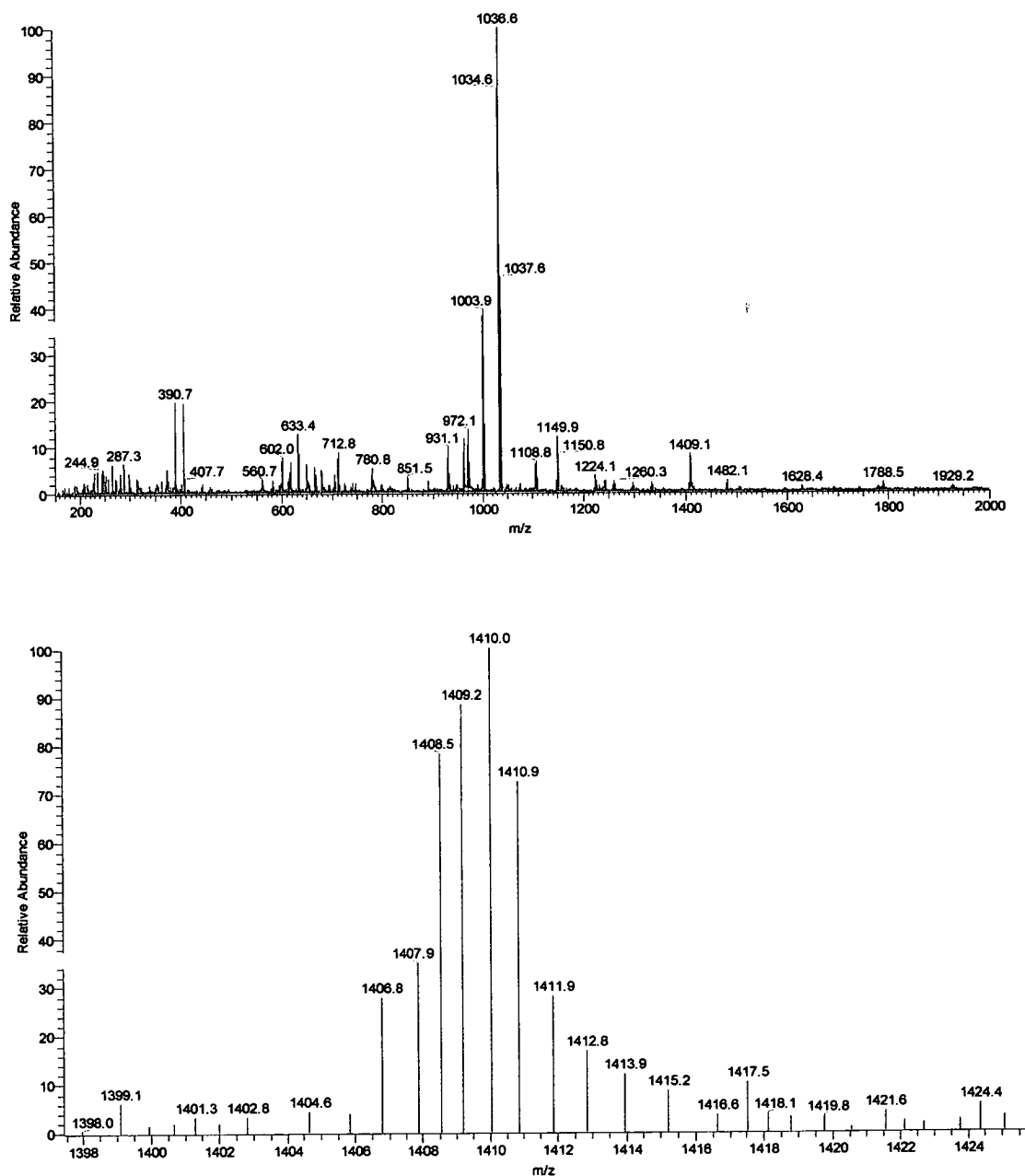
Figure 4.9   ES(+)-MS spectrum of [Eu₂(bis-DBM)₃] (7 × 10⁻⁶ mol dm⁻³) in DMF/CH₃CN/methanoic acid (1 : 99 : 0.1); whole spectrum (top) and expanded region (bottom)

The success of the electrospray technique depends intimately on many factors, such as the ability of the sample to ionise, the nature of the solvent and the solvation processes.[25] It works particularly well with preformed ions in solvents such as water and methanol. The weak signal is probably due to a difficulty in the stable, neutral complex forming MH^+ (despite the 0.1 % methanoic acid present) and possibly also due to the strong solvation by DMF. Evidence for the latter explanation is given by the strong peaks at m/z 1035 and 1036 in the ES(+)-MS spectrum in Figure 4.9, which are tentatively assigned to $[Eu(bis\text{-}DBM)_2\cdot DMF_2 + 2H]^+$.
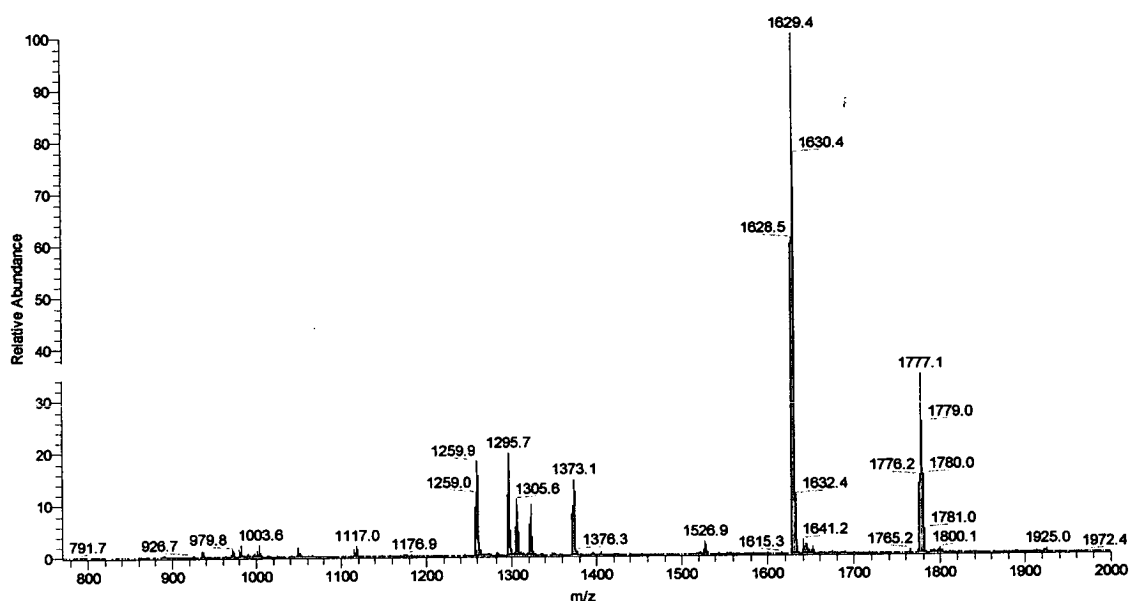
Figure 4.10 ES(–)-MS spectrum of $[Eu_2(bis\text{-}DBM)_3]$ $(7 \times 10^{-6} \text{ mol dm}^{-3})$ in DMF/CH$_3$CN/methanoic acid (1: 99 : 0.1)

The ES(–)-MS spectrum of the same sample is shown in Figure 4.10. In the negative mode, ionisation takes place by loss of the metal ion and/or association with a ligand molecule, leading to intense peaks corresponding to $[Eu(bis\text{-}DBM)_4 + 5H]^-$ and $[Eu_2(bis\text{-}DBM)_4 + H]^-$, centred at m/z 1629 and 1777 respectively. MS-MS of this sample shows that the former peak is not a breakdown product of the latter. The peak centred at m/z 1259 corresponds to $[Eu(bis\text{-}DBM)_3 + 2H]^-$, and MS-MS of this sample shows it to be the main breakdown product of the $[Eu(bis\text{-}DBM)_4 + 5H]^-$ peak at m/z

1629. These ES(−)-MS data support the view that the solution species prior to electrospray ionisation is [Eu₂(bis-DBM)₃]. In addition, the peak at *m/z* 1777 for [Eu₂(bis-DBM)₄ + H]⁻ is particularly interesting because this formula corresponds to the tetrakis dinuclear complex shown in Figure 4.3; this indicates that such a structure is feasible.
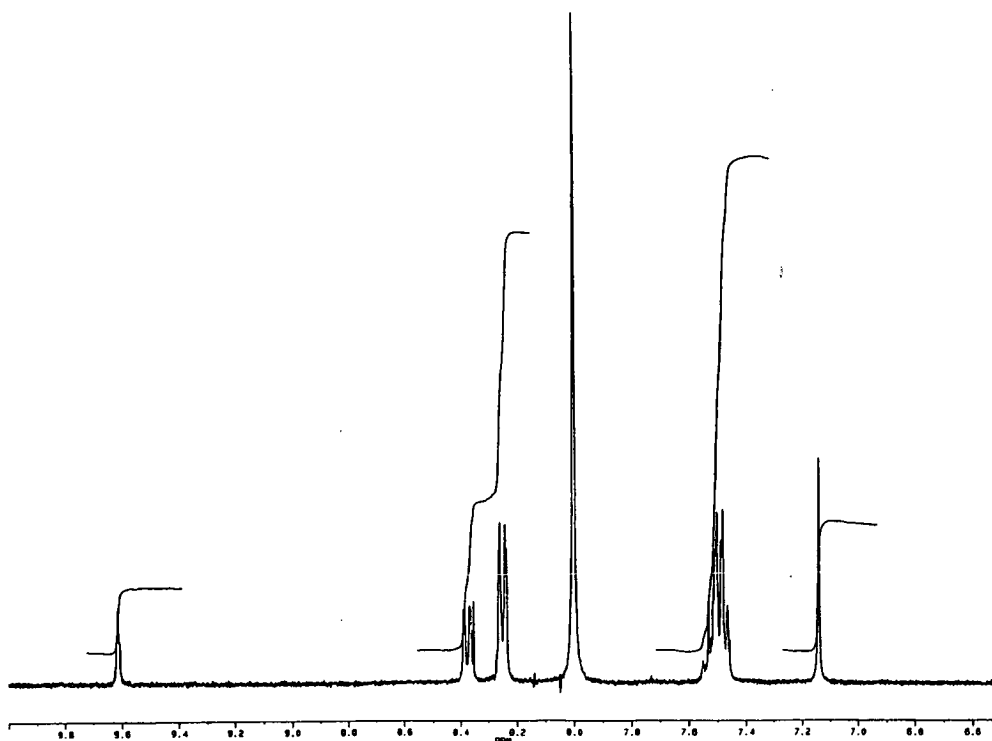
Figure 4.11 ¹H NMR spectrum of [Y₂(bis-DBM)₃] in DMF-*d₇*

The ¹H NMR spectrum of [Y₂(bis-DBM)₃] in DMF-*d₇* is shown in Figure 4.11 (the ion Y³⁺ was chosen because it is a good diamagnetic replacement for Eu³⁺). No signals, other than for the solvent, were found outside the δ 7-10 range shown (the resonance at δ 8.00 is also due to the solvent). The splitting pattern is essentially identical to that of the free ligand (Figure 4.6), the only difference being a shift of the resonances for the complex to higher frequency. This shift is *ca.* 1 ppm for the proton that is *ortho* to both carbonyl substituents in the central phenyl and *ca.* 0.1-0.2 ppm for all of the other resonances. The large shift in the former case is presumably due to the proximity of this proton to two tripositive ions. The presence of a singlet at δ 7.14 for the methine protons

means that, on the NMR timescale, all three ligands are identical and are C_2-symmetric. The $^{13}C\{^1H\}$ NMR spectrum of [Y$_2$(bis-DBM)$_3$] confirms the complex's high symmetry, showing only 11 unique resonances.

The ^1H NMR spectrum of [Eu$_2$(bis-DBM)$_3$] (Figure 4.12) shows quite a different splitting pattern to the free ligand and to [Y$_2$(bis-DBM)$_3$]. In the presence of the paramagnetic Eu^{3+} ion, all of the signals appear at a lower frequency than those of the free ligand (some are shifted by *ca.* 3-4 ppm). While overlap and broadening make it difficult to unambiguously assign the resonances, the singlet at δ 3.62 is probably due to the methine protons. Integration shows that all the other proton signals are accounted for by the multiplets at δ 6.11-6.48 and 4.27-4.30
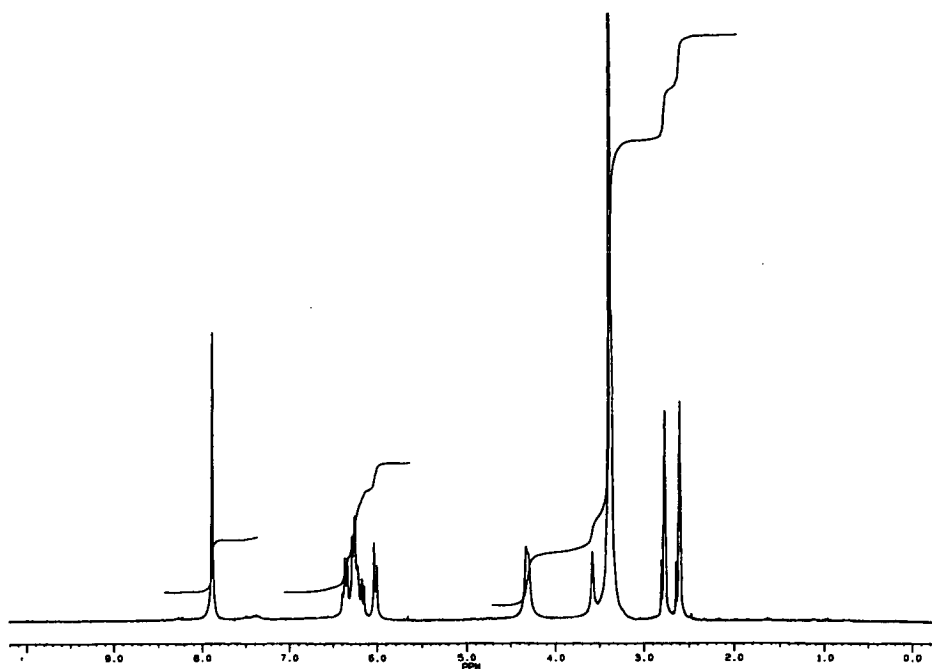
Figure 4.12 ^1H NMR spectrum of [Eu$_2$(bis-DBM)$_3$] in DMF-d_7

In light of the mass spectral and NMR data, the europium and yttrium complexes of bis-DBM can indeed be represented by the "tris" structure shown in Figure 4.3. They are the dinuclear analogues of the well-studied mononuclear tris chelates of β-diketonates.

In Figure 4.3, no attempt was made to specify the numbers of solvent molecules that

might be coordinated to the metal. Many of the tris diketonates of lanthanides are 8-coordinate in the solid state, and this often decreases to 6- or 7-coordination as the ionic radius decreases across the series or for a bulky ligand.[26] Elemental analysis indicates that there are one and two water molecules coordinated to the europium and yttrium complexes of bis-DBM respectively. However, the coordinated water molecules in the mononuclear complexes can usually be removed by vacuum dehydration so that the hydration state of the analysed samples can vary, depending on the specific preparative conditions. The number of coordinated solvent molecules can be ascertained, under certain conditions, using time-resolved luminescence spectroscopy and this approach is used in the next section for [Eu$_2$(bis-DBM)$_3$] in solution.

While the structure in Figure 4.3 is complete in terms of connectivity, there is no information regarding the stereochemistry of the complex. There are essentially two idealised conformations that the complex can adopt: triple helicate or triple mesocate, as mentioned previously. In the first type, the bis-DBM ligands undergo a helical twist along an axis connecting the two metal ions, and in the second case there is no twist. In addition, the adopted conformations may differ between the solid state and solution.

The main method for characterising the stereochemistry of complexes in the solid state is crystallography, whereas NMR spectroscopy is the method of choice for solution. It is not possible to tell whether the complex adopts a helical structure from the ^{1}H NMR spectrum of [Y$_2$(bis-DBM)$_3$] in DMF-d_7. The reasons for this are twofold. Firstly, the structure lacks a NMR handle, such as the protons of a methylene group, to exploit any internal stereoisomerism.[25] Secondly, helical enantiomers in a racemic mixture are not resolvable by NMR. This can be overcome by the use of a chiral auxiliary to convert a racemic mixture into a diastereomeric mixture.[27] The two feasible chiral auxiliaries are lanthanide shift reagents, which are unsuitable in the present context, and chiral solvating agents. Addition of Pirkle's reagent, a well known chiral solvating agent, had no discernible effect on the ^{1}H NMR spectrum of [Y$_2$(bis-DBM)$_3$] in DMF-d_7, though this could be due to the high polarity of the DMF solvent, thereby preventing any interaction between the solvating agent and the complex.

4.3.2 Photophysical studies of tris chelates of bis-DBM

Ligand-centred levels

The absorption spectra of [Y$_2$(bis-DBM)$_3$] and [Eu$_2$(bis-DBM)$_3$] in DMF are very similar, displaying intense $\pi \rightarrow \pi^*$ bands at λ_{max} = 357 nm (ε_{max} = 160 000 dm^3 mol^{-1} cm^{-1}) and 359 nm (ε_{max} = 150 000 dm^3 mol^{-1} cm^{-1}) respectively (Figure 4.13). The absorption spectrum of [Eu$_2$(bis-DBM)$_3$] in methanol matches that of the DMF solution. The profiles of the spectra are very similar to that of the free ligand, and the molar extinction coefficients confirm that there are three ligands per complex. The spectra of these bis-DBM complexes are also very similar to tris lanthanide complexes of DBM,[28] which have λ_{max} = 351 nm (ε_{max} = 66 000 dm^3 mol^{-1} cm^{-1}), in agreement with the previously noted similarities between the free ligands.

The room temperature emission spectrum of [Y$_2$(bis-DBM)$_3$] in DMF exhibits a broad fluorescence band with λ_{max} = 436 nm, attributable to a ligand $\pi^* \rightarrow \pi$ transition (Figure 4.14). More structure is observed in the emission spectrum of [Y$_2$(bis-DBM)$_3$] in a DMF/MeOH (4:1 vol/vol) glass at 77 K, with a fluorescence peak at 439 nm and two new bands centred at 492 nm and 526 nm, due to ligand phosphorescence (Figure 4.14).

It is common in β-diketonate complexes of lanthanides to observe two or three well-defined ligand phosphorescence bands. These are particularly strong when low-lying metal-centred levels are absent, as is the case with yttrium, because energy cannot be transferred from the ligand triplet state to the metal. The phosphorescence yield is also large because of the increased intersystem crossing in the presence of Y^{3+} (heavy-atom effect). As the energy of the ligand-centred triplet state does not depend significantly on the metal,[29] measurement of the short-wavelength, 0-0 transition of [Y$_2$(bis-DBM)$_3$] gives the energy of the $^3\pi\pi^*$ level for all the tris lanthanide chelates of bis-DBM. The 0-0 transition in this case is the band at 492 nm (20 300 cm^{-1}), and this is separated from the next band by *ca.* 1300 cm^{-1}. For comparison, the reported phosphorescence spectrum of [Gd(DBM)$_3$] also has λ_{max} = 492 nm and a vibrational progression of 1300 cm^{-1}, assigned to either C-C or C-O stretching frequencies.[28,30]

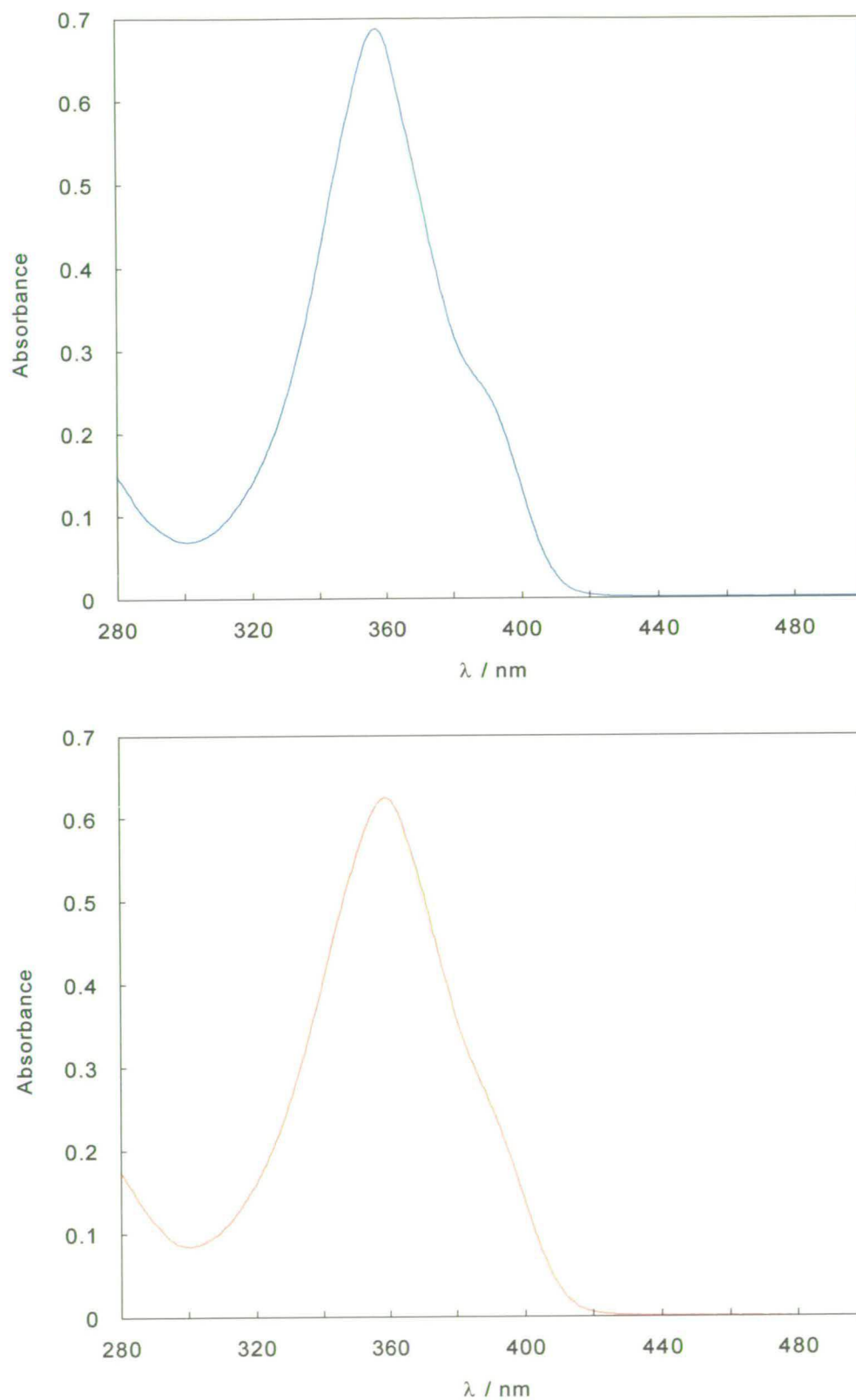**Figure 4.13** Absorption spectra of $[Y_2(bisDBM)_3]$ $(4.4 \times 10^{-6} \text{ mol dm}^{-3})$ in DMF (top) and $[Eu_2(bis\text{-}DBM)_3]$ $(4.2 \times 10^{-6} \text{ mol dm}^{-3})$ in DMF (bottom)
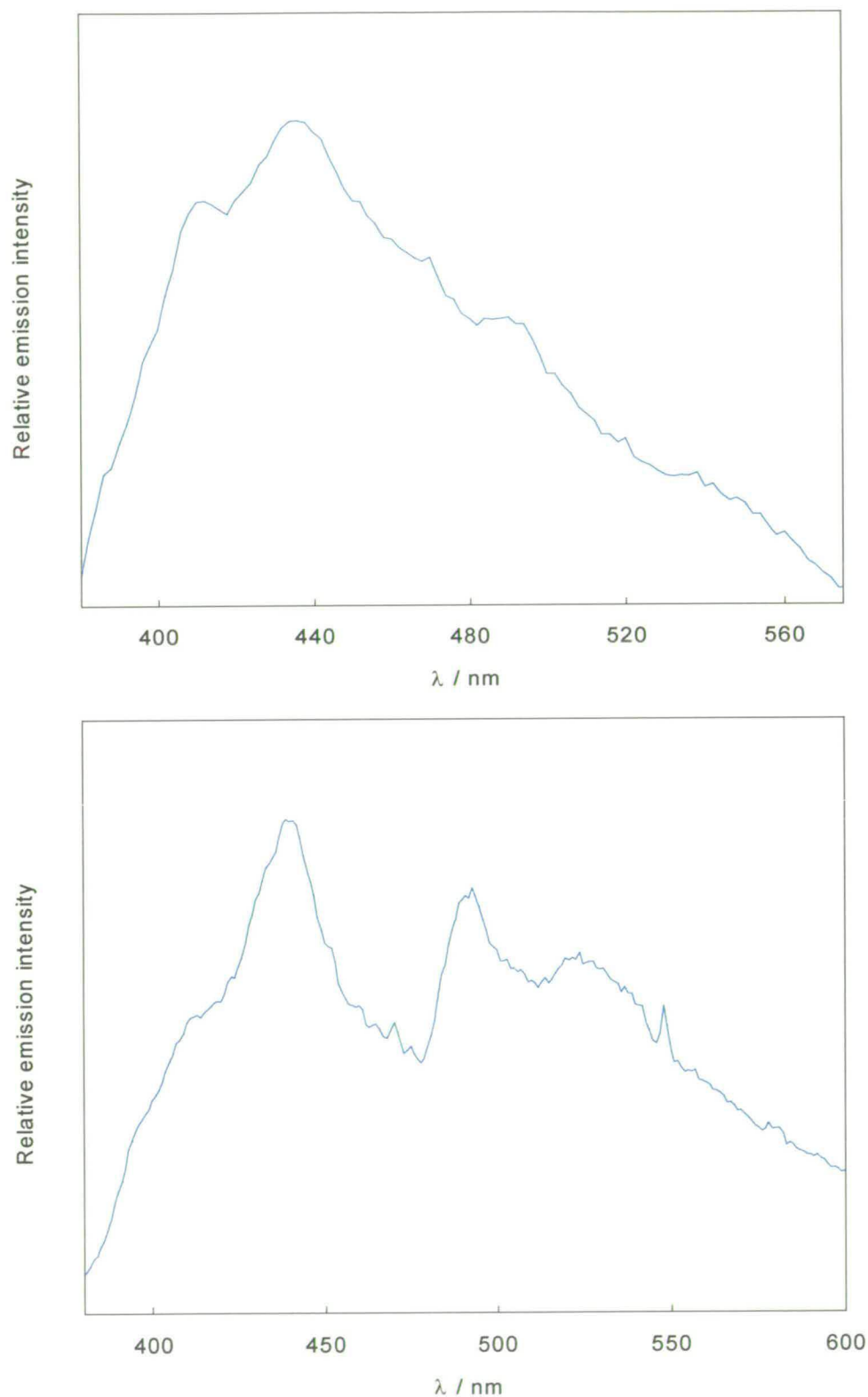
Figure 4.14 Corrected emission spectra of $[Y_2(bis\text{-}DBM)_3]$ ($\lambda_{ex} = 340$ nm): 1.3×10^{-6} mol dm^{-3} in DMF at room temperature with the sample degassed by bubbling with N_2 (top); 1.1×10^{-6} mol dm^{-3} in 1:4 DMF/MeOH at 77K (bottom)
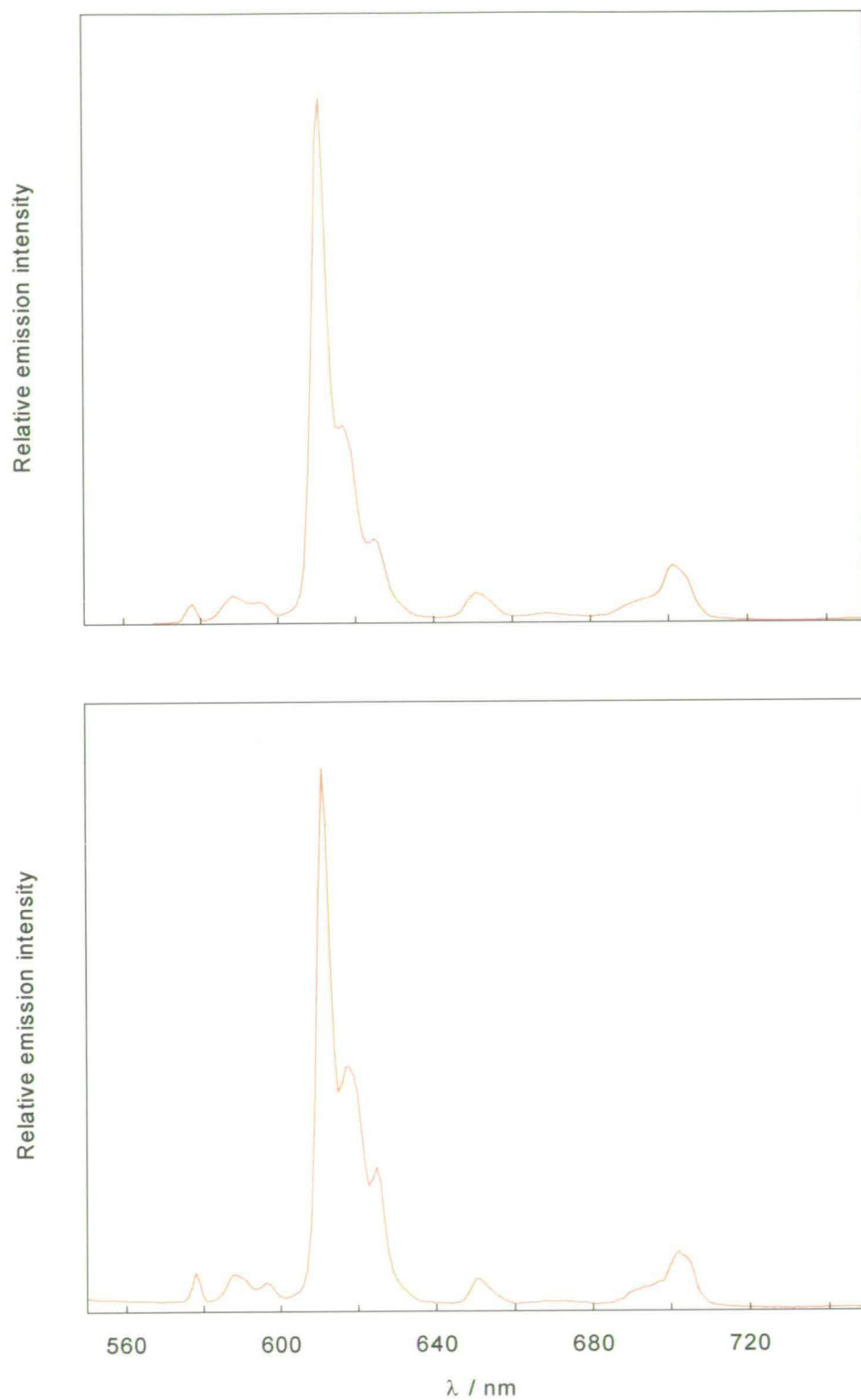
Figure 4.15 Corrected emission spectra of [Eu$_2$(bis-DBM)$_3$] [2 nm bandpass (em.)]: 2×10^{-6} mol dm^{-3} in DMF, $\lambda_{ex} = 350$ nm (top); 2×10^{-7} mol dm^{-3} in MeOH, $\lambda_{ex} = 360$ nm (bottom)

Metal-centred levels

Light excitation into the ligand $^1\pi\pi^*$ state of [Eu$_2$(bis-DBM)$_3$] in DMF (λ_{ex} = 350 nm) at room temperature is followed by strong luminescence, characteristic of the $^5D_0 \rightarrow {}^7F_J$ (J = 0-4) emission bands of Eu^{3+} (Figure 4.15). The emission spectrum of [Eu$_2$(bis-DBM)$_3$] in methanol (λ_{ex} = 360 nm) is also shown in Figure 4.15. Although the resolution of these spectra precludes a detailed analysis of the symmetry of the complexes, it is evident that the structured emission pattern is the same in both solvents, showing that there are no solvent-dependent structural changes. The spectra are dominated by the $^5D_0 \rightarrow {}^7F_2$ transition, which has its most intense peak at 611 nm.

Confirmation that the Eu^{3+} luminescence occurs via excitation of ligand-centred bands is given by the excitation spectrum in DMF (Figure 4.16). This spectrum has a band maximum at 363 nm and matches the corresponding absorption spectrum (Figure 4.13) very closely. Similar results are obtained for the complex in a methanolic solution.
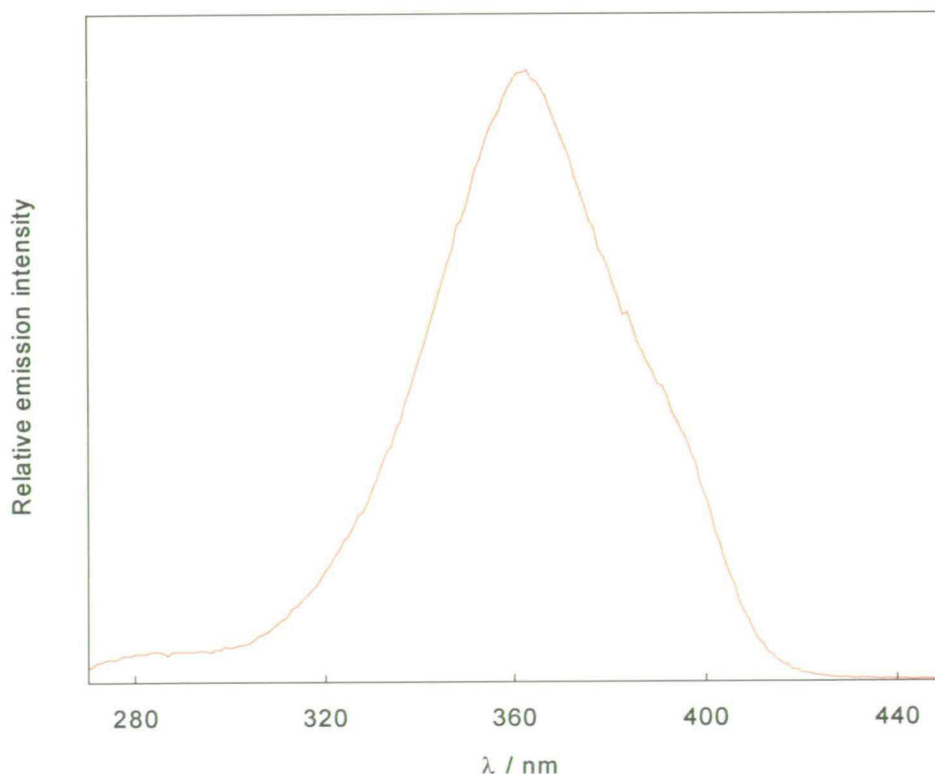
Figure 4.16 Excitation spectrum of [Eu$_2$(bis-DBM)$_3$] (2×10^{-7} mol dm^{-3})

in DMF; λ_{em} = 610 nm

In order to gain a fuller understanding of the photophysical processes involved, a time-resolved study was undertaken. The luminescence lifetimes of [Eu$_2$(bis-DBM)$_3$] in DMF, MeOH and MeOD were measured at room temperature (hereafter indicated as 300 K) and 77 K (Table 4.1), following excitation into ligand-centred bands (λ_{ex} = 355 nm). On each occasion, the $^5D_0 \rightarrow {}^7F_2$ transition was monitored (λ_{em} = 616 nm).

Table 4.1 Luminescence lifetime of the Eu^{3+} ($^5D_0$) level in [Eu$_2$(bis-DBM)$_3$] (λ_{ex} = 355 nm)

Solvent	Concentration / mol dm^{-3}	τ (300 K) / ms	τ (77 K) / ms
DMF	4.2×10^{-6}	0.22	0.46
MeOH	2×10^{-7}	0.20	0.35
MeOD	2×10^{-7}	0.30	0.65

Each of the measured luminescence decays can be described by monoexponential kinetics, even at 77 K, and this suggests that both Eu^{3+} ions have the same environment in the complex. This would certainly agree with the high symmetry observed in the NMR spectra of [Y$_2$(bis-DBM)$_3$]. The measured lifetimes of [Eu$_2$(bis-DBM)$_3$] are also in good agreement with previously studied europium β-diketonates. For example, the reported lifetime of the analogous Eu(DBM)$_3$ complex in methanol is 0.36 ms at 77 K.[31]

It is clear from Table 4.1 that there is a pronounced variation in the $^5D_0$ luminescence decay with solvent. This can be summarised as follows:

$$\tau \text{ (MeOD)} > \tau \text{ (DMF)} > \tau \text{ (MeOH)}$$

This trend can be partly rationalised in terms of the vibrational quenching effect of coordinated solvent molecules. The lifetime is longer in MeOD than in MeOH due to the replacement of the high-energy O–H oscillators with low-energy O–D oscillators. In DMF, the measured lifetimes are intermediate between those for MeOH and MeOD. In this case, the DMF (which was not dried prior to use) probably contains traces of water which coordinate to the metal ion.

As with H_2O/D_2O systems, measurement of lifetimes in MeOH and MeOD allows an estimation of the number of coordinated solvent molecules (q) (equation 4.1):[32]

$$q = A(1/\tau_{MeOH} - 1/\tau_{MeOD})$$
(4.1)

where A is a proportionality constant for a given ion (A is 2.1 and 8.4 for Eu^{3+} and Tb^{3+} respectively) and the lifetimes are given in ms. The error in q is reported to be ± 0.5 by this method.

Application of equation 4.1 to the values given in Table 4.1, gives the values $q = 3.6$ and 2.8 at 300 K and 77 K respectively. Within experimental error, this is good evidence that for $[Eu_2(bis\text{-}DBM)_3]$ in methanol there are three solvent molecules coordinated to each Eu^{3+} ion, giving the Eu^{3+} ions the common solution coordination number of nine.

In addition to a solvent-dependence, the $^5D_0$ luminescence lifetime increases dramatically with a decrease in temperature from room temperature to 77 K in each of the three solvents. To explain such behaviour, it is first important to quantify it. The overall luminescence decay rate constant, k, can be expressed by equation 4.2:

$$k = k_r + k_{nr}(T) + k_{nr}(OH) + k_{nr}(\text{other vibr.})$$
(4.2)

where k_r is the radiative rate constant, $k_{nr}(T)$ is the non-radiative temperature-dependent rate constant, $k_{nr}(OH)$ is the non-radiative temperature-independent rate constant due to O–H oscillators and $k_{nr}(\text{other vibr.})$ is the same rate constant for vibrations other than O–H.[33]

The values of these constants can be obtained for $[Eu_2(bis\text{-}DBM)_3]$ from the measurements made in MeOH and MeOD if the following assumptions are made: $k_{nr}(\text{other vibr.})$ is negligible, coupling with O–D oscillators is inefficient and at 77 K thermally activated processes do not operate. It follows that:

$$k_r = 1 / \tau(77 \text{ K, OD}) \tag{4.3}$$

$$k_{nr}(300 \text{ K}) = 1 / \tau(300 \text{ K, OD}) - 1 / \tau(77 \text{ K, OD}) \tag{4.4}$$

$$k_{nr}(OH) = 1 / \tau(300 \text{ K, OH}) - 1 / \tau(300 \text{ K, OD}) \tag{4.5}$$

Calculations for $[Eu_2(\text{bis-DBM})_3]$ using equations 4.3-4.5 give values of 1500 s^{-1}, 1800 s^{-1} and 1700 s^{-1} for k_r, $k_{nr}(300 \text{ K})$ and $k_{nr}(OH)$ respectively. The term $k_{nr}(OH)$ was used to calculate the number of coordinated solvent molecules in equation 4.1, and the value of 1700 s^{-1} is indicative of an efficient non-radiative pathway.

The temperature dependent rate constant, $k_{nr}(T)$, plays a role when short-lived, higher-energy states are thermally accessible, and in this instance, the calculated value of 1800 s^{-1} for $k_{nr}(300 \text{ K})$ is significant. A common deactivation process encountered in lanthanide complexes is the back transfer of energy from the metal excited state to the ligand triplet state. In view of the similarities between the bis-DBM complexes and previously studied lanthanide β-diketonates, the energy transfer process probably takes place from the triplet level. From the phosphorescence data, the triplet state is at 20 300 cm^{-1}, which is 3000 cm^{-1} above the $^5D_0$ level of Eu^{3+}. This gap is too large, however, to allow the reverse process. This is confirmed by the lack of any changes in lifetime following deaereation of a DMF solution of $[Eu_2(\text{bis-DBM})_3]$ with O_2-free N_2. In fact, it is not uncommon for the luminescence decay of europium β-diketonates to be strongly temperature dependent. In these cases, as in many other europium complexes, the deactivation occurs via a ligand to metal charge transfer state.[34] It is highly probable, therefore, that the thermal quenching of the $^5D_0$ level of Eu^{3+} in $[Eu_2(\text{bis-DBM})_3]$ also occurs by a LMCT process.

The calculated value of 1500 s^{-1} for the radiative rate constant, k_r, seems slightly more unusual than the other terms that have been discussed because k_r for the Eu^{3+} ($^5D_0$) level is normally in the region of 100-900 s^{-1}.[33] Such a fast radiative rate might suggest there are other relaxation pathways that have been ignored. Recent studies with the complex

Eu(thd)$_3$, where thd is the β-diketonate 2,2,6,6-tetramethyl-3,5-heptandionate, demonstrated that vibrations of C$_\alpha$–H (*i.e.* C–H on the chelate ring) contribute 157 s^{-1} to the decay rate and the 18 C–H oscillators from the *tert*-butyl groups contribute 175 s^{-1}.[35] Taking this into account, a radiative rate constant of 1930 s^{-1} was calculated for Eu(thd)$_3$. This high residual rate was attributed to a possible enhancement of the ^{5}D$_0 \rightarrow$ ^{7}F$_J$ transitions by the mixing of some charge transfer character into the ^{5}D$_0$ state. In view of the possibilities of C–H quenching and/or mixing of wavefunctions, the calculated radiative rate for [Eu$_2$(bis-DBM)$_3$] is probably quite reasonable.

The luminescence quantum yield of [Eu$_2$(bis-DBM)$_3$] in DMF at room temperature was measured by the relative method, with λ_{ex} = 365 nm, and was found to be 5%. In comparison, the quantum yield of [Eu(DBM)$_3$] in MeOH at room temperature, following ligand excitation, is reported to be 0.5%.[31] As the room temperature lifetime of [Eu$_2$(bis-DBM)$_3$] is similar in DMF and MeOH (Table 4.1), the lower quantum yield of [Eu(DBM)$_3$] relative to the bis-DBM complex is probably not due to the different solvents used. Instead, it can be attributed to a more efficient ligand to metal energy transfer process in [Eu$_2$(bis-DBM)$_3$]. The difference between the complexes of DBM and bis-DBM is not due to the triplet state energy, since it is similar for both ligands. It may be due to the presence of an additional Eu^{3+} lumophore in [Eu$_2$(bis-DBM)$_3$], thereby increasing the overall efficiency of the energy transfer pathway, or perhaps due to a shorter chromophore-metal distance in the dinuclear complex.

4.4   DINUCLEAR TETRAKIS CHELATES OF BIS-DBM

The main difference between the reported preparations[18,19] of tris complexes of β-diketonates and the corresponding tetrakis complexes is an increase in the ligand to metal ratio to 2:1 in the latter case. Reaction of an ethanolic solution of H$_2$bis-DBM (4 equiv.) and TBAOH·30H$_2$O (8 equiv.) in EtOH with an aqueous solution of EuCl$_3$.6H$_2$O or YCl$_3$.6H$_2$O (2 equiv.) resulted in the immediate formation of a pale yellow precipitate, which was filtered, washed with ice-cold EtOH and H$_2$O and dried under

vacuum. Based on the formulation (TBA)$_2$[Eu$_2$(bis-DBM)$_4$], which was the target product, the yield is 66% (based on Eu$_2$(bis-DBM)$_3$ the yield is > 100%). Similarly, the yield is 76% for the formulation (TBA)$_2$[Y$_2$(bis-DBM)$_4$]).

In the FAB(+)-MS spectrum of the Eu^{3+} product, no peaks that correspond to the tetrakis product are observed, though in view of the dianionic nature of [Eu$_2$(bis-DBM)$_4$]$^{2-}$ this is not surprising. There are, however, strong peaks at *m/z* 1409 and 1651 corresponding to [Eu$_2$(bis-DBM)$_3$ + H]$^+$ and [Eu$_2$(bis-DBM)$_3$ + TBA]$^+$ respectively. Elemental analysis of both complexes confirms the presence of the TBA counterion (*i.e.* presence of N); however, the values found for C, H and N analyses are all low, suggesting that the product is a mixture of the desired compound and another product.

Electrospray mass spectra were recorded for the Eu^{3+} product from the bis-DBM/TBAOH reaction under the same conditions used for [Eu$_2$(bis-DBM)$_3$]. The ES(+)-MS spectrum is shown in Figure 4.17. With the exception of a very strong peak at *m/z* 242 for TBA (not shown), the spectrum is dominated by a peak centred on *m/z* 1650, assigned to [Eu$_2$(bis-DBM)$_3$ + TBA]$^+$. This is much stronger than the [*M* + H]$^+$ signal previously obtained for pure [Eu$_2$(bis-DBM)$_3$] (Figure 4.9), though that signal is also evident in Figure 4.17.

It was expected that the signals at *m/z* 1629 and 1777, corresponding to [Eu(bis-DBM)$_4$ + 5H]$^-$ and [Eu$_2$(bis-DBM)$_4$ + H]$^-$ respectively, that were observed in the ES(−)-MS spectrum of [Eu$_2$(bis-DBM)$_3$] (Figure 4.10) would be stronger in the ES(−)-MS spectrum of the tetrakis product because of the excess ligand. As shown in Figure 4.18, although there is a strong signal centred on *m/z* 1778, the other signal is absent. The most intense signal in the spectrum is centred on *m/z* 1674, and this is tentatively assigned to [Eu$_2$(bis-DBM)$_4$ − PhCO + 2H]$^-$. In fact, loss of the PhCO group from β-diketones is a very common fragmentation in E.I. mass spectrometry,[36] so this assignment seems quite reasonable.
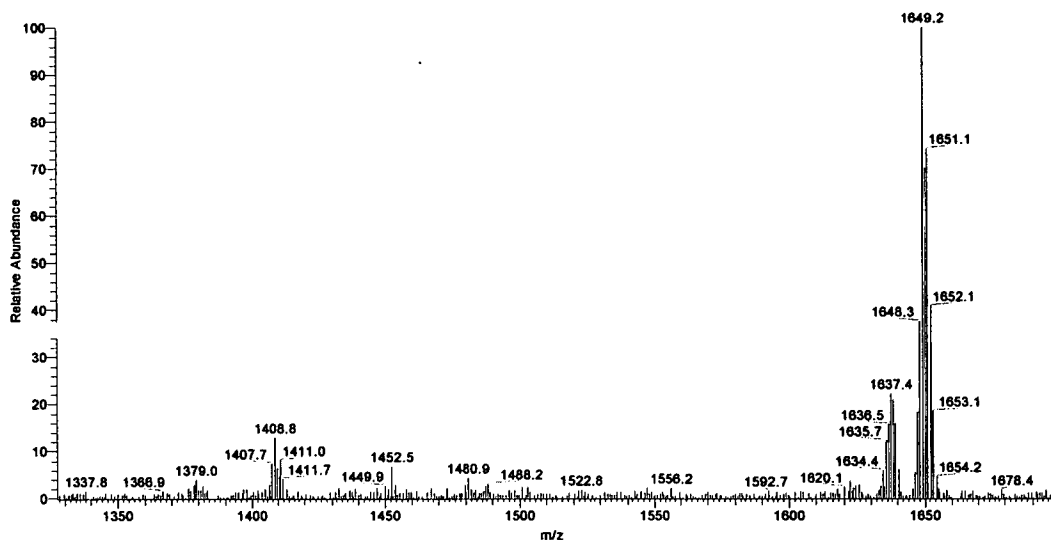
Figure 4.17 ES(+)-MS spectrum of the product of the "tetrakis" reaction between EuCl$_3$, bis-DBM and TBAOH, in DMF/CH$_3$CN/methanoic acid (1: 99 : 0.1) (*ca.* 1 × 10^{-5} mol dm^{-3})
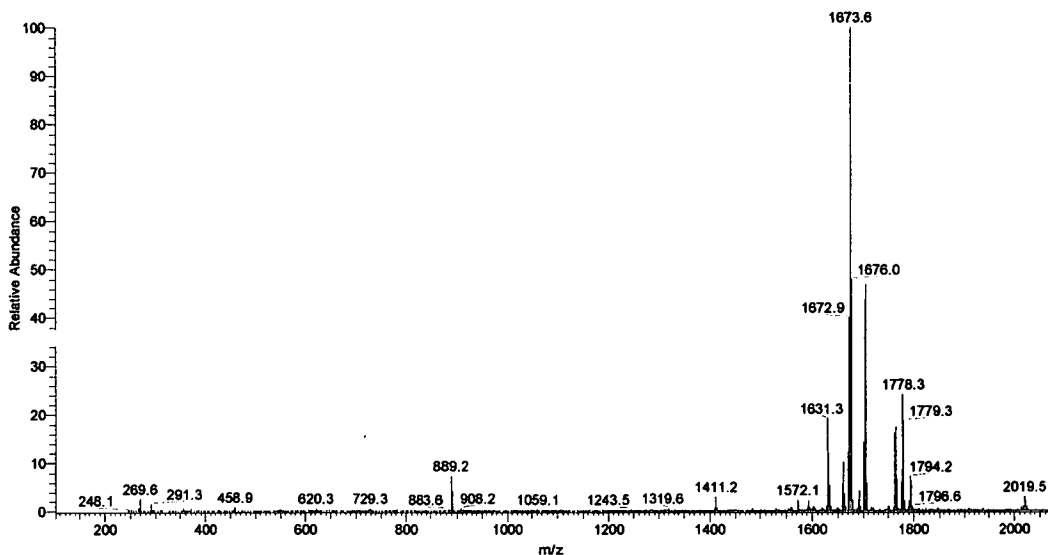

Figure 4.18 ES(−)-MS spectrum of the product of the "tetrakis" reaction between EuCl$_3$, bis-DBM and TBAOH, in DMF/CH$_3$CN/methanoic acid (1: 99 : 0.1) (*ca.* 1 × 10^{-5} mol dm^{-3})

The ^{1}H NMR spectrum, in DMF-d_7, of the Y^{3+} tetrakis product is shown in Figure 4.19. There are two important features of this spectrum. Firstly, the presence of TBA is clear from the four distinctive multiplets with relative intensity 3:2:2:2 between δ 0.95-3.38

(the other resonances in this range are due to solvent). Secondly, the region δ 6.46-9.68 is very complicated with a large number of overlapping resonances, in contrast with the very simple spectrum obtained for $[Y_2(bis\text{-}DBM)_3]$ under the same conditions (Figure 4.11). Assuming all the signals in the region δ 6.46-9.68 are due to bis-DBM, the ligand:TBA ratio can be estimated from the integrated intensities to be 3:1, whereas for pure tetrakis complex this ratio should be 2:1.

An explanation for the aforementioned elemental analyses and NMR spectrum is that the samples are mixtures of the tris and tetrakis complexes. It is well documented that the preparation of mononuclear complexes can result in tris/tetrakis mixtures.[37] It is also well known that tetrakis complexes can undergo partial or complete dissociation to form the tris species.[29] The complicated spectrum in Figure 4.19 may result from a tris/tetrakis equilibrium in solution.
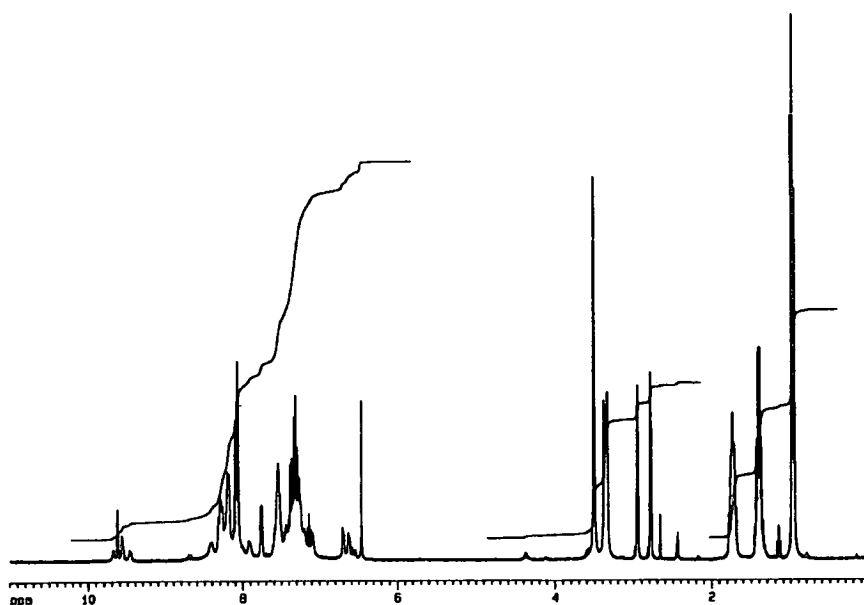
Figure 4.19 ^{1}H NMR spectrum of the product of the "tetrakis" reaction between YCl_3, bis-DBM and TBAOH, in DMF-d_7

More information on this tris/tetrakis equilibrium was provided by a study of the bis-DBM complexes prepared using piperidine (Hpip) as a base. The reaction of bis-DBM (4 equiv.) with hydrated europium or yttrium chloride (2 equiv.) and Hpip (8 equiv.) in a mixed $CHCl_3$/MeOH solvent results in the immediate precipitation of a pale yellow compound.

As with all of the Eu^{3+} complexes of bis-DBM, the product showed strong Eu^{3+} emission following UV excitation. It was observed, however, that washing this solid with MeOH/$CHCl_3$ resulted in a significant reduction in luminescence intensity. Since tetrakis complexes are known to be far more luminescent than the corresponding tris complexes,[29] it was thought that this reduction could be due to the dissociation of the tetrakis species to the tris species. To avoid problems due to dissociation, the same reaction as above was performed using excess piperidine. The FAB(+)-MS spectrum of the product showed strong peaks at *m/z* 1409 and 1494 corresponding to [Eu_2(bis-DBM)$_3$+ H]$^+$ and [Eu_2(bis-DBM)$_3$+ Hpip]$^+$ respectively.

The solid-state reflectance spectrum of this solid at room temperature is shown in Figure 4.20, along with that of pure [Eu_2(bis-DBM)$_3$]. These spectra have two important features. Firstly, the Eu^{3+} luminescence, following UV irradiation, is much weaker for [Eu_2(bis-DBM)$_3$]. Secondly, the fine structure of the hypersensitive $^5D_0 \rightarrow {}^7F_2$ emission band is clearly different in both cases. This indicates that the spectra originate from two different Eu^{3+}-containing species. Furthermore, emission spectra of DMF solutions of the same two solids (Figure 4.21) are identical, within the resolution of the instrument.

These luminescence spectra suggest that the strongly luminescent species formed from the reaction with piperidine is (Hpip)$_2$[Eu_2(bis-DBM)$_4$] and that in solution ligand dissociation occurs to form [Eu_2(bis-DBM)$_3$]. In view of the apparent sensitivity of the tetrakis complexes towards solvent, it is not surprising that attempts to synthesise them result in mixtures of tris and tetrakis species.
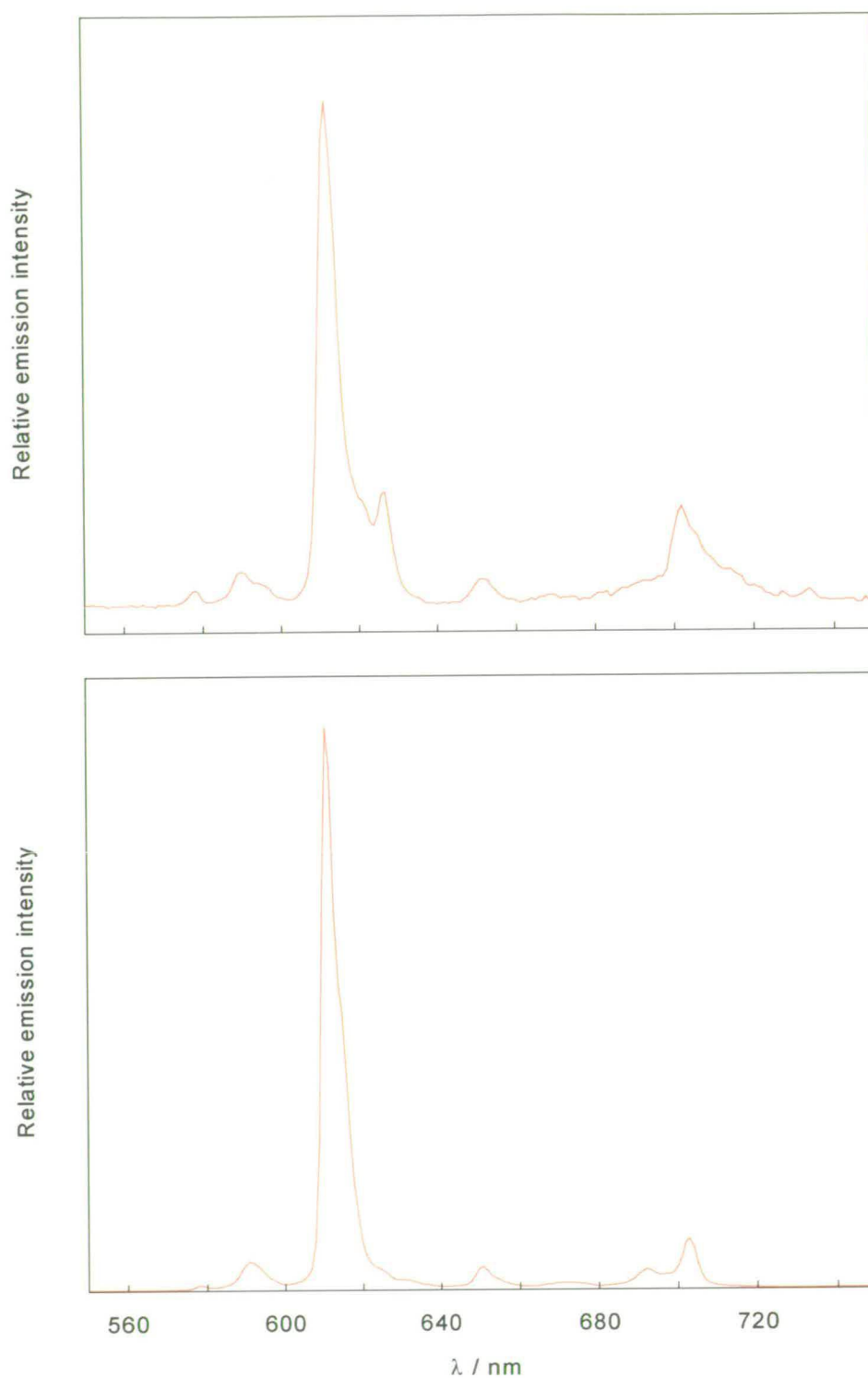
Figure 4.20 Corrected emission spectra of solid [Eu$_2$(bis-DBM)$_3$] (top) and the solid product from the "tetrakis" reaction between EuCl$_3$, bis-DBM and excess Hpip (bottom); λ$_{ex}$ = 350 nm, 2 nm bandpass (em.)
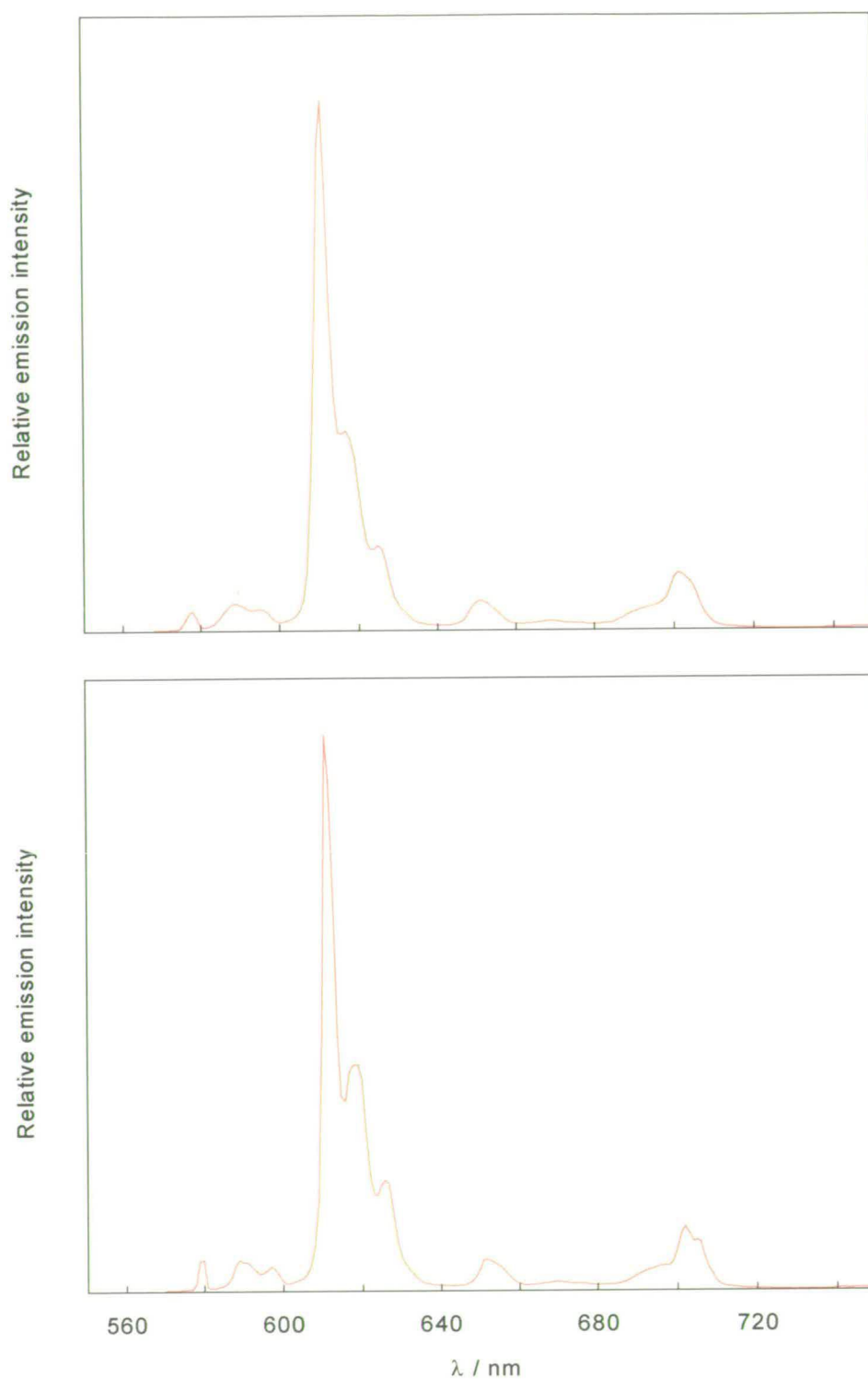
Figure 4.21 Corrected emission spectra in DMF. Top: [Eu$_2$(bis-DBM)$_3$] [2 × 10^{-6} mol dm^{-3}, λ$_{ex}$ = 350 nm, 2 nm bandpass (em.)]; bottom: product from the "tetrakis" reaction between EuCl$_3$, bis-DBM and excess Hpip [3 × 10^{-6} mol dm^{-3}, λ$_{ex}$ = 360 nm, 1 nm bandpass (em.)]

Although attempts to crystallise dinuclear tetrakis complexes of bis-DBM were unsuccessful, if the solubility of dinuclear complexes can be increased, especially in non-coordinating solvents, it should be possible to isolate (and fully characterise) pure tetrakis complexes. Furthermore, as with the tris complexes, there are a number of possibilities for the conformation of dinuclear tetrakis complexes. One of these is a quadruple helix, which would be the first example of such a lanthanide complex. It is of particular interest to study the tetrakis complexes of bis-DBM that are formed when chiral amines are used as the base, since they may result in the formation of diastereomers, which can be investigated by techniques that probe the stereochemistry of molecules in solution (*e.g.* NMR and circular dichroism).

4.5   CONCLUSIONS

The work presented in this chapter represents the first investigation of the formation of dinuclear lanthanide complexes with bis(β-diketone) ligands. Studies with bis-DBM have led to the preparation and full characterisation of the dinuclear complexes [Eu$_2$(bis-DBM)$_3$] and [Y$_2$(bis-DBM)$_3$]. Following a detailed photophysical analysis of these complexes, the processes involved in the conversion of UV to visible light within [Eu$_2$(bis-DBM)$_3$] can be summarised by the energy-level scheme shown in Figure 4.22.

The ligand $^3\pi\pi^*$ state is well placed to allow energy transfer to the upper Eu^{3+} states, following UV absorption. The luminescence quantum yield is high, in spite of the presence of a thermally-activated LMCT pathway that acts to deactivate the $^5D_0$ state of Eu^{3+}, indicating that the energy transfer process is efficient. While the luminescent properties of this complex can be interpreted in a similar manner to the analogous [Eu(DBM)$_3$] complexes, the greater efficiency of the sensitisation process and very large absorbance of the dinuclear complex justify this study, and illustrate the potential benefits of polynuclear lanthanide systems.

Overall, this work has shown that suitably designed bis(β-diketonates) can react with

lanthanide ions to give dinuclear lanthanide complexes as the sole product. The synthetic versatility of these binucleating ligands should allow an interesting and varied array of dinuclear complexes to be synthesised.
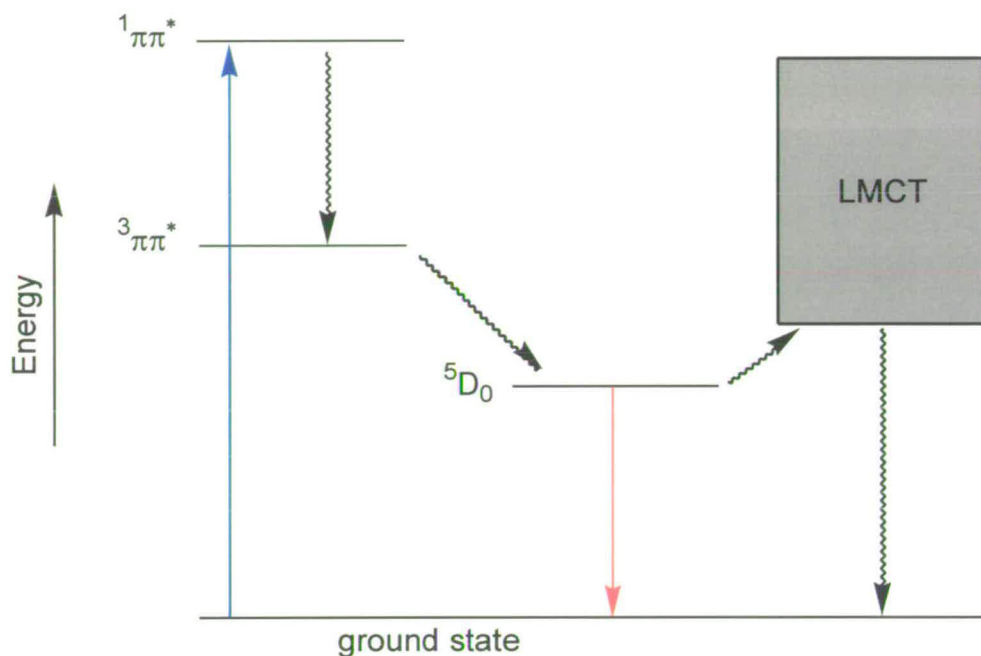

Figure 4.22 Schematic energy-level diagram for [Eu$_2$(bis-DBM)$_3$]

4.6   REFERENCES

1.   C. Piguet and J.-C. G. Bünzli, *Chem. Soc. Rev.*, 1999, **28**, 347.

2.   P. Guerriero, S. Tamburini and P. A. Vigato, *Coord. Chem. Rev.*, 1995, **139**, 17.

3.   K. D. Matthews, R. A. Fairman, A. Johnson, K. V. N. Spence, I. A. Kahwa. G. L. McPherson and H. Robotham, *J. Chem. Soc., Dalton Trans.*, 1993, 1719 and references therein.

4.   P. Guerriero, P. A. Vigato, J.-C. G. Bünzli and E. Moret, *J. Chem. Soc., Dalton Trans.*, 1990, 647.

5.   M. Elhabiri, R. Scopelliti, J.-C. G. Bünzli and C. Piguet, *J. Am. Chem. Soc.*,1999, **121**, 10747.

6.   J.-P. Costes, F. Dahan, A. Dupuis, S. Lagrave and J.-P. Laurent, *Inorg. Chem.*,

1998, **37**, 153.

7.   F. Avecilla, A. de Blas, R. Bastida, D. E. Fenton, J. Mahía, A. Macías, C. Platas, A. Rodríguez and T. Rodríguez-Blas, *Chem. Commun.*, 1999, 125.

8.   J.-M. Lehn, *Angew. Chem. Int. Ed. Engl.*, 1988, **27**, 89.

9.   *Comprehensive Supramolecular Chemistry*, eds. J. L. Atwood, J. E. D. Davies, D. D. MacNicol and F. Vögtle, Elsevier, Oxford, 1996, **9**.

10. E. C. Constable, *Prog. Inorg. Chem.*, 1994, **42**, 67.

11. D. L. Caulder and K. N. Raymond, *J. Chem. Soc., Dalton Trans.*, 1999, 1185.

12. J.-C. G. Bünzli, S. Petoud, C. Piguet and F. Renaud, *J. Alloys Compd.*, 1997, **249**, 14.

13. M. Elhabiri, R. Scopelliti, J.-C. G. Bünzli and C. Piguet, *Chem. Commun.*, 1998, 2347.

14. A. R. Siedle in *Comprehensive Coordination Chemistry*, Vol. 2, ed. G. Wilkinson, Pergamon Press, Oxford, 1987, ch. 15.4.

15. V. A. Grillo, E. J. Seddon, C. M. Grant, G. Aromí, J. C. Bollinger, K. Folting and G. Christou, *Chem. Commun.*, 1997, 1561.

16. A. W. Maverick and F. E. Klavetter, *Inorg. Chem.*, 1984, **23**, 4129.

17. A. W. Maverick, S. C. Buckingham, Q. Yao, J. R. Bradbury and G. G. Stanley, *J. Am. Chem. Soc.*, 1986, **108**, 7430.

18. L. R. Melby, N. J. Rose, E. Abramson and J. C. Caris, *J. Am. Chem. Soc.*, 1964, **86**, 5117.

19. H. Bauer, J. Blanc and D. L. Ross, *J. Am. Chem. Soc.*, 1964, **86**, 5125.

20. D. Horiguchi, K. Maeda, K. Sasamoto and Y. Ohkura, *Chem. Pharm. Bull.*, 1993, **41**, 1411.

21. J. Yuan, K. Matsumoto and H. Kimura, *Anal. Chem.*, 1998, **70**, 596.

22. D. F. Martin, M. Shamma and W.C. Fernelius, *J. Am. Chem. Soc.*, 1958, **80**, 4891.

23. J. Emsley, *Struct. Bonding (Berlin)*, 1984, **57**, 147.

24. D. E. Williams, *Acta Crystallogr.*, 1966, **21**, 340.

25. C. Piguet, G. Bernardinelli and G. Hopfgartner, *Chem. Rev.*, 1997, **97**, 2005.

26. S. Cotton, *Lanthanides and Actinides*, Macmillan Education, London, 1991, ch. 2.

27. D. Parker, *Chem. Rev.*, 1991, **91**, 1441.

28. R. E. Whan and G. A. Crosby, *J. Mol. Spectroscopy*, 1962, **8**, 315.

29. A. P. B. Sinha, in *Spectroscopy in Inorganic Chemistry*, eds. C. N. R. Rao and J. R. Ferrare, Academic Press, New York, 1971, Vol. 2.

30. W. F. Sager, N. Filipesen and F. A. Serafin, *J. Phys. Chem.*, 1965, **69**, 1092.

31. W. R. Dawson, J. L. Kropp and M. W. Windsor, *J. Chem Phys.* 1966, **45**, 2410

32. R. C. Holz, C. A. Chang and W. DeW. Horrocks, Jr., *Inorg. Chem.*, 1991, **30**, 3270.

33. N. Sabbatini, M. Guardigli and J.-M. Lehn, *Coord. Chem. Rev.*, 1993, **123**, 201.

34. M. T. Berry, P. S. May and H. Xu, *J. Phys. Chem.*, 1996, **100**, 9216.

35. T. C. Schwendemann, P. S. May, M. T. Berry, Y. Hou and C. Y. Meyers, *J. Phys. Chem. A*, 1998, **102**, 8690.

36. J. H. Bowie, D. H. Williams, S.-O. Lawesson and G. Schroll, *J. Org. Chem.*, 1966, **31**, 1384.

37. J. F. Desreux, in *Lanthanide Probes in Life, Chemical and Earth Sciences*, eds. J.-C. G. Bünzli and G. R. Chopin, Elsevier, Amsterdam, 1989, ch. 2.

Chapter Five

Ternary complexes of lanthanides with crown ethers and aromatic acids

5.1 INTRODUCTION

As discussed in Chapter 2, a significant application of lanthanide complexes is as luminescent labels for biomolecules, especially for use in time-resolved fluoroimmunoassays (TR-FIA). While there are many successful assay procedures in use at the present time, there is a continual drive towards systems with increased sensitivity, efficiency and simplicity. Heterogeneous assays (*e.g.* DELFIA[1]) are limited by labour-intensive, multi-step procedures with a corresponding increase in error. In homogeneous assays, the label must be luminescent and stable *in situ*, and permit monitoring of the immunoreaction without a separation stage,[2] making this approach harder to realise in practice.

One successful homogeneous assay based on energy transfer involves a Eu^{3+} cryptate as an energy donor and the fluorescent protein allophycocyanin as the energy acceptor.[3] This interaction is non-specific, however, as the two components are simply brought in close proximity. This is often called fluorescence or luminescence resonance energy transfer (FRET or LRET respectively) and has been used primarily to measure distances between energy transfer components (see Chapter 2).[4,5]

The work described in this chapter is the first step in an approach to luminescent labelling based on energy transfer between organised components. The key feature of this strategy is the controlled formation of a stable ternary luminescent lanthanide complex following an immunoreaction; the intensity of lanthanide luminescence gives a direct quantification of the target analyte.

A potential homogeneous assay that utilises this approach is illustrated in Figure 5.1. This is an example of a sandwich assay as it involves three components; two labelled antibodies (Ab) bind at different sites (epitopes) of the corresponding antigen (Ag), which is the analyte. A stable, non-luminescent complex of a Eu^{3+} ion with a non-absorbing ligand (NAL) is attached to one antibody, while a light-harvesting ligand is attached to the other antibody. The immunoreaction brings the [EuNAL] label in close proximity with the LHC label, and ternary complex formation occurs. Upon excitation

with UV light, energy transfer can occur from the LHC to the Eu^{3+} ion followed by characteristic $^5D_0 \rightarrow {}^7F_J$ emission of the metal.
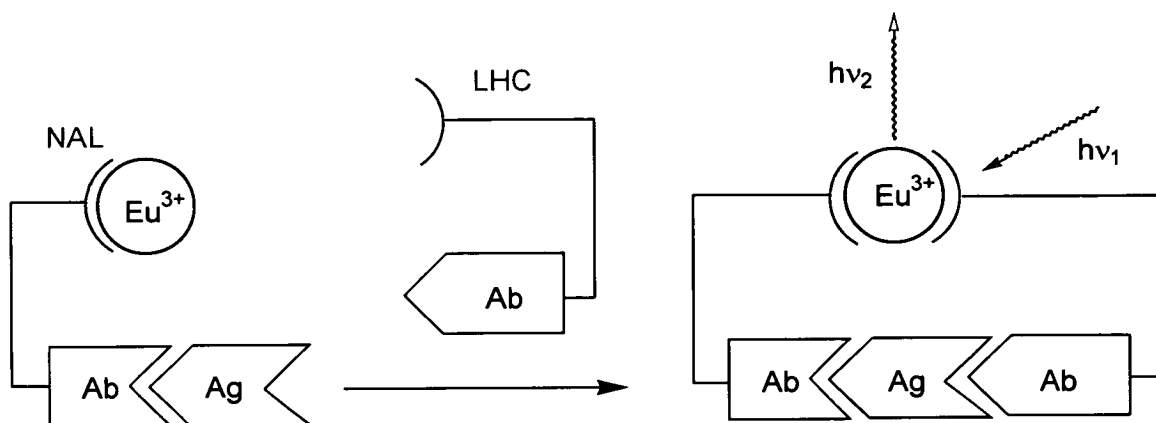

Figure 5.1 Potential homogeneous immunoassay involving an antigen (Ag) as the analyte and two labelled antibodies (Ab) [one antibody is labelled with a complex of Eu^{3+} and a non-absorbing ligand (NAL), the other with a light-harvesting ligand (LHC)]: immunoreaction results in the formation of a luminescent ternary lanthanide complex

Developing an immunoassay such as that depicted in Figure 5.1 requires a detailed study of the ternary complex formation of the [LnNAL] and LHC components prior to their attachment to biomolecules. The process can be more simply described as shown in Figure 5.2.
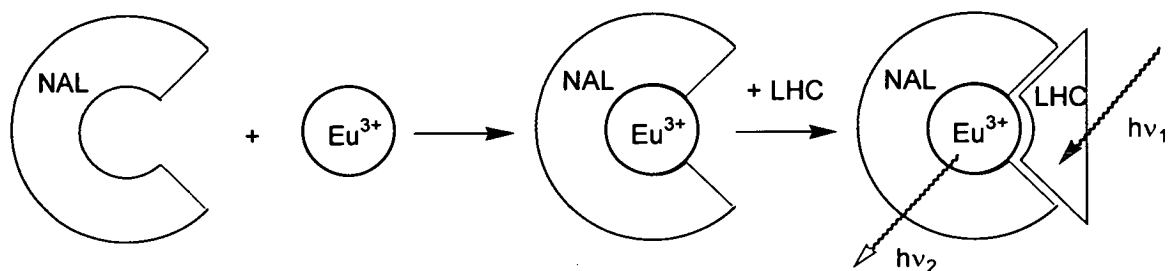
Figure 5.2 Schematic of the formation of luminescent ternary lanthanide complexes

The choice of NAL is very important as it must form a thermodynamically stable and kinetically inert complex with the Ln^{3+} ion, but also leave the metal coordinatively

unsaturated. Solvent molecules will occupy the "free" coordination sites, and these can be removed upon binding of the LHC. The intensity of metal-centred luminescence will be increased by the sensitisation process and also by the replacement of quenching solvent molecules.

Upon surveying the literature concerning lanthanide complexes, it is clear that there have been comparatively few reports of ternary complex formation. There are, however, a number of important studies with direct relevance to this work that require some discussion.

One of the earliest studies was of the photophysics of mixed ligand complexes formed upon addition of 5-substituted salicylic acids (*e.g.* 5-fluorosalicylic acid, **35**) to [TbEDTA]⁻ in aqueous solution.[6] Formation of the ternary complex, [Tb(EDTA)(ligand)], occurs between pH 2.5 and 3 and is associated with deprotonation of the carboxylic acid. The ternary complexes are fully formed at 1:1:1 mole ratios, and an energy transfer process takes place from the bound salicylate ligand to the Tb^{3+} ion. The strong pH dependence of the lifetime and intensity of Tb^{3+} luminescence between pH 8 and 11.5 is associated with ionisation of the phenolic proton. Subsequent binding of the phenolate group to the metal probably results in the expulsion of coordinated water molecules.
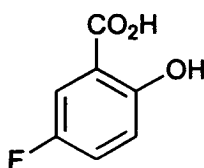
35

Salicylates have also been used in a DNA hybridisation assay involving pairs of oligonucleotide probes that have been chemically modified to form a ternary Tb^{3+} complex after hybridisation with a template nucleic acid.[7] The salicylate energy donor is

attached to the 3′ end of one oligonucleotide and an energy acceptor TbDTPA complex is attached to the 5′ end of another oligonucleotide. After hybridisation to the complementary DNA strand, the donor and acceptor are brought close enough for ternary complex formation, and energy transfer, to occur. In the preceding examples involving salicylates, both the light-harvesting ligand and the [LnNAL] complex have a negative charge, which is not ideal for strong binding.

The ternary systems involving Eu^{3+} ions, 1,7-diaza-4,10,13-trioxacyclopentadecane-N,N′-diacetic acid (**36**) and 1,10-phenanthroline-2,9-dicarboxylic acid (**37**) utilise a similar approach to that illustrated in Figure 5.2.[8] The crown forms a stable complex with Eu^{3+} ions (log K = 11.9),[9] and addition of ligand **37** leads to ternary complex formation; irradiation of **37** results in the sensitisation of Eu^{3+} luminescence. This system and others like it, involving **36** and EDTA as non-absorbing ligands with a range of sensitising ligands,[10] are limited for use in labelling applications, however, by complicated solution behaviour.
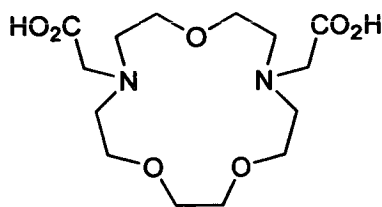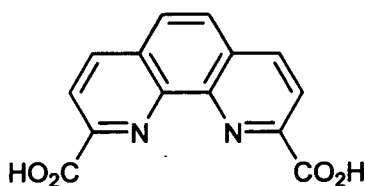

36   **37**

The macrocyclic ligands 1,10-diaza-4,7,13,16-tetraoxacyclooctadecane-*N,N*′-diacetic acid (H_2DACDA, **38**) and 1,4,7,10-tetraoxa-13-azacyclopentadecane-13-acetic acid (HMACMA, **39**) were chosen for the role of the NAL in this work. They can be described as nitrogen-pivot lariat crown ethers[11] due to the carboxylic acid pendant arms that are attached to the nitrogen atoms of the crown. Macrocycles with ionisable pendant donor groups greatly increase the thermodynamic and kinetic stability of their complexes compared with the non-functionalised analogues. This results from the greater preorganisation[12] of the ligand for metal binding (*i.e.* it is held in a conformation close to that required for complex formation) and the electrostatic metal-ligand

interactions introduced by the ionisable pendant arms.[13]
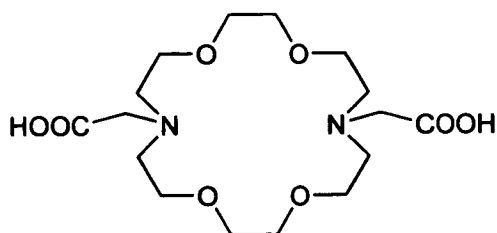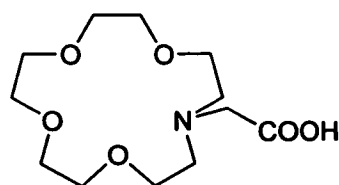
38   39

Although there are no reports of the complexation of Ln^{3+} ions with MACMA, there have been a number of studies involving Ln^{3+} ions and DACDA.[14-18] These have been primarily concerned with the structure and behaviour of the DACDA complexes in solution; no reports have been made of their isolation or solid-state characterisation of the complexes. Measurement of the stability constants of various DACDA complexes demonstrated ligand selectivity for Ln^{3+} ions as a group ($\log K = 10.8$-12.2), rather than transition metals or alkaline earth metals.[14]

The DACDA complexes of Ln^{3+} ions have a reasonably high kinetic stability. They exhibit both acid-dependent and acid-independent dissociation pathways, described by the simple rate law given in equation 5.1:[16]

$$k_{obsd} = k_d + k_H[H^+] \tag{5.1}$$

where k_{obsd} is the observed pseudo-first order rate constant, and k_d and k_H are the rate constants for direct dissociation and acid catalysed pathways respectively. For the Eu^{3+} complex at 25 °C and 0.1 mol dm^{-3} ionic strength, for example, k_d and k_H are $(4.31 \pm 1.47) \times 10^{-4}$ s^{-1} and $(5.70 \pm 0.96) \times 10^{-1}$ mol^{-1} dm^3 s^{-1} respectively.[16] It is believed that the self-dissociation pathway does not occur in one step but involves a rate-determining distortion of the complex to yield an intermediate that is rapidly scavenged (*e.g.* by H^+) to give the products.

By analogy with other crown ethers, the cavity radius of DACDA has been estimated to

be 1.45 ± 0.15 Å,[18] allowing the Ln^{3+} ion to enter the cavity and bind with the four oxygen and two nitrogen atoms of the ring. There have been a number of reports regarding the solution structure. One study involved lifetime measurements of the Eu^{3+} complex in H_2O and D_2O, showing there are 1-2 water molecules coordinated to the metal. On the basis of NMR spectroscopy of the Y^{3+} complex and excitation spectroscopy of the Eu^{3+} complex, this study suggested that the ligand undergoes fluxional processes, possibly due to the ether oxygen atoms fluctuating between bound and unbound states.[17] Following a thermodynamic study, it was concluded that the Eu^{3+} ion fits well, due to encapsulation of the metal by the eight donor atoms.[18]

As the ligand MACMA has only one pendant arm, its lanthanide complexes will possess a 2+ charge. It also provides two fewer donor atoms than DACDA; four oxygen atoms and one nitrogen atom in the ring, and the carboxylate group. It was hoped that a comparison of the interaction of DACDA and MACMA complexes with light-harvesting ligands would reveal the factors controlling ternary complex formation.

The simple aromatic acids picolinic acid (**40**) and phthalic acid (**41**) were chosen for the role of the LHC because pyridinecarboxylic acids and benzenecarboxylic acids form stable complexes with lanthanides and are known sensitisers of Ln^{3+} luminescence.[19, 20] While picolinic acid has one ionisable carboxylic acid and a nitrogen atom available for metal binding, phthalic acid has two ionisable carboxylic acid groups. It was envisaged that there would be a favourable electrostatic interaction with the cationic crown complexes upon deprotonation of these ligands.
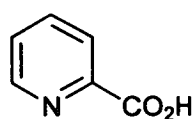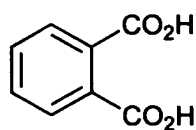
40   **41**

5.2 SYNTHESIS AND CHARACTERISATION OF CROWN COMPLEXES

5.2.1 Lanthanide complexes of DACDA

Preparation

Attempts to isolate the complexes [LnDACDA]Cl (Ln = La, Eu, Tb) were made by essentially the same procedure for each metal. This involved deprotonation of H_2DACDA with a suitable base, addition of the $LnCl_3$ and precipitation of the complex from the aqueous solution by adding acetone. The crystalline sample obtained from the europium reaction analysed as [EuDACDA]Cl·$2H_2O$ (73% yield). The products obtained from the reaction of DACDA with either $LaCl_3$ or $TbCl_3$ analysed less satisfactorily; the analysis of the lanthanum product differed only slightly (by 0.5-1%) from the formulation [LaDACDA]Cl·$2H_2O$, whereas analysis of the terbium product suggested that an inorganic salt is present. Confirmation that the [LnDACDA]Cl (Ln = La, Tb) complexes had formed was obtained from FAB-MS, with each spectrum showing intense signals corresponding to $[M-Cl]^+$.

Solid-state structure of [LnDACDA]Cl

Although the solid-state structure of a complex is not necessarily the same as that found in solution, it can give a useful indication of the interactions between the ligand(s) and the metal. In view of the conflicting reports regarding the structure of [EuDACDA]Cl in solution, attempts were made to crystallise [LnDACDA]Cl complexes. Single crystals of [LnDACDA]Cl (Ln = Eu and Tb) suitable for an X-ray diffraction analysis were grown by slow evaporation of acetonitrile solutions.

The crystal structure of [EuDACDA]Cl is shown in Figure 5.3. Each Eu^{3+} ion is ten-coordinate, and is bound to four oxygen and two nitrogen atoms of the DACDA ring, one oxygen atom from each of the ligand's carboxylate arms and a water molecule [see (a) in Figure 5.3]. One of the carboxylate arms is monodentate, whilst the other is 1,3-binucleating, linking adjacent Eu^{3+} centres to form a polymeric chain [see (b) in Figure 5.3]. The bridging carboxylate arm from a neighbouring ligand completes the coordination sphere of the metal.
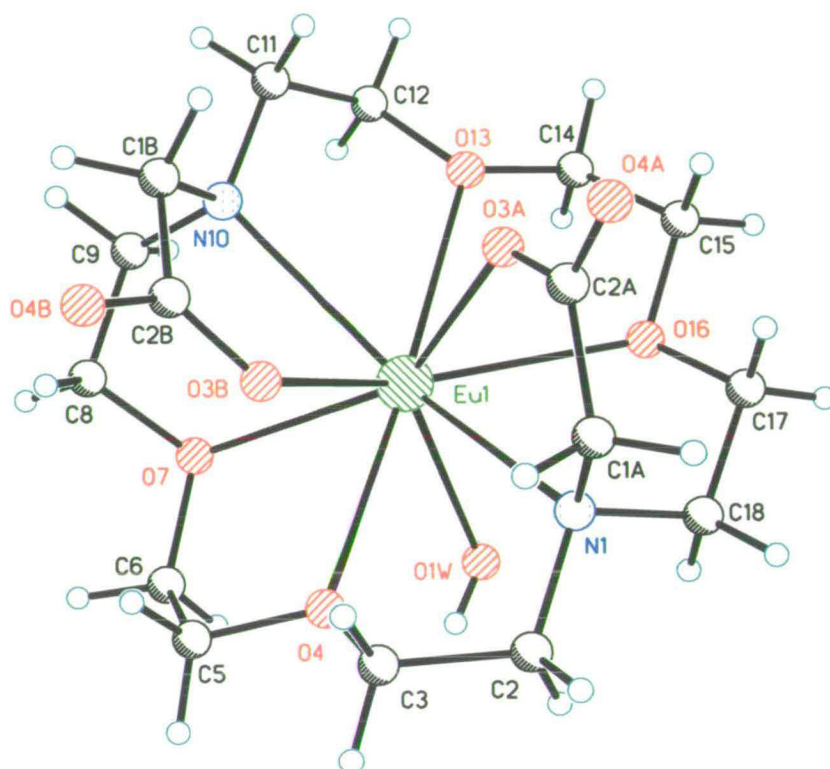
(a)
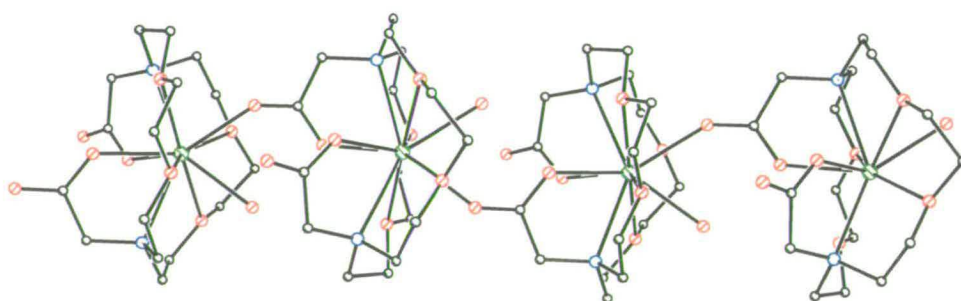
(b)

Figure 5.3 Molecular structure of {[EuDACDA(H$_2$O)]Cl}$_n$·6nH$_2$O showing (a) the Eu^{3+} coordination sphere with the atomic numbering scheme [selected bond distances (Å): Eu(1)–O(3B) 2.396(3), Eu(1)–O(3A) 2.402(3), Eu(1)–O(4A)#1 2.459(3), Eu(1)–O(1W) 2.461(3), Eu(1)–O(7) 2.528(3), Eu(1)–O(13) 2.612(3), Eu(1)–O(16) 2.613(3), Eu(1)–O(4) 2.629(3), Eu(1)–N(1) 2.686(4), Eu(1)–N(10) 2.738(4), O(4A)–Eu(1)#2 2.459(3)] and (b) part of one of the polymeric chains

143

The Eu^{3+} ion is situated in the middle of the DACDA ring, the two carboxylate arms from the same ligand are on one side of the ring, and the other carboxylate and water molecule are on the other side of the ring. While it is difficult to directly infer the solution structure from this polymeric crystal structure, it is clear that the ligand is able to wrap around the metal, yet still leave coordination sites free. This is obviously important when considering ternary complex formation.

The metal-ligand bond distances depend primarily on the donor atom. The intracomplex carboxylate bonds have an average Ln–O distance of 2.40 Å. These are of a similar length to those found in other complexes (*e.g.* the average Ln–O bond distance for the coordinated carboxylates in $[EuDOTA]^-$ is 2.39 Å).[21] Bond distances from the metal to ether oxygens (average 2.60 Å) and nitrogen (average 2.71 Å)' are longer, as are the Ln–O distances for the bridging carboxylate ligand and the water molecule (both are 2.46 Å).

It is interesting to compare the structure of [EuDACDA]Cl with the reported structure of Eu^{3+} complexed with 1,10-diaza-4,7,13,16-tetraoxacyclooctadecane, an analogue of DACDA with no carboxylate arms. In this structure, $[Eu(NO_3)_2(C_{12}H_{26}N_2O_4)](NO_3)$, the Eu^{3+} ion is also ten-coordinate, bonding to the six donor atoms of the macrocycle and to the four oxygen atoms of two bidentate nitrates.[22] The average bond distances for. Eu–O(ether), Eu–O(NO_3) and Eu–N are 2.60, 2.47 and 2.62 Å respectively. The addition of the carboxylate arms appears to weaken the Eu–N bonds, possibly due to steric factors.

The flexibility of the DACDA ligand allows it to optimise bonding interactions with the Ln^{3+} ion by adopting a polymeric structure. In fact, this type of behaviour does not appear to be unusual for complexes of lariat crown ethers. The structure of the cadmium complex of MACMA is a tetrameric cluster, $[Cd_4(MACMA)_4][CdCl_4]_2 \cdot 3H_2O$, with bridging acetate groups.[23] The structure of the cadmium complex with the ligand 1,4,7,10-tetraoxa-13-azacyclopentadecane, a MACMA analogue without the pendant arm, is monomeric $[Cd(MACMA)(NO_3)_2]$.[23] Thus, the introduction of pendant carboxylates to crown ethers can result in significant changes to the solid-state structure

144

of the macrocyclic complexes formed.

Although the polymeric structure of [EuDACDA]Cl was not predicted, it is worth noting that there is currently much interest in the crystal engineering of polymeric lanthanide complexes and the control of their properties.[24] The crystal packing diagram of [EuDACDA]Cl (Figure 5.4) shows that the polymeric chains are aligned parallel to the *b* axis and are separated by hydrophilic channels of water molecules and Cl⁻ ions. There is an intermolecular network of hydrogen bonds, involving coordinated and non-coordinated water molecules, Cl⁻ ions and ethylenic protons that help to cement the structure.
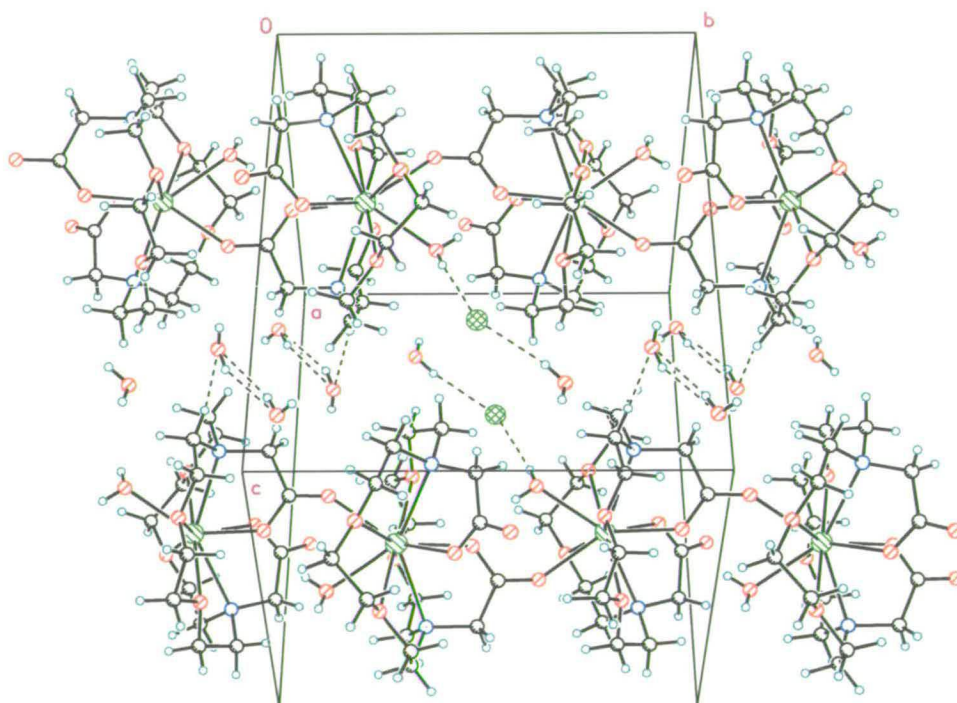

Figure 5.4 Crystal packing of $\{[EuDACDA(H_2O)]Cl\}_n \cdot 6nH_2O$

For polymeric structures to be of use as functional materials, it is necessary to have a synthetic route that can consistently produce the desired structure. In this respect, one indication that lanthanide complexes of lariat crown ethers could be useful is that the crystal structure of [TbDACDA]Cl, with crystals grown under the same conditions, is

isostructural with that of the Eu^{3+} complex. One of the polymeric chains of the [TbDACDA]Cl structure is shown in Figure 5.5, and as can be seen, the only difference is a shortening of the metal-ligand bond distances and the absence of a coordinated water molecule. Both of these differences can be attributed to the lanthanide contraction.
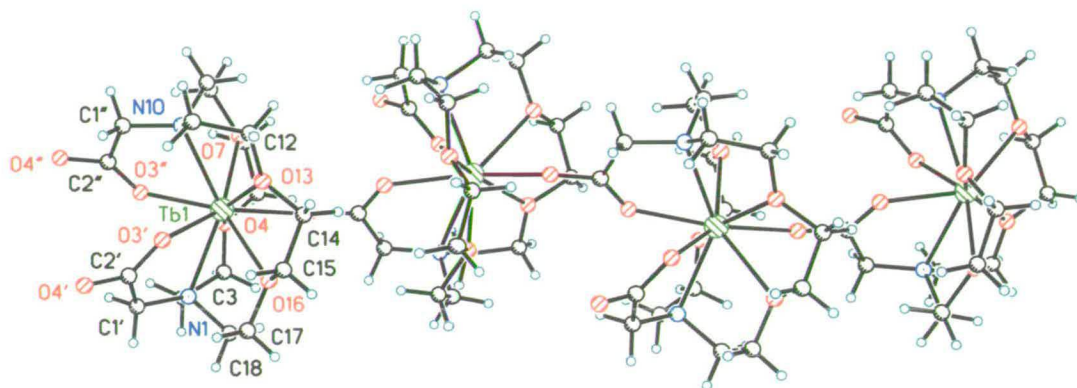

Figure 5.5 Molecular structure of $[TbDACDA]_n \cdot Cl_n \cdot 6nH_2O$ showing one of the polymeric chains with the atomic numbering scheme; selected bond distances (Å): Tb(1)–O(4″)#1 2.271(10), Tb(1)–O(3″) 2.305(13), Tb(1)–O(3′) 2.310(8), Tb(1)–O(13) 2.437(8), Tb(1)–O(4) 2.463(7), Tb(1)–O(7) 2.512(7), Tb(1)–O(16) 2.555(9), Tb(1)–N(1) 2.559(10), Tb(1)–N(10) 2.593(9), O(4″)–Tb(1)#2 2.271(10)

Solution structure of [LnDACDA]Cl: NMR spectroscopy

The previous NMR studies regarding the solution structure of [LnDACDA]Cl have been inconclusive. The ^1H NMR spectrum of the Y^{3+} complex in D_2O was reported to consist of several poorly resolved multiplets, yielding no useful structural data at all temperatures studied.[17] On the other hand, the ^{13}C NMR spectrum of the same complex was quite informative.[17] At 3 °C eight resonances were observed, reducing to five resonances at 81 °C. Two singlets were attributed to the acetate carbons and carboxylate carbons respectively, while the other resonances were attributed to the ethylenic carbons. At low temperature the ethylenic carbons undergo slow exchange, but at higher temperature they rapidly exchange and three singlets are observed.

In an attempt to gain more information about their solution structure, the DACDA complexes were studied by NMR spectroscopy. The ^{1}H NMR spectra of both [EuDACDA]Cl and [TbDACDA]Cl consisted of unresolved, overlapping multiplets and will not be discussed further. However, NMR spectroscopy of the diamagnetic La^{3+} complex was far more revealing. The ^{1}H, ^{13}C and ^{1}H–^{13}C COSY NMR spectra of [LaDACDA]Cl in D$_2$O at room temperature and 360 MHz are shown in Figures 5.6, 5.7 and 5.8 respectively.

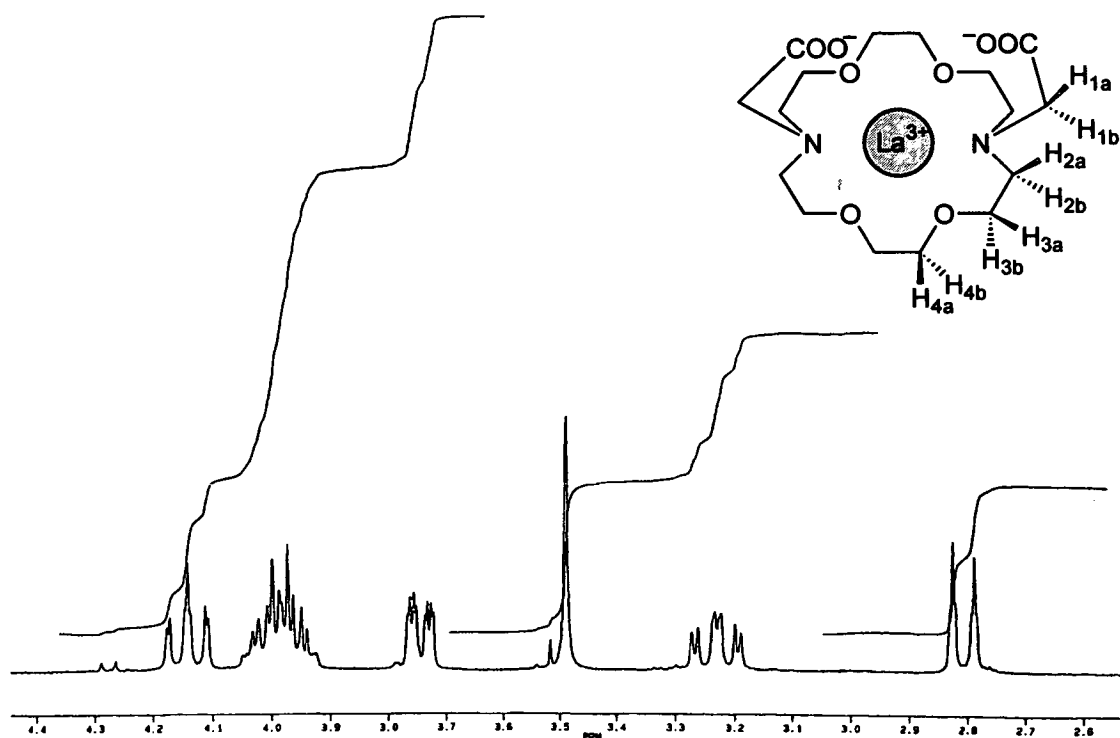**Figure 5.6** ^{1}H NMR spectrum of [LaDACDA]Cl at room temperature in D$_2$O (360 MHz); the inset shows a labelled structure (see text for assignments)

There are six intense signals in the ^{1}H NMR spectrum. The singlet at δ 3.49 is assigned to four equivalent acetate protons (*e.g.* H$_{1a}$ and H$_{1b}$), indicating that on the NMR timescale the complex has high symmetry. This high symmetry is confirmed by the presence of only five resonances in the ^{13}C NMR spectrum, which must be due to the five unique carbon environments that are labelled 1-5 in Figure 5.7. The signal at δ 180.55 can be assigned to the carboxylate carbon (carbon 5). From the ^{1}H–^{13}C COSY

NMR spectrum, the ^{13}C resonance at δ 59.92 is assigned to the acetate carbon (carbon 1). Similarly the multiplet at δ 3.94-4.03 in the ^{1}H NMR spectrum can be assigned as the eight diether-ethylenic protons (*e.g.* H$_{4a/b}$), allowing assignment of the carbon resonance at δ 69.87 to carbon 4 in Figure 5.7. This leaves four ^{1}H resonances and two carbon resonances still to be assigned. The ^{1}H–^{13}C COSY shows that each of the remaining carbon resonances correlates with two proton resonances. Based on chemical shift, the carbon resonance at δ 69.05, which correlates with the proton resonances at δ 4.11-4.18 and 3.72-3.77, is assigned to carbon 3 in Figure 5.7 because it is adjacent to an ether oxygen. Similarly, the carbon resonance at δ 59.12, which correlates with the proton resonances at δ 3.19-3.27 and 2.79-2.83, is assigned to carbon 2 in Figure 5.7 because it is adjacent to an amine nitrogen.
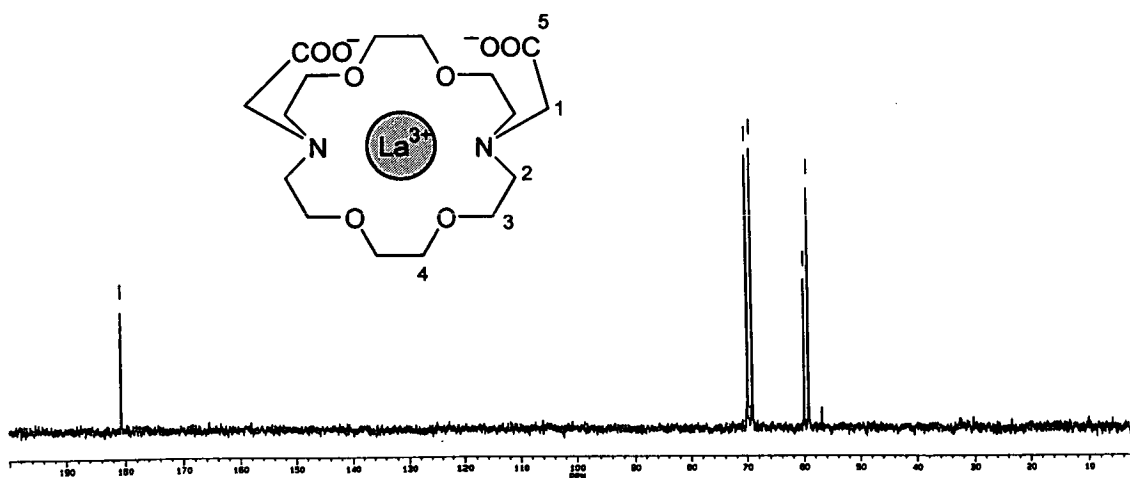

Figure 5.7 ^{13}C NMR spectrum of [LaDACDA]Cl at room temperature in D$_2$O (360 MHz); the inset shows a labelled structure (see text for assignments)

Upon closer inspection of the ^{1}H NMR spectrum of [LaDACDA]Cl it is evident that there are some smaller peaks, in addition to the six intense resonances. These peaks could be due to a small impurity in the sample, as was suggested by the analysis of the [LaDACDA]Cl sample. However, there was no apparent difference in the intensities of these smaller peaks, relative to the larger peaks, after recrystallisation of the sample used for the spectrum in Figure 5.6. In addition, the peaks are not observed in any of the starting materials and do not correspond to any obvious possible side-products, such
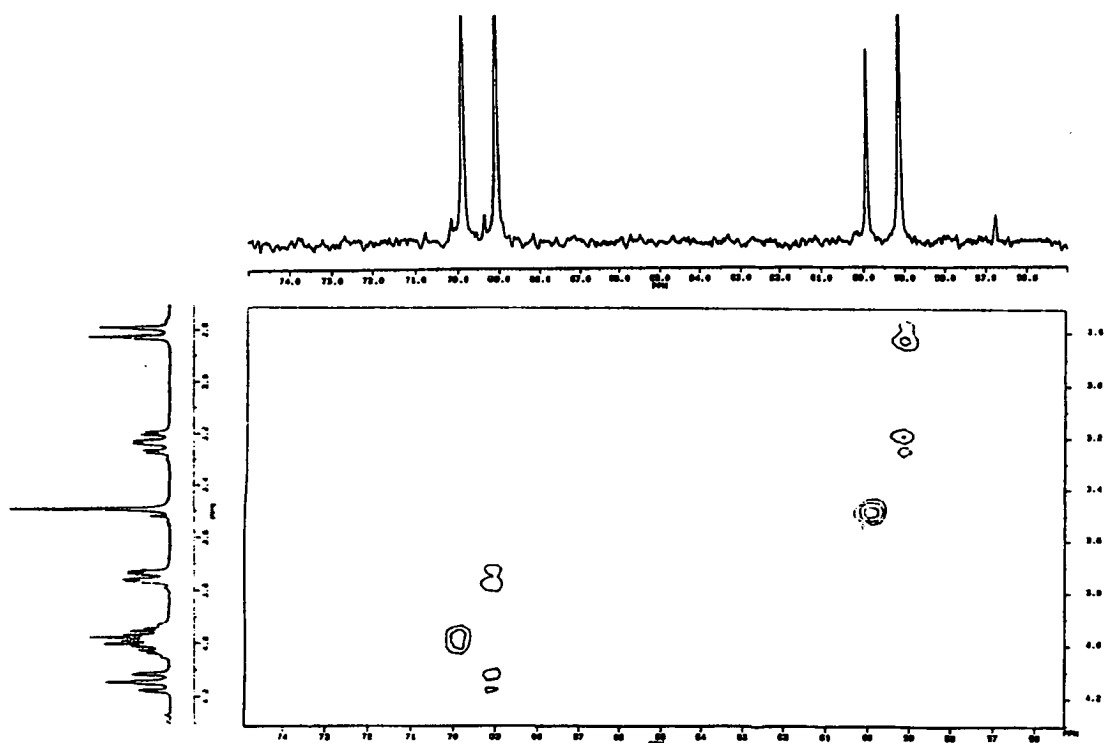
as the sodium salt of the ligand.

Figure 5.8 ^{1}H–^{13}C COSY spectrum of [LaDACDA]Cl at room temperature in D$_2$O (360 MHz)

It was thought that these smaller peaks might be due to the presence of a small amount of an isomeric form of the complex. Such solution behaviour is not uncommon for macrocyclic complexes. For example, two isomers are observed in solution in the ^{1}H NMR spectra of [LnDOTA]$^-$ complexes,[25] though only one of these is observed in the solid state. To investigate this possibility, ^{1}H NMR spectra of [LaDACDA]Cl were recorded at 600 MHz at 5, 25 and 45 °C (Figures A5 –A7 in Appendix I). The small peaks appear to be quite structured, as would be expected from an isomeric form of [LaDACDA]Cl, although they are too weak to attempt their proper assignment.

The other feature of these spectra is the broadening of all the resonances with a lowering of the temperature. This corresponds to the slowing down of fluxional processes and is in agreement with the observed ^{13}C NMR spectra reported for the

149

[YDACDA]Cl complex.[17] There were no significant changes in the relative intensities of the weak and strong resonances upon varying the temperature, as might be expected for an equilibrium between isomers. However, these studies were performed over a limited temperature range, and changes may not have been readily discernible due to the small intensity of the peaks.

The high symmetry observed for [LaDACDA]Cl is not consistent with the polymeric structure observed for the crystal structure of the Eu^{3+} and Tb^{3+} complexes, though this is perhaps unsurprising in aqueous solution. It is also worth noting at this point that although the structure of [LaDACDA]Cl in Figures 5.6 and 5.7 is drawn with the carboxylate arms on the same side of the ring, the NMR data does not exclude a structure with the arms on opposite sides of the ring. Indeed, 'if isomeric forms are present, they may result from changes in the conformation of the acetate arms.

Solution structure of [LnDACDA]Cl: luminescence spectroscopy

As ligand deprotonation and the dissociation kinetics of [LnDACDA]Cl complexes are pH-dependent, the pH of all solutions used for luminescence studies in this chapter were either measured prior to use or maintained at a constant value by dissolving the complex in a buffer solution. The buffer used was 0.05 mol dm^{-3} Tris [tris(hydroxymethyl)-aminomethane], with pH of 7.7 (25 °C), and this was chosen to avoid problems associated with complexation of the buffer.[19]

The steady-state excitation and emission spectra for [EuDACDA]Cl in Tris buffer are shown in Figure 5.9. Both spectra have differences to those reported for the free Eu^{3+} ion in aqueous solution,[26] which can be attributed to complexation by DACDA. The excitation spectrum consists of sharp *f-f* transitions, such as the strong $^7F_0 \rightarrow {}^5L_6$ transition at 394 nm, and broad UV bands centred at 280-290 nm, which can be attributed to LMCT transitions associated with oxidation of the amine nitrogens. Similar broad LMCT bands are observed in the excitation spectrum of the Eu^{3+} complex of the 2.2.1 cryptand (1), which was discussed in Chapter 2.[27]
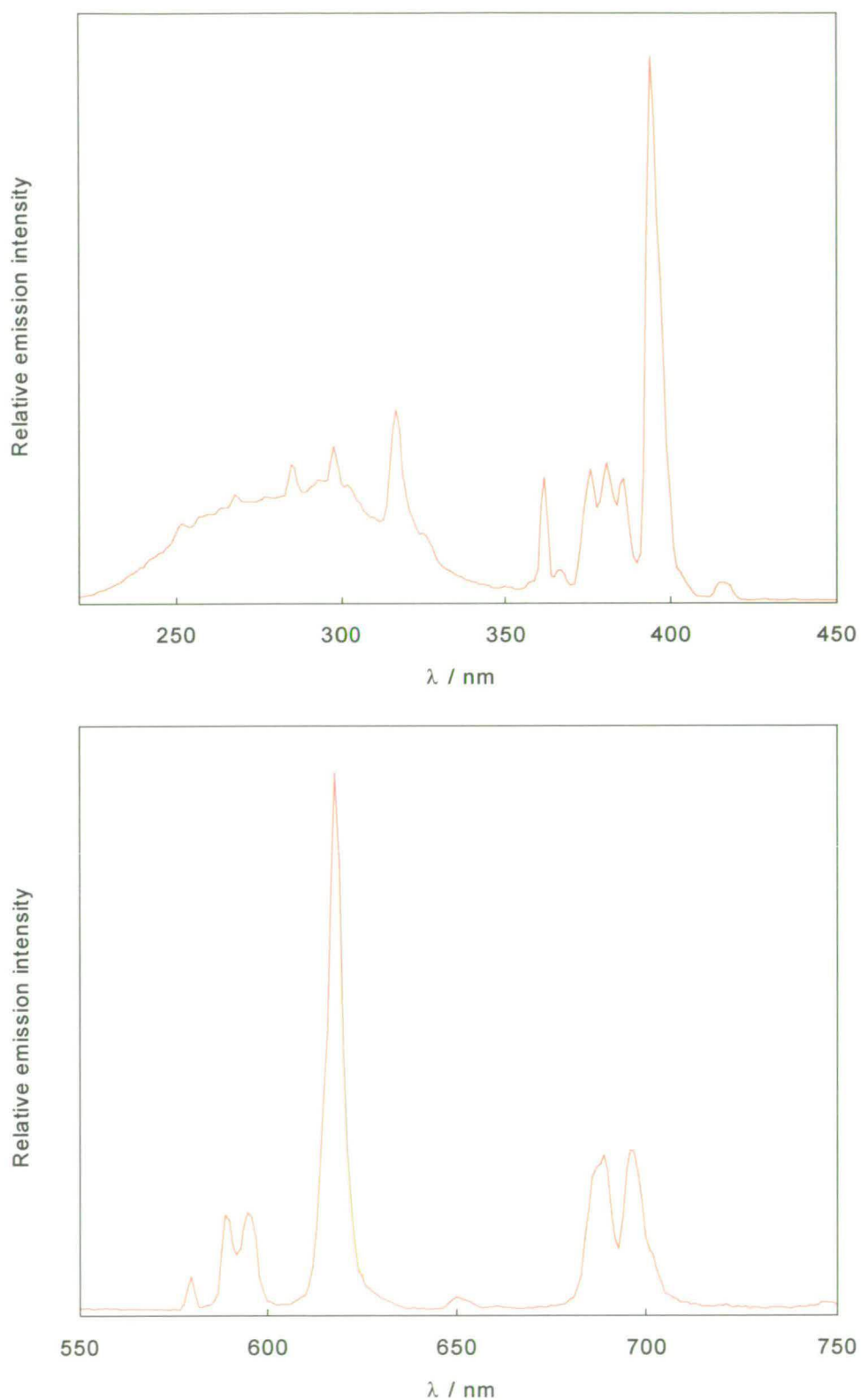
Figure 5.9 Excitation spectrum (top) and corrected emission spectrum (bottom) of [EuDACDA]Cl (1.2 × 10^{-3} mol dm^{-3}) in 0.05 mol dm^{-3} Tris buffer (pH 7.7); λ_{em} = 618 nm, λ_{ex} = 270 nm

The $^5D_0 \rightarrow {}^7F_J$ (J = 0-4) transitions of Eu^{3+} dominate the emission spectrum of [EuDACDA]Cl. A change in the relative intensity of these bands upon complexation is common. In this case, the high intensity of the structured $^5D_0 \rightarrow {}^7F_4$ transition (*ca.* 695 nm) relative to the other $^5D_0 \rightarrow {}^7F_J$ transitions is noteworthy. Such an enhancement of the $^5D_0 \rightarrow {}^7F_4$ intensity has also been observed for Eu^{3+} complexes of DOTA and related aza macrocycles.[28,29] An explanation for this phenomenon, beyond the simple one of complexation, is outside the scope of this work as the intensities of *f-f* transitions are still the subject of much theoretical analysis.[30]

Confirmation that [EuDACDA]$^+$ is maintained in solution is given by luminescence lifetime measurements. The Eu^{3+} ($^5D_0$) lifetimes of [EuDACDA]Cl (1×10^{-3} mol dm^{-3}) in H_2O and D_2O are 0.43 ms and 1.50 ms respectively. The samples were excited at 355 nm, measurements were made at the natural pH (*ca.* 7) of the solutions and monoexponential decays were obtained. As discussed in Chapter 2, the number of coordinated water molecules can be calculated using equation 2.7, giving a q-value of 1.7. If equation 2.8 is used, thereby taking into account any outer sphere water molecules, a q_{corr}-value of 1.7 is also obtained.

A previous study of [EuDACDA]Cl in aqueous solution at pH 6 reported lifetimes of 0.46 and 1.19 ms in H_2O and D_2O respectively, giving a q-value of 1.4 and a q_{corr}-value of 1.3.[17] The authors of this report suggested that the q-value possibly reflected a weighted average of complexes with one and two coordinated water molecules, in agreement with the multiple bands they observed in the $^7F_0 \rightarrow {}^5D_0$ high-resolution excitation spectrum.

Since the preformed [EuDACDA]Cl complex used in the present study shows a 10-coordinate Eu^{3+} in the crystal structure, the slightly higher q-values obtained do not seem unreasonable. The negligible difference between corrected and uncorrected q-values suggests that the non-integral q-values can be attributed to complexes with different numbers of coordinated waters rather than to the error in the estimation of q.

5.2.2 Lanthanide complexes of MACMA

Preparation

The ligand HMACMA was prepared as the hydrochloride hydrate (HMACMA.HCl.nH₂O) (1 < n < 2) by the hydrolysis of ethyl 1,4,7,10-tetraoxa-13-azacyclopentadecane-13-acetate (42) according to a literature procedure.[23]

42
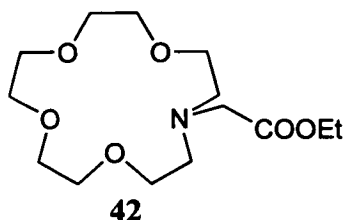
For the complex syntheses, a solution of HMACMA·HCl in dry acetonitrile was added to a solution of M(NO₃)₃ (M = Eu, Y) and triethylorthoformate in dry acetonitrile. The use of triethylorthoformate as a drying agent for the preparation of lanthanide complexes in acetonitrile is well documented.[31] The crystalline sample obtained from the Eu³⁺ reaction analysed as [EuMACMA](NO₃)₂·3H₂O (20% yield). The FAB-MS spectrum of this product showed an intense peak at *m/z* 489 corresponding to [*M*–NO₃]⁺. Similarly, the FAB-MS spectrum of the Y³⁺ product showed an intense peak at *m/z* 427 assigned as [*M*–NO₃]⁺. Since attempts to crystallise the Eu³⁺ complex of MACMA were unsuccessful, studies focused on the solution phase.

Solution structure of [LnMACMA](NO₃)₂

The positive-ion electrospray mass spectrum of [EuMACMA](NO₃)₂ in H₂O (Figure A8 in Appendix I) shows peaks at *m/z* 489 and 491, corresponding to [*M*–NO₃]⁺, as found in the FAB-MS spectrum. This is a good indication that the complex is maintained in solution. There is also an intense peak at *m/z* 278 that can be assigned to the free ligand, [MACMA + 2H]⁺.

In the ¹H NMR spectrum of [YMACMA](NO₃)₂ in D₂O, all of the protons can be accounted for by a poorly resolved multiplet at δ 3.68-3.97 and a broad singlet at δ 3.42, which integrate as 18 and 4 protons respectively. Similarly, the ¹H NMR spectrum of

[EuMACMA](NO$_3$)$_2$ in CD$_3$NO$_2$ shows an unresolved multiplet at δ 3.37-3.70 and a broad singlet at δ 2.89, which integrate as 6 and 16 protons respectively (this is an approximation as the signals were weak). These spectra suggest that fluxional processes, which are slow on the NMR timescale, are operative for these complexes in solution.

Both steady-state excitation and emission spectra were recorded for solutions of [EuMACMA](NO$_3$)$_2$ in Tris buffer (Figure 5.10). The comments made for the luminescence spectra of [EuDACDA]Cl also apply to the [EuMACMA](NO$_3$)$_2$ spectra. Complexation by MACMA is demonstrated by the broad UV bands attributed to LMCT transitions, while the emission spectrum displays a relatively high intensity $^5D_0 \rightarrow {^7F_4}$ transition (*ca.* 695 nm). Despite being recorded under the same conditions (*eg.* excitation wavelength and instrument settings), the emission spectrum of [EuMACMA](NO$_3$)$_2$ is significantly weaker than that of Eu[DACDA]Cl. Although the stability constant of [EuMACMA](NO$_3$)$_2$ has not been measured, the 1×10^{-3} mol dm^{-3} solution concentration used should ensure that the complex is the predominant species. Since the excitation spectra of both complexes have very similar profiles, the dramatic reduction in intensity was thought to be due to more deactivating water molecules coordinating the metal in the MACMA complex. This was confirmed by lifetime measurements.

The Eu ($^5D_0$) level of 1×10^{-3} mol dm^{-3} [EuMACMA](NO$_3$)$_2$ in H$_2$O and D$_2$O exhibits lifetimes of 0.18 ms and 1.0 ms respectively. Samples were excited at 355 nm, the solution pH was *ca.* 7.5 and monoexponential decays were obtained. The calculated values of q and q_{corr} for this complex are 4.8 and 5.2, indicating five water molecules are coordinated to the Eu^{3+} ion. This high q-value is due to the presence of only five ring donor atoms and one carboxylate group on the ligand.
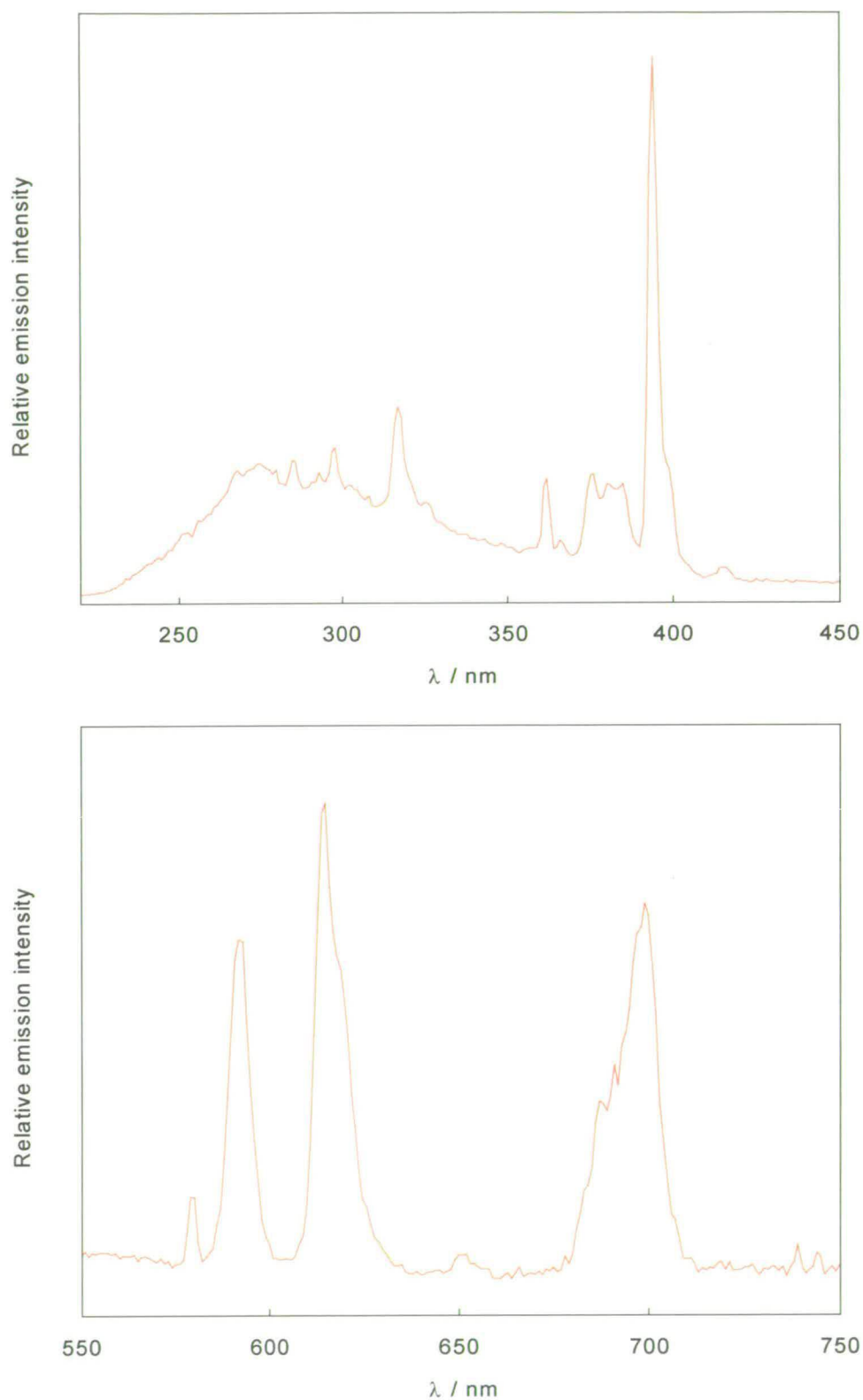
Figure 5.10 Excitation spectrum (top) and corrected emission spectrum (bottom) of [EuMACMA](NO$_3$)$_2$ (1.6 × 10^{-3} mol dm^{-3}) in 0.05 mol dm^{-3} Tris buffer (pH 7.7); λ$_{em}$ = 618 nm, λ$_{ex}$ = 270 nm

5.3   PRELIMINARY STUDIES OF TERNARY COMPLEX FORMATION

This section details the preliminary investigation of the interaction of [EuDACDA]Cl and [EuMACMA](NO$_3$)$_2$ with aromatic acids, using electrospray mass spectrometry (ES-MS) and luminescence spectroscopy. These two techniques are increasingly being used together for the characterisation of lanthanide complexes in solution.[32]

5.3.1 Electrospray MS studies of ternary complex formation

ES-MS allows complexes to be studied in the same solvents used for complementary techniques such as NMR and luminescence spectroscopy. It is a very soft ionisation technique and in many cases has been shown to qualitatively reflect the species that exist in solution (see Chapter 4). In spite of it's advantages and widespread use, however, the processes involved in the electrospray technique are not yet fully understood.[33] Apart from the effect of the specific instrumentation and settings employed, important factors that could influence the observed spectra obtained for complexes include the charge on the complex, the stability of the complex, the concentration and the solvent.[32]

The samples used for ES-MS were aqueous solutions of [EuDACDA]Cl, [TbDACDA]Cl or [EuMACMA](NO$_3$)$_2$ mixed with an aqueous solution of either picolinic or phthalic acid. The concentration of the crown complex was 1×10^{-4} mol dm^{-3}, while the concentration of the aromatic acids ranged from 1×10^{-4} to 1×10^{-3} mol dm^{-3}. For [EuDACDA]Cl and [TbDACDA]Cl mixtures, the pH was adjusted to *ca.* 7.5 with NaOH (aq), while for the [EuMACMA](NO$_3$)$_2$ mixtures the pH of the solutions was adjusted to *ca.* 7.5 with either NaOH (aq) or aqueous tetrabutylammonium hydroxide (TBAOH). Both picolinic acid (pKa *ca.* 5.4)[34] and phthalic acid (pKa *ca.* 2.8 and 5.4)[35] exist almost completely in their fully deprotonated forms at pH 7.5, giving the picolinate (PCA$^-$) and phthalate (Phth^{2-}) anions respectively.

The ES(+)-MS spectrum of a solution of [EuDACDA]Cl with two equivalents of picolinic acid (Figure A9 in Appendix I) shows reasonably strong peaks at *m/z* 527 and

529, corresponding to [EuDACDA]$^+$, as observed in the FAB-MS spectrum. The expansion shows that there are also weaker peaks at *m/z* 672 and 674 which are assigned as [EuDACDA + PCA + Na]$^+$. This is a good indication that the neutral ternary complex [Eu(DACDA)(PCA)] is present in solution, with the association of a Na$^+$ ion during the electrospray process producing the charged species observed. No peaks identified as Eu^{3+}-containing species were observed in the ES(–)-MS spectrum; the strongest peak was for free picolinate at *m/z* 122.

Similarly, the ES(+)-MS spectrum of a solution of [EuDACDA]Cl with two equivalents of phthalic acid (Figures A10 and A11 in Appendix I) shows peaks due to [EuDACDA]$^+$ at *m/z* 527 and 529, and peaks corresponding to the ternary species [EuDACDA + Phth + Na + H]$^+$ at *m/z* 715 and 717. While a ternary complex of [EuDACDA]$^+$ with picolinate is neutral, the ternary complex with phthalate should have a negative charge at pH 7.5. The ES(–)-MS spectrum of the phthalic acid mixture (Figures A10 and A11 in Appendix I) clearly shows peaks at *m/z* 691 and 693, corresponding to the ternary species [EuDACDA + Phth]$^-$, in addition to a peak at *m/z* 165 due to free phthalate. It should be noted that no peaks due to free DACDA were observed in either the positive or negative ion mode spectra of both picolinate and phthalate mixtures, suggesting that the [EuDACDA]Cl complex survives the ionisation process intact.

ES-MS spectra of [TbDACDA]Cl with aromatic acids corroborates the results obtained for [EuDACDA]Cl. The mixtures investigated also contained two equivalents of acid, though the actual concentration of [TbDACDA]Cl will be slightly lower than 1×10^{-4} mol dm^{-3} as the sample is not pure. The spectra are very similar to those obtained for the [EuDACDA]Cl mixtures. In the ES(+)-MS spectrum of the picolinate mixture, peaks are observed at *m/z* 535 and 680 due to [TbDACDA]$^+$ and [TbDACDA + PCA + Na]$^+$ respectively. For the phthalate mixture, the ES(+)-MS spectrum shows peaks at *m/z* 535 and 680 due to [TbDACDA]$^+$ and [TbDACDA + Phth + Na + H]$^+$ respectively, while the ES(–)-MS spectrum shows a peak at *m/z* 699 due to [TbDACDA + Phth]$^-$. Again, no peaks assigned to the free DACDA ligand were observed.

In contrast to the ES-MS data obtained for the DACDA complexes, no peaks attributed to Eu^{3+}-containing species were observed in any of the mixtures of [EuMACMA](NO_3)$_2$ with picolinic or phthalic acid. For solutions containing one or two equivalents of acid, with the pH adjusted with NaOH (aq), the strongest peaks in the ES(−) spectra are attributed to nitrate ion (*m/z* 62), the free aromatic acid (*m/z* 122 and 165 for picolinate and phthalate respectively) and free MACMA (*m/z* 276); the strongest peaks in the ES(+) spectra are at *m/z* 300 due to [MACMA + Na + H]$^+$. For solutions containing one, two or ten equivalents of acid, with the pH adjusted with TBAOH (aq), the strongest peaks observed in the ES(−) spectra are for the nitrate ion and the free acid; the strongest peaks in the ES(+) spectra are assigned to TBA$^+$ (*m/z* 242), [MACMA + TBA + H]$^+$ (*m/z* 519) and [(TBA)$_2$ + NO_3]$^+$ (*m/z* 546).

As discussed previously, ES-MS of an aqueous solution of [EuMACMA](NO_3)$_2$ showed peaks at *m/z* 489 and 491, corresponding to [EuMACMA + NO_3]$^+$ (Figure A8 in Appendix I). Although the concentration of this sample was not recorded, the concentration would have been in the region of 10^{-4}-10^{-5} mol dm^{-3} (*ie.* a suitable concentration for the ES-MS experiment). In other words, the addition of the picolinic or phthalic acid solution to the [EuMACMA](NO_3)$_2$ solution appears to result in the disappearance of the [EuMACMA + NO_3]$^+$ peak and the appearance of new peaks that correspond to association of MACMA with either Na$^+$ or TBA$^+$.

One possible explanation is that the presence of the Na$^+$ or TBA$^+$ ions results in the removal of the Eu^{3+} ion from the crown. Indeed, the pH of the [EuMACMA](NO_3)$_2$ solution used for the ES-MS spectrum shown in Figure A8 was not altered, thus the concentration of other cations would have been minimal. Another explanation is that the observed peaks are simply due to the electrospray ionisation process. In order to properly rationalise these results, a thermodynamic and kinetic analysis of [EuMACMA](NO_3)$_2$, analogous to that reported for [EuDACDA]Cl, is needed. This would clarify the amount of free ligand expected at a given concentration and the dissociation pathways of the complex.

5.3.2 Luminescence studies of ternary complex formation

The motivation for studying ternary complex formation was the development of new homogeneous fluoroimmunoassays, in which energy transfer occurs from a light-harvesting ligand to a Ln^{3+} ion that is complexed to a non-absorbing ligand. These preliminary studies investigate the effect of addition of a light-harvesting ligand on the photophysical properties of a solution containing a Eu^{3+}-crown complex.

Emission spectra were recorded for aqueous solutions containing [EuDACDA]Cl or [EuMACMA]$(NO_3)_2$, before and after the addition of picolinic or phthalic acid. The pH of all solutions used was kept constant by dissolving the species in Tris buffer (pH 7.7). The concentration of the acid solutions was much greater than that of the Eu^{3+} solutions, thereby ensuring negligible volume change upon addition of the acid.

As shown in Figures 5.11 and 5.12, addition of picolinic acid to solutions of [EuDACDA]Cl or [EuMACMA]$(NO_3)_2$ results in a new peak in the excitation spectra at *ca.* 271 nm. From the emission spectrum it is clear that this new excitation peak is due an increase in Eu^{3+} luminescence, and it can be attributed to energy transfer from bound picolinate; picolinate has an absorption band at 270 nm (ε_{max} *ca.* 3500 dm^3 mol^{-1} cm^{-1}).

In selecting ligands to act as light harvesters, it is important that their stability constants with the Ln^{3+} ion are reasonably high, but not so high that replacement of the crown ether may occur. For the 1:1 complexation with Eu^{3+}, log K = 3.99 and 3.70 for picolinic[34] and phthalic[35] acid respectively. These stability constants are much lower than the value reported for [EuDACDA]$^+$ (log K = 12.02), so ligand exchange should not be a problem.[36] In view of this, the change in the spectra shown in Figures 5.11 and 5.12 can be attributed to the binding of picolinate to [EuDACDA]$^+$. Following the addition of picolinic acid, the growth of Eu^{3+} emission of a [EuDACDA]Cl solution was monitored with time and equilibration was found to have occurred within a few seconds. As [EuDACDA]$^+$ is relatively inert,[16] this supports the conclusion that picolinate binds to [EuDACDA]$^+$.
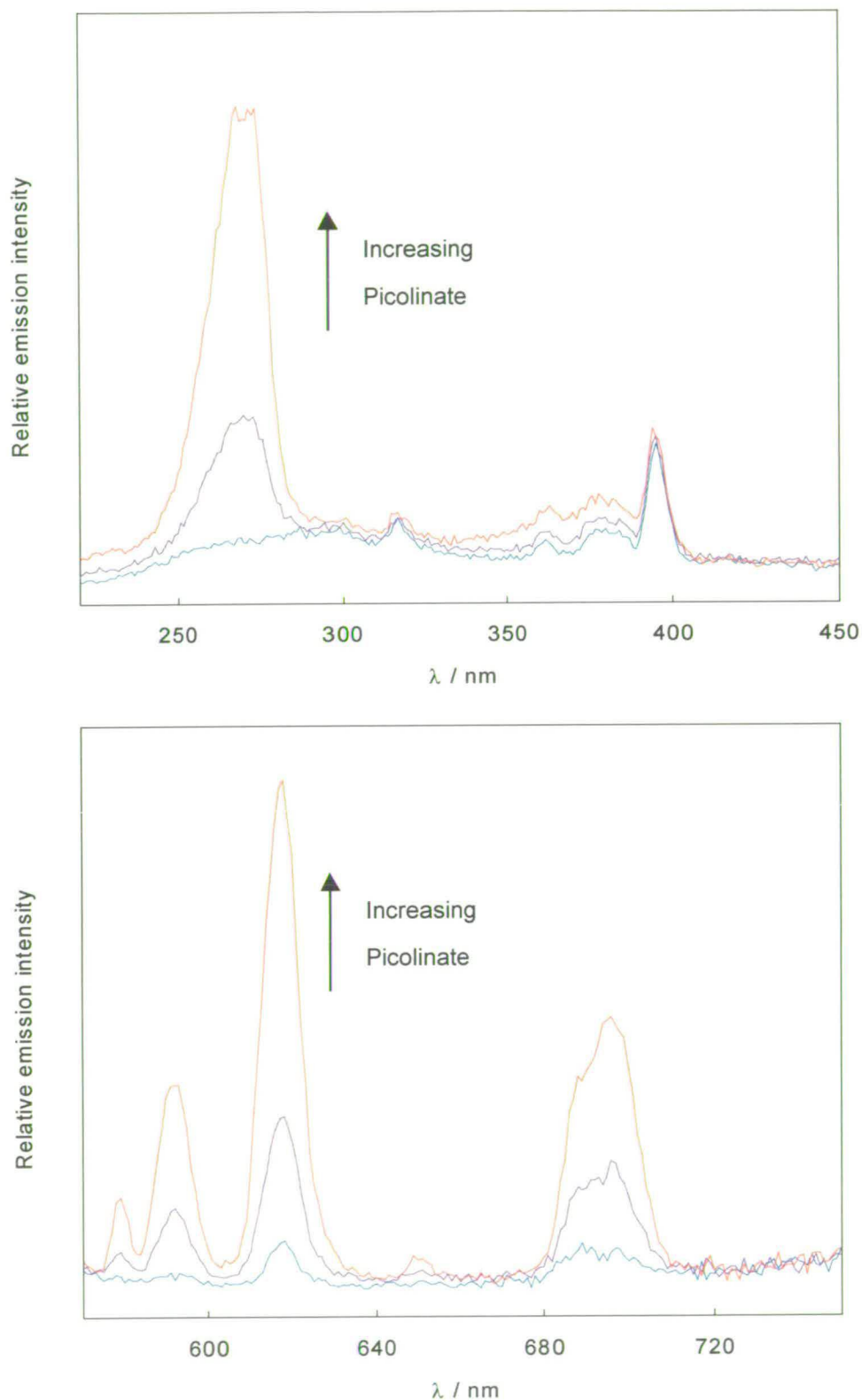
Figure 5.11 Excitation (top) and corrected emission spectra (bottom) of [EuDACDA]Cl $(1.2 \times 10^{-5} \text{ mol dm}^{-3})$ in 0.05 mol dm^{-3} Tris buffer (pH 7.7) containing no picolinate, 1 equiv. of picolinate or 4 equiv. of picolinate; $\lambda_{ex} = 270$ nm, $\lambda_{em} = 618$ nm

Figure 5.12 Excitation (top) and corrected emission spectra (bottom) of [EuMACMA](NO$_3$)$_2$ (1.6 × 10^{-5} mol dm^{-3}) in 0.05 mol dm^{-3} Tris buffer (pH 7.7) containing no picolinate, 1 equiv. of picolinate or 4 equiv. of picolinate; λ_{ex} = 270 nm, λ_{ex} = 617 nm

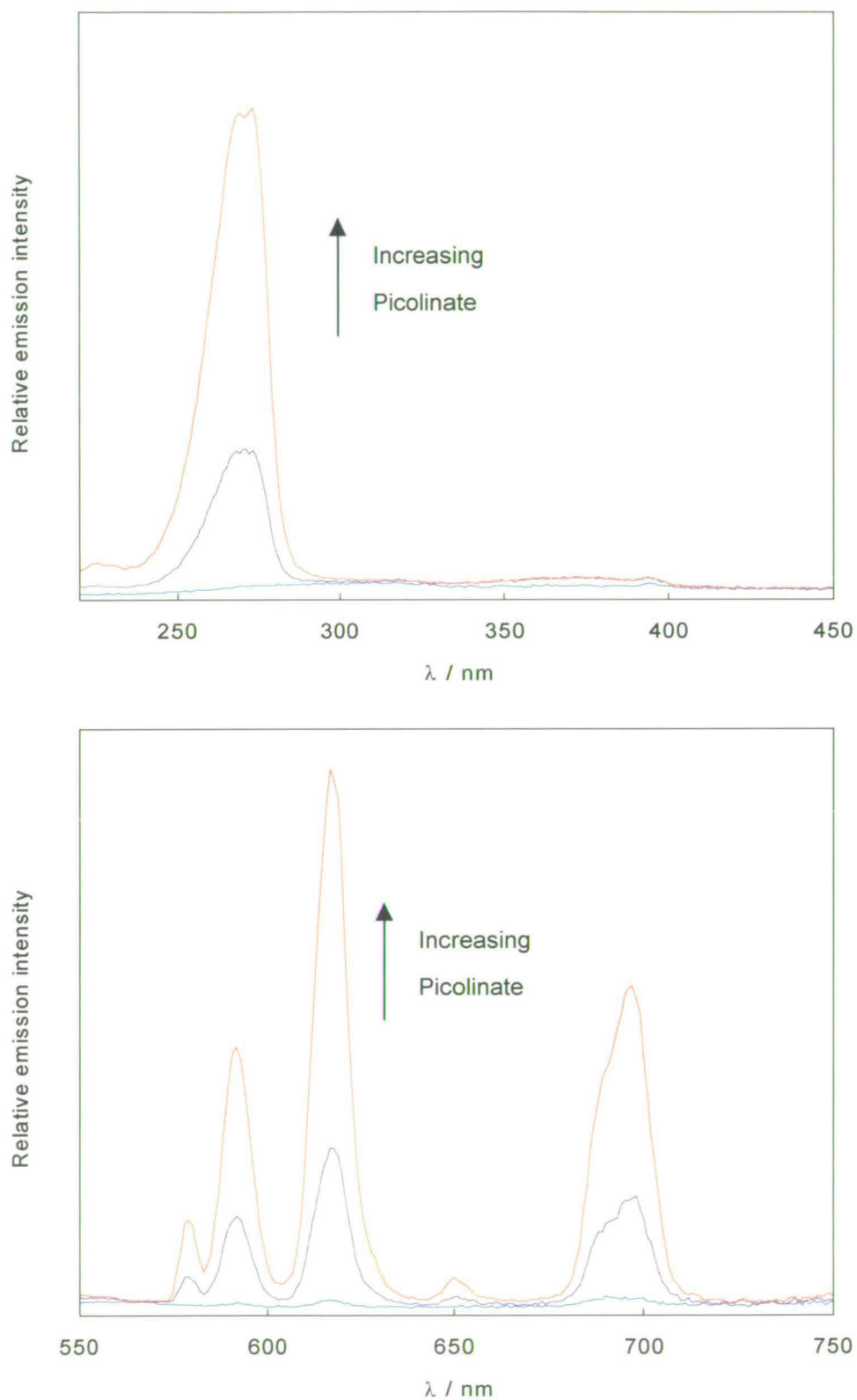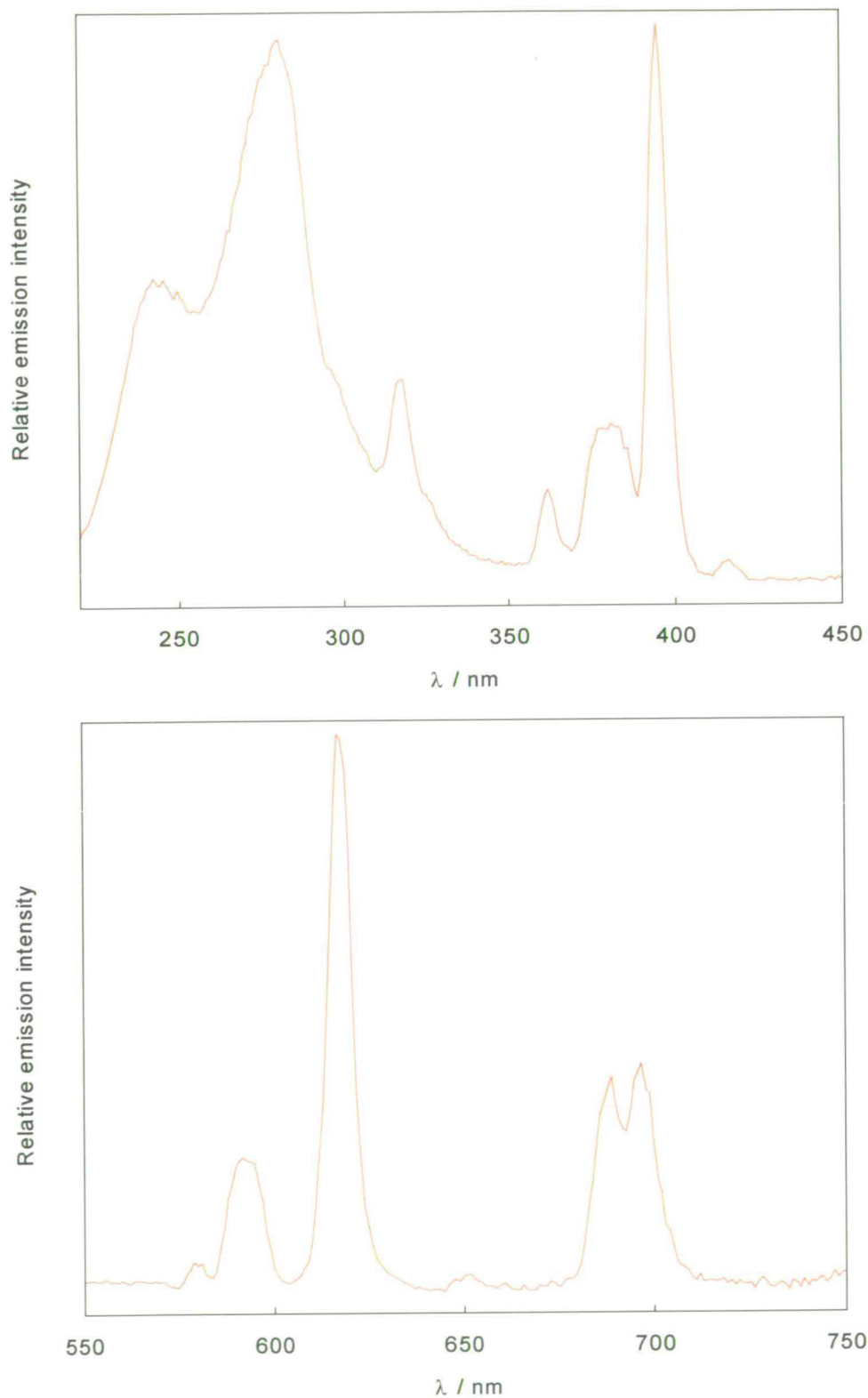**Figure 5.13** Excitation (top) and corrected emission spectra (bottom) of [EuDACDA]Cl (1.2×10^{-4} mol dm^{-3}) in 0.05 mol dm^{-3} Tris buffer (pH 7.7) containing 1 equiv. of phthalate; $\lambda_{ex} = 270$ nm, $\lambda_{ex} = 617$ nm

As the number of free Eu^{3+} coordination sites in $[EuDACDA]^+$ is limited to two, the most plausible explanation for the data in Figure 5.11 is that the ternary complex has formed, in agreement with the ES-MS data previously discussed. Figure 5.11 also shows that upon addition of four equivalents of picolinic acid, there is a further substantial increase in both Eu^{3+} emission and the excitation peak at 271 nm. Assuming that the ternary complex is formed, this means that the binding of picolinate to $[EuDACDA]^+$ is not quantitative at these concentrations.

The solution equilibria play a more obvious role in the binding experiments involving phthalate. At solution concentrations of *ca.* 1×10^{-5} mol dm^{-3}, as used for picolinate binding, no change in the emission or excitation spectra was observed, even after addition of four equivalents of phthalic acid. However, the emission and excitation spectra of a 1.2×10^{-4} mol dm^{-3} solution of [EuDACDA]Cl and one equivalent of phthalic acid (Figure 5.13) indicates energy transfer from phthalate to Eu^{3+} has occurred. The peak at 280 nm in the excitation spectrum correlates with a phthalate absorption band (ε_{270} *ca.* 1500 dm^3 mol^{-1} cm^{-1}). The luminescence spectra for $[EuMACMA](NO_3)_2$ and phthalate were not recorded at higher concentration.

Lifetime measurements provide additional means to monitor and assess ternary complex formation. The Eu ($^5D_0$) lifetime of a 1.3×10^{-4} mol dm^{-3} solution of [EuDACDA]Cl in 0.05 mol dm^{-3} Tris buffer (pH 7.7) was found to be 0.42 ms, in agreement with that measured in non-buffered H_2O. The excitation wavelength was 355 nm and the decay was found to be monoexponential. After addition of seven equivalents of picolinic acid (also in buffer) the lifetime was 0.39 ms, which is the same within experimental error. An excitation spectrum of this solution was recorded, confirming that the picolinate had interacted with the metal as discussed above.

It was originally envisaged that binding of the picolinate would result in expulsion of the water molecule, with a corresponding increase in the luminescence lifetime. Since $[EuDACDA]^+$ has at least one coordinated water molecule, the lifetime data seemed quite surprising. Assuming ternary complex formation has occurred, there are a number of explanations for these data. One possibility is that picolinate removes the coordinated

water molecule but provides an additional deactivating pathway. This was the explanation given for the reduction in the Eu ($^5D_0$) lifetime of certain 1:1 Eu^{3+}:β-diketonate complexes in aqueous solution.[37] The authors suggested a ligand-centred triplet level may be involved, though LMCT states could presumably play a part.

Another explanation is that picolinate binds to $[EuDACDA]^+$ but does not displace the remaining water molecule(s). Indeed, a number of Eu^{3+} complexes, with q-values > 1, appear unable to have their remaining water molecule displaced by carbonate and phosphate anions, perhaps due to steric effects.[38] A final explanation for the small change in lifetime is that the amount of ternary complex in solution is small and in fast exchange with $[EuDACDA]^+$. This would result in the observed luminescence being predominately from $[EuDACDA]^+$. Knowledge of the equilibria of these systems, together with lifetime measurements in H_2O and D_2O, would help to clarify all of the luminescence results discussed in this section.

5.4 CONCLUSIONS

This chapter is concerned with the ternary complexation of lanthanides with crown ethers and aromatic acids, with a view to the development of improved methods of luminescent labelling. Complexes of the ligand DACDA with lanthanides (La^{3+}, Eu^{3+} and Tb^{3+}) have been isolated for the first time, and the europium and terbium complexes adopt an interesting polymeric structure in the solid state; these complexes have also been characterised by NMR and luminescence spectroscopy. The first studies of lanthanide complexes of the crown ether MACMA have been performed; lifetime measurements show that the europium complex has five water molecules coordinated to the metal ion in aqueous solution, in contrast to the 1-2 coordinated water molecules in [EuDACDA]Cl.

The results of the preliminary investigation into ternary complex formation are very promising. Luminescence spectra confirm the interaction of picolinate and phthalate with $[EuDACDA]^+$, and ES-MS spectra show signals corresponding to the ternary

species. Similarly, luminescence spectra indicate that picolinate coordinates to [EuMACMA]$^{2+}$ in aqueous solution. While the data obtained for the mixtures of crown complexes and aromatic acids strongly suggest that ternary complexes are formed, this must be firmly established before embarking on further studies.

It should be reasonably straightforward, however, to quantify the binding process between [EuDACDA]$^+$ or [EuMACMA]$^{2+}$ and picolinate or phthalate by standard titration methods. The stoichiometry of the new complexes could be determined by monitoring changes in the emission spectra following addition of the light-harvesting ligand to the crown complex, under conditions in which quantitative binding occurs.[39] The effect of the number of H_2O-occupied coordination sites on the stoichiometry of the complexes that are formed is of particular interest.

5.5   REFERENCES

1.   E. P. Diamandis and T. K. Christopoulos, *Anal. Chem.*, 1990, **62**, 1449A.

2.   I. Hemillä, *J. Alloys Compd.*, 1995, **225**, 480.

3.   G. Mathis, *Clin. Chem.*, 1993, **39**, 1953.

4.   P. R. Selvin, T. M. Rana and J. E. Hearst, *J. Am. Chem. Soc.*, 1994, **116**, 6029.

5.   C. F. Meares and T. G. Wensel, *Acc. Chem. Res.*, 1984, **17**, 202.

6.   H. G. Brittain and S. Rivera, *Inorg. Chim. Acta*, 1985, **110**, 35.

7.   A. Oser and G. Valet, *Angew. Chem. Int. Ed. Engl.*, 1990, **29**, 1167.

8.   P. G. Sammes, G. Yahioglu and G. D. Yearwood, *Chem. Commun.*, 1992, 1282.

9.   C. A. Chang and V. O. Ochaya, *Inorg. Chem.*, 1986, **25**, 355.

10.   J. Coates, P. G. Sammes and R. M. West, *J. Chem. Soc., Perkin Trans. 2*, 1996, 1283.

11.   G. W. Gokel, *Chem. Soc. Rev.*, 1992, 39.

12.   D. J. Cram, T. Kaneda, R. G. Helgeson, S. B. Brown, C. B. Knobler, E. Maverick and K. N. Trueblood, *J. Am. Chem. Soc.*, 1985, **107**, 3645.

13.   F. Arnaud-Neu, *Chem. Soc. Rev.*, 1994, 235.

14.   C. A. Chang and M. E. Rowland, *Inorg. Chem.*, 1983, **22**, 3866.

15. C. A. Chang, B. S. Garg, V. K. Manchanda, V. O. Ochaya and V. C. Sekhar, *Inorg. Chim. Acta*, 1986, **115**, 101.

16. C. A. Chang and V. C. Sekhar, *Inorg. Chem.*, 1987, **26**, 1981.

17. R. C. Holz, S. L. Klakamp, C. A. Chang and W. DeW. Horrocks, Jr., *Inorg. Chem.*, 1990, **29**, 2650.

18. V. K. Manchanda, P. K. Mohapatra, C. Zhu and R. M. Izatt, *J. Chem. Soc., Dalton Trans.*, 1995, 1583.

19. G. R. Choppin, in *Lanthanide Probes in Life, Chemical and Earth Sciences*, eds. J.-C. G. Bünzli and G. R. Chopin, Elsevier, Amsterdam, 1989, ch. 1.

20. H. G. Brittain, *Inorg. Chem.*, 1979, **18**, 1740 and reference therein.

21. M.-R. Spirlet, J. Rebizant, J. F. Desreux and M.-F. Loncin, *Inorg. Chem.*, 1984, **23**, 359.

22. J.-C. G. Bünzli, G. A. Leonard, D. Plancharel and G. Chapuis, *Helv. Chim. Acta.*, 1986, **69**, 288.

23. K. A. Byriel, L. R. Gahan, C. H. L. Kennard, J. L. Latten and P. C. Healy, *Aust. J. Chem.*, 1993, **46**, 713.

24. A. S. Gajadhar-Plummer, I. A. Kahwa, A. J. P. White and D. J. Williams, *Inorg. Chem.*, 1999, **38**, 1745 and references therein.

25. S. Aime, M. Botta, M. Fasano, M. P. M. Marques, C. F. G. C. Geraldes, D. Pubanz and A. E. Merbach, *Inorg. Chem.*, 1997, **36**, 2059.

26. S. P. Sinha, in *Systematics and the Properties of the Lanthanides*, ed. S. P. Sinha, D. Reidel Publishing Company, Dordrecht, 1983, ch. 10.

27. N. Sabbatini, S. Dellonte, M. Ciano, A. Bonazzi and V. Balzani, *Chem. Phys. Lett.*, 1984, **107**, 212.

28. C. C. Bryden and C. N. Reilley, *Anal. Chem.*, 1982, **54**, 610.

29. S. Aime, A. S. Batsanov, M. Botta, J. A. K. Howard, D. Parker, K. Senanayake and G. Williams, *Inorg. Chem.*, 1994, **33**, 4696.

30. G. F. de Sá, O. L. Malta, C. de Mello Donegá, A. M. Simas, R. L. Longa, P. A. Santa-Cruz and E. F. da Silva Jr., *Coord. Chem. Rev.*, 2000, **196**, 165.

31. O. A. Gansow and A. R. Kauser, *Inorg. Chim. Acta*, 1985, **95**, 1.

32. C. Piguet, G. Bernardinelli and G. Hopfgartner, *Chem. Rev.*, 1997, **97**, 2005.

33. M. Goodall, P. M. Kelly, D. Parker, K. Gloe and H. Stephan, *J. Chem. Soc.,*

Perkin Trans. 2, 1997, 59 and references therein.

34. A. E. Martell and R. M. Smith, *Critical Stability Constants, Vol. 1*, Plenum Press, New York, 1974.

35. A. E. Martell and R. M. Smith, *Critical Stability Constants, Vol. 3*, Plenum Press, New York, 1977.

36. L. C. Thompson and J. A. Loraas, *Inorg. Chem.*, 1963, **2**, 89.

37. S. T. Frey, M. L. Gong and W. DeW. Horrocks, Jr., *Inorg. Chem.*, 1994, **33**, 3229.

38. R. M. Supkowski and W. DeW. Horrocks, Jr., *Inorg. Chem.*, 1999, **38**, 5616.

39. *Fluorescence Spectroscopy: An Introduction for Biology and Medicine*, eds. A. J. Pesce, C. G. Rosén and T. L. Pasby, Marcel Dekker Inc., New York, 1971, ch. 7.

Chapter Six

Experimental

6.1   GENERAL PROCEDURES AND CHARACTERISATION TECHNIQUES

6.1.1 Solvents, starting materials and syntheses

Starting materials were of reagent grade, obtained from Aldrich or Acros, and used without further purification, unless otherwise stated. Lanthanide(III) chlorides and lanthanide(III) nitrates were obtained from Aldrich or Acros (99.9%) and used as received. Deuterated solvents were obtained from Goss Scientific and used as received. Anhydrous solvents, when required, were freshly distilled over the appropriate drying agents under dinitrogen.[1]

Reactions requiring anhydrous conditions were performed under dinitrogen using standard Schlenck and vacuum line techniques.[2] Subsequent work-up of products was carried out without precautions to exclude air. Thin layer chromatography was performed using glass plates precoated with Merck Kieselgel 60 PF$_{254}$.

6.1.2 Spectroscopic and analytical measurements

^{1}H-, ^{13}C{^{1}H}- and ^{31}P{^{1}H}-NMR spectra were performed by the departmental service on Bruker AC-200, 250, 360 MHz and Varian INOVA 600 MHz spectrometers. ^{1}H and ^{13}C{^{1}H} shifts were referenced to external SiMe$_4$, while ^{31}P{^{1}H} shifts were referenced to external 85% aqueous phosphoric acid. Positive ion FAB mass spectrometry was performed by the departmental service on a Kratos MS-50 mass spectrometer, using a *m*-nitrobenzyl alcohol matrix, unless otherwise stated. Elemental analyses were performed by the departmental service using a Perkin-Elmer 2400 CHN elemental analyser. Routine UV absorption spectra were recorded on a Unicam UV/Vis UV2-100 spectrometer. IR spectra were obtained from KBr pellets with a Perkin-Elmer 1710 Fourier Transform spectrometer. Electrospray mass spectra were performed at the EPSRC Mass Spectrometry Service Centre, University of Wales, Swansea using a Micromass Quattro II low resolution triple quadrupole mass spectrometer or performed by the departmental service using a Finnigan LCQ spectrometer. A Metrohm electrode

and pH meter (E632) were used for pH measurements and were calibrated using buffers (pH 4, 7 and 9) obtained from Fluka.

6.1.3 Crystallography

Single-crystal x-ray crystallography was performed by Dr. Simon Parsons. Diffraction data were collected with either Mo-Kα or Cu-Kα radiation on a Stoe Stadi-4 diffractometer equipped with an Oxford Cryosystems low temperature device. On one occasion data were collected using synchrotron radiation (λ = 0.6875 Å) on Station 9.8 at Daresbury Laboratory. Structures were solved by direct or Patterson methods (SHELXS, SIR 92 or DIRDIF) and refined against F^2 (SHELXL) or F (CRYSTALS).

6.2   LUMINESCENCE MEASUREMENTS

6.2.1 General

UV absorption spectra for luminescence studies were recorded on a Perkin-Elmer Lambda 9 spectrometer. All measurements were made at room temperature (*ca.* 20 °C) in aerated solutions, unless otherwise stated. DMF and methanol were of spectroscopic grade and used as received. CH$_3$CN was dried over P$_2$O$_5$ (5% w/v) and freshly distilled prior to use. Water was purified by a Millipore (Milli-RO 15) water purification system. Deuterated solvents for photophysical studies were obtained from Goss Scientific and used as received. Tris buffer (0.05 mol dm^{-3}) at pH 7.7 (25 °C) was prepared by mixing the appropriate amounts of tris(hydroxymethyl)aminomethane and [tris(hydroxymethyl)-aminomethane]hydrochloride in water.

6.2.2 Steady-state luminescence spectroscopy

Luminescence emission and excitation spectra were recorded on a Photon Technology International (PTI) QM-1 emission spectrometer. Data were acquired using FeliX

software. The excitation source was either a 75 or 150 W xenon arc lamp. Emission and excitation monochromators (PTI model 101) were in a f/4 0.2-metre Czerny-Turner configuration with standard 1200 lines/mm grating. Luminescence emission was collected at 90° and detected, after passing through appropriate cut-off filters, by a R928 Hamamatsu photomultiplier tube (PMT). Emission spectra were typically obtained using an excitation and emission bandpass of 5 nm, with the most highly resolved spectra having an emission bandpass of 1 nm. Emission spectra were corrected for the wavelength dependence of the PMT. Uncorrected excitation spectra were typically obtained using an excitation and emission bandpass of 5 nm, with the most highly resolved spectra having an excitation bandpass of 1 nm. The absorbance of solutions was kept low (≤ 0.1) over the wavelength region examined when obtaining excitation spectra.

6.2.3 Luminescence lifetime measurements

Data acquisition

Lifetime measurements were carried out using a nanosecond Nd-YAG laser (Continuum, Surelite II) as the excitation source. The experimental set-up is shown in Figure 6.1. The third or fourth harmonic output of the laser was used for excitation at 355 nm or 266 nm respectively. Emission from the sample was collected at 90°, passed through appropriate cut-off filters and detected by a photomultiplier tube (Hamamatsu R928) following wavelength selection by a PC-controlled monochromator (PTI model 101) with a bandpass of 5 nm. Emission was monitored at 616 nm for Eu^{3+} ($^{5}D_0$), 545 nm for Tb^{3+} ($^{5}D_4$), 647 nm for Sm^{3+} ($^{4}G_{5/2}$) and 574 nm for Dy^{3+} ($^{4}F_{9/2}$). The signal from the photomultiplier tube was processed through a digital storage oscilloscope (LeCroy 9350 AM, 500 MHz), triggered by the laser pulse. The emission decay curves were averaged over 1000 laser shots and transferred to a PC for analysis. For room temperature measurements, solution samples were placed in 1 cm quartz cuvette and powdered solid samples in a quartz tube. For measurements at 77 K, samples were placed in a quartz tube and cooled in a quartz dewar filled with liquid nitrogen.

Data analysis

The obtained, unweighted, data were analysed by a nonlinear, least-squares, iterative technique (Marquardt-Levenberg algorithm) using Kaleidagraph software. The luminescence decay curves were fitted to a single exponential, equation 6.1:

$$I(t) = I(0)\exp(-t / \tau)$$ (6.1)

where $I(t)$ is the intensity at time t after the excitation flash, $I(0)$ is the initial intensity at $t = 0$ and τ is the luminescence lifetime. High Pearson's correlation coefficients ($\geq$ 0.999) were observed in all cases. Lifetimes were reproducible to $\pm$ 5%.
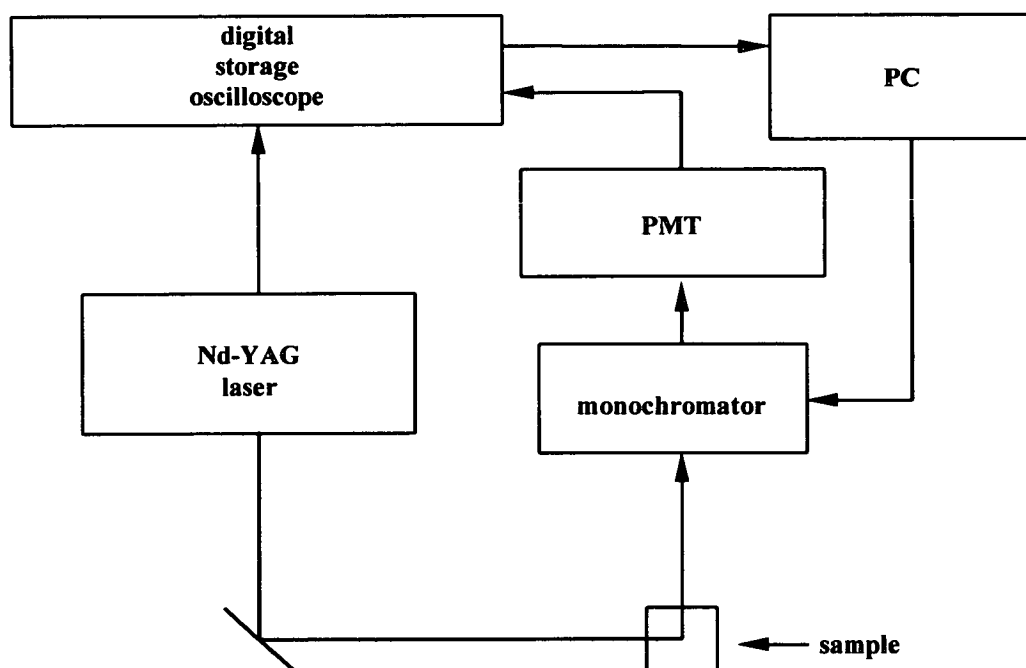
Figure 6.1 Experimental set-up for luminescence lifetime measurements

In order to establish the accuracy of the lifetime measurement, it was necessary to measure the lifetime of a suitable standard for which a reliable literature value exists. The lifetime of a solution of $EuCl_3$ in H_2O (0.1 mol dm^{-3}) is reported to be 0.10 ms $\pm$

172

10%.[3] The lifetime of this standard was measured regularly and was in good agreement with the reported value.

6.2.4 Luminescence quantum yield measurement

Luminescence quantum yields were measured by a relative method, which is the method of choice for solution determinations.[4] In the same apparatus, the quantum yield of an unknown is related to that of a standard by equation 6.2:

$$\Phi_u / \Phi_s = [A_s / A_u][I_s / I_u][n^2 / n_o^2][L_u / L_s] \tag{6.2}$$

where the u subscript refers to the unknown and s to the standard and other symbols have the following meanings: Φ is quantum yield, A is the absorbance at the excitation wavelength, I is the relative intensity of the exciting light, L is the integrated emission area across the band, n is the index of refraction of the solvent containing the unknown and n_o is the index of refraction of the solvent containing the standard. [Ru(2,2'-bipyridyl)$_3$]Cl$_2$ ($\Phi = 0.028$ in aerated H$_2$O)[5] and quinine sulfate ($\Phi = 0.546$ in aerated 0.5 mol dm^{-3} H$_2$SO$_4$)[6] were used as standards for complexes of europium(III) and terbium(III) respectively. Europium(III) emission was measured between 550 nm and 750 nm, corresponding to the dominant $^5D_0 \rightarrow {}^7F_J$ ($J = 0$-4) transitions, while terbium(III) emission was measured between 450 nm and 700 nm, corresponding to the $^5D_4 \rightarrow {}^7F_J$ ($J = 0$-6) transitions.

The relative intensity at different excitation wavelengths was measured using the emission spectrometer's reference photodiode, by comparing corrected and uncorrected excitation spectra, and also by the use of standards whose quantum yields are known to be constant over appropriate wavelength regions (quinine sulfate in 0.05 mol dm^{-3} H$_2$SO$_4$ and [Ru(2,2'-bipyridyl)$_3$]Cl$_2$ in methanol).[4,7] The absorbance of sample and standard were similar (within *ca.* 5%) and small (≤ 0.1) to minimise errors due to inner filter effects. The accuracy of these procedures is estimated to be $\pm$ 30%, due to possible cumulative systematic errors.[7]

6.3 EXPERIMENTAL DETAILS FOR CHAPTER 3

The [Sm(tpip)$_3$] and [Dy(tpip)$_3$] samples were prepared by Ross Blackwood, following the method described in this section.

Preparation of N-(P,P-diphenylphosphinoyl)-P,P-diphenylphosphinimidic acid (Htpip, 23)[8]
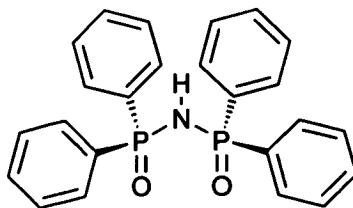
23

A solution of chlorodiphenylphosphine (4.07 g, 18.4 mmol) and hexamethyldisilazane (1.49 g, 9.23 mmol) in toluene (30 cm^3) was refluxed for 3 hours, after which time Me$_3$SiCl was distilled off. The mixture was cooled for 10 minutes in an ice bath and a solution of H$_2$O$_2$ (2 cm^3, 27.5% Wt in H$_2$O) in THF (4 cm^3) was added dropwise. This solution was added to diethyl ether (50 cm^3) resulting in the formation of a white precipitate. This solid was washed several times with water and recrystallised from methanol, giving the desired product (1.0 g, 26%) on the basis of the following spectroscopic evidence and by comparison with a sample kindly supplied by Professor J. D. Woolins (Department of Chemistry, Loughborough University). δ_H (200 MHz, CDCl$_3$) 7.27-7.7.48 (12H, m, Ar), 7.65-7.80 (8H, m, Ar); $\delta_P\{^1H\}$ (101 MHz, CDCl$_3$) 21.0 (s); FAB-MS *m/z* 418 [M + H]$^+$, 219 [M-Ph$_2$PO+2H]$^+$; λ_{max}/nm (EtOH) ε/dm^3 mol^{-1} cm^{-1} 261 (2060), 266 (2460), 273 (1940).

Preparation of potassium tetraphenylimidodiphosphinate (Ktpip)[9]

Htpip (0.30 g, 0.72 mmol) was dissolved in a 2% methanolic KOH solution (10 cm^3). The solvent volume was decreased to 2 cm^3 under reduced pressure and diethyl ether

was added (20 cm^3). The resultant solid was recrystallised from ethanol to give the desired product (0.187 g, 58%). δ_H (360 MHz, D$_2$O) 7.79-7.73 (8H, m, Ar), 7.52-7.41 (12H, m, Ar); $\delta_P\{^1H\}$ (146 MHz, D$_2$O) 17.0 (s); FAB-MS *m/z* 456 [*M* + H]$^+$.

Preparation of lanthanide complexes of tetraphenylimidodiphosphinate (tpip) [9]

To a solution of three equivalents of Ktpip (0.187 g, 0.41 mmol) in H$_2$O, one equivalent of LnCl$_3$·6H$_2$O (L = Sm, Eu, Gd, Tb, Dy), dissolved in H$_2$O, was added dropwise. The white solid that immediately precipitated was filtered, washed with H$_2$O several times and dried under vacuum, giving Ln(tpip)$_3$ in 70-80% yield. In addition to the spectroscopic data shown below it should be noted that the UV/Vis absorption spectra of these compounds have identical profiles.

[Eu(tpip)$_3$] : δ_H (360 MHz, CDCl$_3$) 7.48-7.54 (24H, m, Ar), 7.21 (12H, t, ^3J (H,H) = 7.4 Hz, Ar), 6.95-6.99 (24H, m, Ar); $\delta_C\{^1H\}$ (91 MHz, CDCl$_3$) 129.8 (d, ^1J (P,C) = 137 Hz, quart. C), 129.4 (s), 128.9 (d, *J* (P,C) = 10 Hz), 127.0 (d, *J* (P,C) = 13 Hz); $\delta_P\{^1H\}$ (146 MHz, CDCl$_3$) 37.7 (s); FAB-MS *m/z* 1400 [*M* + H]$^+$, 983 [*M*–tpip]$^+$; λ_{max}/nm (CHCl$_3$) 273 (ε = 5000 dm^3 mol^{-1} cm^{-1}). (Found: C, 59.16; H, 4.24; N, 2.83%. C$_{72}$H$_{60}$EuN$_3$O$_6$·3H$_2$O requires C, 59.43; H, 4.57; N, 2.89%).

Single crystals of [Eu(tpip)$_3$] suitable for an X-ray diffraction analysis were grown, by slow evaporation, from both a CHCl$_3$ solution (a) and an ethyl acetate solution (b).

(a) Crystallographic data for [Eu(tpip)$_3$]·0.67 H$_2$O: C$_{72}$ H$_{61.33}$ Eu N$_3$ O$_{6.67}$ P$_6$, M = 1411.75, trigonal, space group *P*-3, a = 23.418(2), c = 21.185(3) Å, *V* = 10061.85 Å^3, Z = 6, ρ_{calcd} = 1.40 g cm^{-3}, F(000) = 4324.65, Mo$_{K\alpha}$ radiation (λ = 0.71073 Å), *T* = 220 K, μ = 0.30 mm^{-1}, R_1 = 0.0426, *wR* = 0.0418 for 8591 independent reflections (*I* > 2.00σ(*I*), θ_{max} = 25°), GOF = 1.1338.

(b) Crystallographic data for [Eu(tpip)$_3$]·0.5 EtOAc: C$_{74}$ H$_{64}$ Eu N$_3$ O$_7$ P$_6$, M = 1445.06, triclinic, space group *P*-1, a = 13.304(7), b = 14.076(6), c = 21.368(11) Å, α = 72.47(3), β = 83.76(2), γ = 63.41(2) °, *V* = 3410(3) Å^3, Z = 2, ρ_{calcd} = 1.407 g cm^{-3}, F(000) = 1476, Mo$_{K\alpha}$ radiation (λ = 0.71073 Å), *T* = 220 K, μ = 1.116 mm^{-1}, R_1 = 0.0314 [θ_{max} =

25°, 10697 data $F > 4\sigma$ (F)], $wR = 0.0693$ for 11950 independent reflections, GOF = 1.061.

[Tb(tpip)$_3$] : δ_H (360 MHz, CDCl$_3$) 7.97 (24H, br s, Ar), 7.35 (12H, s, p-Ar), 6.28 (24H, s, Ar); $\delta_C\{^1H\}$ (91 MHz, CDCl$_3$) 159.3 (quart. C), 134.5 (s), 130.4 (s), 128.6 (s); $\delta_P\{^1H\}$ (146 MHz, CDCl$_3$) 200.7 (s); FAB-MS m/z 1408 [M + H]$^+$, 991 [M–tpip]$^+$.

Single crystals of [Tb(tpip)$_3$] suitable for an X-ray diffraction analysis were grown by slow evaporation from a CHCl$_3$ solution.

Crystallographic data for [Tb(tpip)$_3$]·0.75 H$_2$O: C$_{72}$ H$_{61.50}$ N$_3$ O$_{6.75}$ P$_6$ Tb, M = 1421.48, rhombohedral, space group R-3, a = 23.372(4), c = 42.956(8) Å, V = 20320(6) Å^3, Z = 12, ρ_{calcd} = 1.394 g cm^{-3}, $F(000)$ = 8682, Mo$_{K\alpha}$ radiation (λ = 0.71073 Å), T = 220 K, μ = 1.24 mm^{-1}, R_1 = 0.0624 [θ_{max} = 25°, 5674 data $F > 4\sigma$ (F)], wR_2 = 0.1744 for 7979 independent reflections, GOF = 1.033.

[Sm(tpip)$_3$] : δ_H (250 MHz, CDCl$_3$) 7.58-7.66 (24H, m, Ar), 7.19-7.26 (12H, m, p-Ar), 7.03-7.08 (12H, m, Ar); $\delta_C\{^1H\}$ (63 MHz, CDCl$_3$) 131.1, 131.0, 130.9, 129.8, 127.5, 127.4, 127.3 [(s), (d), (d), (d)]; $\delta_P\{^1H\}$ (101 MHz, CDCl$_3$) 25.1 (s); FAB-MS m/z 1403 [M + H]$^+$, 985 [M–tpip]$^+$.

[Dy(tpip)$_3$] : δ_H (250 MHz, CDCl$_3$) 8.1 (24H, br s, Ar), 7.45 (12H, br s, p-Ar), 6.57 (24H, br s, Ar); $\delta_C\{^1H\}$ (63 MHz, CDCl$_3$) 154 (br s), 132.6 (s), 130.2 (s), 128.3 (s); $\delta_P\{^1H\}$ (101 MHz, CDCl$_3$) 147.9 (s); FAB-MS m/z 1414 [M + H]$^+$, 997 [M–tpip]$^+$.

[Gd(tpip)$_3$] : FAB-MS m/z 1407 [M + H]$^+$, 992 [M–tpip]$^+$.

Preparation of chlorodi-2-methylphenylphosphine **(24)**[10]
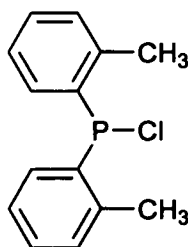
24

A solution of *o*-bromotoluene (10.0 g, 57.9 mmol) in dry THF (10 cm^3) was added dropwise to dry magnesium turnings (1.57 g, 64.6 mmol). The reaction mixture was stirred for 1 hour, after which time formation of the Grignard reagent was complete. The Grignard reagent, and washings in dry THF (7 cm^3), were added dropwise to a solution of phosphorus trichloride (2.2 cm^3, 25 mmol) in dry THF (10 cm^3) cooled in an ice bath. After a few minutes, a large amount of white precipitate formed. This mixture was left stirring at room temperature for 23 hours, filtered and washed with dry toluene (20 cm^3). The solvent was removed from a small sample of this solution, and the resultant material was identified as the desired compound by ^{1}H and ^{31}P NMR spectroscopy. Due to the sensitivity of the material, the THF/toluene solution of this compound was used without further purification. δ_H (250 MHz, CDCl$_3$) 2.47 (6H, d, ^4J (P,H) = 2.7 Hz, CH$_3$); $\delta_P\{^1H\}$ (101 MHz, CDCl$_3$) 74.4 (s).

Preparation of N-(P,P-di-2-methylphenylphosphinoyl)-P,P-di-2-methylphenyl-phosphinimidic acid (Httip, 25)
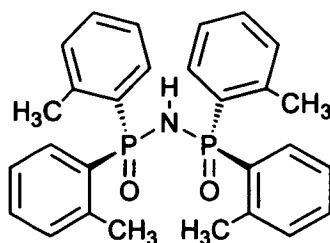
25

Hexamethyldisilazane (1.59 g, 9.85 mmol) was dissolved in dry toluene (2 cm^3) and added dropwise to a solution of chlorodi-2-methylphenylphosphine in toluene/THF (25 mmol, assuming 100% yield of preparation described above). This solution was refluxed for 4.5 hours, after which time Me$_3$SiCl and THF were distilled off. The solution was cooled in an ice bath for 30 minutes, H$_2$O$_2$ (1.7 cm^3, 35% Wt in H$_2$O) in THF (2 cm^3) was added dropwise, and the solution stirred for 18 hours. This solution was added to diethyl ether (50 cm^3), resulting in the immediate precipitation of a white solid. This solid was filtered and washed with water and MeOH, giving the desired product [0.71 g, 15% (based on hexamethyldisilazane)]. δ_H (250 MHz, CDCl$_3$) 7.82-7.74 (4H, m, Ar), 7.33-7.27 (4H, m, Ar), 7.14-7.00 (8H, m, Ar), 2.18 (12H, s, CH$_3$); $\delta_P\{^1H\}$ (101 MHz, CDCl$_3$) 25.4 (s); IR (cm^{-1}): 1196, 1215 and 1229 [ν(PNP)] and 1068, 1094 [ν(PO)]; FAB-MS m/z 474 [M + H]$^+$. (Found: C, 69.89; H, 6.10; N, 2.77%. C$_{28}$H$_{29}$NO$_2$P$_2$·0.5H$_2$O requires C, 69.70; H, 6.27; N, 2.90%).

Preparation of Kttip

Httip (0.615 g, 1.30 mmol) was heated at reflux for 1 hour in a 10% methanolic KOH solution (30 cm^3). The solvent was removed under reduced pressure and the resultant white solid washed with water (5 cm^3). This solid was recrystallised from ethanol to give the desired product (0.390 g, 59%). Single crystals of Kttip suitable for an X-ray diffraction analysis were grown by slow evaporation from a methanolic solution. δ_H (200 MHz, CD$_3$OD) 8.31-8.20 (4H, m, Ar), 7.29-6.99 (12H, m, Ar), 2.12 (12H, s, CH$_3$); $\delta_P\{^1H\}$ (81 MHz, CD$_3$OD) 9.1 (s); FAB-MS m/z 512 [M + H]$^+$, 550 [M + K]$^+$. λ_{max}/nm (MeOH) 270 (ε = 2700 dm^3 mol^{-1} cm^{-1}), 277 (2500). (Found: C, 58.19; H, 6.30; N, 2.25%. C$_{28}$H$_{28}$KNO$_2$P$_2$·3.5H$_2$O requires C, 58.53; H, 6.14; N, 2.44%).

Crystallographic data for [K(ttip)(MeOH)$_2$(H$_2$O)]$_n$: C$_{30}$ H$_{38}$ K N O$_5$ P$_2$, M = 593.65, orthorhombic, space group *Pna2$_1$*, a = 16.956(7), b = 22.495(5), c = 8.0303(19) Å, V = 3063.0(16) Å^3, Z = 4, ρ_{calcd} = 1.287 g cm^{-3}, F(000) = 1256, Cu$_{K\alpha}$ radiation (λ = 1.54178 Å), T = 220 K, μ = 2.817 mm^{-1}, R_1 = 0.0709 [θ_{max} = 70°, 1556 data F > 4σ (F)], wR_2 = 0.1716 for 2854 independent reflections, GOF = 0.977.

Preparation of [Eu(ttip)₃]

EuCl$_3$.6H$_2$O (0.016 g, 0.044 mmol) dissolved in methanol (1 cm^3) was added dropwise to a solution of Kttip (0.067 g, 0.13 mmol) in methanol (5 cm^3). The white solid that immediately precipitated was filtered, washed with methanol (2 × 2 cm^3) and dried under vacuum (0.054 g, 78%). Single crystals, suitable for an X-ray diffraction analysis, were grown by slow evaporation from a CHCl$_3$ solution. δ_H (250 MHz, CDCl$_3$) 7.15-7.16 (24H, m, Ar), 6.10-6.31 (24H, m, Ar), 3.06 (36H, s, CH$_3$); $\delta_P\{^1H\}$ (101 MHz, CDCl$_3$) 25.7 (s); IR (cm^{-1}): 1224, 1195 [ν(PNP)] and 1098, 1071 [ν(PO)]; FAB-MS *m/z* 1571 [*M* + H]$^+$, 1097 [*M*–ttip]$^+$; λ_{max}/nm (CH$_3$CN) 278 (ε = 6800 dm^3 mol^{-1} cm^{-1}), 271 (6200). (Found: C, 63.95; H, 5.55; N, 2.52%. C$_{84}$H$_{84}$EuN$_3$O$_6$P$_6$ requires C, 64.29; H, 5.39; N, 2.68%).

Crystallographic data for [Eu(ttip)₃]·CHCl$_3$: C$_{85}$ H$_{85}$ Cl$_3$ Eu N$_3$ O$_6$ P$_6$, M = 1688.69, rhombohedral, space group *R*-3, a = b = 15.2788(6), c = 30.532(5) Å, α = β = 90, γ = 120 °, *V* = 6172.5(10) Å^3, *Z* = 3, ρ_{calcd} = 1.363 g cm^{-3}, *F*(000) = 2604, Mo$_{K\alpha}$ radiation (λ = 0.71073 Å), *T* = 220 K, μ = 1.029 mm^{-1}, R_1 = 0.0549 [θ_{max} = 25°, 2217 data *F* > 4σ (*F*)], *wR* = 0.1296 for 2418 independent reflections, GOF = 1.113.

Preparation of [Tb(ttip)₃]

TbCl$_3$.6H$_2$O (0.014 g, 0.037 mmol) dissolved in methanol (1 cm^3) was added dropwise to a solution of Kttip (0.053 g, 0.10 mmol) in methanol (8 cm^3). The white solid that immediately precipitated was filtered, washed with methanol (2 × 2 cm^3) and dried under vacuum (0.050 g, 86%). $\delta_P\{^1H\}$ (101 MHz, CDCl$_3$) 142 (br.s); IR (cm^{-1}): 1224, 1195 [ν(PNP)] and 1098, 1071 [ν(PO)]; FAB-MS *m/z* 1576 [*M* + H]$^+$, 1103 [*M*–ttip]$^+$. (Found: C, 63.62; H, 5.47; N, 2.57%. C$_{84}$H$_{84}$TbN$_3$O$_6$P$_6$ requires C, 64.00; H, 5.37; N, 2.67%).

6.4   EXPERIMENTAL DETAILS FOR CHAPTER 4

Preparation of 1,3-bis(3-phenyl-3-oxopropanoyl)benzene (H₂bis-DBM) (30)[11]
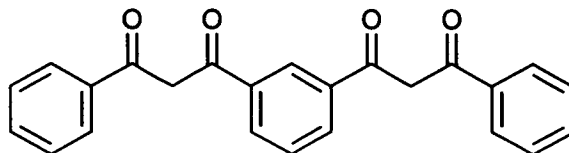
30

A solution of dimethyl isophthalate (6.53 g, 0.033 mol) and acetophenone (10 g, 0.083 mol) in THF (100 cm³) was added to NaH (4.0 g, 0.10 mol), forming an orange precipitate. The mixture was stirred at 0-5 °C for 2 hours and for a further 2 hours at room temperature. The NaH was quenched with water and the mixture filtered. Addition of dilute HCl to the yellow/orange solution yielded a pale yellow solid, which was identified as the desired product (2.16 g, 18%). Single crystals of H₂bis-DBM suitable for an X-ray diffraction analysis were grown by slow evaporation from a methanol solution. δ_H (360 MHz, CDCl₃) 8.65 (1H, t, J = 2 Hz, COPhCO, *o*-Ar), 8.17 (2H, dd, J = 8, 2 Hz, COPhCO, *o*-Ar), 7.98-8.04 (4H, m, PhCO, *o*-Ar), 7.50-7.66 (7H, m, *m*- and *p*-Ar), 6.94 (2H, s, CH); FAB-MS *m/z* 371[M + H]$^+$ (thioglycerol matrix), 266 [M–COPh]$^+$; λ_{max}/nm (MeOH) 357 (ε = 48 000 dm³ mol⁻¹ cm⁻¹).

Crystallographic data for H₂bis-DBM: C₂₄ H₁₈ O₄, M = 370.38, orthorhombic, space group $P2_12_12_1$, a = 5.2013(5), b = 16.6336(15), c = 20.8923(18) Å, V = 1807.5(3) Å³, Z = 4, ρ_{calcd} = 1.361 g cm⁻³, F(000) = 776, synchrotron radiation (λ = 0.68750 Å), T = 160 K, μ = 0.092 mm⁻¹, R_1 = 0.0793 [θ_{max} = 27 °, 2798 data F > 4σ (F)], wR_2 = 0.2499 for 3580 independent reflections, GOF = 1.102.

Preparation of Y₂(bis-DBM)₃

A solution of YCl₃.6H₂O (0.0514 g, 0.17 mmol) in MeOH (2 cm³) was added dropwise to a solution of H₂bis-DBM (0.0915 g, 0.25 mmol) in CHCl₃ (8 cm³), resulting in a pale yellow solution. A solution of NEt₃ (0.052 g, 0.51 mmol) in MeOH (2 cm³) was added dropwise to this solution, producing a deeper yellow colour. A pale yellow precipitate

formed after a few seconds. The mixture was stirred for one hour, filtered and washed with; $CHCl_3$ (2×2 cm^3), methanol (4×2 cm^3), H_2O (2×2 cm^3) and ether (2×2 cm^3) and dried under vacuum to give the desired product (0.067 g, 60%). δ_H (360 MHz, DMF-d_7) 9.61 (3H, t, ^4J = 2 Hz Ar), 8.39-8.35 (6H, m, Ar), 8.26-8.24 (12H, m, Ar), 7.55-7.46 (21H, m, Ar), 7.14 (6H, s, COCHCO); δ_C\{^1H\} (90.56 MHz, DMF-d_7) 184.5 (6C, CO), 183.5 (6C, CO), 140.5, 140.1, 131.4, 130.5, 128.6, 128.4, 128.1, 127.9, 94.3; FAB-MS m/z 1283 [M + H]$^+$; λ_{max}/nm (DMF) 357 (ε = 160 000 dm^3 mol^{-1} cm^{-1}). (Found: C, 65.71; H, 3.84%. $C_{72}H_{48}O_{12}Y_2 \cdot 2H_2O$ requires C, 65.56; H, 3.97%).

Preparation of Eu$_2$(bis-DBM)$_3$

A solution of $EuCl_3.6H_2O$ (0.0507 g, 0.14 mmol) in MeOH (2 cm^3) was added dropwise to a solution of H$_2$bis-DBM (0.0724 g, 0.20 mmol) in $CHCl_3$ (8 cm^3), resulting in a pale yellow solution. A solution of NEt$_3$ (0.0396 g, 0.39 mmol) in MeOH (2 cm^3) was added dropwise to this solution, producing a deeper yellow colour. The mixture was stirred for two hours at room temperature and cooled overnight in a refrigerator. The pale yellow precipitate that had formed was filtered and washed with; $CHCl_3$ (2×2 cm^3), methanol (4×2 cm^3), H_2O (2×2 cm^3) and ether (2×2 cm^3), then dried under vacuum to give the desired product (0.0395 g, 40%). δ_H (250 MHz, DMF-d_7) 6.11-6.48 (30H, m, Ar), 4.27-4.30 (12H, m, Ar), 3.62 (6H, s, COCHCO); FAB-MS m/z 1409 [M + H]$^+$; λ_{max}/nm (DMF) 359 (ε = 150 000 dm^3 mol^{-1} cm^{-1}). (Found: C, 60.66; H, 3.31%. $C_{72}H_{48}O_{12}Eu_2 \cdot H_2O$ requires C, 60.60; H, 3.53%).

Attempted synthesis of (TBA)$_2$[Eu$_2$(bis-DBM)$_4$]

A solution of H$_2$bis-DBM (0.062 g, 0.17 mmol) and TBAOH·30H$_2$O (0.268 g, 0.34 mmol) in EtOH (5 cm^3) was warmed to 70 °C and a solution of $EuCl_3.6H_2O$ (0.031 g, 0.083 mmol) in H_2O (2 cm^3) was added dropwise, along with washings of EtOH/H$_2$O (5:1, 1 cm^3). The pale yellow precipitate that immediately formed was filtered, washed with ice-cold EtOH (2×2 cm^3) and H_2O (2×2 cm^3), and dried under vacuum (0.062 g, 66% based on (TBA)$_2$[Eu$_2$(bis-DBM)$_4$]). As described in Chapter 4, the product obtained from the above reaction is thought to be a mixture of Eu$_2$(bis-DBM)$_3$ and (TBA)$_2$[Eu$_2$(bis-DBM)$_4$]. FAB-MS m/z 1409 [Eu$_2$(bis-DBM)$_3$+ H]$^+$, 1651 [Eu$_2$(bis-

DBM)$_3$+ TBA]$^+$; (Found: C, 61.37; H, 5.41; N, 0.77%. $C_{128}H_{136}N_2O_{16}Eu_2$ requires C, 67.95; H, 6.06; N, 1.24%).

Attempted synthesis of (TBA)$_2$[Y$_2$(bis-DBM)$_4$]

A solution of H$_2$bis-DBM (0.053 g, 0.14 mmol) and TBAOH·30H$_2$O (0.230 g, 0.288 mmol) in EtOH (5 cm^3) was warmed to 70 °C and a solution of YCl$_3$.6H$_2$O (0.022 g, 0.073 mmol) in H$_2$O (2 cm^3) was added dropwise. The pale yellow precipitate that immediately formed was filtered, washed with ice-cold EtOH (2 × 2 cm^3) and H$_2$O (2 × 2 cm^3), and dried under vacuum (0.057 g, 76% based on (TBA)$_2$[Y$_2$(bis-DBM)$_4$]). As described in Chapter 4, the product obtained from the above reaction is thought to be a mixture of Y$_2$(bis-DBM)$_3$ and (TBA)$_2$[Y$_2$(bis-DBM)$_4$].(Found: C, 66.53; H, 5.64; N, 0.78%. $C_{128}H_{136}N_2O_{16}Y_2$ requires C, 71.97; H, 6.42; N, 1.31%).

Attempted synthesis of (Hpip)$_2$[Eu$_2$(bis-DBM)$_4$]

A solution of EuCl$_3$.6H$_2$O (0.083 g, 0.22 mmol) in MeOH (6 cm^3) was added dropwise to a solution of H$_2$bis-DBM (0.041 g, 0.11 mmol) in CHCl$_3$ (20 cm^3), giving a pale yellow solution. An excess amount of piperidine (Hpip) was added to this solution, resulting in the immediate formation of a pale yellow precipitate which was filtered and dried under vacuum. As described in Chapter 4, the product obtained from the above reaction is thought to be a mixture of Eu$_2$(bis-DBM)$_3$ and (Hpip)$_2$[Eu$_2$(bis-DBM)$_4$], on the basis of luminescence measurements. FAB-MS *m/z* 1409 [Eu$_2$(bis-DBM)$_3$+ H]$^+$, 1494 [Eu$_2$(bis-DBM)$_3$+ Hpip]$^+$.

6.5   EXPERIMENTAL DETAILS FOR CHAPTER 5

H$_2$DACDA (**38**) was a gift from Dr. Neil Robertson. Ethyl 1,4,7,10-tetraoxa-13-azacyclopentadecane-13-acetate (**42**) was prepared by Jennifer L. Craig, following a literature procedure.[12] The ES-MS samples of [EuDACDA]Cl and [TbDACDA]Cl with aromatic acids, which were discussed in Chapter 5, were also prepared by Jennifer L. Craig.
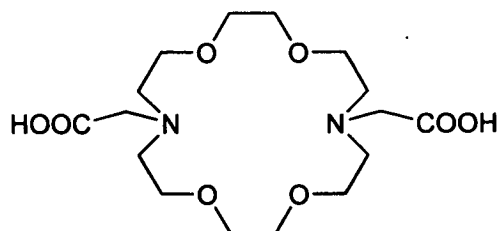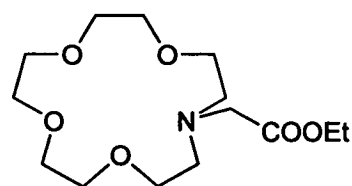
38   **42**

Preparation of [EuDACDA]Cl

H_2DACDA (0.097 g, 0.26 mmol) and NaOMe (0.028 g, 0.53 mmol) were dissolved in methanol (3 cm^3) and EuCl$_3$ (0.110 g, 0.30 mmol) in H$_2$O (2 cm^3) was added dropwise to this solution. After stirring for 30 minutes, the solution was filtered and acetone (50 cm^3) added. The white solid that crystallised overnight was filtered, washed with a 5% H$_2$O/acetone mixture (1 cm^3) and dried under vacuum (0.11 g, 73%). Single crystals of [EuDACDA]Cl suitable for an X-ray diffraction analysis were grown by slow evaporation from an acetonitrile solution. FAB-MS *m/z* 527 [*M*–Cl]$^+$. (Found: C, 32.38; H, 5.33; N, 4.73%. C$_{16}$H$_{28}$ClEuN$_2$O$_8$·2H$_2$O requires C, 32.04; H, 5.38; N, 4.67%).

Crystallographic data for {[EuDACDA(H$_2$O)]Cl}$_n$·6nH$_2$O: C$_{16}$ H$_{42}$ Cl Eu N$_2$ O$_{15}$, M = 689.93, monoclinic, space group $P2_1/n$, a = 13.207(4), b = 12.110(4), c = 16.681(5) Å, α = γ = 90, β = 96.28(3) °, *V* = 2651.8(13) Å^3, Z = 4, ρ_{calcd} = 1.728 g cm^{-3}, F(000) = 1408, Mo$_{K\alpha}$ radiation (λ = 0.71073 Å), *T* = 220 K, μ = 2.536 mm^{-1}, R$_1$ = 0.0317 [θ_{max} = 25°, 3889 data *F* > 4σ (*F*)], *wR* = 0.0701 for 4602 independent reflections, GOF = 1.060.

Preparation of [LaDACDA]Cl

A mixture of LaCl$_3$.7H$_2$O (0.20 g, 0.53 mmol), H$_2$DACDA (0.21 g, 0.53 mmol) and NaHCO$_3$ (0.10 g, 1.2 mmol) was dissolved in H$_2$O (100 cm^3). This, initially effervescent, solution was stirred for 1 hour, and the initial white precipitate that formed was filtered off and discarded. The volume was reduced to 10 cm^3 and acetone (120 cm^3) was added, resulting in the precipitation of a white solid, which was isolated and identified as the desired product (0.17 g, 56%). This product may contain a small

impurity (see analysis and Chapter 5 discussion). δ_H (360 MHz, D_2O) 4.11-4.18 (4H, m, OCH_2CH$_2$N), 3.94-4.03 (8H, m, OCH_2CH$_2$O), 3.72-3.77 (4H, m, OCH_2CH$_2$N), 3.49 (4H, s, NCH_2COO), 3.19-3.27 (4H, m, OCH$_2$CH_2N), 2.79-2.83 (4H, m, OCH$_2$CH_2N); $\delta_C\{^1H\}$ (91 MHz, CDCl$_3$) 180.6 (CO), 69.9 (OCH$_2$CH$_2$O), 69.1 (OCH$_2$CH$_2$N), 59.9 (NCH$_2$COO), 59.1 (OCH$_2$$CH_2$N); FAB-MS m/z 515 $[M$–Cl$]^+$. (Found: C, 33.69; H, 5.96; N, 4.23%. $C_{16}H_{28}ClLaN_2O_8 \cdot 2H_2O$ requires C, 32.75; H, 5.50; N, 4.77%).

Preparation of [TbDACDA]Cl

H$_2$DACDA (0.077 g, 0.20 mmol) and KOH (0.024 g, 0.43 mmol) were dissolved in H$_2$O (10 cm^3) and TbCl$_3$ (0.075 g, 0.20 mmol) in H$_2$O (2 cm^3) was added dropwise to this solution. The volume was reduced to 3 cm^3 under reduced pressure and acetone (40 cm^3) added. The white solid that crystallised was filtered, washed with a 5% H$_2$O/acetone mixture (1 cm^3) and dried under vacuum (0.10 g, 85%). This sample probably has a salt impurity (see analysis). Single crystals of [TbDACDA]Cl suitable for an X-ray diffraction analysis were grown by slow evaporation from an acetonitrile solution. FAB-MS m/z 535 $[M$–Cl$]^+$(thioglycerol matrix). (Found: C, 24.55; H, 4.91; N, 3.53%. $C_{16}H_{28}ClTbN_2O_8 \cdot 2H_2O$ requires C, 31.67; H, 5.32; N, 4.62%).

Crystallographic data for [TbDACDA]$_n \cdot$Cl$_n \cdot 4n$H$_2$O: C_{16} H$_{36}$ Cl N$_2$ O$_{12}$ Tb, $M =$ 642.84, orthorhombic, space group *Pna*2$_1$, a = 12.634(3), b = 14.828(2), c = 12.620(6) Å, $\alpha = \beta = \gamma = 90$ °, $V =$ 2364.3(12) Å^3, $Z =$ 4, $\rho_{calcd} =$ 1.806 g cm^{-3}, $F(000) =$ 1296, Mo$_{K\alpha}$ radiation ($\lambda =$ 0.71073 Å), $T =$ 293 K, $\mu =$ 3.166 mm^{-1}, $R_1 =$ 0.0412 [$\theta_{max} =$ 25°, 2284 data $F >$ 4σ (F)], $wR =$ 0.0975 for 2976 independent reflections, GOF = 1.019.

Preparation of 1,4,7,10-tetraoxa-13-azacyclopentadecane-13-acetic acid (HMACMA, 39) as the hydrochloride hydrate (HMACMA.HCl.nH$_2$O) (1 < n < 2)[13]
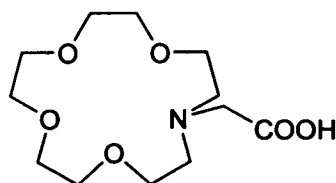
39

Ethyl 1,4,7,10-tetraoxa-13-azacyclopentadecane-13-acetate (**42**) (1.6 g, 5.2 mmol) was stirred at reflux with concentrated hydrochloric acid (3 cm^3) in H$_2$O (300 cm^3) for 67 hours. The clear solution was cooled, the solvent removed under reduced pressure and the compound dried under vacuum, yielding a viscous, pale yellow oil that turned to a glass on standing (quantitative yield based on ^{1}H NMR spectrum). δ_H (250 MHz, CDCl$_3$) 8.18 (1H, br s, CO$_2$H), 4.47 (2H, s, NCH_2COOH), 4.17-3.65 (20H, m, CH$_2$); $\delta_C\{^1H\}$ (62.9 MHz, CDCl$_3$) 167.1 (CO$_2$H), 70.3 (OCH$_2$CH$_2$O), 69.8 (OCH$_2$CH$_2$O), 69.6 (OCH$_2$CH$_2$O), 65.0 (OCH$_2$CH$_2$N), 55.1 (OCH$_2$CH$_2$N), 54.6 (NCH$_2$CO$_2$H).

Preparation of [EuMACMA](NO$_3$)$_2$

Eu(NO$_3$)$_3$.5H$_2$O (0.219 g, 0.511 mmol) was dissolved in dry acetonitrile (10 cm^3) and heated under reflux with triethylorthoformate (1 cm^3) for 4 hours, followed by the dropwise addition of a solution of HMACMA.HCl (0.157 g, 0.494 mmol) in dry acetonitrile (4 cm^3). The solution was heated under reflux for 24 hours. Diethyl ether (20 cm^3) was added and the resultant solid was washed with diethyl ether (2 × 10 cm^3) and dried under vacuum (0.12 g, 20%). δ_H (200 MHz, CD$_3$NO$_2$) 3.37-3.70 (6 H, m, CH$_2$), 2.89 (16H, br s, CH$_2$); FAB-MS *m/z* 489 [*M*–NO$_3$]$^+$. (Found: C, 23.75; H, 4.21; N, 7.16%. C$_{12}$H$_{22}$EuN$_3$O$_{12}$·3H$_2$O requires C, 23.77; H, 4.65; N, 6.93%).

Preparation of [YMACMA](NO$_3$)$_2$

Y(NO$_3$)$_3$.6H$_2$O (0.201 g, 0.525 mmol) was dissolved in dry acetonitrile (10 cm^3) and heated under reflux with triethylorthoformate (1 cm^3) for 4 hours, followed by the dropwise addition of a solution of HMACMA.HCl (0.168 g, 0.529 mmol) in dry

acetonitrile (3 cm^3). The solution was heated under reflux for 17 hours. Diethyl ether (20 cm^3) was added and the resultant solid was washed with diethyl ether (2 × 10 cm^3) and dried under vacuum (0.191 g, 67%). δ_H (360 MHz, D$_2$O) 3.68-3.97 (18H, m, CH$_2$), 3.42 (4H, br s, CH$_2$); FAB-MS *m/z* 427 [*M*–NO$_3$]$^+$.

6.6 REFERENCES

1. W. L. F. Armarego and D. D. Perrin, *Purification of Laboratory Chemicals*, 4th Ed., Butterworth-Heinemann, Oxford, 1995.

2. D. F. Shriver, *Manipulation of Air-Sensitive Compounds*, McGraw-Hill, New York, 1969.

3. J. L. Kropp and M. W. Windsor, *J. Chem. Phys.*, 1965, **42**, 1599.

4. J. N. Demas and G. A. Crosby, *J. Phys. Chem.*, 1971, **75**, 991.

5. K. Nakamura, *Bull. Chem. Soc. Jpn.*, 1982, **55**, 2697.

6. S. R. Meech and D. Phillips, *J. Photochem.*, 1983, **23**, 193.

7. J. N. Demas and G. A. Crosby, *J. Am. Chem. Soc.*,1971, **93**, 2841.

8. D. J. Williams, *Inorg. Nucl. Chem. Lett.*, 1980, **16**, 189.

9. I. Rodríguez, C. Alvarez, J. Gómez-Lara and R. Cea-Olivares, *Lanthanide-Actinide Res.*, 1986, **1**, 253.

10. P. W. Clark and B. J. Mulraney, *J. Organomet. Chem.*, 1981, **217**, 51.

11. D. F. Martin, M. Shamma and W.C. Fernelius, *J. Am. Chem. Soc.*,1958, **80**, 4891.

12. F. R. Fronczek, V. J. Gatto, C. Minganti, R. A. Schultz, R. D. Gandour and G. W. Gokel, *J. Am. Chem. Soc.*,1984, **106**, 7244.

13. K. A. Byriel, L. R. Gahan, C. H. L. Kennard, J. L. Latten and P. C. Healy, *Aust. J. Chem.*, 1993, **46**, 713.
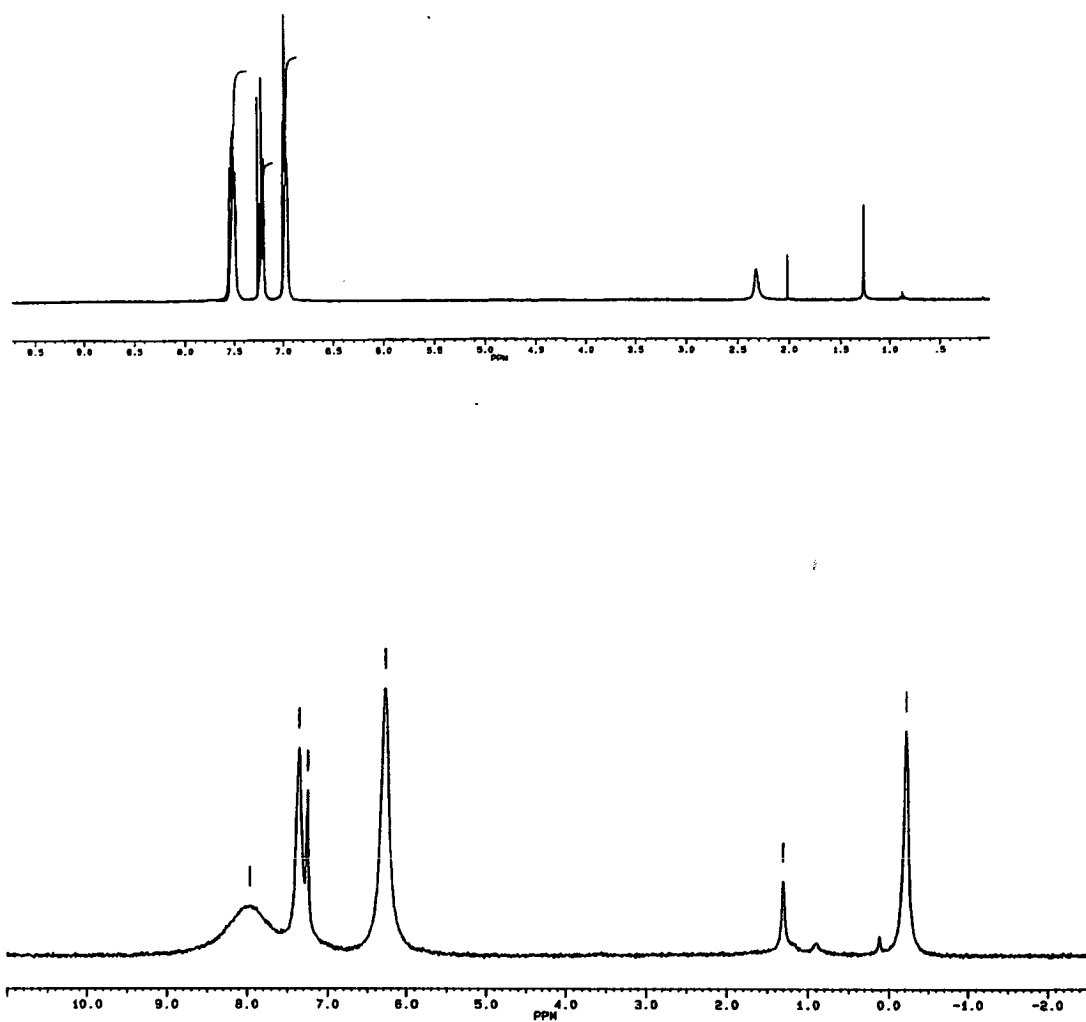
Appendix I

NMR and ES-MS spectra

Figure A1 ^{1}H NMR spectra of [Eu(tpip)$_3$] (top) and [Tb(tpip)$_3$] (bottom); CDCl$_3$, 360 MHz
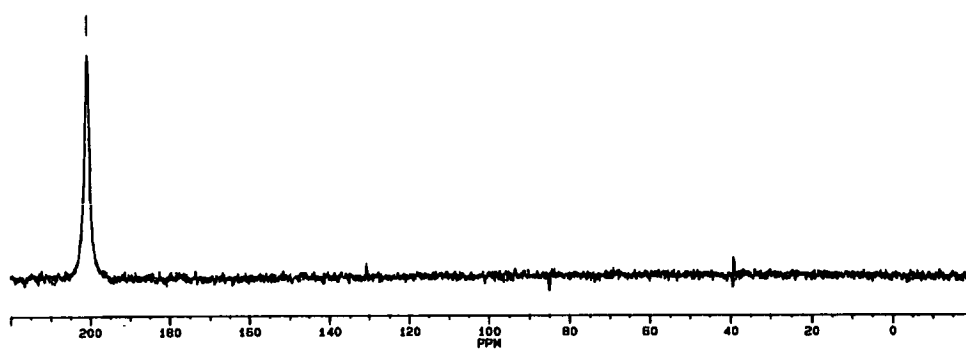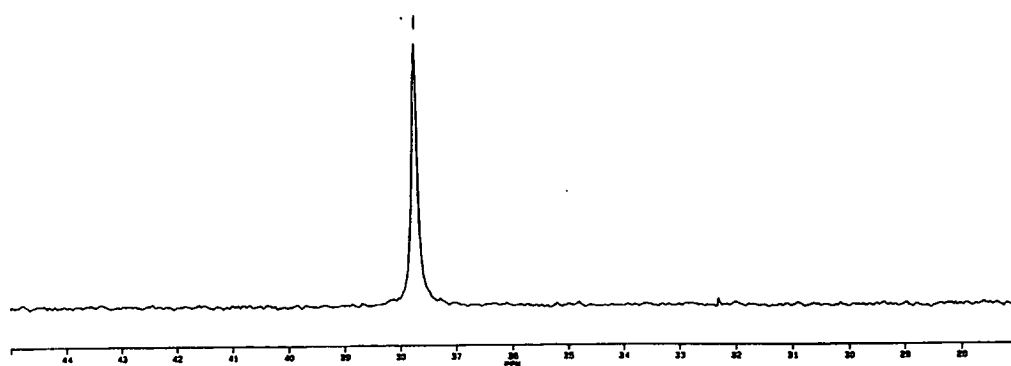
Figure A2 ^{31}P NMR spectra of [Eu(tpip)$_3$] (top) and [Tb(tpip)$_3$] (bottom); CDCl$_3$, 146 MHz
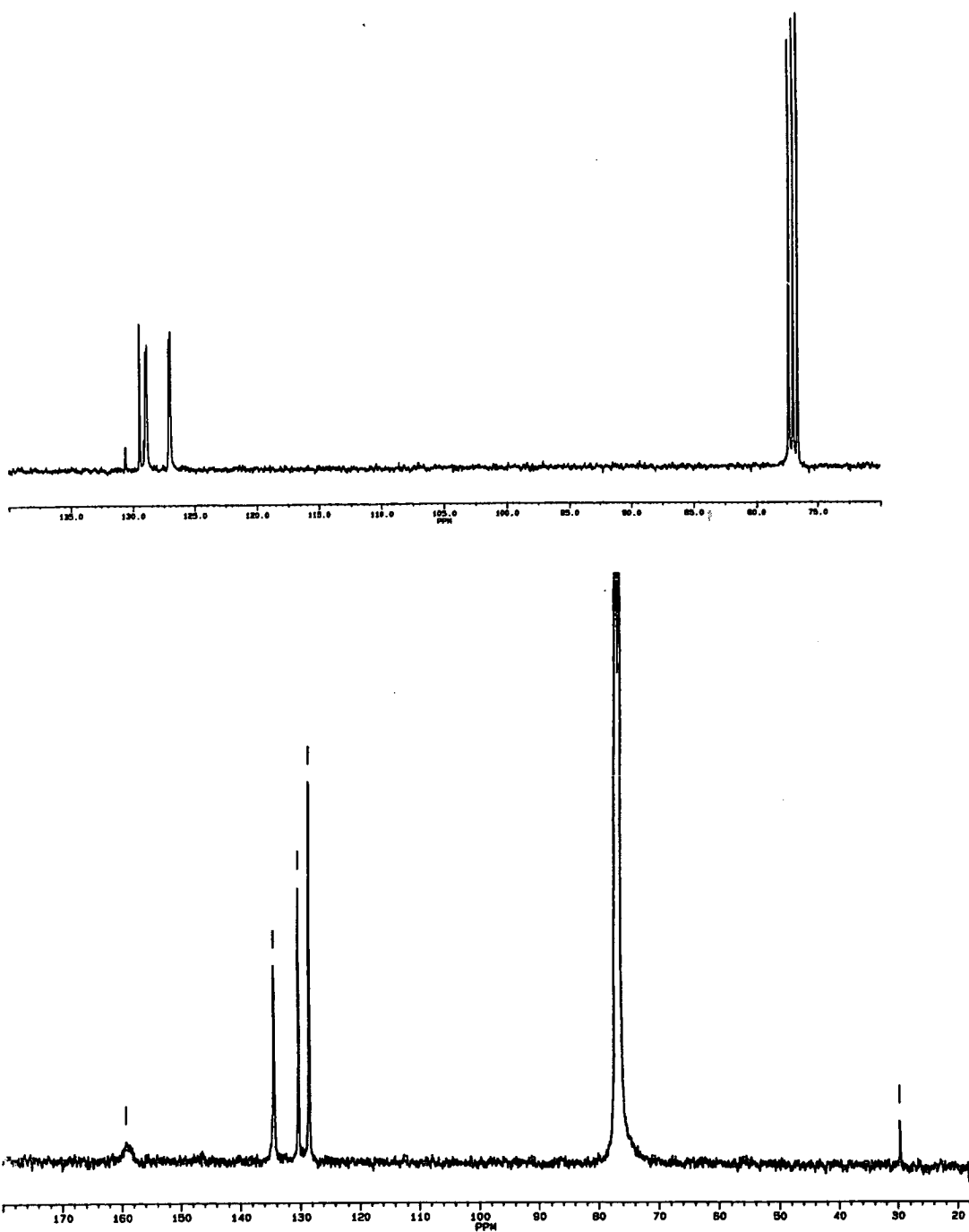
Figure A3 ^{13}C NMR spectra of [Eu(tpip)$_3$] (top) and [Tb(tpip)$_3$] (bottom); CDCl$_3$, 91 MHz
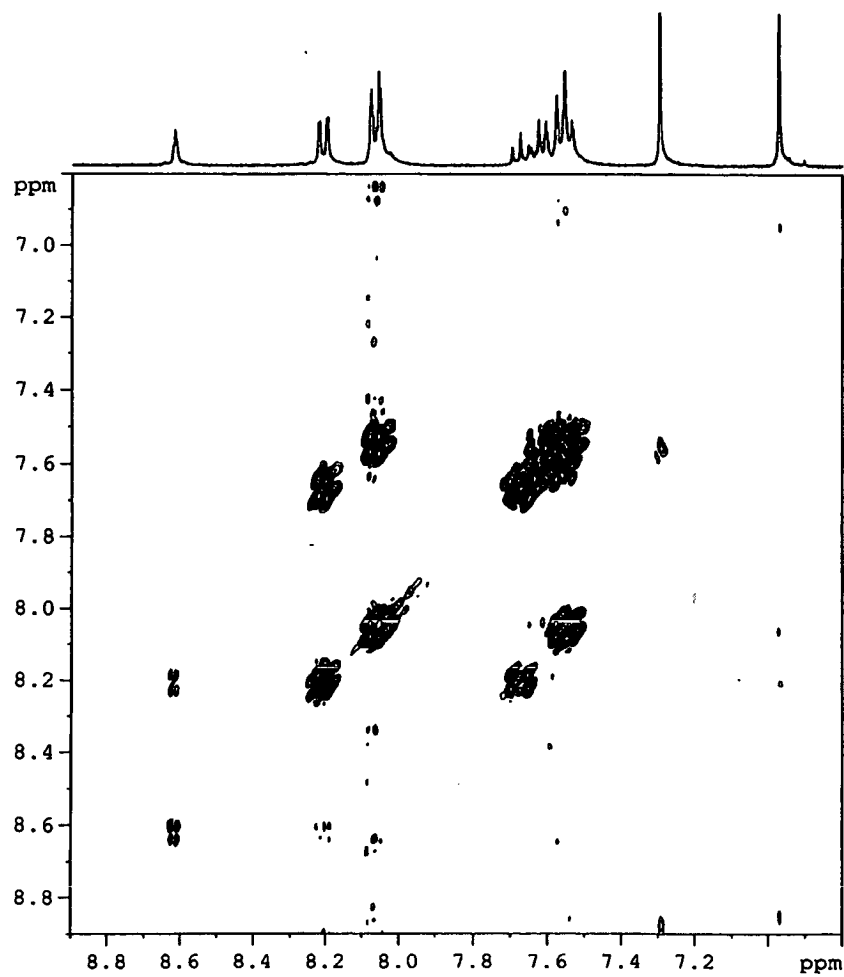
Figure A4 ^{1}H-^{1}H COSY spectrum of H$_2$bis-DBM; CDCl$_3$, 360 MHz
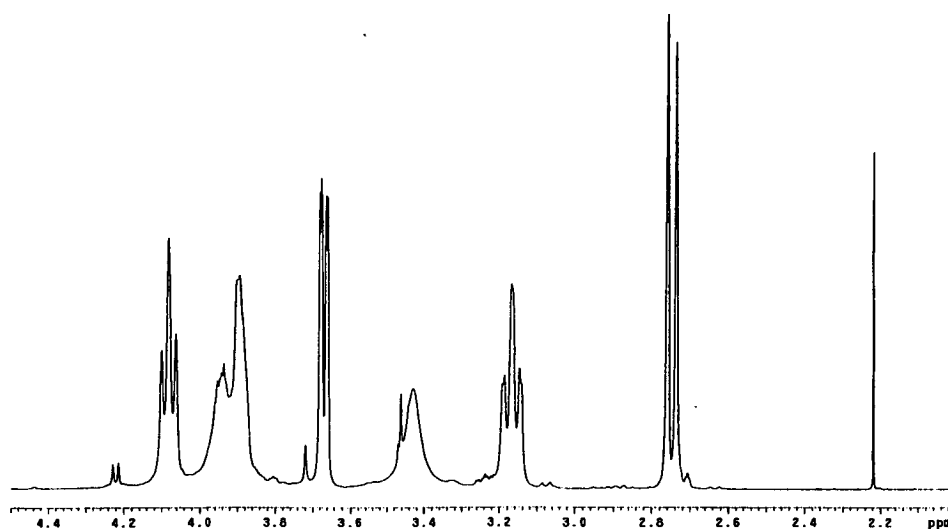
Figure A5 ^{1}H NMR spectrum of [LaDACDA]Cl at 5 °C; D$_2$O, 600 MHz
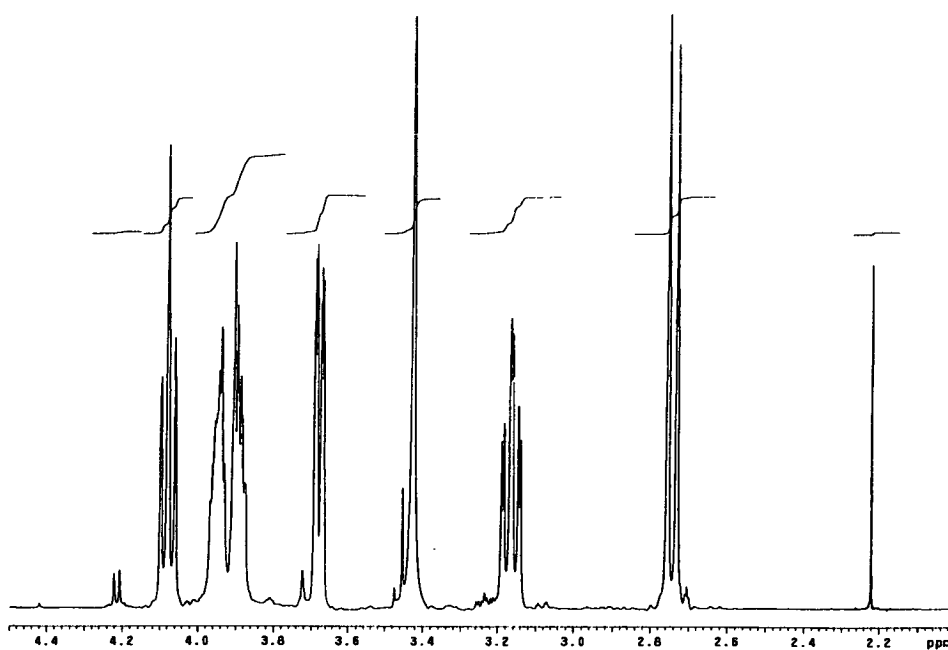
Figure A6 ^{1}H NMR spectrum of [LaDACDA]Cl at 25 °C; D$_2$O, 600 MHz
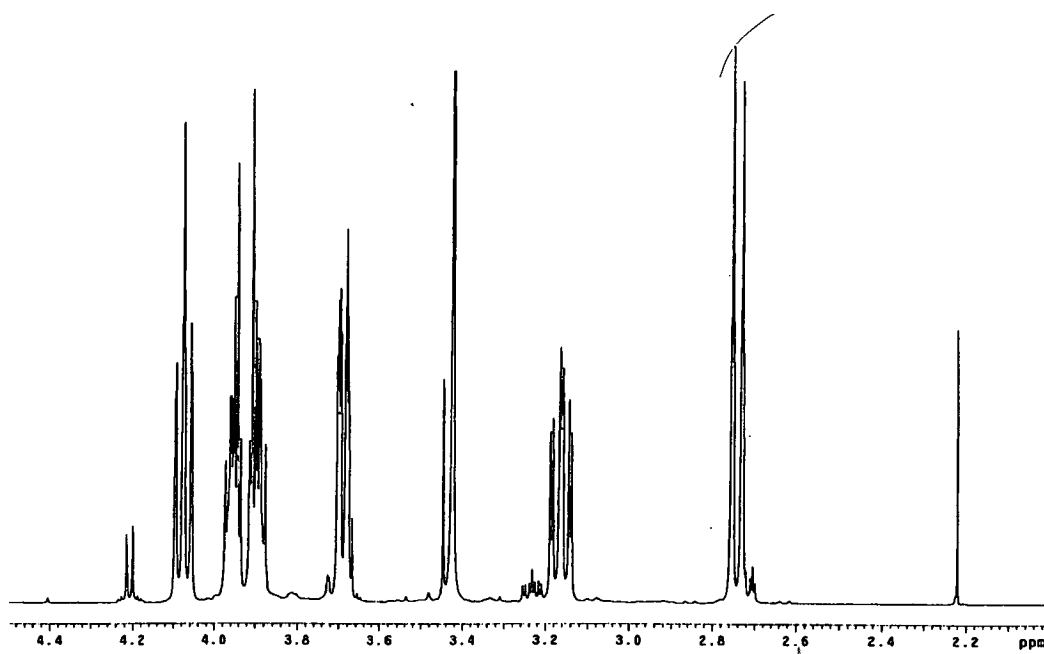
Figure A7 ^{1}H NMR spectrum of [LaDACDA]Cl at 45 °C; D_2O, 600 MHz

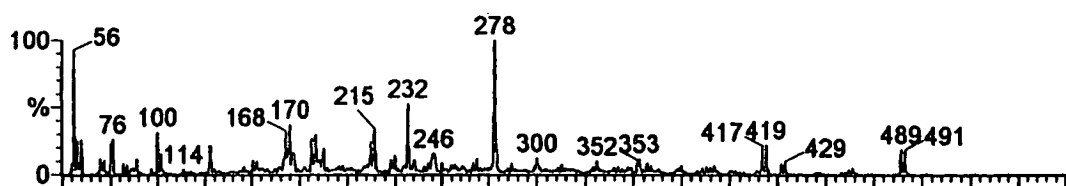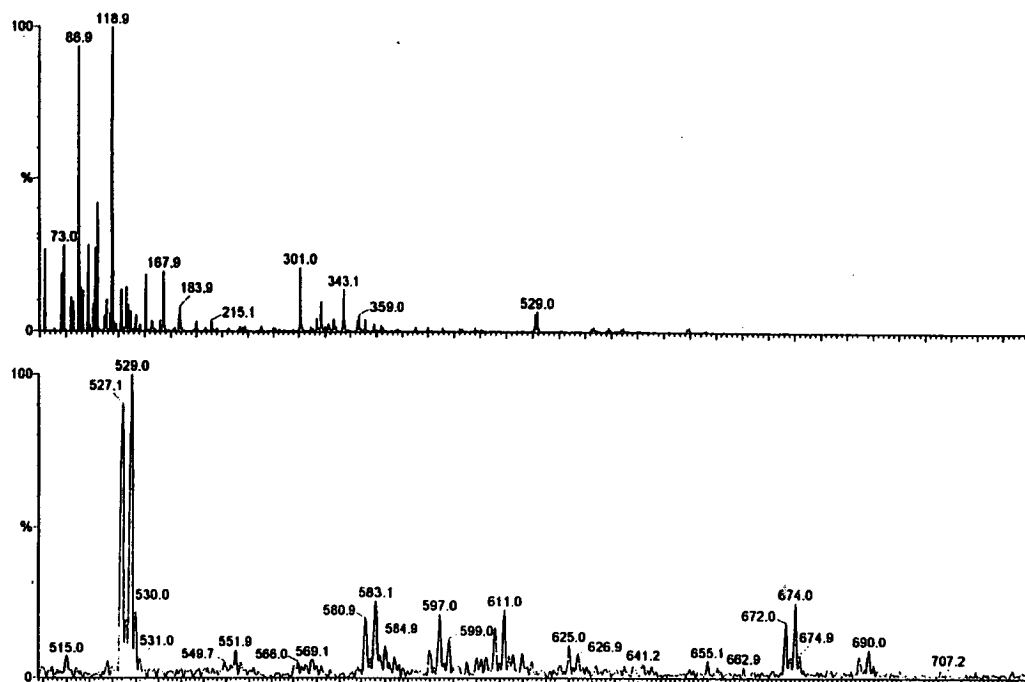**Figure A8** ES(+)-MS spectrum of [EuMACMA]$(NO_3)_2$ in H_2O

Figure A9 ES(+)-MS spectrum of [EuDACDA]Cl (1 × 10^{-4} mol dm^{-3}) and picolinic acid (2 × 10^{-4} mol dm^{-3}) in 0.05 mol dm^{-3} Tris buffer (pH 7.7); whole spectrum (top) and expanded region (bottom)
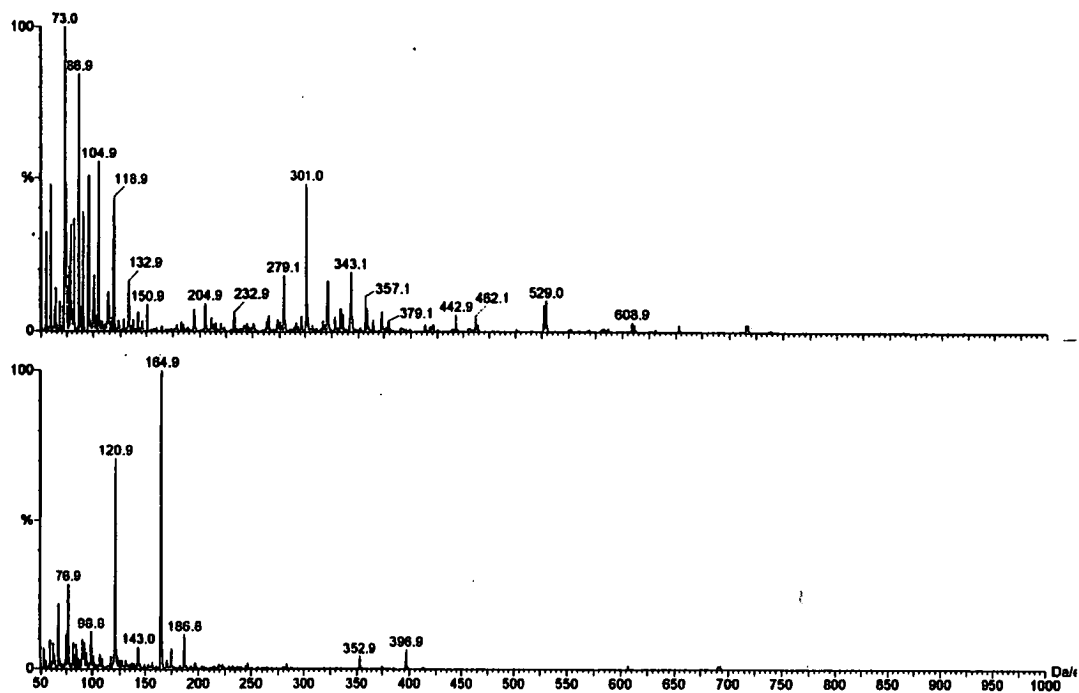
Figure A10 ES(+)-MS spectrum (top) and ES(−)-MS spectrum (bottom) of [EuDACDA]Cl $(1 \times 10^{-4}$ mol dm$^{-3})$ and phthalic acid $(2 \times 10^{-4}$ mol dm$^{-3})$ in 0.05 mol dm^{-3} Tris buffer (pH 7.7); whole spectrum
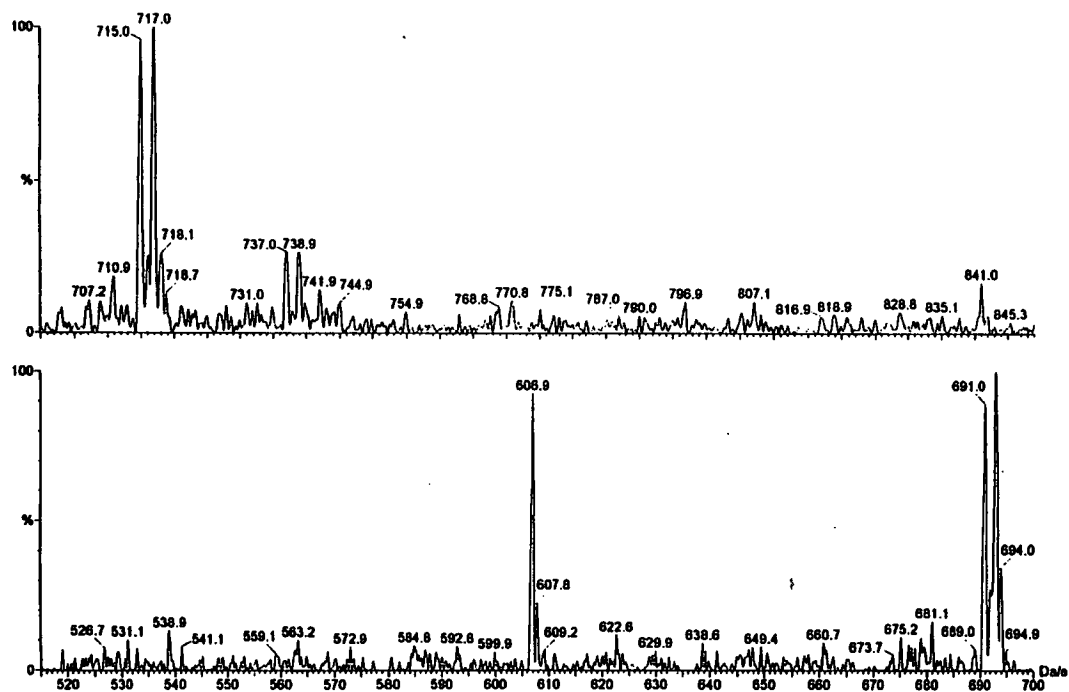
Figure A11 ES(+)-MS spectrum (top) and ES(−)-MS spectrum (bottom) of [EuDACDA]Cl (1×10^{-4} mol dm^{-3}) and phthalic acid (2×10^{-4} mol dm^{-3}) in 0.05 mol dm^{-3} Tris buffer (pH 7.7); expanded region

Appendix II

Courses and conferences attended

Postgraduate Lecture Courses

- Surface Imaging and Analysis   April 1997

- Computers in Chemistry   May 1998

- Inorganic Synthesis Workshop   February 1999

- University of Edinburgh Inorganic Section Meetings   1997-1999

Conferences

- R. S. C. Scottish Dalton Symposium,   February 1997
  University of Edinburgh

- Universities of Scotland Inorganic (USIC) Conference,   September 1997
  University of Edinburgh, Poster Presentation

- R. S. C. U.K. Macrocycles and Supramolecular   January 1998
  Chemistry Conference,
  University of Nottingham, Poster Presentation

- Universities of Scotland Inorganic (USIC) Conference   September 1998
  University of Strathclyde, Oral Presentation

Appendix III

Reprint of published material

Imidodiphosphinate ligands as antenna units in luminescent lanthanide complexes

Steven W. Magennis,[a] Simon Parsons,[a] Anne Corval,[b] J. Derek Woollins[c] and Zoe Pikramenou*[a]

[a] Department of Chemistry, The University of Edinburgh, King's Buildings, West Mains Road, Edinburgh, UK EH9 3JJ. E-mail: z.pikramenou@ed.ac.uk

[b] Laboratoire de Spectrométrie Physique, Université Joseph Fourier, BP 87 38402, Saint Martin d'Hères Cedex, France

[c] Department of Chemistry, Loughborough University, Loughborough, Leics., UK LE11 3TU

Imidodiphosphinate ligands form a hydrophobic shell around terbium and europium ions leading to long-lived, highly luminescent complexes.

The design of miniature 'antenna' systems based on lanthanides for collecting light and converting it to a different frequency has important applications in the development of photonic devices and sensors.[1] Europium and terbium ions are attractive luminescent centers due to their visible, long-lived emission. A breakthrough in lanthanide chemistry came with the design of cryptand ligands that encapsulate the lanthanide ion, protecting it from coordinating solvent molecules that quench its emission.[2] When the arms of the cryptand are light-harvesting units they act as an antenna for collecting light and transferring the energy to the lanthanide.[1,3] Research efforts have focused on the development of ligand systems for lanthanides based on podand-type structures,[3,4] calixarenes[5] or helicates.[6] We are interested in the development of neutral lanthanide complexes with ligands that completely encapsulate the ion forming a hydrophobic shell around the metal ion. Rather than using a highly designed cryptate ligand we aim to use simple lanthanide complexation principles to govern the formation of such species. In order to achieve this, we need strong binding sites that coordinate to the lanthanide and bulky aromatic units that are 'independent/remote' from the binding site and which form the hydrophobic shell. By using remote light-harvesters (rather than harvesters that are themselves the binding units, e.g. polypyridines) we can optimize the ion emission by choosing the best sensitizer, aromatic unit, for the ion; this is important as it is rare to find systems that are ideal both for europium and terbium emission. While remote harvesting units have previously been successfully employed in macrocyclic supramolecular structures to enhance the lanthanide emission,[7,8] using lanthanide complexation principles should allow less synthetically challenging open chain ligands to be used.

We have chosen tetraphenyl imidodiphosphinate (tpip) as an ideal ligand with which to test our design.[9] The imidodiphosphi-

Htpip
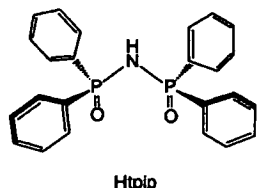
nate binding site can chelate to the lanthanide and does not contain any O–H, C–H or N–H bonds in the binding site that can contribute to the quenching of the lanthanide emission.[10] Attached to each of these binding units are four phenyl groups that (i) play the role of remote light-harvesting units and (ii) form a hydrophobic shell around the ion. We wish now to report our studies on the europium and terbium complexes of tpip

which demonstrate that the ligands act as light-collector units forming a hydrophobic shell around the ion resulting in highly luminescent europium and terbium complexes. The chemistry contrasts with the analogous lanthanide β-diketonates where the binding site is surrounded by two rather than four aryl units and short lifetimes result from lack of protection of the lanthanide from the water (which limits their applications as sensors or biolabels).[11]

Reaction of K(tpip) with $EuCl_3$ or $TbCl_3$, in 3:1 molar ratio, leads to the formation of the neutral complexes [Eu(tpip)₃] and [Tb(tpip)₃], respectively. The complexes have been fully characterized and analysed by spectroscopic methods.† X-Ray quality crystals of [Tb(tpip)₃] were obtained by slow evaporation from chloroform. The crystal structure (Fig. 1)‡ shows that the twelve phenyl groups surround the lanthanide ion, forming a hydrophobic cage leading to a six-coordinate terbium ion. Two molecules in the unit cell which are different in the symmetry around terbium are observed; 1 being a distorted octahedron and 2 trigonal prismatic. Edge-to-face π stacking is present in both structures with C–H to centroid distance of ca. 3.0 Å of two phenyl groups in different ligands. Although there is no water coordinated to terbium, in contrast with the praseodymium crystal structure, there is a short van der Waals contact, observed only in 2, between the terbium ion and a water molecule situated at the top of the trigonal prism with a Tb–O distance of 3.85 Å (expected van der Waals 4.08 Å). The [Eu(tpip)₃] crystal structure is similar to the terbium one with three molecules in the unit cell, in two of which the symmetry around europium is trigonal prismatic and the other one is a
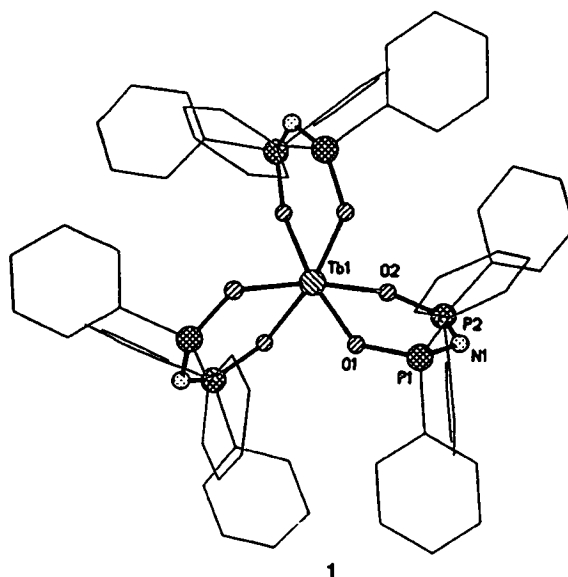

1

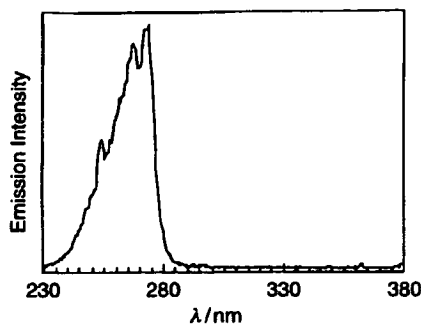Fig. 1 Crystal structure of [Tb(tpip)₃].

Fig. 2 Excitation spectrum of [Eu(tpip)₃] in CHCl₃, λ_{em} = 620 nm.

distorted octahedron. The short water van der Waals distance is again observed only in the trigonal prismatic molecules. The low coordination numbers of europium and terbium are attributed to the bulkiness of the ligands, with the twelve phenyl groups forming a cage around the ion.

Upon excitation at 273 nm (ε = 5,000 dm³ mol⁻¹ cm⁻¹) the [Eu(tpip)₃] and [Tb(tpip)₃] complexes exhibit strong emission, red and green respectively, characteristic of the ion. The excitation spectra of the complexes show a band centered at 270 nm, characteristic of the absorption of the ligand confirming that the emission of the complex is due to energy transfer from the ligand to the lanthanide luminescent center (Fig. 2).

Both europium and terbium complexes exhibit long lifetimes in solution compared with previously reported antenna complexes where lifetimes are optimized either for europium or for terbium. The emission lifetimes were found to be 1.8 ms for [Eu(tpip)₃] and 2.8 ms for [Tb(tpip)₃] in dry acetonitrile. Although there is no evidence of water coordination in the crystal structure, addition of water in the acetonitrile solution of [Tb(tpip)₃] and [Eu(tpip)₃] leads to shortening of the emission lifetime by 25 and 43%, respectively. The shortening in the lifetime indicates some involvement of the water molecules in the coordination sphere of the lanthanide. It may be attributed to a twist of the complex conformation in solution to fit the water molecule and agrees with the observed short water van der Waals contacts. The larger effect of water quenching in europium complexes has been well documented.[12]

The quantum yields of the complexes were measured in dry acetonitrile and determined using the method established by Haas and Stein, using [Ru(bipy)₃]Cl₂ (Φ = 0.028 in water) and quinine sulfate (Φ = 0.546 in 0.5 M H₂SO₄) as standards for the europium and terbium complex, respectively, taking into account the different excitation wavelength correction.[13] The values obtained are 1.3% for [Eu(tpip)₃] and 20% for [Tb(tpip)₃]. We postulate that the quenching of the europium emission via an LMCT state is not as effective as in the case of calixarene complexes where the quantum yields of the europium and terbium complexes can differ by more than three orders of magnitude.[5] Further photophysical experiments are currently underway to obtain more information about the mechanism of the energy transfer. The lack of any back energy transfer processes observed when bipyridine ligands are employed in terbium complexes leads to a high quantum yield for terbium.

We have introduced the imidodiphosphinate ligands as successful 'antenna' ligands for sensitizing both europium and terbium emission. The crystal structures of the complexes show unusual six-coordinate lanthanide ions where the ligands form a hydrophobic cage around the ion. We are currently further investigating the formation of these encapsulated lanthanide complexes based on these design principles.

Notes and references

† *Selected spectroscopic data* [Tb(tpip)₃]: ¹H NMR (360 MHz, CDCl₃, 25 °C, TMS) δ 7.97 (24H, Ar), 7.35 (12H, *p*-Ar), 6.28 (24H, Ar); ³¹P{¹H}

NMR (146 MHz, CDCl₃, 25 °C, 85% H₃PO₄) δ 200.7(s); MS (FAB⁺ in *m*-NBA) *m/z* 1408 (MH⁺), 991 (*M⁺* − tpip). [Eu(tpip)₃]: ¹H NMR (360 MHz, CDCl₃, 25 °C, TMS) δ 7.48–7.54 (m, 24H, *o*-Ar), 7.21 [t, ³*J* (HH) 7.4 Hz, 12H, *p*-Ar], 6.95–6.99 (m, 24H, *m*-Ar); ³¹P{¹H} NMR (146 MHz, CDCl₃, 25 °C, 85% H₃PO₄) δ 37.7(s); MS (FAB⁺ in *m*-NBA) *m/z* 1400 (MH⁺), 983 (*M⁺* − tpip). The ³¹P and ¹H NMR spectra at low temperature in deuterated dichloromethane or acetone reveal only one solution species which contains only one ligand environment. The lifetime measurements are mono-exponential. The paramagnetic shifts on ³¹P confirm the metal coordination. From these observations, we can conclude that (i) there is only one solution species (ii) all three ligands are in identical environments (iii) the ligand is bound to the metal centre. We believe that the only formulation that satisfies all these requirements is [ML₃] similar to that observed in the solid state.

‡ *Crystal data* [Tb(tpip)₃]·0.75 H₂O: C₇₂H₆₁.₅₀TbN₃O₆.₇₅P₆, *M* = 1421.48, rhombohedral, space group *R3̄*, *Z* = 12, *a* = 23.372(4), *c* = 42.956(8) Å, *U* = 20320(6) Å³, *T* = 220 K, μ = 1.240 mm⁻¹, final *R* = 0.0624 [based on *F* and 5674 data with *F*>4σ(*F*)], w*R*₂ = 0.1744 (based on *F²* and all 7979 unique data used in refinement) for 535 parameters. The structure was solved by direct methods (SIR 92) and refined by full-matrix least-squares procedures on *F²* (SHELXL-97).[14]

[Eu(tpip)₃]·0.67H₂O: C₇₂H₆₁.₃₃EuN₃O₆.₆₇P₆, *M* = 1411.75, trigonal, space group *P3̄*, *Z* = 6, *a* = 23.418(2), *c* = 21.185(3) Å, *U* = 10061.4(19) Å³, *T* = 220 K, μ = 1.13 mm⁻¹; final *R* = 0.0426 and *R*ᵥᵥ = 0.0418 [both based on 8591 out of 11861 unique data with *F*>4σ(*F*)], for 800 parameters. The structure was solved by Patterson methods (DIRDIF) and refined by full-matrix least-squares procedures on *F* (CRYSTALS).[15] CCDC 182/1097. See http://www.rsc.org/suppdata/cc/1999/61/ for crystallographic files in .cif format.

1 V. Balzani and F. Scandola, *Supramolecular Photochemistry*, Ellis Horwood, Chichester, UK, 1991; A. P. de Silva, H. Q. Nimal Gunaratne, T. Gunnlaugsson, A. J. M. Huxley, C. P. McCoy, J. T. Rademacher and T. E. Rice, *Chem. Rev.*, 1997, 97, 1515; T. Gunnlaugsson and D. Parker, *Chem. Commun.*, 1998, 511.

2 J.-M. Lehn, *Angew. Chem., Int. Ed. Engl.*, 1988, 27, 89; *Supramolecular Chemistry*, VCH, Weinheim, 1995.

3 N. Sabbatini, M. Guardigli and J.-M. Lehn, *Coord. Chem. Rev.*, 1993, 123, 201 and references therein.

4 M. P. Lowe, P. Caravan, S. J. Rettig and C. Orvig, *Inorg. Chem.*, 1998, 37, 1637; G. Ulrich, M. Hissler, R. Ziessel, I. Manet, G. Sarti and N. Sabbatini, *New J. Chem.*, 1997, 21, 147; D. A. Bardwell, J. C. Jeffery, P. L. Jones, J. A. McCleverty, E. Psillakis, Z. Reeves and M. D. Ward, *J. Chem. Soc., Dalton Trans.*, 1997, 2079.

5 L. J. Charbonnière, C. Balsiger, K. J. Schenk and J.-C. G. Bünzli, *J. Chem. Soc., Dalton Trans.*, 1998, 505; M. P. Oude Wolbers, F. C. J. M. van Veggel, R. H. M. Heeringa, J. W. Hofstraat, F. A. J. Geurts, G. J. van Hummel, S. Harkema and D. N. Reinhoudt, *Liebigs Ann./Recueil*, 1997, 2587; G. Ulrich, R. Ziessel, I. Manet, M. Guardigli, N. Sabbatini, F. Fraternali and G. Wipff, *Chem. Eur. J.*, 1997, 3, 1815; N. Sabbatini, M. Guardigli, A. Mecati, V. Balzani, R. Ungaro, E. Ghidini, A. Casnati and A. Pochini, *J. Chem. Soc., Chem. Commun.*, 1990, 878.

6 C. Piguet, G. Bernardinelli and G. Hopfgartner, *Chem. Rev.*, 1997, 97, 2005.

7 S. Aime, M. Botta, R. S. Dickins, C. L. Maupin, D. Parker, J. P. Riehl and J. A. G. Williams, *J. Chem. Soc., Dalton Trans.*, 1998, 881; P. R. Selvin, J. Jancarik, M. Li and L.-W. Hung, *Inorg. Chem.*, 1996, 35, 700; N. Sato and S. Shinkai, *J. Chem. Soc., Perkin Trans. 2*, 1993, 621.

8 M. A. Mortellaro and D. G. Nocera, *J. Am. Chem. Soc.*, 1996, 118, 7414; Z. Pikramenou, J-a Yu, A. Ponce and D. G. Nocera, *Coord. Chem. Rev.*, 1994, 132, 181; Z. Pikramenou and D. G. Nocera, *Inorg. Chem.*, 1992, 31, 532.

9 Some lanthanide complexes of tpip have previously been prepared as NMR shift reagents: N. Platzer, H. Rudler, C. Alvarez, L. Barkaoui, B. Denise, N. Goasdoué, M.-N. Rager, J. Vaissermann and J.-C. Daran, *Bull. Soc. Chim. Fr.*, 1995, 132, 95; I. Rodriguez, C. Alvarez, J. Gomez-Lara, R. A. Toscano, N. Platzer, C. Mulheim and H. Rudler, *J. Chem. Soc., Chem. Commun.*, 1987, 1502.

10 Y. Haas and G. Stein, *J. Phys. Chem.*, 1972, 76, 1093. D. Parker and J. A. G. Williams, *J. Chem. Soc., Dalton Trans.*, 1996, 3613.

11 The presence of a C–H bond in the binding site of the diketonates is further detrimental to the lifetimes of these complexes. For a general reference see: G. E. Buono-Core, H. Li and B. Marciniak, *Coord. Chem. Rev.*, 1990, 99, 55.

12 W. DeW. Horrocks, Jr. and D. R. Sudnick, *Acc. Chem. Res.*, 1981, 14, 384.

13 Y. Haas and G. Stein, *J. Phys. Chem.*, 1971, 75, 3668.

14 G. M. Sheldrick, SHELXL-97, Siemens Analytical X-ray, 1995.

15 D. J. Watkin, C. K. Pront, J. R. Carruthus and P. W. Betteridge, CRYSTALS, University of Oxford, 1996.

Communication 8/08046A